SIMPLE TECHNIQUES FOR THE IMPLEMENTATION OF THE MECHANICS OF UNSATURATED SOILS INTO ENGINEERING PRACTICE

by

Won Taek Oh

A thesis
Submitted to the faculty of graduate and postdoctoral studies
Under the supervision of
Dr. Sai K. Vanapalli, P.Eng.

In partial fulfillment of the requirements for the degree of
Doctor of Philosophy in Civil Engineering

Department of Civil Engineering
University of Ottawa
Ottawa, Ontario, Canada K1N 6N5

November 2012

The doctor of philosophy in Civil Engineering is a joint program between Carleton University and University of Ottawa, which is administered by the Ottawa-Carleton institute for Civil Engineering

ABSTRACT

Over the past 50 years, several advancements have been made in the research area of the mechanics of unsaturated soils. These advancements can be categorized into two groups; (i) development (or improvement) of testing techniques (or apparatus) to determine the mechanical properties of unsaturated soils and (ii) development of (numerical, empirical or semi-empirical) models to estimate the variation of mechanical properties of unsaturated soils with respect to suction based on the experimental results. Implementation of the mechanics of unsaturated soils in conventional geotechnical engineering practice, however, has been rather limited. The key reasons for the limited practical applications may be attributed to the lack of simple and reliable methods for (i) measuring soil suction in the field quickly and reliably and (ii) estimating the variation of mechanical properties of unsaturated soils with respect to suction.

The main objective of this thesis research is to develop simple and reliable techniques, models or approaches that can be used in geotechnical engineering practice to estimate sol suction and the mechanical properties of unsaturated soils. This research can be categorized into three parts.

In the First Part, simple techniques are proposed to estimate the suction values of as-compacted unsaturated fine-grained soils using a pocket penetrometer and a conventional tensiometer. The suction values less than 300 kPa can be estimated using a strong relationship between the compressive strength measured using a pocket penetrometer and matric suction value. The high suction values in the range of 1,200 kPa to 60,000 kPa can be estimated using the unique relationship between the initial tangent of conventional tensiometer response versus time behavior and suction value.

In the Second Part, approaches or semi-empirical models are proposed to estimate the variation of mechanical properties of unsaturated soils with respect to suction, which include:

- Bearing capacity of unsaturated fine-grained soils
- Variation of bearing capacity of unsaturated fine-grained soils with respect to matric suction
- Variation of initial tangent elastic modulus of unsaturated soils below shallow foundations with respect to matric suction
- Variation of maximum shear modulus with respect to matric suction for unsaturated non-plastic sandy soils (i.e. plasticity index, I_p = 0 %)

In the Third Part, approaches (or methodologies) are suggested to simulate the vertically applied stress versus surface settlement behavior of shallow foundations in unsaturated coarse-grained soils assuming elastic-perfectly plastic behavior. These methodologies are extended to simulate the stress versus settlement behavior of both model footings and in-situ plates in unsaturated coarse-grained soils.

The results show that there is a reasonably good comparison between the measured values (i.e. soil suction, bearing capacity, elastic and shear modulus) and those estimated using the techniques or models proposed in this thesis research.

The models (or methodologies) proposed in this thesis research are promising and encouraging for modeling studies and practicing engineers to estimate the variation of mechanical behavior of unsaturated soils with respect to matric suction.

ACKNOWLEDGEMENTS

The work presented in this thesis was conducted at the Department of Civil Engineering at the University of Ottawa under the supervision of Dr. Sai K. Vanapalli. I would like to express my sincere appreciation to Dr. Sai Vanapalli. The completion of this thesis would not have been possible without his encouragement, invaluable suggestions, and continuous support throughout this research program.

The financial supports from the Natural Sciences and Engineering Research Council (NSERC), Ontario graduate Scholarship (OGS), and Ontario Graduate Scholarship in Science and Technology (OGSST) are gratefully acknowledged.

Thanks are also extended to the technical officers, Kulan and Celestin and my colleagues, Jules, Fathi, Othman, Hana, Joseph, Ali, Afshin, and Farzad at the Geotechnical lab, University of Ottawa for their help, assistances, and good company.

I would like to express my gratitude to my mother, parents-in-law, brothers, sisters-in-law for their encouragements. Finally, Special appreciations go to my lovely wife, Jiyoung for her patience, continuous support and encouragement during this long journey. I love you and am so proud of you.

LIST OF CONTENTS

LIST OF FIGURES

LIST OF TABLES

LIST OF SYMBOLS

SUBSCRIPT

i	= initial value
f	= value at failure
sat	= saturated condition
$unsat$	= unsaturated condition
max	= maximum value
min	= minimum value

SYMBOLS

α, β	= fitting parameters for elastic modulus
ζ, ξ	= fitting parameters for shear modulus
υ, μ	= fitting parameters for shear strength of unsaturated fine-grained soils
γ_d	= dry unit weight of soil
γ_t	= total unit weight of soil
$\Delta\delta$	= increment of settlement in elastic range
Δq	= increment of applied stress in elastic range
δ	= settlement of model footing or in-situ plate
ε_a	= axial strain in shear strength tests
θ	= volumetric water content
θ_r	= residual volumetric water content
κ	= fitting parameter for shear strength
K	= slope of matric suction versus compression strength from pocket penetrometer
ν	= Poisson's ratio
ξ_c, ξ_q, ξ_γ	= shape factors
$(\sigma_n - u_a)$	= net normal stress
σ	= applied stress in shear strength tests

σ_1	= major principal stress (total)
σ_3	= minor principal stress (total)
σ'_1	= major principal stress (effective)
σ'_3	= minor principal stress (effective)
τ	= shear strength of soil
ϕ'	= effective internal friction angle for saturated condition
ϕ^b	= contribution of soil suction towards the shear strength of unsaturated soil
ϕ^*	= modified internal friction angle with respect to local shear failure
ϕ_u	= internal friction angle for undrained condition under saturated condition
ϕ'_{AS}	= internal friction angle obtained under axisymmetric condition
ϕ'_{PS}	= internal friction angle obtained under plain strain condition
ψ	= fitting parameter for bearing capacity
Ψ	= soil suction
Ψ_r	= residual suction value
$(1/a)$	= initial tangent of hyperbolic relationship
B	= width of a (model) footing
c	= total cohesion
c'	= effective cohesion for saturated condition
c_u	= undrained shear strength
c^*	= modified effective cohesion with respect to local shear failure
C_U	= coefficient of uniformity
D	= diameter of a circular footing
D'	= diameter of a tank used for the model footing test
D_f	= depth from the surface of (model) footing
e	= void ratio
E	= elastic modulus
E_i	= initial tangent elastic modulus
$E_{i(B)}$	= E_i representing a soil layer in the range of 0 to B
$E_{i(1.5B)}$	= E_i representing a soil layer in the range of 0 to 1.5B
G	= shear modulus

G_s	= specific gravity
H'	= height of a box used for model footing test
I_D	= relative density
I_p	= plasticity index
I_w	= influence factor
k_{is}	= initial tangent modulus of subgrade reaction
K_0	= coefficient of lateral earth pressure at rest
L'	= length of a box used for model footing test
L	= length of (model) footing
N_c, N_q, N_γ	= bearing capacity factors
p'	= $(\sigma'_1 + \sigma'_3)/2$
p	= $(\sigma_1 + \sigma_3)/2$
q (q')	= $(\sigma_1 - \sigma_3)/2$
$\overline{q}$	= overburden pressure
q_u	= unconfined compressive strength
q_{ult}	= ultimate bearing capacity
S	= degree of saturation
$(u_a - u_w)$	= matric suction
$(u_a - u_w)_{AVR}$	= average matric suction value
$(u_a - u_w)_b$	= air-entry value
u_a	= pore-air pressure
u_w	= pore-water pressure
w	= water content
w_L	= liquid limit
w_P	= plastic limit
W'	= width of a box used for model footing test

CHAPTER 1

GENERAL INTRODUCTION

1.1 Justification for Using the Mechanics of Unsaturated Soils

Approximately one-third of the earth's surface is constituted of arid or semi-arid regions. In these regions, natural ground water table is deep and soils are typically in a state of unsaturated condition. Hence, the stresses associated with the constructed infrastructure such as shallow foundations, retaining walls, tunnels, pipe lines are mostly distributed in the zone above natural ground water table where pore-water pressures are negative with respect to the atmospheric pressure (i.e. matric suction). This implies that rational design of geotechnical infrastructure listed above in arid or semi-arid regions should be carried out based on the mechanics of unsaturated soils. In other words, the influence of matric suction on the mechanical behavior of geotechnical structures should be taken into account in the engineering practice.

1.2 Objectives of the Thesis

Fredlund and Rahardjo (1993) provided comprehensive framework that can be used to interpret the mechanical properties of unsaturated soils such as the shear strength, the volume change and the flow behavior. The primary objective of this thesis is to develop a rational and yet simple techniques, approaches or methodologies to implement their framework into conventional geotechnical engineering practice. Keeping this key objective in perspective, several secondary objectives are addressed through this thesis as follows.

- Techniques to estimate the suction values of as-compacted unsaturated fine-grained soils in low and high suction range

- An approach to estimate the bearing capacity of unsaturated fine-grained soils
- A semi-empirical model to estimate the variation of bearing capacity of unsaturated fine-grained soils with respect to matric suction
- A semi-empirical model to estimate the variation of elastic modulus of unsaturated soils with respect to matric suction
- A semi-empirical model to estimate the variation of shear modulus of non-plastic sandy soils (i.e. I_p = 0%) with respect to matric suction
- Methodologies to simulate the vertically applied stress versus settlement behavior of shallow foundations in unsaturated coarse-grained soils

1.3 Scope of the Thesis

The scope of this thesis can be summarized into the following four categories.

1.3.1 Simple Techniques for Estimating the Suction Value of As-Compacted Soils

Two simple techniques are proposed to estimate the suction value of as-compacted unsaturated fine-grained soils over a range of 0 to 60,000 kPa. The first technique uses a conventional pocket penetrometer in the estimation of matric suction values lower than 300 kPa. This technique is developed based on the assumption that there is a strong relationship between matric suction and the compressive strength measured using a pocket penetrometer. The second technique uses conventional tensiometer to estimate relatively high suction values in the range of 1,200 to 60,000 kPa using a (conventional) tensiometer response versus time behavior for the matric suction values in the range of 0 to 50 kPa. This technique is developed based on the assumption that the tensiometer response versus time behavior can be represented using the hyperbolic model and there is a unique relationship between the initial tangent of tensiometer response versus time behavior and a certain matric suction value. The equilibrium suction values of the as-compacted specimens are measured using axis-translation technique and a psychrometer for low and high suction values respectively and compared with those estimated using the techniques proposed in this thesis.

1.3.2 Bearing Capacity of Unsaturated Fine-grained Soils

A series of model footing ($B \times L$ = 50 mm × 50 mm) tests are conducted on statically compacted fine-grained soil samples using specially designed equipment. The compacted soil samples are first saturated and then subjected to varying degrees of natural air-drying to achieve different average matric suction values (i.e. 0, 55, 100, 160, 205 kPa) prior to loading them to failure conditions at constant rate [i.e. 1.14 mm/min (0.045 in/min)]. Based on the experiment results, an approach is suggested to interpret the bearing capacity of unsaturated fine-grained soils by extending the Skempton (1948)'s bearing capacity theory. The proposed approach uses only unconfined compressive strength of unsaturated soils without matric suction measurement. In addition, a model is also proposed to estimate the variation of bearing capacity of unsaturated fine-grained soils with respect to matric suction using the Soil-Water Characteristic Curve (*SWCC*) and the undrained shear strength for saturated condition along with two fitting parameters. Discussions on the reasonable approach to interpret the bearing capacity of unsaturated soils taking account of soil types (coarse- or fine-grained soils) and drainage conditions of pore-air and pore-water are also presented.

1.3.3 Elastic and Shear Modulus of Unsaturated Soils

A semi-empirical model is developed to estimate the variation of elastic modulus of unsaturated soils with respect to matric suction. The model footing tests undertaken at the University of Ottawa (Mohamed and Vanapalli 2007) and other studies (i.e. model footing and in-situ plate load tests results) published in the literature are used to develop the model. The proposed model requires *SWCC* and elastic modulus under saturated condition along with two fitting parameters. Comparisons are provided between the measured elastic moduli obtained from model footing and in-situ plate load tests in unsaturated soils and those estimated using the proposed model in this thesis. Extending the concepts used to develop the model for elastic modulus, another model is also proposed to estimate the variation of shear modulus of unsaturated non-plastic soils (i.e. I_p = 0%) with respect to matric suction.

1.3.4 Modelling the Stress versus Settlement Behavior of Shallow Foundations in Unsaturated Coarse-Grained Soils

Two methodologies are proposed to simulate the vertically applied stress versus surface settlement behavior of shallow foundations in unsaturated coarse-grained soils. In the first method (*Method I*), the stress versus settlement behavior is simplified as elastic - perfectly plastic behavior. In other words, the behavior is idealized using two straight lines, which represent elastic and perfectly plastic behavior, respectively. The linear lines that represent elastic and perfectly plastic behavior are obtained using the elastic modulus model proposed in this thesis and bearing capacity model available in the literature (Vanapalli and Mohamed 2007), respectively. In the second method (*Method II*), finite element analysis is carried out using elastic - perfectly plastic model with Mohr-Coulomb yield criterion (Chen and Zhang 1991). The finite element analysis is undertaken using the commercial finite element software, *SIGMA*/*W* (Krahn 2007), a software product of *GEO-SLOPE* (i.e. Geostudio 2007). The validity of '*Method I*' is tested using the model footing tests results in unsaturated sand (Mohamed and Vanapalli 2006). In addition, '*Method II*' (i.e. finite element analysis) is extended to simulate the stress versus settlement behavior of an in-situ footing load test in an unsaturated sandy soil (Briaud and Gibbens 1992).

Moreover, discussion on the influence of plate (or footing) size on the stress versus settlement behavior (i.e. scale effect) in unsaturated soils is presented. Unlike saturated soils, two aspects such as plate size and matric suction distribution profile should be considered to investigate the scale effect in unsaturated soils. This is attributed to the fact that the stress versus settlement behavior of an unsaturated soil below a shallow foundation is influenced by not only footing size but also representative matric suction value. Extending this concept, details of Large Tempe Cell that can be used to achieve uniform matric suction distribution profile with depth are presented in the appendix. This Large Tempe Cell can be effectively used to better understand the scale effect of plate size in unsaturated soils.

1.4 Organization of the Thesis

This thesis consists of seven chapters including 'General Introduction' and 'Summary and Conclusions'. Each chapter deals with different topic and has been published in a journal. Hence, a separate chapter on the 'Literature Review' is not presented since each chapter has a separate section which provides background information regarding the topic.

The First Chapter describes the need for the mechanics of unsaturated soils, objective of this thesis research and the scopes and the organization of the thesis.

In the Second Chapter, two simple techniques are proposed that can be used to estimate soil suction values of as-compacted unsaturated fine-grained soils in the range of 0 to 60,000 kPa. Contents of this chapter have been published in the ASTM Geotechnical Testing Journal (**Vanapalli and Oh 2011**).

In the Third Chapter, an approach is suggested to interpret the bearing capacity of unsaturated fine-grained soils based on a series of model footing tests results in unsaturated fine-grained soils. In addition, a simple model is proposed to estimate the variation of bearing capacity of unsaturated fine-grained soils with respect to matric suction. Contents of this chapter have been accepted for the publication in the ASCE International Journal of Geomechanics (**Oh and Vanapalli 2012a**).

In the Fourth Chapter, a semi-empirical model is developed to estimate the variation of elastic modulus of unsaturated soils below shallow foundations with respect to matric suction using model footing and in-situ plate load tests results in unsaturated soils. Contents of this chapter have been published in the Canadian Geotechnical Journal (**Oh and Vanapalli 2009**).

In the Fifth Chapter, two methodologies are suggested to estimate the vertically applied stress versus surface settlement behavior of shallow foundations in unsaturated coarse-grained soils assuming elastic-perfectly plastic behavior. The justification of the proposed methodologies is checked by comparing the measured stress versus settlement behaviors from the model footing and in-situ footing load tests and those estimated using the proposed methodologies. Contents of this chapter have been published in the Canadian Geotechnical Journal (**Oh and Vanapalli 2011**).

In the Sixth Chapter, a semi-empirical model is proposed to estimate the variation of shear modulus of unsaturated non-plastic sandy soils by analyzing the measured shear moduli from bender element and resonant column tests. Contents of this chapter have been accepted for the publication in the Journal of Geotechnical and Geological Engineering (**Oh and Vanapalli 2012b**).

In the Seventh Chapter, conclusions from different studies undertaken through this thesis are succinctly summarized. In addition, recommendations and future works that would be useful for implementing the mechanics of unsaturated soils in engineering practice are suggested.

REFERENCES

Briaud, J.-L. and Gibbens, R. 1994. Predicted and measured behavior of five large spread footings on sand. *In* Proceedings of Prediction Symposium, ASCE, Geotechnical Special Publication, 41.

Chen, W.F. and Zhang, H. 1991. Structural plasticity: theory, problems, and CAE software. Springer-Verlag.Fredlund, D. G. and Rahardjo, H. 1993. *Soil mechanics for unsaturated soils*. John Wiley and Sons, INC., New York.

Krahn, J. 2007. Stress and deformation modelling with SIGMA/W (SIGMA/W manual). Geo-slope International Ltd.

Mohamed, F.M.O and Vanapalli, S.K. 2006. Laboratory investigations for the measurement of the bearing capacity of an unsaturated coarse-grained soil. *In* Proceedings of the 59th Canadian Geotechnical Conference, Vancouver.

Oh, W.T., Vanapalli, S.K. and Puppala, J. 2009. Semi-empirical model for the prediction of modulus of elasticity for unsaturated soils. *Canadian Geotechnical Journal*, 48(6): 903-914.

Oh, W.T. and Vanapalli, S.K. 2011. Modelling the applied vertical stress and settlement relationship of shallow foundations in saturated and unsaturated sans. *Canadian Geotechnical Journal*, 48(3): 425-438.

Oh, W.T. and Vanapalli, S.K. 2012a. Interpreting the bearing capacity of unsaturated fine-grained soils using modified effective and total stress approaches. *ASCE International Journal of Geomechanics*. (Accepted for publication)

Oh, W.T. and Vanapalli, S.K. 2012b. Semi-empirical model for estimating the small-strain shear modulus of unsaturated non-plastic sandy soils. *Journal of Geotechnical and Geological Engineering*. (Accepted for publication)

Skempton, A.W. 1948. The $\phi_u = 0$ analysis for stability and its theoretical basis. *In* Proceedings of the 2nd International Conference of Soil Mechanics and Foundation Engineering, 1, 72-77.

Vanapalli, S.K. and Mohamed, F.M.O. 2007. Bearing capacity of model footings in unsaturated soils. Experimental Unsaturated Soil Mechanics. *In* Proceedings of the 2nd International Conference on Unsaturated Soils, Weimar, 483-493.

Vanapalli, S.K. and Oh, W.T. 2011. Simple techniques for the estimation of suction in compacted soils in the range of 0 to 60,000 kPa. *ASTM Geotechnical Testing Journal*, 34(6).

CHAPTER 2

SIMPLE TECHNIQUES FOR ESTIMATING SOIL SUCTION OF UNSATURATED SOILS

2.1 Introduction

The conventional tensiometer (i.e. jet fill tensiometer or small tip tensiometer) is regarded to be reliable, simple and economical device that can be used in the direct measurement of matric suction both in the laboratory and in the field. However, effective continuous measurements of matric suction using the conventional tensiometers are limited to 90 kPa or even lower due to the problems associated with cavitation (Stannard 1990). The limitation associated with the conventional tensiometers could be overcome using the high capacity tensiometers (Ridley and Burland 1993, Guan and Fredlund 1997, Tarantino and Mongiovì 2003). The presently used high capacity tensiometers are capable of measuring soil suction values up to 1,500 kPa (Ridley and Burland 1995); however, they are expensive and are mostly used for research purposes in the laboratories.

In this chapter, two simple techniques (one for low and the other for high suction) are proposed to estimate suction values of as-compacted soils in the range of 0 to 60,000 kPa. These techniques are developed based on a series of laboratory tests conducted on statically compacted fine-grained soil at different water contents (i.e. soil suctions). A glacial till obtained from Indian Head, Saskatchewan, Canada was chosen as a candidate material in the present study. Compacted glacial tills are commonly used in the construction of pavements and embankments in Western Canada and also in several regions of the *U.K* and the *U.S.A* (Oh and Vanapalli 2010).

The first technique uses a pocket penetrometer that is commonly used in the site investigation studies to classify the fine-grained soils based on compression strength (i.e. approximate undrained shear strength). This technique is based on the assumption that there is a strong relationship between the compression strength determined using a pocket penetrometer, PP_{cs} and the matric suction of as-compacted soils. The conventional pocket penetrometers are typically capable of measuring compression strength of 450 kPa. In other words, this technique is dependent on the capacity of the pocket penetrometer and the matric suction values that can be estimated using this technique is relatively low. The matric suction values of the as-compacted soils less than 500 kPa were measured using the modified null pressure plate apparatus extending axis-translation technique (Power and Vanapalli 2010) to provide comparisons between the measured matric suction values and those estimated using the proposed technique.

The second technique uses a conventional tensiometer to estimate suction values in the range of 1,200 kPa to 60,000 kPa. This technique is based on the assumption that there is a unique relationship between the initial tangent of conventional tensiometer response versus time behavior and suction value of as-compacted soils. This assumption was found to be valid for the data published in the literature for several soils. The tensiometer response versus time behaviors measured in the suction range of only 0 to 50 kPa is required to use this technique. This data is then used in a hyperbolic model to estimate initial tangent of tensiometer response versus time behavior. The equilibrium suction values of the as-compacted soils greater than 1000 kPa were measured using a psychrometer (i.e. WP4-T).

2.2 Soil Sample Preparation for the Testing Program

The required soil (i.e. Indian Head till) for the testing program was prepared by first air-drying and subjecting it to gentle pulverization to separate the individual soil particles and then passed through a 2 mm sieve. The soil has 23%, 48%, and 29% of sand, silt, clay content, respectively and can be classified as *CL* as per the *USCS* classification. The plasticity index, I_p is 15.5% and the specific gravity, G_s is 2.72. Figure 2.1 shows the grain size distribution curve for the Indian Head till along with basic soil properties. The prepared soil was mixed with distilled water at different water contents chosen for the study and placed in sealed polyethylene bags. The soil bags were stored in a humidity controlled chamber for at least 5 days to ensure uniform distribution of water throughout the samples.

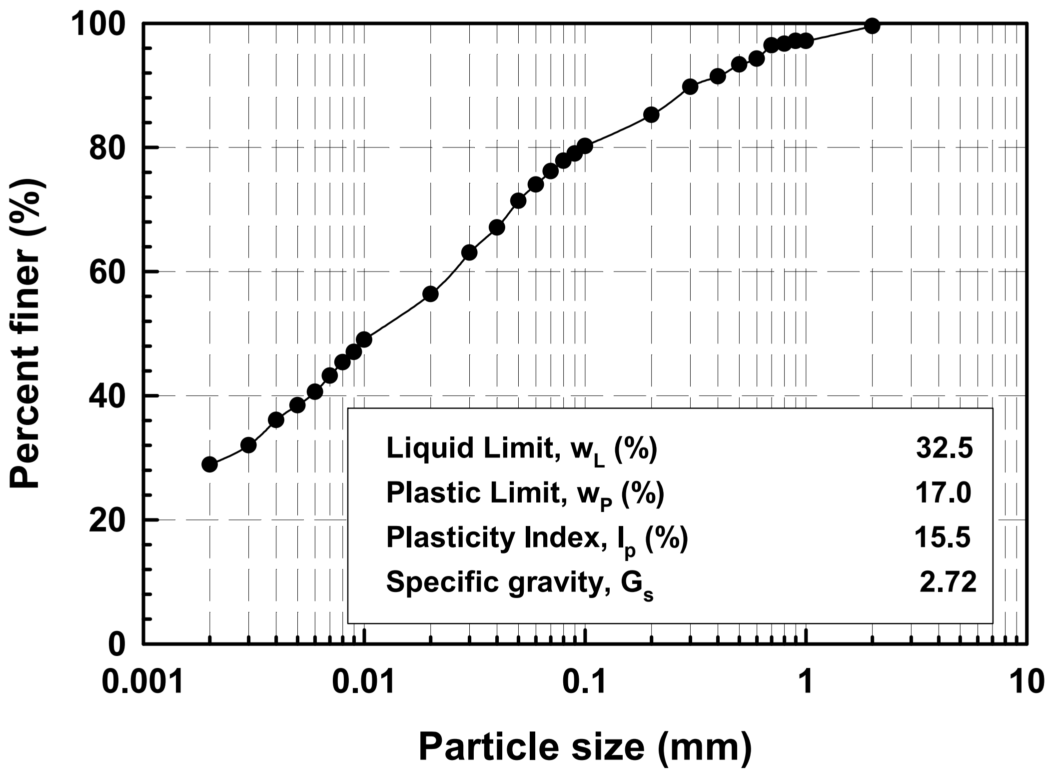

Figure 2.1 Grain size distribution curve of the soil (Indian Head till) used in the research.

The soil-water mixtures were compacted in metal rings [50 mm in diameter and 20 mm in height; Figure 2.2(a)] under three different static compaction stresses (i.e. 375, 750, and 1125 kPa) using a metal mould (50 mm in diameter and 100 mm in height) and a compactor [Figure 2.2(b)]. The specimens compacted in metal rings were used to (i) determine compaction characteristics, (ii) perform pocket penetrometer tests and (iii) perform suction measurements. The specimens compacted (in five layers) in metal mould were used for conducting unconfined compression tests at a constant rate (i.e. 1.14 mm/min; 0.045 in/min).

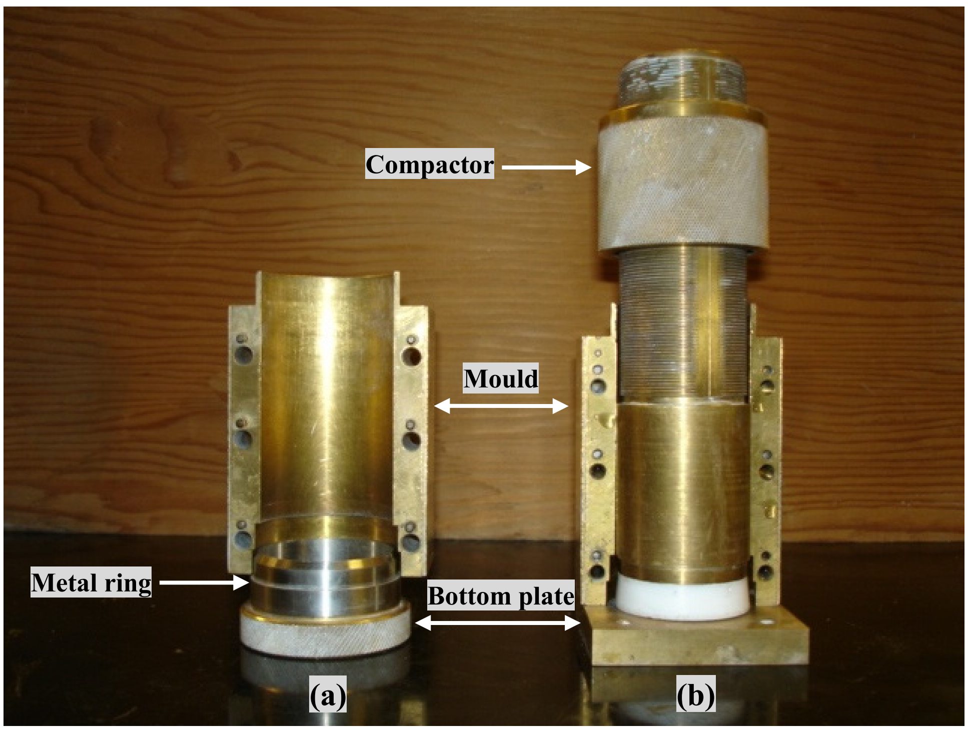

Figure 2.2 Accessories used to compact soil-water mixtures for (a) pocket penetrometer and (b) unconfined compression tests.

Figure 2.3 shows the compaction curves for the three compaction stresses. Three specimens that represent varying soil structures (i.e. dry of optimum moisture content, optimum moisture content and wet of optimum moisture content; Vanapalli et al. 1999) were chosen from each compaction curve (i.e. specimens *A*, *B*, *C* for 375 kPa, *A′*, *B′*, *C′* for 750 kPa, and *A″*, *B″*, *C″* for 1125 kPa). Three more specimens [i.e. *X* for 375 kPa, *Y* for 750 kPa and *Z* (same as *B″*) for 1125 kPa] compacted at the same water content (w = 14.8 %) were prepared to investigate the variation of matric suction and degree of saturation with respect to compaction stress. Table 2.1 summarizes the water content and dry density for the specimens used in the testing program.

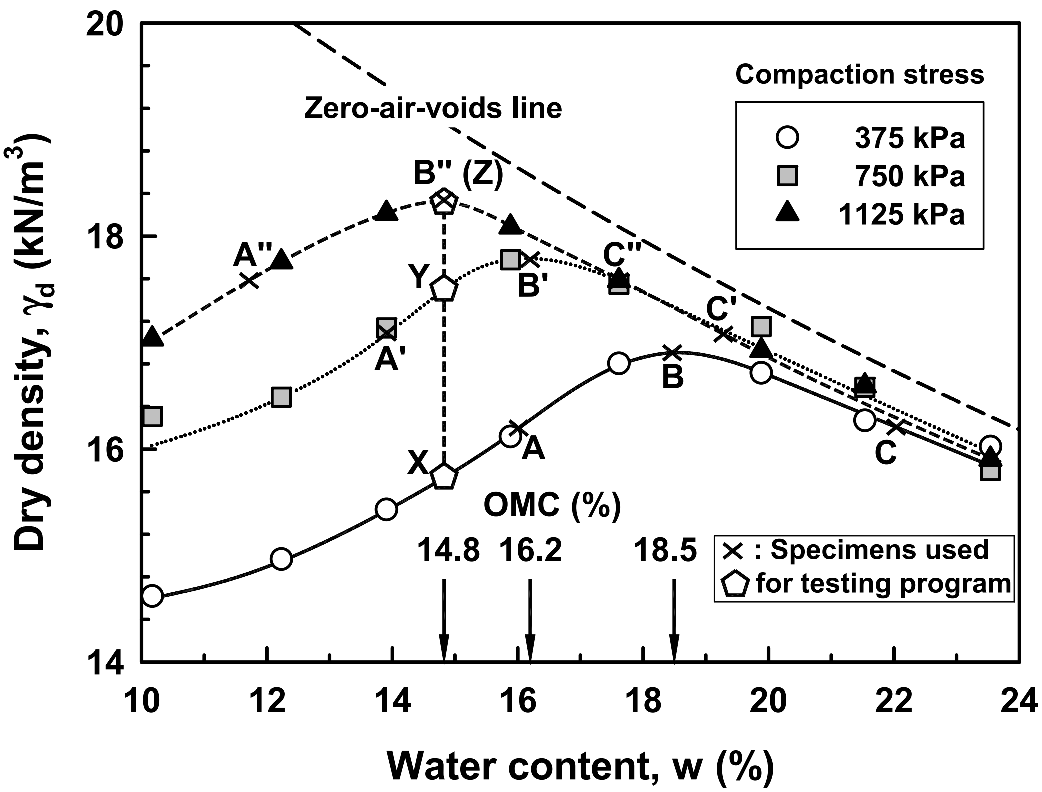

Figure 2.3 Compaction curves for different compaction stresses and specimens used for the testing program (*OMC* = optimum moisture content).

Table 2.1 Soil specimens used for testing program.

Specimens	Compaction stress (kPa)					
	375		750		1125	
	w (%)	γ_d (kN/m^3)	w (%)	γ_d (kN/m^3)	w (%)	γ_d (kN/m^3)
A, A', A'' (Dry of optimum)	16.0	16.2	13.9	17.1	11.7	17.6
B, B', B'' (Optimum)	18.5	16.9	16.2	17.8	14.8	18.3
C, C', C'' (Wet of optimum)	22.0	16.2	19.3	17.1	17.6	17.6
X (Dry of optimum)	14.8	15.7				
Y (Dry of optimum)			14.8	17.5		
Z (Optimum)					14.8	18.3

2.3 Estimation of Low Suction Values Using a Pocket Penetrometer

2.3.1 Pocket Penetrometer Test

Pocket penetrometer (Figure 2.4) is a device that is conventionally used to estimate approximate undrained shear strength of fine-grained soil samples collected from site investigation studies (ASTM D 6169-98 2005) based on compression strength from the pocket penetrometer (PP_{cs}). The PP_{cs} values can be directly read on the compression strength scale using the red slide ring which shifts to a certain distance as the piston end of pocket penetrometer is pushed into a soil specimen to a depth of 6.35 mm (1/4″). The diameter of the piston end is 6.35 mm (1/4″) and the range of measurement is between 25 kPa and 450 kPa (each division is 25 kPa). Approximations can be easily made with naked eyes or with the assistance of a simple hand lens to measure PP_{cs} with 5 kPa sensitivity.

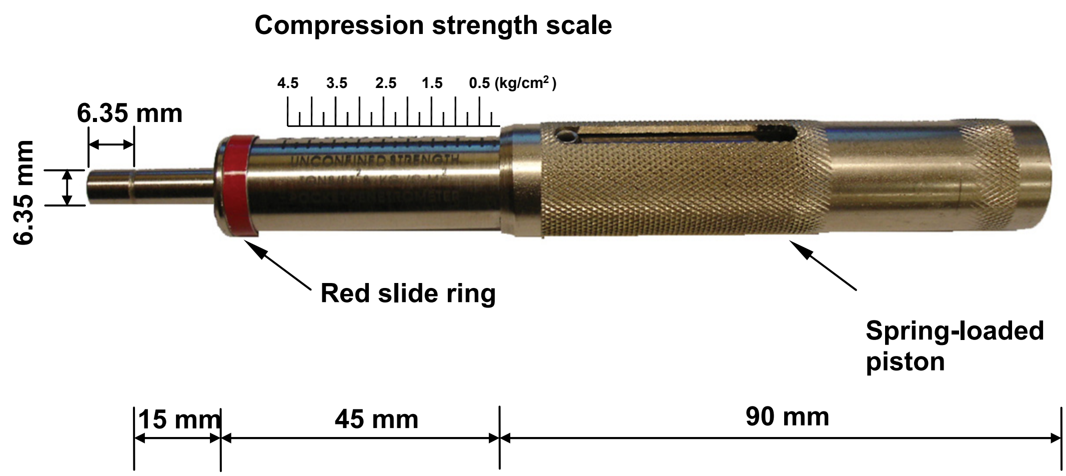

Figure 2.4 Pocket penetrometer used in the research.

To measure the PP_{cs} values, the piston end of the pocket penetrometer was first located in the center of the compacted specimens in metal rings. The specimen was then slowly loaded with the pocket penetrometer using both hands until the piston end penetrates to a depth of 6.35 mm (Figure 2.5). The tests were conducted on two identical specimens and the average PP_{cs} values were used for the analysis. The difference between two PP_{cs} values were less than 7 kPa for the matric suction value less than 120 kPa and less than 30 kPa for the matric suction values greater than 180 kPa. For all practical purposes, the test results on the compacted specimens can be considered to be repeatable.

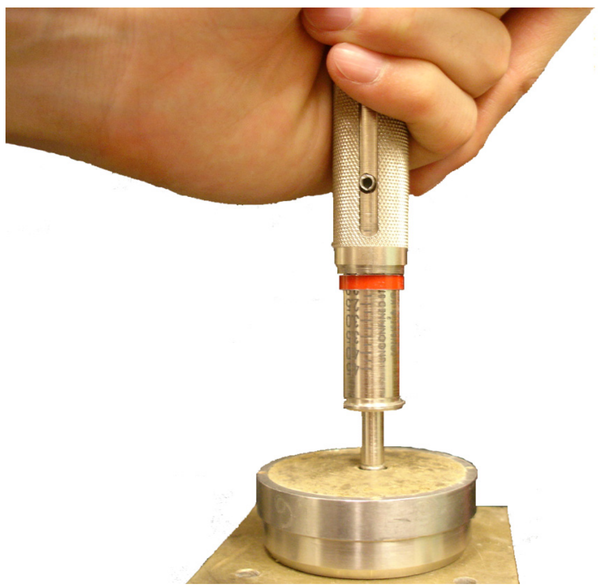

Figure 2.5 Penetration of piston end of a pocket penetrometer into a compacted specimen to measure compression strength.

2.3.2 Matric Suction Measurement

The matric suction values of the as-compacted specimens used for pocket penetrometer tests were measured using axis-translation technique (ASTM D 68736-02 2008, Power and Vanapalli 2010, Figure 2.6). Figure 2.7 shows the constant matric suction contours based on the measured matric suction values. The constant matric suction contours show positive slope for all the water contents and compaction stresses used in the present study. The slopes tend to be vertical as compaction water content decreases (Tarantino and Tombolato 2005, Catana 2006, González and Colmenares 2006, Tarantino and De Col 2008). Such a behavior indicates that (i) matric suction values of specimens compacted at the same water content increases with increasing degree of saturation (i.e. compaction stress) and (ii) the influence of compaction water content on matric suction becomes predominant in comparison to compaction stress and dry density as compaction water content decreases.

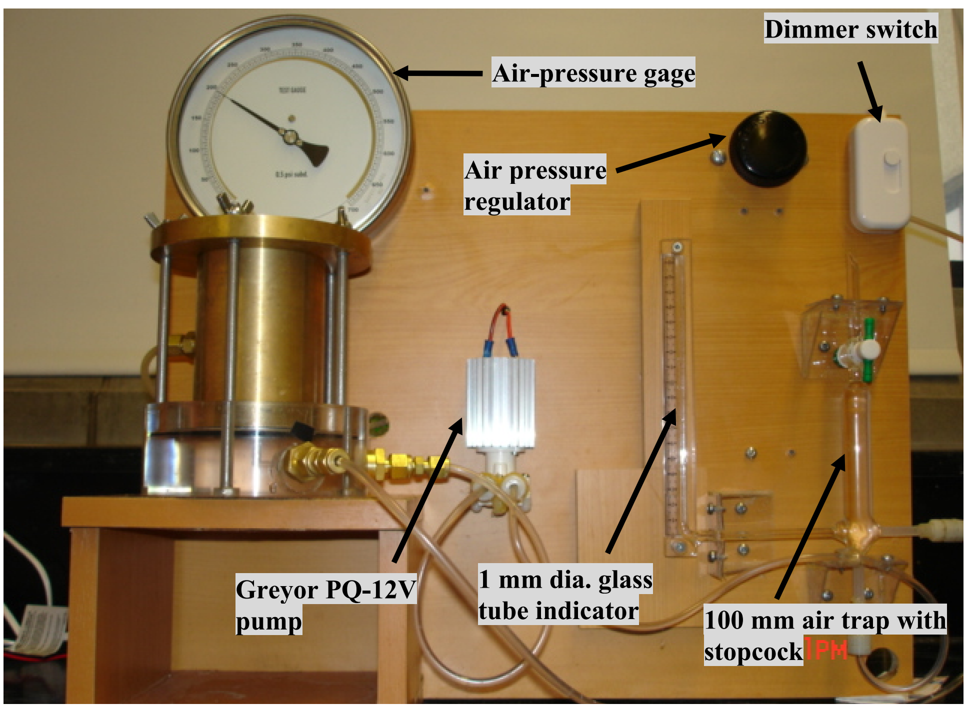

Figure 2.6 Equipment setup used to measure matric suction values of as-compacted soils extending axis-translation technique.

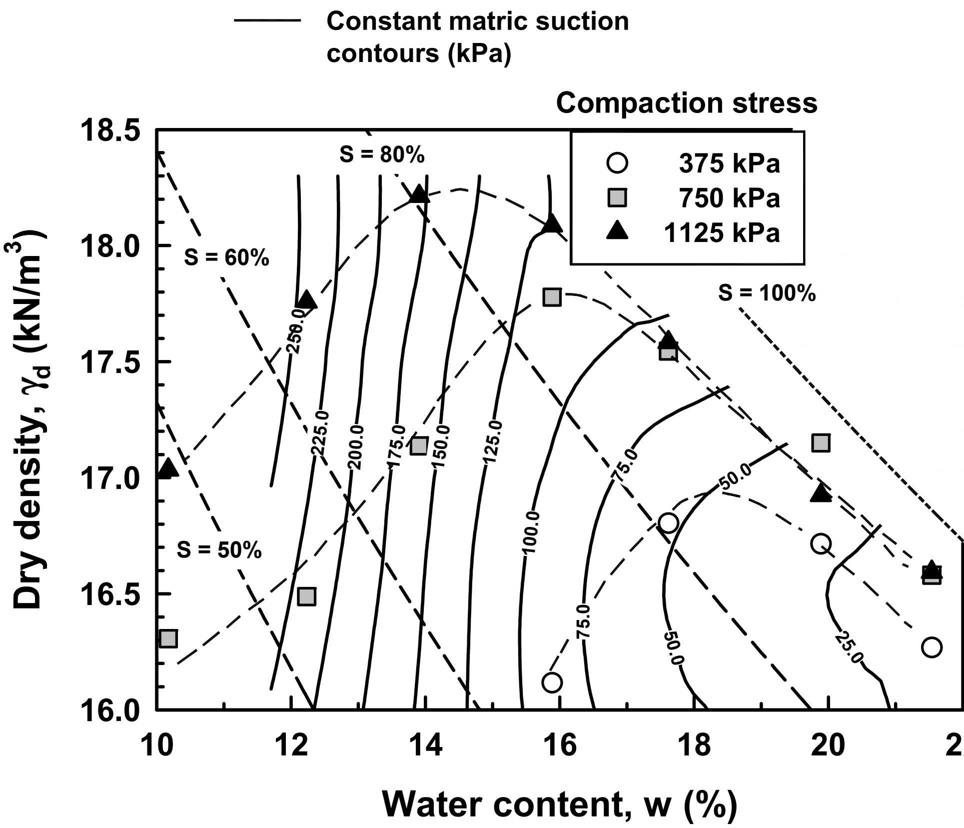

Figure 2.7 Contours of constant matric suction for the as-compacted specimens.

Tarantino and Tombolato (2005) provided detailed explanations for this characteristic behavior using the 'void-dependent retention curve' concept (see Figure 2.8). A soil specimen on compaction reaches point A_1 that is located on a main-wetting curve associated with void ratio e_A. Upon unloading the compaction stress, the state of the soil specimen moves from point A_1 to point A_2 that represents a new degree of saturation, S and matric suction, $(u_a - u_w)$ for the as-compacted condition. When the soil specimen at point A_2 is reloaded under higher compaction stress, the main-wetting curve moves upward and the soil specimen follows the paths $A_2 \rightarrow A_1 \rightarrow B_1$. Unloading of the compaction stress from point B_1 drags the soil specimen to point B_2 whose matric suction value is greater than that of A_1 in spite of higher degree of saturation. Figure 2.9 shows matric suction versus degree of saturation relationships for the three specimens, X, Y, and Z compacted at the same water content (w = 14.8 %), but different compaction stresses (i.e. 375, 750 , and 1125 kPa) (see Figure 2.3 and Table 2.1). As can be seen, the matric suction value of the specimen, Z is greater than those of the specimens, X and Y even though the degree of saturation of the specimen Z is greater than other specimens.

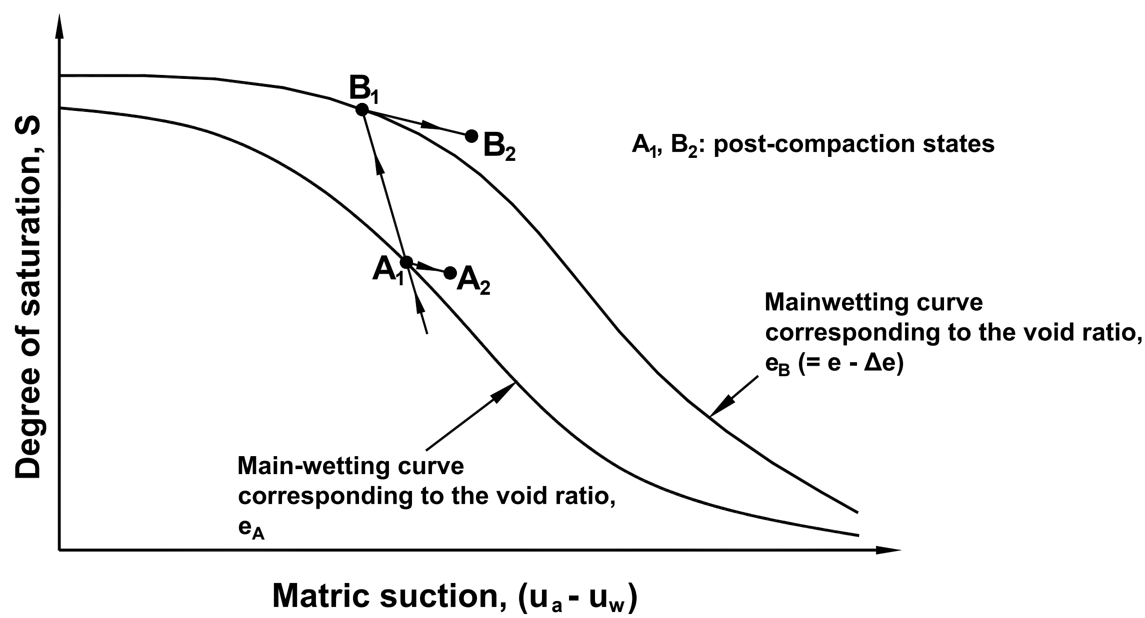

Figure 2.8 Effect of void-dependent retention curve on post-compaction (Tarantino and Tombolato 2005).

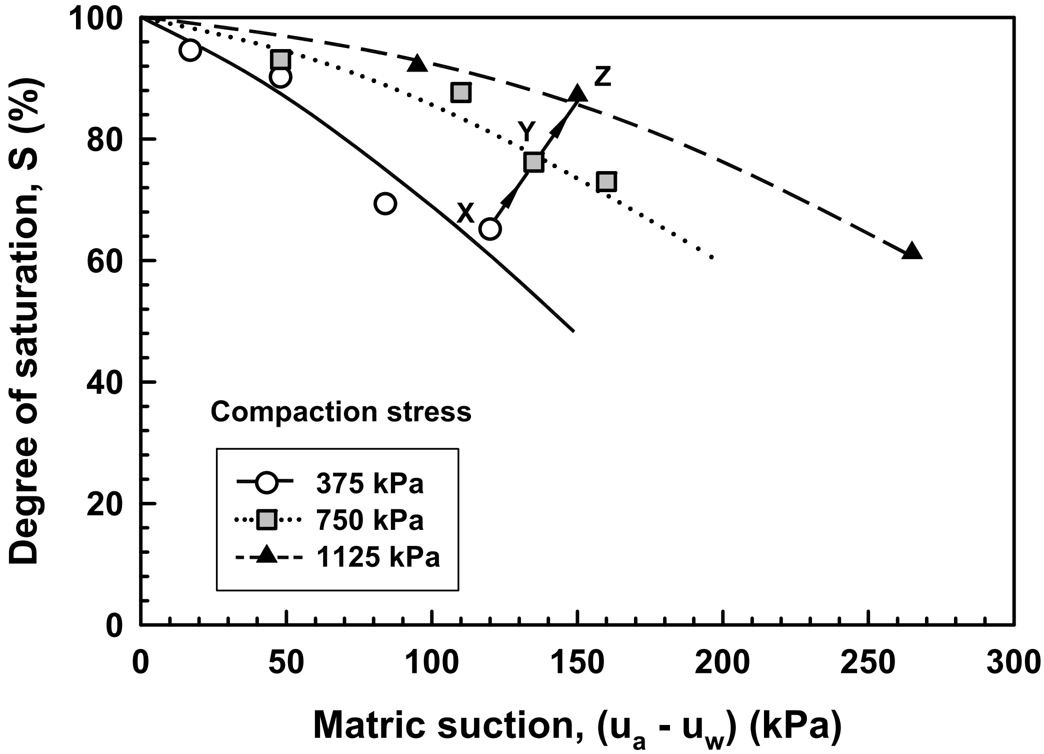

Figure 2.9 Relationship between degree of saturation and matric suction for different compaction stresses and the variation of degree of saturation and matric suction with respect to compaction stress for the specimens (*X*, *Y* and *Z*) compacted at the same water content (w = 14.8 %).

2.3.3 Relationship between PP_{cs} and Matric Suction

Figure 2.10 shows the relationship between the compression strength from the pocket penetrometer, PP_{cs} and matric suction for the soil specimens prepared with compaction stress of 375 kPa. The pocket penetrometer penetrated into the soil specimens by its own weight (or with low resistance) for the soil specimens compacted at higher water contents ($w \geq 24\%$; $S \approx 100$; Figure 2.11) since the matric suction values were close to 0 kPa with relatively low dry density. Hence, the PP_{cs} values corresponding to 0 kPa of matric suction were considered to be zero. The PP_{cs} for the specimen, A'' could not be plotted in Figure 2.10 since the value was beyond the maximum measurable capacity of the pocket penetrometer used (i.e. greater than 450 kPa). Based on the results shown in Figure 2.10, a relationship to estimate the matric suction of the as-compacted glacial till specimens is developed as shown in Eq. (2.1).

$$\left(u_a - u_w\right) = K \cdot PP_{cs} \tag{2.1}$$

where K is the slope of the matric suction versus PP_{cs} relationship, which is equal to 0.43 in the present study

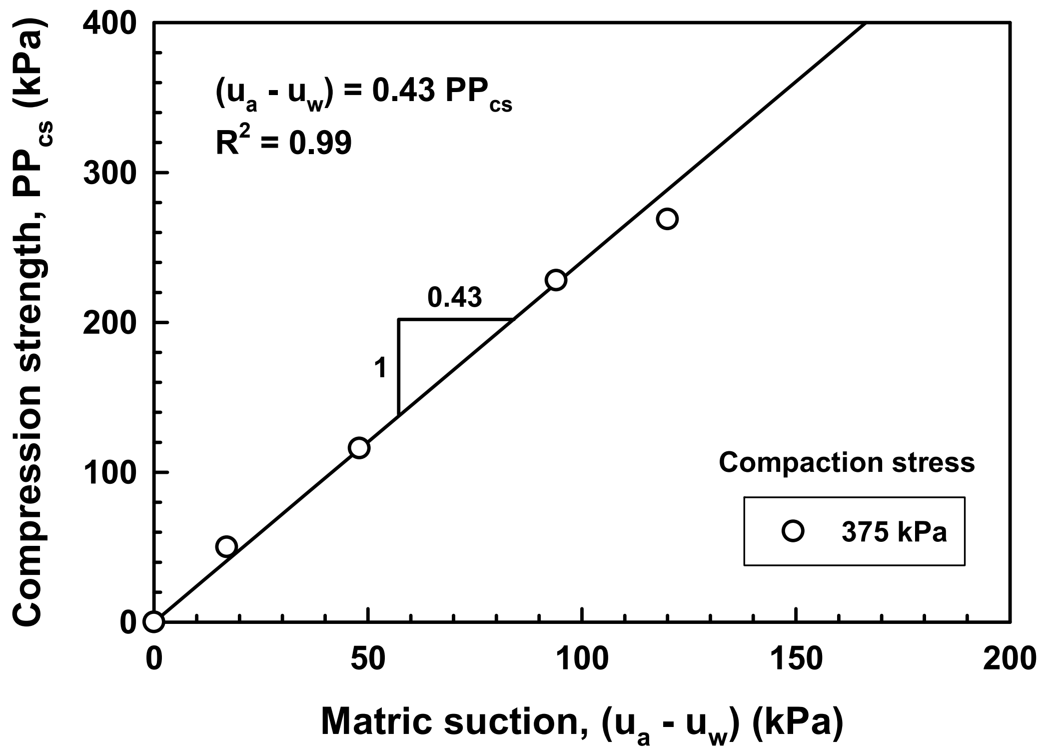

Figure 2.10 Relationship between compression strength from pocket penetrometer and matric suction for the soil specimens compacted under the stress of 375 kPa.

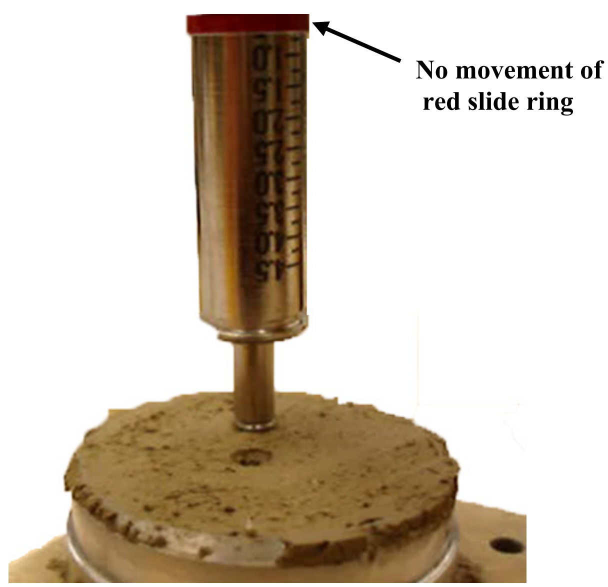

Figure 2.11 Pocket penetrometer test that shows zero resistance (i.e. no movement of red slide ring) for the specimen at the degree of saturation close to 100%.

2.3.4 Verification of the Proposed Technique

To check the validity of the proposed technique [i.e. Eq. (2.1)], comparisons are provided between the measured matric suction values using the axis-translation technique and those estimated using Eq. (2.1) for the soil specimens prepared with different compaction stresses (i.e. 750 and 1125 kPa). As can be seen in Figure 2.12, there is a reasonably good agreement between the measured and the estimated matric suction values.

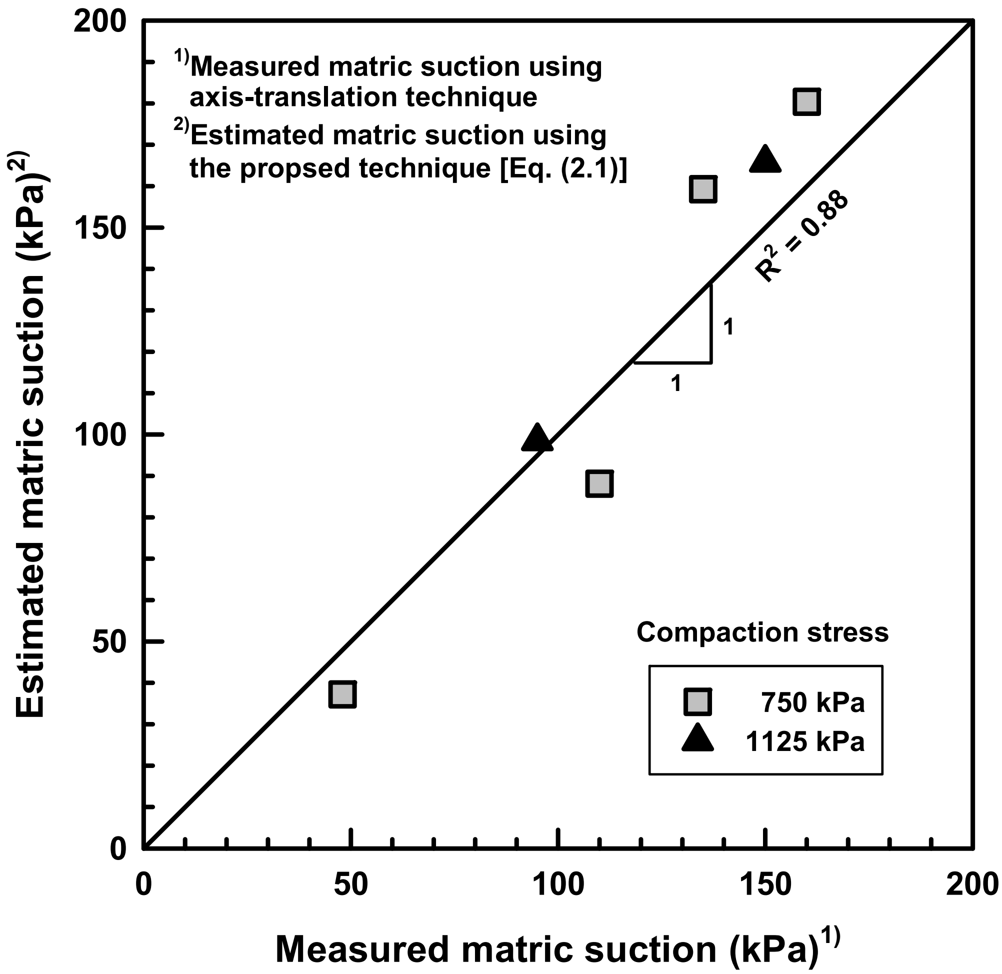

Figure 2.12 Comparison between the measured and the estimated matric suction values.

Figure 2.13(a), (b) and (c) show the unconfined compression test results for the specimens compacted with the compaction stress of 375 kPa, 750 kPa, and 1125 kPa, respectively.

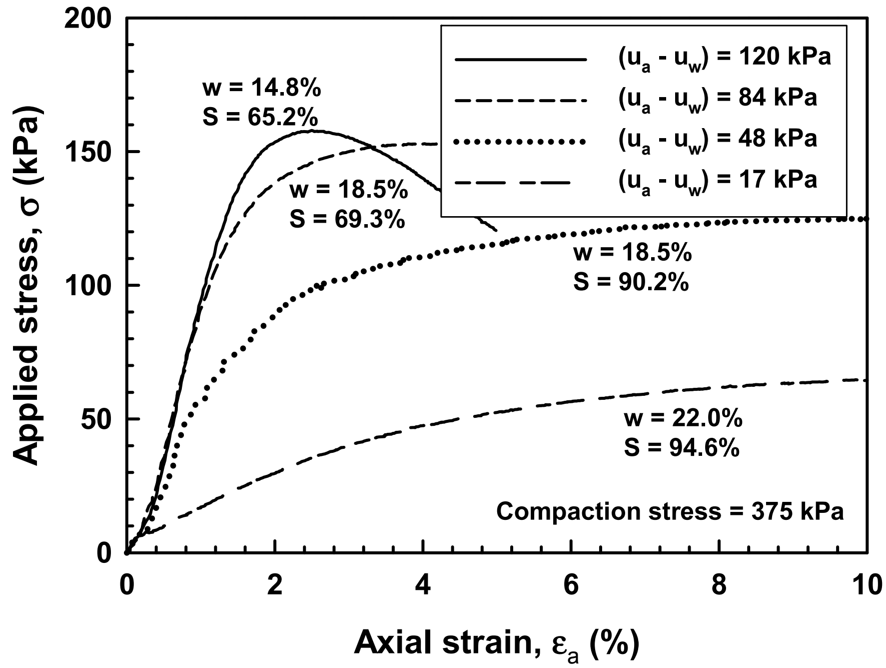

Figure 2.13(a) Unconfined compression test results for the soil specimens compacted with compaction stress of 375 kPa.

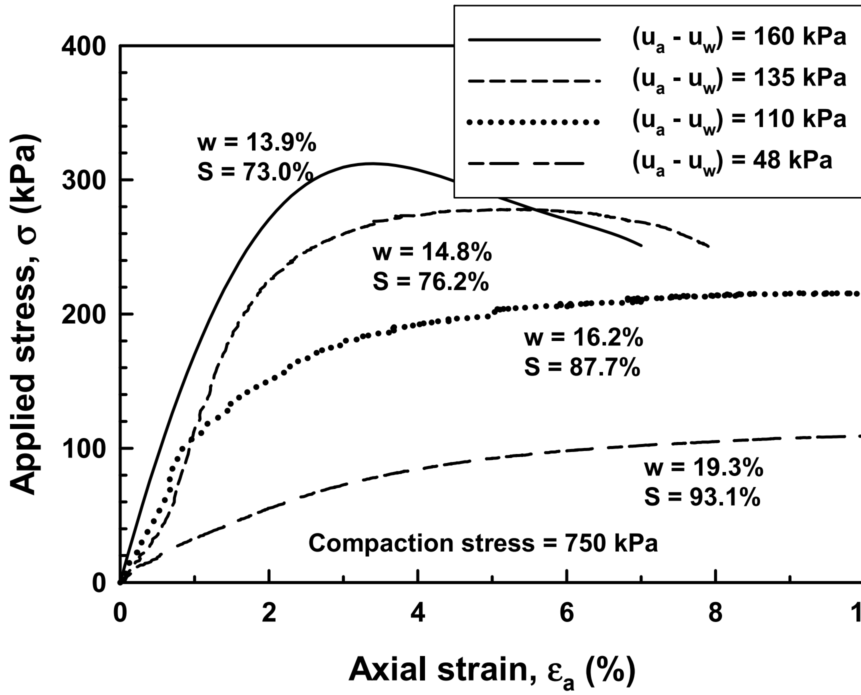

Figure 2.13(b) Unconfined compression test results for the soil specimens compacted with compaction stress of 750 kPa.

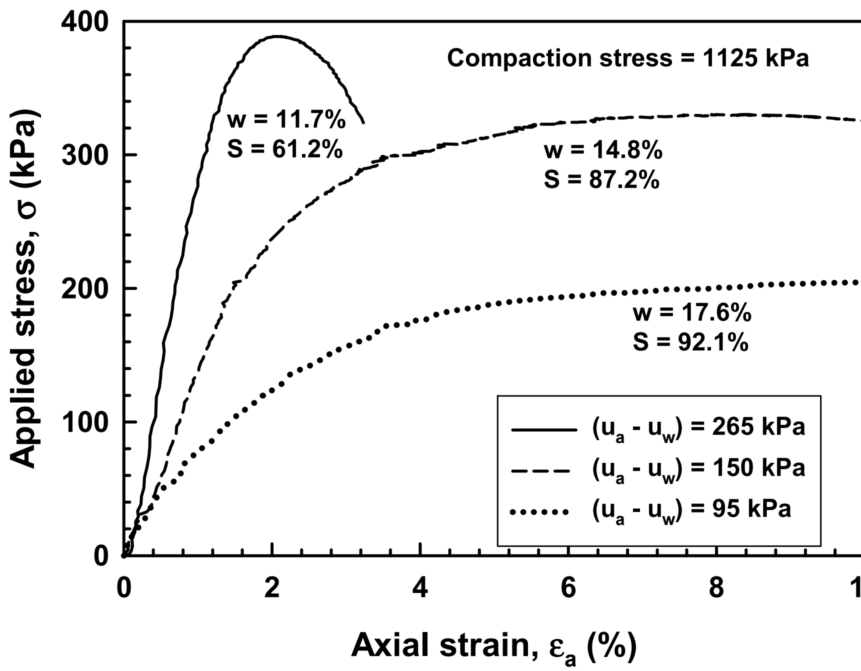

Figure 2.13(c) Unconfined compression test results for the soil specimens compacted with compaction stress of 1125 kPa.

Figure 2.14 shows the variation of unconfined compressive strength (i.e. q_u) and PP_{cs} with respect to matric suction. The unconfined compressive strength increases nonlinearly with increasing matric suction; similar trends are observed with respect to the shear strength behavior of unsaturated soils (Toll 1990, Vanapalli et al. 1996). However, the pocket penetrometer tests results show that the PP_{cs} values increases with a low degree of non-linearity for the matric suction values studied. Such a behavior may be attributed to the mechanism of soil deformation during the pocket penetrometer tests.

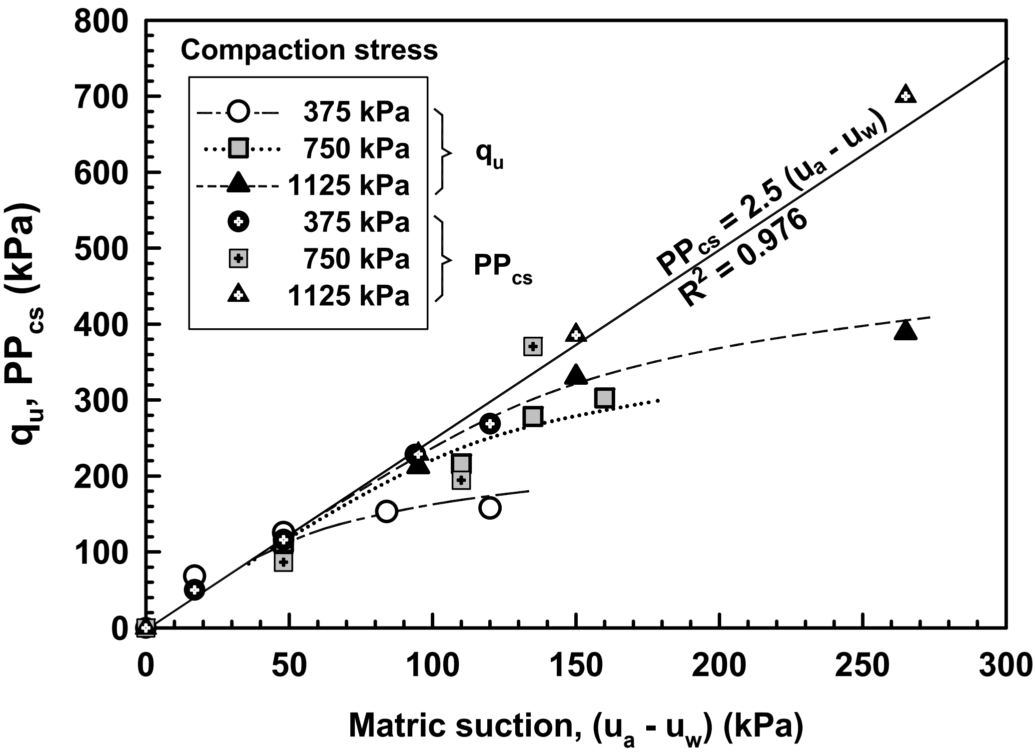

Figure 2.14 Variation of unconfined compressive strength and compression strength with respect to matric suction for the soil specimens compacted with different compaction stresses.

Unlike shear strength tests, the deformation of soil specimens during the penetration of the pocket penetrometer takes place only due to the compression of soils below the piston end of the pocket penetrometer without heave on the soil surfaces. This behavior is similar to that of punching failure in model footing or in-situ plate load (Schnaid et al. 1995, Consoli et al. 1998) tests in unsaturated fine-grained soils. The model footing ($B \times L$ = 50 mm × 50 mm) and unconfined compression test results conducted on statically compacted Indian Head till soil samples (details will be discussed in Chapter 3) also demonstrated similar trends as shown in Figure 2.15(a) and (b). In other words, the ultimate bearing capacity linearly increases with increasing matric suction, whereas the rate of increase in unconfined compressive strength with respect to the matric suction is nonlinear in nature. It can, therefore, be postulated that the decrease in the contribution of matric suction towards PP_{cs} with increasing matric suction can be negligible when compared to the shear strength tests.

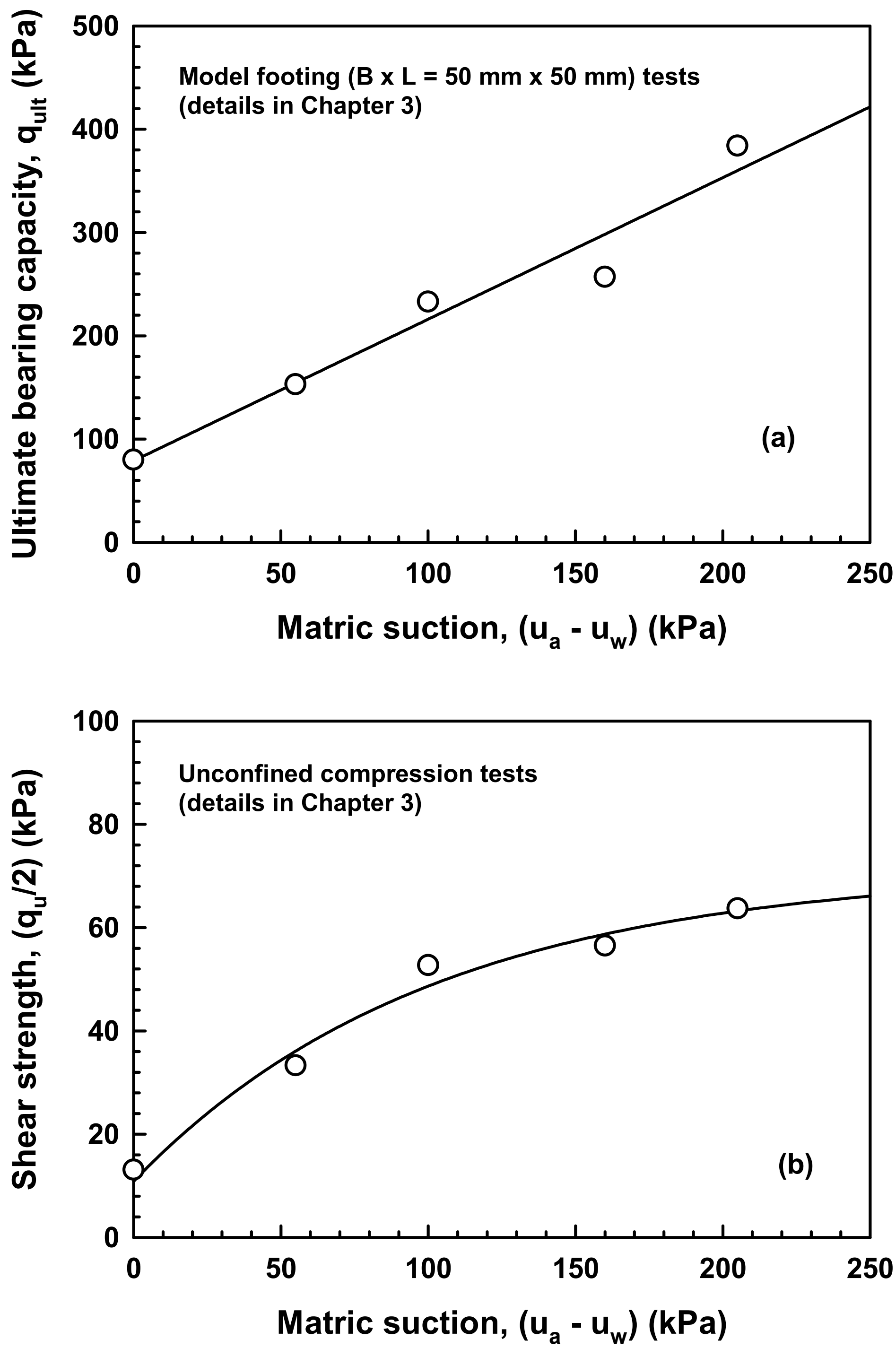

Figure 2.15 Variation of (a) ultimate bearing capacity and (b) unconfined compressive strength with respect to matric suction (details in Chapter 3).

Table 2.2 summarizes the compaction properties (i.e. water content, degree of saturation, matric suction, dry unit weight, and void ratio) of as-compacted soils along with pocket penetrometer and unconfined compression test results.

Table 2.2 Summary of compaction properties of as-compacted soil samples along with pocket penetrometer and unconfined compression test results.

Compaction stress (kPa)	w (%)	S (%)	$(u_a - u_w)$ (kPa)	γ_d (kN/m^3)	E	PP_{cs1} 1) (kPa)	PP_{cs2} 2) (kPa)	PP_{cs_ave} 3) (kPa)	q_u 4) (kPa)
375	16	69.3	84	16.2	0.63	233	223	228	153
	18.5	90.2	48	16.9	0.56	119	113	116	125
	22	94.6	17	16.2	0.64	50	50	50	68
	14.8	65.2	120	15.7	0.62	263	275	269	158
750	13.9	73.0	160	17.1	0.52	429	410	420	303
	16.2	87.7	110	17.8	0.50	179	210	205	216
	19.3	93.1	48	17.1	0.57	83	90	86.5	112
	14.8	76.2	135	17.5	0.53	371	370	370	278
1125	11.7	61.2	265	17.6	0.52				389
	14.8	87.2	150	18.3	0.46	400	371	385	330
	17.6	92.1	95	17.6	0.52	233	225	229	212

1) 2) PP_{cs1} and $P3P_{cs2}$: PP_{cs} for the two identical specimens
3) PP_{cs_ave}: average PP_{cs} [= $(PP_{cs1}+ PP_{cs2})/2$]
4) q_u: unconfined compressive strength

2.3.5 Influence of Hysteresis on Compression Strength from Pocket Penetrometer

Additional pocket penetrometer tests were conducted on the three specimens, *X*, *Y*, and *Z* (see Table 2.1 and Figure 2.3) to check the influence of hysteresis on the PP_{cs} results. Each test was carried out on two identical specimens. The compacted specimens were first allowed to imbibe distilled water for 2 days in a pressure plate apparatus for achieving saturation condition. During this process a large porous metal was placed on the compacted specimens to prevent any possible volume change in the compacted specimens (Figure 2.16).

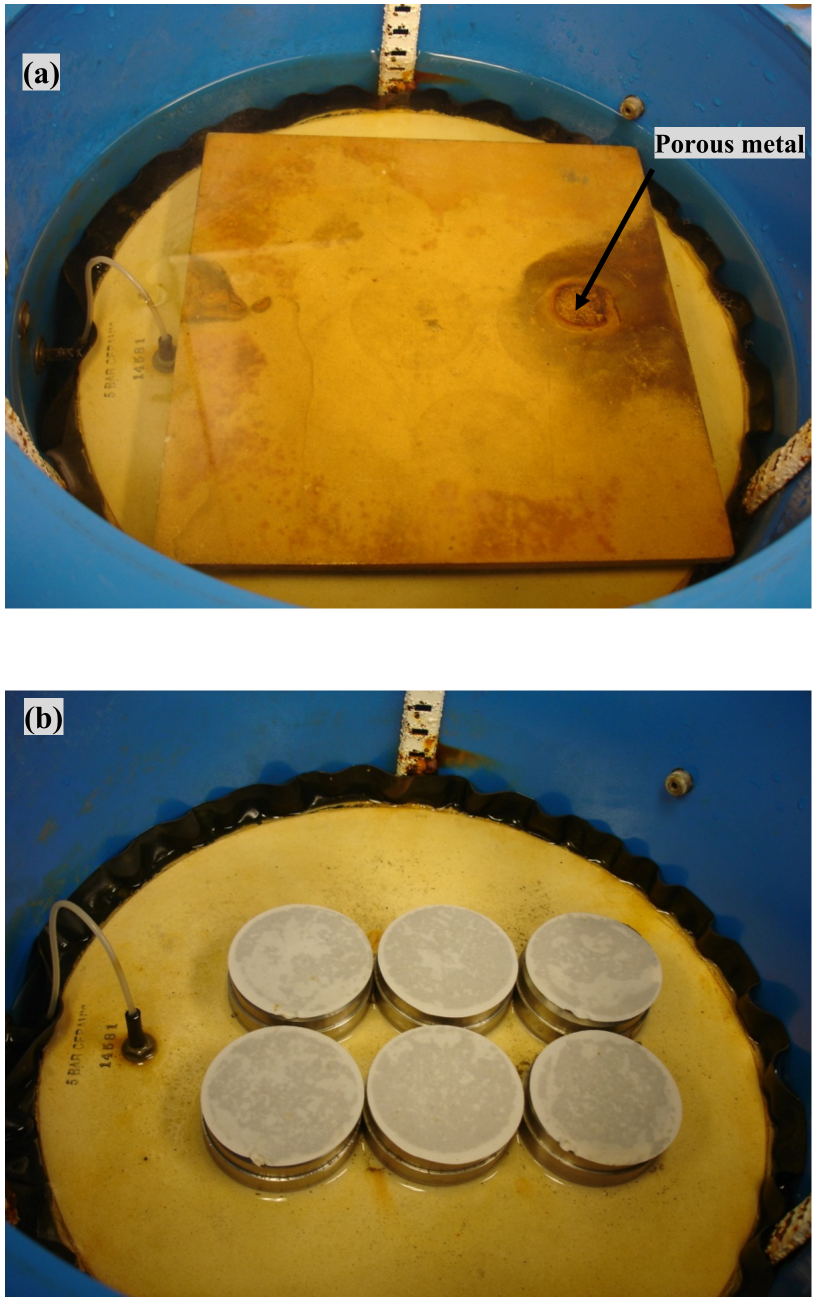

Figure 2.16 (a) Saturation process and (b) saturated specimens in a pressure plate apparatus.

The saturation of the specimens was verified using mass-volume relationship. The targeted air-pressure (i.e. 70 kPa) was then applied to the specimens using axis-translation technique. In other words, the matric suction value of the three specimens became the same with the value of 70 kPa at equilibrium conditions. The average PP_{cs} values for each specimen is plotted in Figure 2.17 (★) along with those of the as-compacted specimens. The PP_{cs} value for the specimen *Z* was estimated to be highest (180 kPa) followed by *Y* (163 kPa) and *X* (100 kPa).

This result indicates that the matric suction versus PP_{cs} relationship is influenced by wetting-drying process (i.e. hysteresis); however, the difference between the measured and the estimated PP_{cs} values for the specimen *X* (375 kPa) can be regarded to be experimental errors. The results also suggest that the influence of hysteresis reduces with increasing compaction stress.

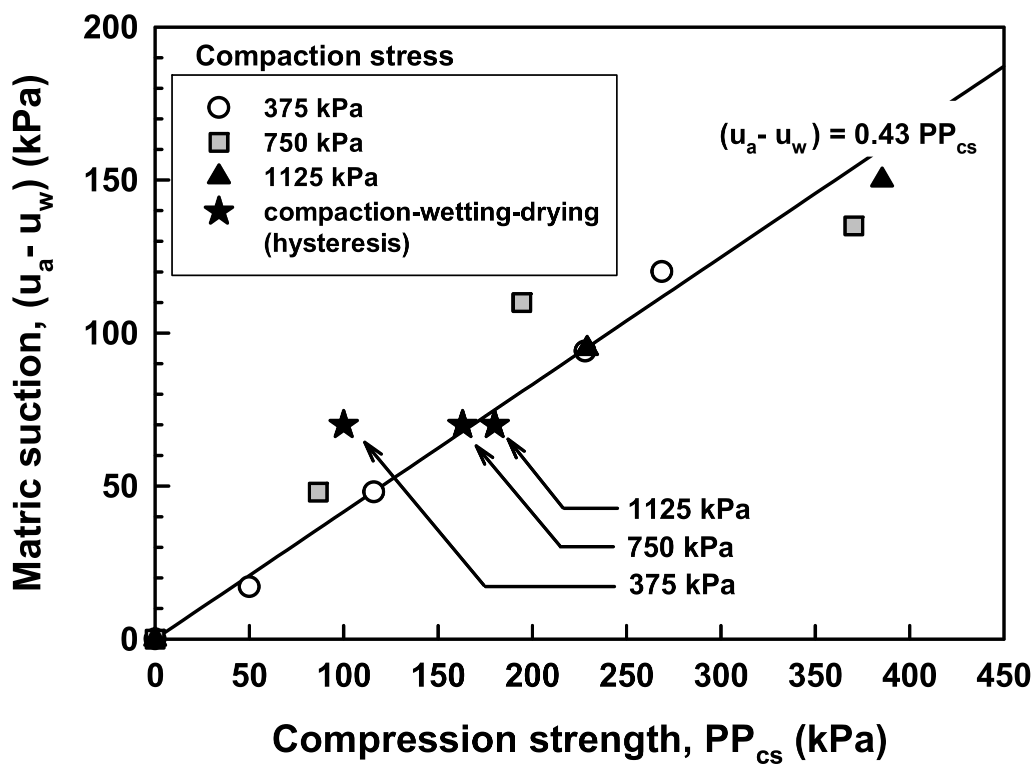

Figure 2.17 Influence of hysteresis (wetting-drying) on compression strength from the pocket penetrometer for the matric suction of 70 kPa along with the results for the as-compacted specimens.

2.4 Estimation of High Suction Value Using a Conventional Tensiometer

2.4.1 Hyperbolic Model

The two-constant hyperbolic model [Eq. (2.2); Figure 2.18] has been widely used in various geotechnical engineering fields such as stress-strain relationship (Kondner 1963, Duncan and Chang 1970) and ultimate settlement in field conditions (Kodandaramaswamy and Narasimha Rao 1980). According to Kondner (1963), hyperbolic relationship may not provide exact fit for entire range of non-linear experimental data. However, several studies have shown that initial tangent of typical hyperbolic relationship [i.e. Eq. (2.3)] can be reliably used to estimate ultimate value of non-linear relationship.

$$y = \frac{x}{a + bx} \tag{2.2}$$

$$\left(\frac{dy}{dx}\right)_{x=0} = \frac{1}{a} \tag{2.3}$$

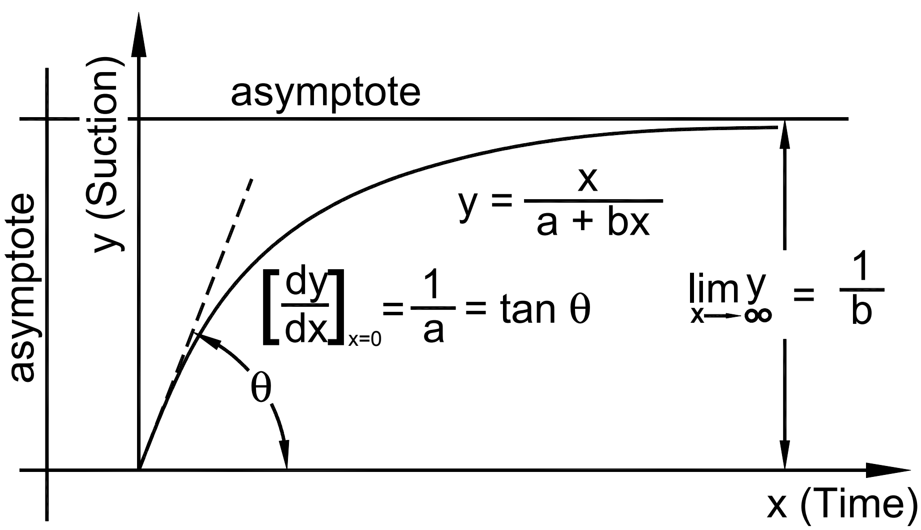

Figure 2.18 Typical hyperbolic relationship (Kondner 1963).

Figure 2.19 shows typical tensiometer response versus time behavior obtained using high capacity tensiometers (Ridley and Burland 1993, Guan and Fredlund 1997). Two key observations can be derived from these results; (i) the tensiometer response versus time behavior can be reasonably represented using the Kondner's (1963) hyperbolic model for entire range (i.e. from zero to equilibration suction value) and (ii) initial tangent of the tensiometer response versus time behavior (i.e. *1/a* in Figure 2.18) is dependent on the suction value of the unsaturated soils tested. This characteristic behavior implies that suction value of an unsaturated soil can be estimated by establishing the relationship between tensiometer response versus time behavior and equilibrium suction value. This approach can be indirectly supported by the studies provided by Oliveira and Marinho (2008). They suggested that the equilibration time (i.e. time at which suction readings are close to actual values) increases as the suction value increases. In other words, the tensiometer response versus time behavior can be used as a tool to estimate the equilibrium suction value of a specimen. The equilibration time was defined as a time at which the average rate of suction change over an interval of ten seconds is less than 0.0025(s^{-1}) from the tensiometer response versus time behaviors (Figure 2.20).

Extending this concept, in this chapter, a relationship between the equilibrium suction value and initial tangent of tensiometer response versus time behavior [i.e. $1/a$ in Eq. (2.3)] is developed using a conventional tensiometer. The tensiometer response versus time behaviors measured for a short period of time (typically less than 5 minutes) is required for studying the validity of the proposed assumption.

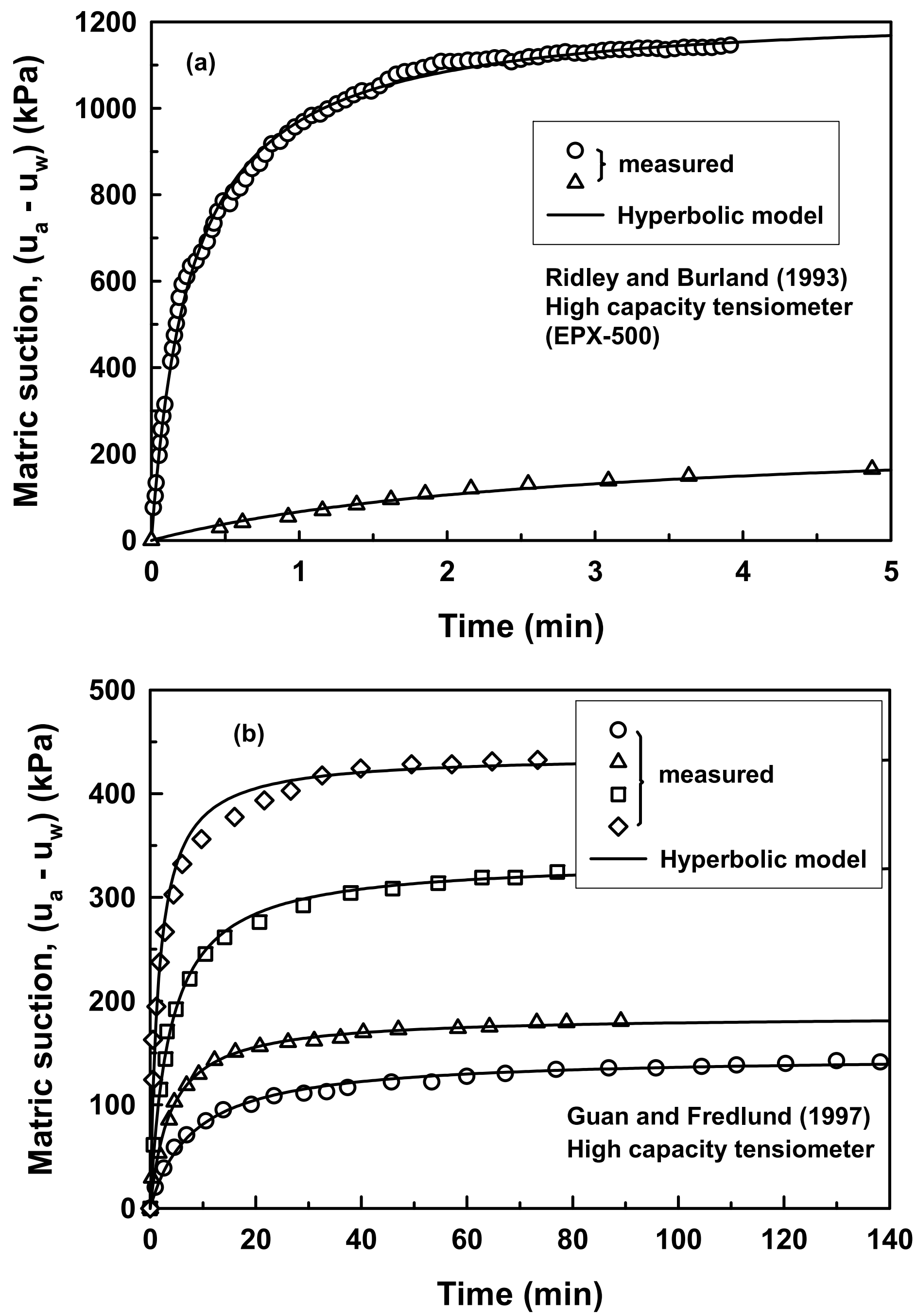

Figure 2.19 Comparison between the measured tensiometer response versus time behaviors and those estimated using hyperbolic model [data from (a) Ridley and Burland 1993 and (b) Guan and Fredlund (1997)].

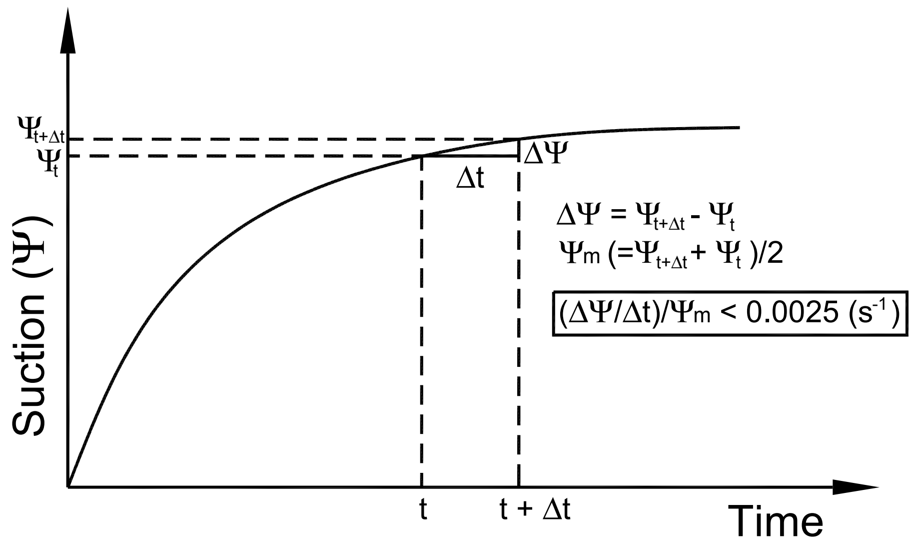

Figure 2.20 Illustrative diagram to define suction equilibration time measured with the high capacity tensiometer (Oliveira and Marinho 2008).

2.4.2 Sample Preparation for Conventional Tensiometer Tests

The Indian Head till samples for the conventional tensiometer tests were prepared using the accessories shown in Figure 2.21. Metal ring (i.e. 64 mm in diameter and 64 mm in height) was first placed on a metal plate and filled with soil-water mixtures. The compactor (assembly of compactor plate and compactor bar) was then placed on the surface of the soil-water mixtures and a load (i.e. equivalent to the compaction stress of 350 kPa) was applied on the compactor bar using a loading machine (Figure 2.22). After compaction, a thin-wall tube (i.e. 5 mm in outer diameter) was penetrated into the prepared compacted soil specimens (Figure 2.23) to make a cylindrical aperture (i.e. 5 mm in diameter and 9 mm in depth; Figure 2.24) in order to insert the ceramic cup of the conventional tensiometer (i.e. 5 mm in diameter and 7 mm in height; Figure 2.25). The tests were conducted for five different water contents (i.e. 3.6, 5.3, 7.0, 9.3, and 11.2 %).

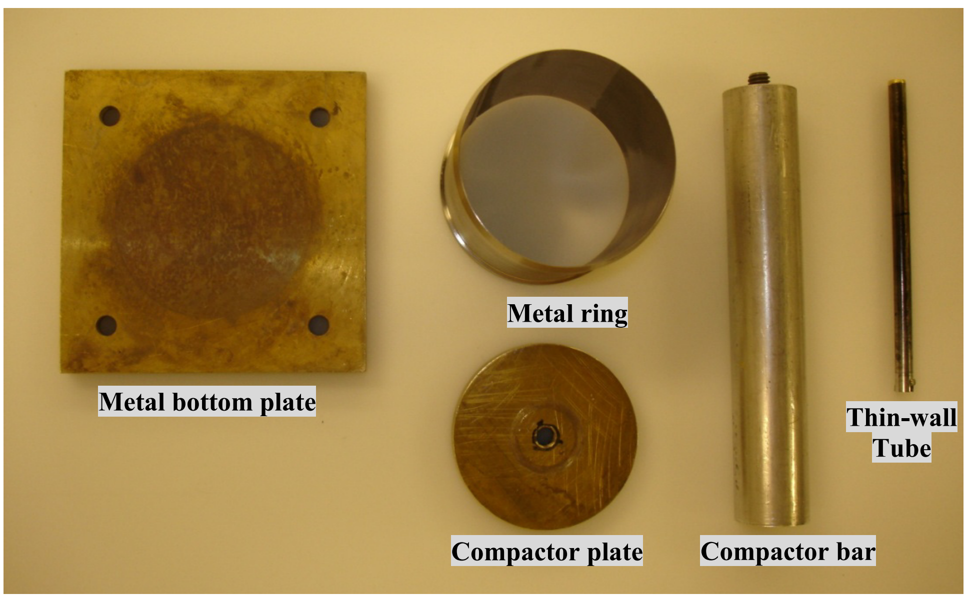

Figure 2.21 Accessories used to compact soil specimens for conventional tensiometer tests.

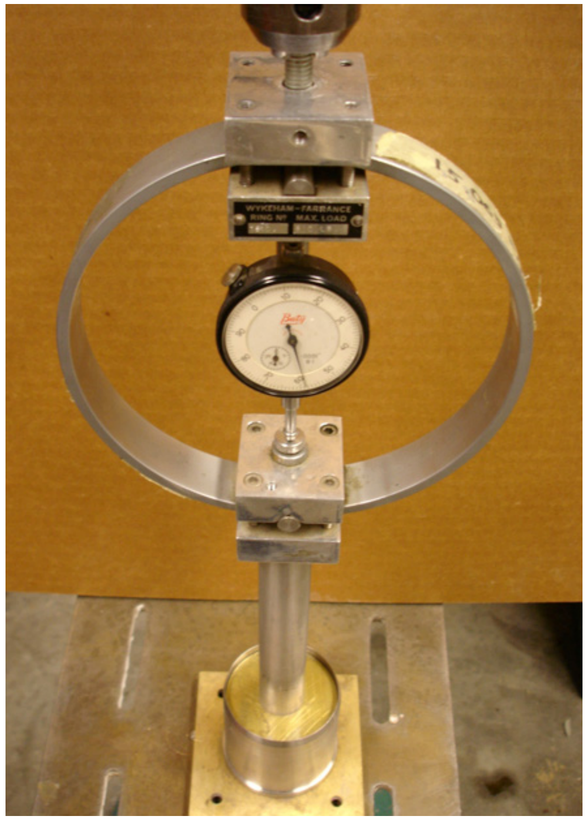

Figure 2.22 Static compaction of the soil-water mixtures.

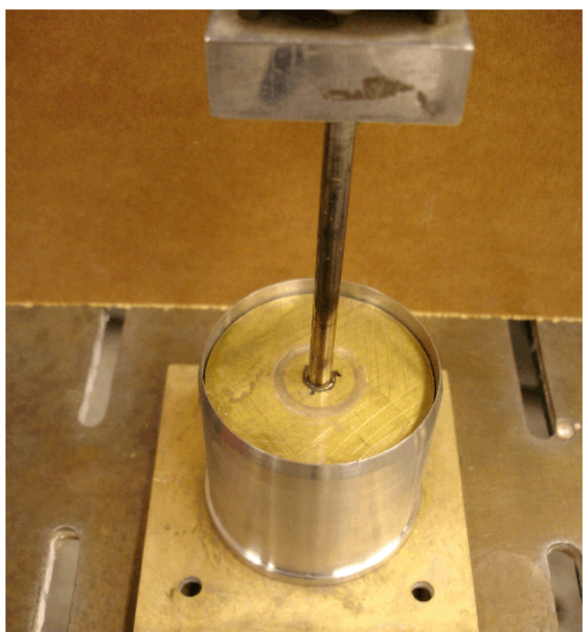

Figure 2.23 Penetration of a thin-wall tube into a prepared compacted soil specimen to make a cylindrical aperture.

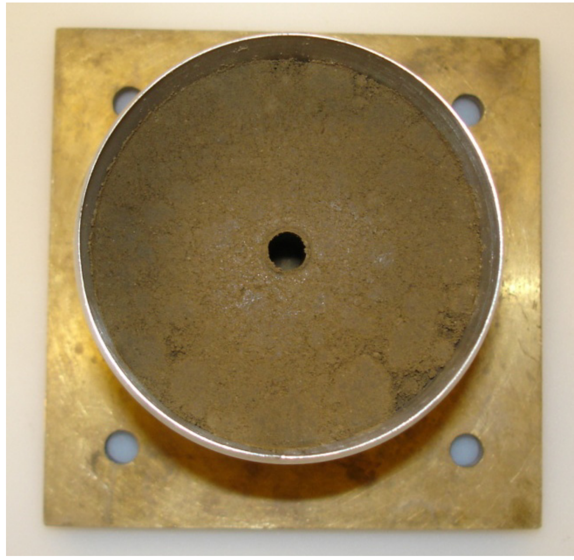

Figure 2.24 A cylindrical aperture in a compacted soil specimen to insert the ceramic cup of the conventional tensiometer.

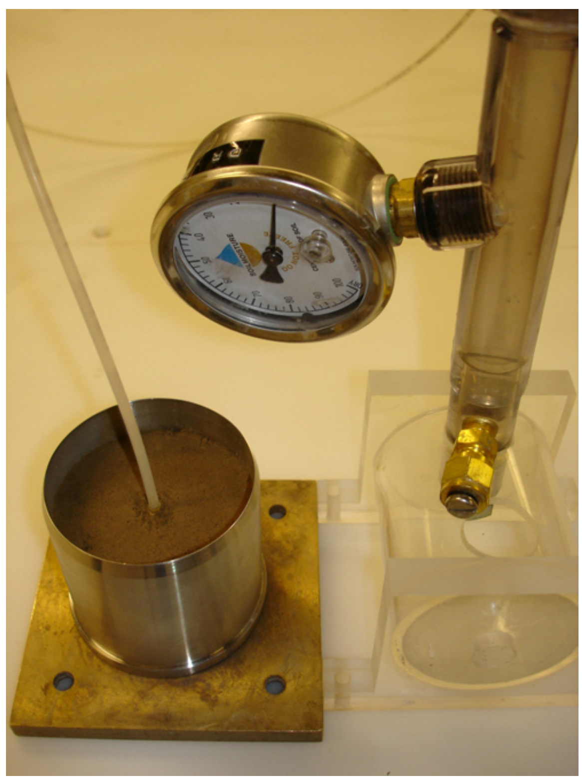

Figure 2.25 Measurement of conventional tensiometer response versus time behavior.

Take and Bolton (2003) showed that the measurements of suction values using tensiometers are significantly influenced by saturation effort of filter elements. However, in this study, the conventional tensiometer was used to measure *TRT* behaviors in the suction range of 0 to 50 kPa rather than equilibrium matric suction value of the specimens. In other words, the procedures of the ceramic tip saturation are not relevant to the proposed technique as long as the ceramic tip is saturated using consistent procedures. The variation of matric suction with time from the conventional tensiometer was videotaped using a video camera with the real-time function to improve the accuracy and reliability of the measurements (Figure 2.25).

After the tensiometer response versus time behavior in the suction range of 0 to 50 kPa or less was measured (typically for a time period of less than 5 min) a small piece of soil sample was removed from the compacted specimen used for testing. The specimen was placed in a test container (40 mm in diameter and 15 mm in height) and the equilibrium suction value was measured using a psychrometer (WP4-T; Figure 2.26). This instrument can measure water potential in less than 20 minutes (depending on soil type; Leong et al. 2003; Campbell et al. 2007) in the range of 0 to 300 MPa with an accuracy of ±0.1 MPa from 0 to 10 MPa and ±1% from 10 to 300 MPa (WP4-T Operator's Manual, Decagon Services, Inc.). The calibration curve for the WP4-T is shown in Figure 2.27.

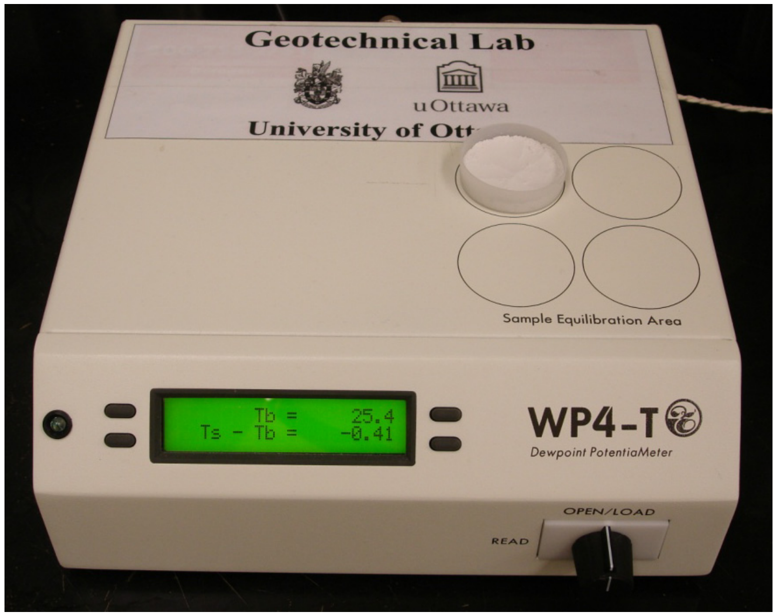

Figure 2.26 Psychrometer (WP4-T) used for high soil suction measurement in the research.

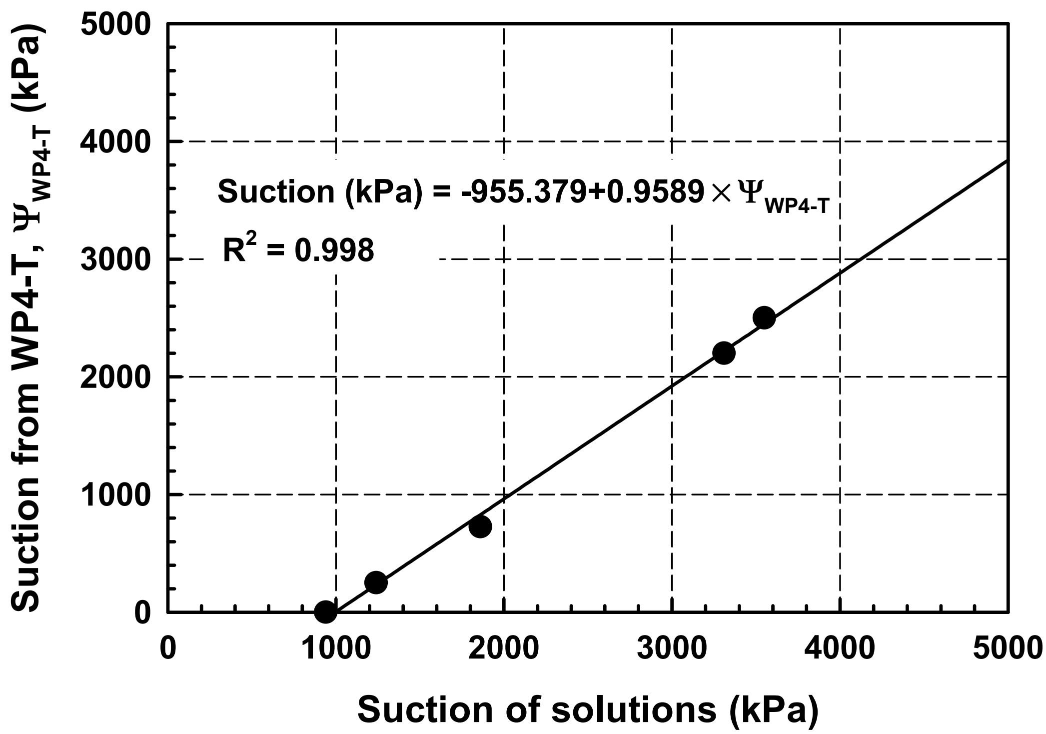

Figure 2.27 Calibration curve for the WP4-T used in the research.

2.4.3 Measured and Estimated Tensiometer Response versus Time Behaviors

The tensiometer response versus time behaviors in the matric suction range of 0 to 50 kPa for five different compaction water contents are shown in Figure 2.28 along with the equilibrium suction values (Ψ) measured using a psychrometer. The parameter, a of the best-fitting curve [i.e. hyperbolic model; Eq. (2.3)] for each suction value are summarized in Table 2.3. There are differences in the tensiometer response versus time behaviors between conventional tensiometers (i.e. Figure 2.28) and high capacity tensiometers (i.e. Figure 2.19). These differences are attributed to the following reasons: (i) conventional tensiometers are designed to measure the matric suction values less than 100 kPa and (ii) the response with time is dependent on the sensitivity of the vacuum gage and the type of water used in the study (i.e. de-aired water or distilled water).

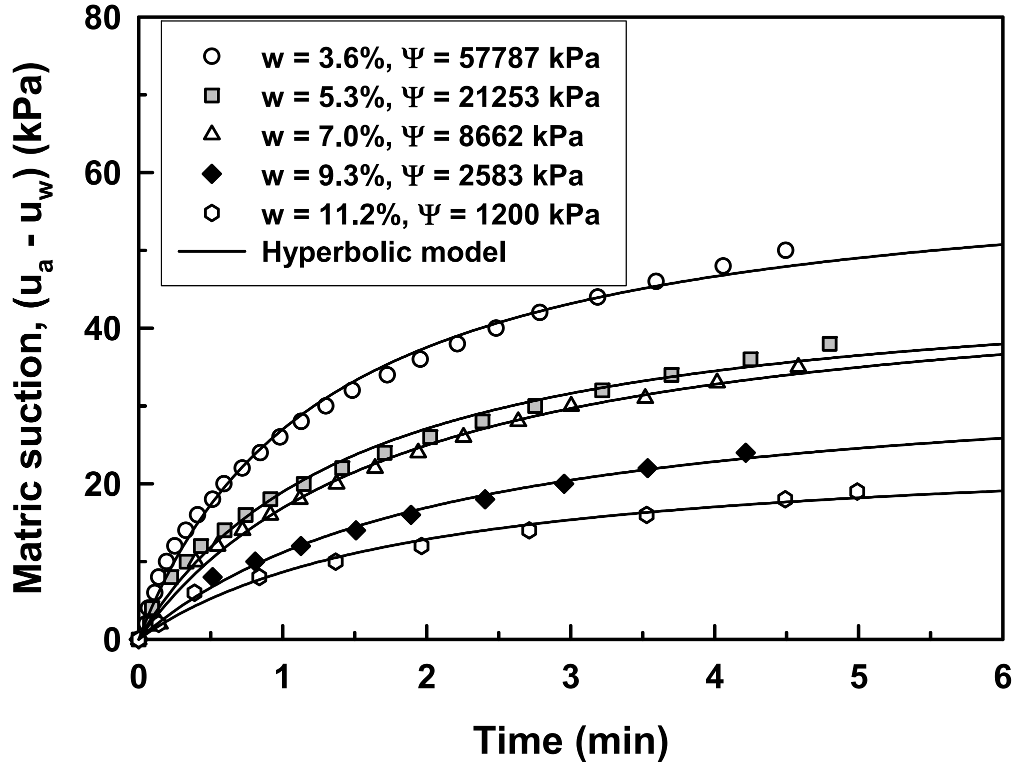

Figure 2.28 Conventional tensiometer response versus time behaviors for the specimens compacted at different water contents.

Table 2.3 Summary of the initial tangent of tensiometer response versus time behaviors (i.e. *1/a*) for each compaction water content (or suction).

Water content, *w* (%)	Suction, Ψ (kPa)	*a*	*1/a*
3.6	57,787	0.0208	48.08
5.3	21,253	0.0318	31.45
7.0	8,662	0.0384	26.04
9.3	2,583	0.0612	16.34
11.2	1,200	0.0795	12.58

Figure 2.29 shows the relationship between the soil suction and initial tangent of the tensiometer response versus time behaviors (i.e. *1/a*) on an arithmetic scale plot. The value of *1/a* was assumed to be equal to zero at saturated condition. The results show that the suction value starts rapidly increasing in the suction range of 1,200 and 2,583 kPa. The results in Figure 2.29 show a linear relationship [Eq. (2.4)] when plotted on a logarithmic scale (Figure 2.30) for the suction values studied in this study [i.e. $1{,}200 \leq \Psi$ (kPa) $\leq 60{,}000$]. The calibrated relationship summarized in Figure 2.30 is useful to estimate the equilibrium suction values (i.e. typically greater than 1500 kPa) of the compacted glacial till specimens tested with conventional tensiometer readings in the suction range of 0 to 50 kPa.

$$\Psi\,(\mathrm{kPa}) = 0.7771(1/a)^{2.9037} \tag{2.4}$$

The relationship for the suction values less than 1,200 kPa (which is influenced by the liquid phase flow for the glacial till studied in the research program) was not investigated since the measurement of suction using the psychrometer (i.e. WP4-T) in that range is not reliable (Bulut et al. 2002). The relationship in that range can be obtained by measuring suction values using high capacity tensiometers, the axis-translation technique or the proposed method in the present study (i.e. using high capacity pocket penetrometer) depending on the range of matric suction values.

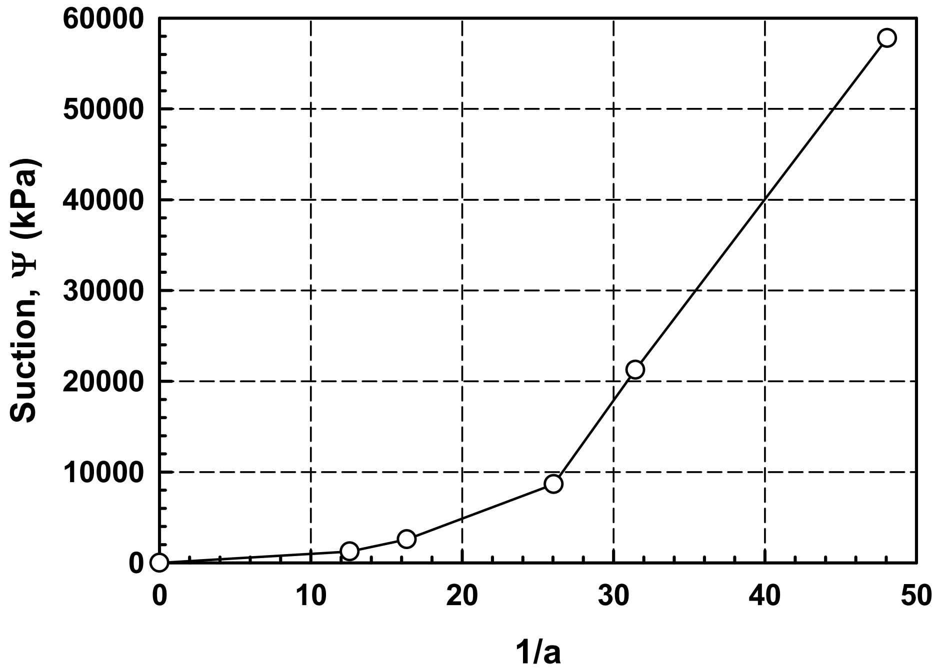

Figure 2.29 Relationship between suction and initial tangent of tensiometer response versus time behavior, 1/*a* (arithmetic scale plot).

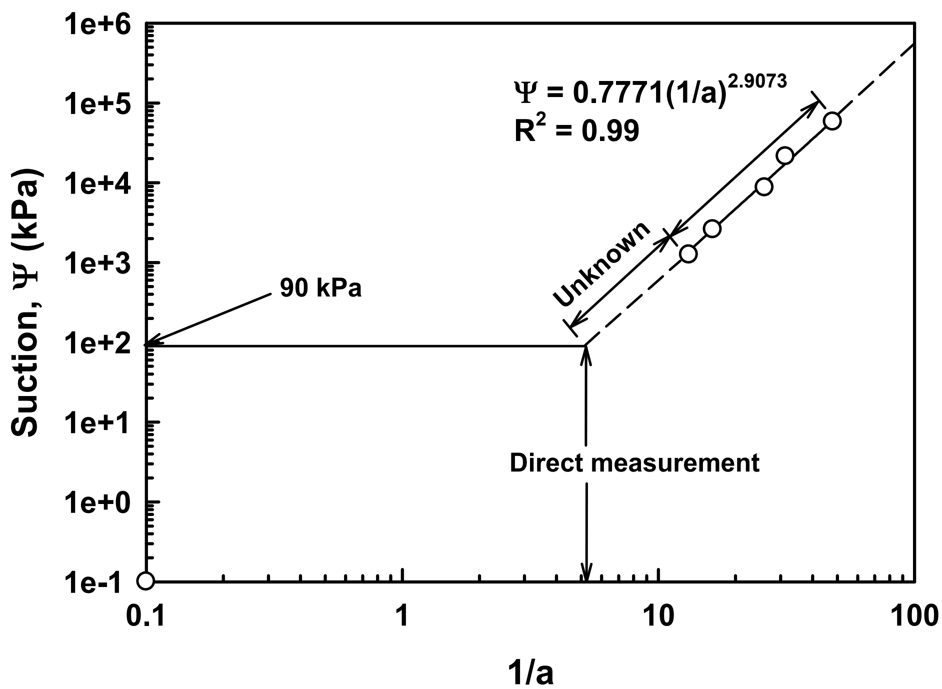

Figure 2.30 Relationship between suction and initial tangent of tensiometer response versus time behavior, 1/*a* (log scale plot).

2.4.4 Procedures Followed to Obtain the Tensiometer Response versus Time Behavior

The relationship in Eq. (2.4) is sensitive and can be influenced by conventional tensiometer used and the techniques followed in the measurement of suction. The procedure followed in the present study to measure the tensiometer response versus time behavior is summarized below;

(i) The ceramic cup of the conventional tensiometer was saturated by submerging it in distilled water for a period of 24 hrs.

(ii) The body of the tensiometer was filled using commercial distilled water. In this program, de-aired water was not used to avoid possible inconsistencies between lab and field conditions.

(iii) The service cap of the tensiometer should be securely tightened (Rahardjo and Leong 2006).

(iv) The tensiometer response versus time behavior can be influenced by the initial wetting condition of the surface of the ceramic cup (Ridley et al. 2003). Hence, the moisture on the surface of the tensiometer ceramic cup should be removed following standard protocols before the ceramic cup is driven into the specimen.

2.5 Summary and Conclusions

Soil suction is a key stress state variable that influences the engineering behavior of unsaturated soils. However, in spite of significant advances made in the interpretation of mechanical behavior of unsaturated soils, there are no simple instruments that are available to quickly measure soil suction in the laboratory or in the field. Rapid measurement of matric suction in many practical applications such as the assessment of pavement performance and the stability of embankment slopes would be of significant value.

In this chapter, two simple techniques are proposed to estimate the soil suction using pocket penetrometer and conventional tensiometer for low (0 to 300 kPa) and high (1,200 to 60,000 kPa) suction values, respectively. These techniques were developed and tested by conducting a series of laboratory tests on a glacial till (i.e. Indian Head till) specimens that were statically compacted at different water contents and compaction stresses.

The first technique is proposed using a pocket penetrometer for estimating low suction values based on the assumption that there is a strong relationship between the matric suction and compression strength measured using pocket penetrometer. The range of matric suction values that can be estimated using this technique is dependent on the capacity of pocket penetrometer used. The developed relationship between matric suction and compression strength from the pocket penetrometer [Eq. (2.1)] is only valid for the soil tested in this chapter.

The second technique is proposed using conventional tensiometer to measure high suction values based on the assumption that the tensiometer response versus time behavior can be reasonably represented using hyperbolic model (Kondner 1963) and the initial tangents of tensiometer response versus time behaviors are a function of the equilibrium suction values of the specimens. Once the initial tangent value (i.e. $1/a$) is determined based on the measured tensiometer response versus time behavior, suction value of an unsaturated soil can be estimated using the calibration curve shown in Eq. (2.4). The calibration curve is influenced by the conventional tensiometer used and the technical protocols followed for measuring tensiometer response versus time behaviors. Hence, it is recommended to standardize the protocols for obtaining reliable relationship between suction and (*1/a*).

There is a reasonably good comparison between the measured and the estimated suction values for both proposed techniques. The proposed techniques are promising and can be tested on different fine-grained compacted soils to develop generalized relationships as function of plasticity index [i.e. I_p versus K in Eq. (2.1)]. Such relationships will be valuable for the practicing engineers to estimate suction values of unsaturated soils easily.

REFERENCES

ASTM D 6169-98. 2005. Standard guide for selection of soil and rock sampling devices used with drill rigs for environmental investigation, *Annual Book of ASTM Standards*, ASTM International, West Conshohocken, PA.

ASTM D6836-02. 2008. Standard test methods for determination of the soil water characteristic curve for desorption using hanging column, pressure extractor, chilled mirror hygrometer, or centrifuge, Annual Book of ASTM Standards, ASTM International, West Conshohocken, PA.

Bulut, R., Hineidi, S.M. and Bailey, B. 2002. Suction measurements - filter paper and chilled mirror psychrometer. *In* Proceedings of the Texas Section American Society of Civil Engineers, Fall Meeting, Waco, Texas.

Campbell, G.S., Smith, D.M. and Teare, B.L. 2007. Application of a dew point method to obtain the soil water characteristic. Springer Proceedings in Physics, 112(2): 71-77.

Catana, M.C. 2006. Compaction and water retention characteristics of Champlain Sea clay. MASc Thesis, Civil Engineering Department, University of Ottawa, Ottawa, Canada.

Consoli, N.C., Schnaid, F. and Milititsky, J. 1998. Interpretation of plate load tests on residual soil site. *Journal of Geotechnical and Geoenvironmental Engineering*, 124(9): 857-867.

Decagon Services, Inc.WP4-T operator’s manual (Ver. 5). Washington, DC.

Duncan, J.M. and Chang, C.Y. 1970. Non-linear analysis of stress and strain in soils. *Journal of the Soil and Mechanics and Foundation Division*, ASCE, 96(SM5): 1655-1681.

González, N.A. and Colmenares, J.E. 2006. Influence of matric suction on the volume change behavior of a compacted clayey soil. *In* Proceedings of the 4th International Conference on Unsaturated Soils, Carefree, Arizona, ASCE, 825-836.

Guan, Y. and Fredlund, D.G. 1997. Use of tensile strength of water for the direct measurement of high soil suction. *Canadian Geotechnical Journal*, 34(4): 604-614.

Kodandaramaswamy, K. and Narasimha Rao, S. 1980. The prediction of settlements and heave in clay," *Canadian Geotechnical Journal*, 17(4): 623-631.

Kondner, R.L. 1963. Hyperbolic stress-strain response: cohesive soils. *Journal of the Soil and Mechanics and Foundation Division*, ASCE, 89(1): 115-143.

Leong, E.C., Tripathy, S. and Rahardjo, H. 2003. Total suction measurement of unsaturated soils with a device using the chilled-mirror dew-point technique. *Géotechnique*, 53(2): 173-182.

Oh, W.T. and Vanapalli, S.K. 2010. Influence of rain infiltration on the stability of compacted soil slopes. *Computers and Geotechnics*, 37(5): 649-657.

Oliveira, O.M. and Marinho, F.A.M. 2008. Suction equilibration time for a high capacity tensiometer. *Geotechnical Testing Journal*, 31(1): 101-105.

Power, K.C. and Vanapalli, S.K. 2010. Modified null pressure plate apparatus for measurement of matric suction. *Geotechnical Testing Journal*, 33(4).

Rahardjo, H. and E.C. Leong. 2006. Suction measurements. Keynote lecture. *In* Proceedings of 4th International Conference on Unsaturated Soils Conference. Geo Institute. Phoenix, Arizona, 81 – 104.

Ridley A.M. and Burland, J.B. 1993. A new instrument for the measurement of soil moisture suction. *Géotechnique*, 43(2): 321-324.

Ridley, A.M. and Burland J.B. 1995. Measurement of suction in materials which swell. *Applied Mechanics Reviews*, 48(9): 727-732.

Ridley, A.M., Dineen, L., Burland, J.B. and Vaughan, P.R. 2003. Soil matric suction: some examples of its measurement and application in geotechnical engineering. *Géotechnique*, 53(2): 241-253.

Schnaid, F., Consoli, N.C., Cumdani, R. and Milititsky, J. 1995. Load-settlement response of shallow foundations in structured unsaturated soils. *In* Proceedings of the 1st International Conference on Unsaturated Soils, Paris, 999-1004.

Stannard, D.I. 1990. Tensiometers - theory, construction, and use. *Groundwater and Vadose Zone Monitoring*, D.M. Neilson and A. I. Johnson (eds), ASTM STP 1053, 34-51.

Take, W.A. and Bolton, M.D. 2003. Tensiometer saturation and the reliable measurement of soil suction. *Géotechnique*, 53(2): 159-172.

Tarantino, A. and De Col, E. 2008. Compaction behavior of clay. *Géotechnique*, 58(3): 199-213.

Tarantino, A. and Mongiovì, L. 2003. Calibration of tensiometer for direct measurement of matric suction. *Géotechnique*, 53(1): 137-141.

Tarantino, A. and Tombolato, S. 2005. Coupling of hydraulic and mechanical behavior in unsaturated compacted clay. *Géotechnique*. 55(4): 307-317.

Toll, D.G. 1990. A frame work for unsaturated soil behavior. *Géotechnique*, 40(1): 31-44.

Vanapalli, S.K., Fredlund, D.G. and Pufahl, D.E. 1996. The relationship between the soil-water characteristic curve and the unsaturated shear strength of a compacted glacial till. *Geotechnical Testing Journal*, 19(3): 259-268.

Vanapalli, S.K., Fredlund, D.G. and Pufahl, D.E. 1999. Influence of soil structure and stress history on the soil-water characteristics of a compacted till. *Géotechnique*, 49(2): 143-159.

CHAPTER 3

BEARING CAPACITY OF UNSATURATED SOILS

3.1 Introduction

The bearing capacity of soils can be reliably determined using the vertically applied stress versus surface settlement behaviour from in-situ plate load test. In-situ plate load tests are commonly carried out on soils that are typically in a state of unsaturated condition. The influence of suction, however, is not considered in the interpretation of the bearing capacity from in-situ plate load tests.

Several researchers performed model footing (Steensen-Bach et al. 1987, Oloo 1994, Mohamed and Vanapalli 2006, Vanapalli and Mohamed 2007) and in-situ plate load tests (Consoli et al. 1998, Costa et al. 2003, Rojas et al. 2007) in unsaturated coarse- and fine-grained soils to study the influence of suction on the bearing capacity. The bearing capacity of saturated soils are conventionally estimated using either the effective stress approach (i.e. c' and ϕ'; Terzaghi 1943; hereafter referred to as *ESA*) or the total stress approach (i.e. $\phi_u = 0$; Skempton 1948; hereafter referred to as *TSA*) depending on the soil type and drainage condition. However, the bearing capacity of both coarse- and fine-grained soils are commonly estimated by extending Terzaghi (1943)'s effective stress approach considering the influence of suction (i.e. ϕ^b) regardless of soil type and drainage condition. The *ESA* can be extended to reliably estimate the bearing capacity of unsaturated coarse-grained soils since the drainage conditions for both the pore-air and the pore-water are under drained condition. However, this approach may not be applicable to the in-situ plate load tests in unsaturated fine-grained soils due to the following reasons. The in-situ plate load tests are generally conducted in accordance with ASTM D1194-94 (standard 1998). Typically, each load is applied (i) for a period of 15 minutes or greater or (ii) until the settlement has ceased or the rate of settlement meets standards guidelines. Due to this reason, there are uncertainties with respect to the drainage conditions of pore-air and pore-water while conducting the in-situ plate load tests in unsaturated fine-grained soils in comparison to unsaturated coarse-grained soils.

In this chapter, a series of model footing tests are conducted in a statically compacted unsaturated fine-grained soil to investigate the bearing capacity of unsaturated fine-grained soils. The results are interpreted using two different approaches introducing modifications to the conventional effective and total stress approaches (i.e. modified effective and total stress approaches). The validity of using modified total stress approach is also tested on in-situ plate load tests carried out in an unsaturated fine-grained soil. The advantages, disadvantages, and limitations of using the modified effective and total stress approach for geotechnical engineering practice applications are discussed. In addition, a semi-empirical model is also proposed to estimate the variation of bearing capacity of unsaturated fine-grained soils with respect to matric suction. Finally, a suggestion is made for interpreting the bearing capacity of low plastic unsaturated soils (i.e. $0 < I_p$ (%) < 8).

3.2 Estimation of Bearing Capacity of Unsaturated Fine-Grained Soils Extending Effective Stress Approach (ESA)

3.2.1 Effective Stress Approach using Reduced Shear Strength Parameters

Schnaid et al. (1995) and Consoli et al. (1998) conducted in-situ plate load tests in unsaturated fine-grained soils. The bearing capacity values were estimated using the *ESA* combined with reduction factors approach (i.e. punching shear failure) [Eq. (3.1) and Eq. (3.2)] without considering the influence of suction on the bearing capacity. There was a good agreement between the measured and the estimated bearing capacity values. However, discussing the results, they stated that the good agreement using the reduction factors approach was a '*surprising*' case. In other words, the reduction factors approach without considering the influence of suction may not be generalized for all types of unsaturated fine-grained soils and for different matric suction values.

$$c^* = 0.67c' \tag{3.1}$$

$$\tan \phi^* = 0.67 \tan \phi' \tag{3.2}$$

where c', ϕ' = effective cohesion and internal friction angle, and c^*, ϕ^* = modified effective cohesion and internal friction angle with respect to local (or punching) shear failure

3.2.2 Modified Effective Stress Approach

Oloo et al. (1997) proposed an equation [Eq. (3.3)] to estimate the bearing capacity of unsaturated fine-grained soils extending the Terzaghi (1943)'s *ESA* considering the influence of matric suction. In this chapter, modified equations for estimating the bearing capacity of unsaturated soils extending the *ESA* is termed as '*Modified Effective Stress Approach'* (hereafter referred to as *MESA*) to distinguish it from the conventional *ESA*.

$$q_{ult(unsat)} = \left\{ c' + (u_a - u_w) \tan \phi^b \right\} N_c \xi_c + \overline{q} N_q \xi_q + \frac{1}{2} B \gamma N_\gamma \xi_\gamma \tag{3.3}$$

where $q_{ult(unsat)}$ = ultimate bearing capacity of unsaturated soil, c' = effective cohesion, $(u_a - u_w)$ = matric suction, ϕ^b = internal friction angle due to the contribution of matric suction, N_c, N_q, N_γ = bearing capacity factors, ξ_c, ξ_q, ξ_γ = shape factors, $\overline{q}$ = overburden pressure, and B = width of footing.

Eq. (3.3) was developed based on the assumption that shear strength failure envelope of unsaturated soils is bilinear (Gan et al. 1988). Figure 3.1 shows the variation of bearing capacity with respect to matric suction based on bilinear behavior [curve (i)] and typical behaviors for coarse-grained [curve (ii); Mohamed and Vanapalli 2006] and fine-grained [curve (iii); Costa et al. 2003, Rojas et al. 2007, Leong et al. 2001] soils. In unsaturated coarse-grained soils, bearing capacity increases with increasing matric suction; however, it starts decreasing as matric suction approaches residual suction values. On the other hand, for unsaturated fine-grained soils, bearing capacity increases with increasing matric suction and then converges to a certain value at large suction value. Such behavior can be attributed to the increase in bonding between soil particles due to phenomena similar to cementation. The typical bearing capacity behavior for unsaturated coarse- and fine-grained soils indicates that interpreting the bearing capacity of unsaturated soils assuming bilinear behavior can lead to discrepancy between the measured and the estimated bearing capacity values for the matric suction values greater than air-entry value of soils.

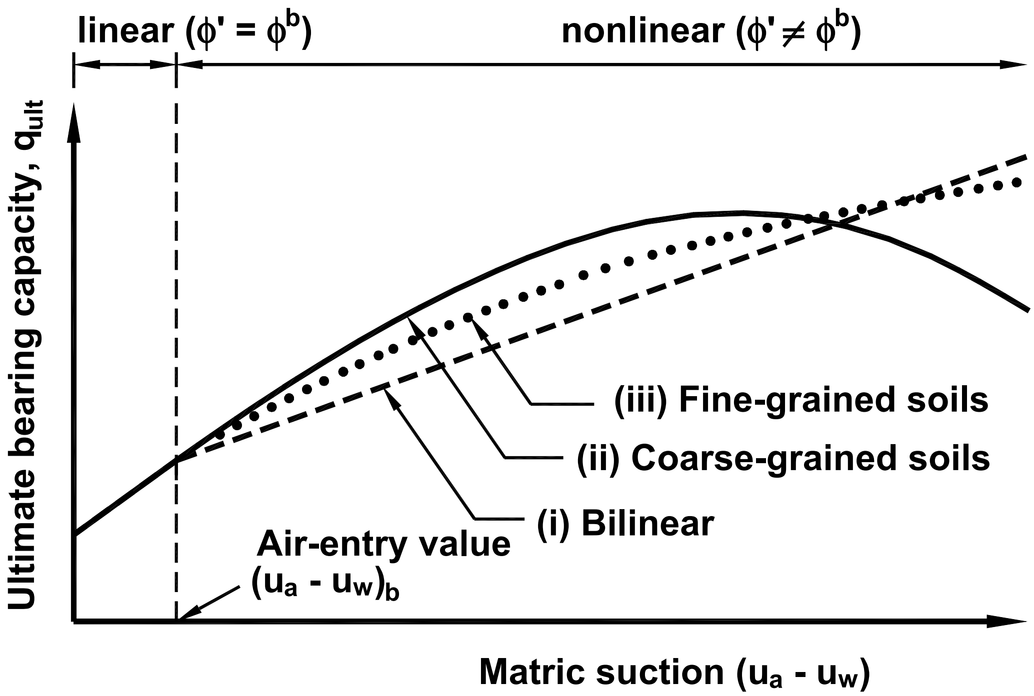

Figure 3.1 Variation of ultimate bearing capacity with respect to suction for different types of soils.

Several investigators proposed empirical or semi-empirical models to estimate the shear strength of unsaturated soils. In many of these models, the Soil-Water Characteristic Curve (*SWCC*) is used as a main tool. Eq. (3.4) shows semi-empirical model proposed by Vanapalli et al. (1996) and Fredlund et al. (1996) to estimate the variation of the shear strength with respect to matric suction. The relationship between suction and degree of saturated can be determined based on *SWCC*.

$$\tau_{unsat} = c' + (\sigma_n - u_a)\tan\phi' + (u_a - u_w)(S^{\kappa})(\tan\phi') \tag{3.4}$$

where τ_{unsat} = shear strength of unsaturated soil, c', ϕ' = effective cohesion and internal friction angle for saturated condition, $(\sigma_n - u_a)$ = net normal stress, $(u_a - u_w)$ = matric suction, S = degree of saturation, and κ = fitting parameter (i.e. function of plasticity index, I_p and $\kappa = 1$ for cohesionless soils; Garven and Vanapalli 2006)

Vanapalli et al. (1996) and Fredlund et al. (1996) provided mathematical relationship towards explaining the nonlinear variation of shear strength with respect to matric suction using the differential form of Eq. (3.4) [see Eq. (3.5)]. For matric suction values less than air-entry value, shear strength linearly increases since $S = 1$ and $[d(S^{\kappa})]/[d(u_a - u_w)] = 0$ (i.e. $\phi^b = \phi'$). The ϕ^b value then starts decreasing with further increase in matric suction value due to the decrease in degree of saturation and the term $[d(S^{\kappa})]/[d(u_a - u_w)]$ becomes negative. Finally, the ϕ^b value becomes close to zero when suction value is greater than residual suction value since both S and $[d(S^{\kappa})/d(u_a - u_w)]$ becomes close to zero) (Figure 3.2).

$$\begin{aligned} \tan\phi^b &= \frac{d\tau_{unsat}}{d(u_a - u_w)} \\ &= \left[(S^{\kappa}) + (u_a - u_w)\frac{d(S^{\kappa})}{d(u_a - u_w)}\right]\tan\phi' \end{aligned} \tag{3.5}$$

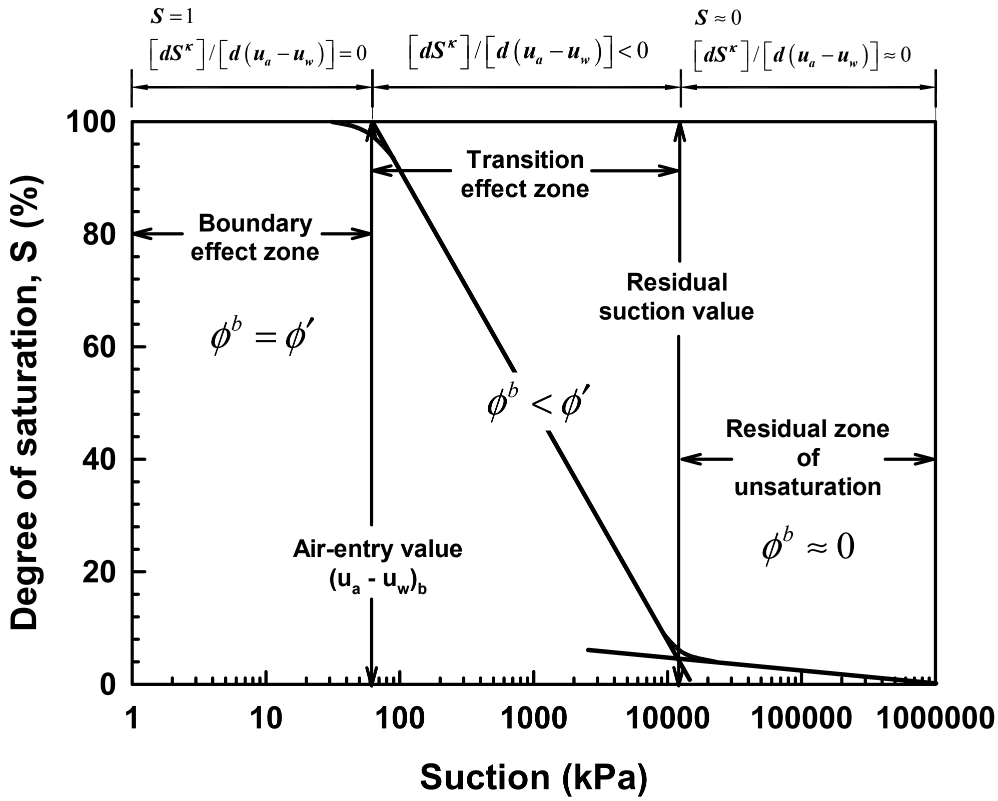

Figure 3.2 Variation of ϕ^b with respect to suction in three zones of *SWCC*.

This characteristic behavior shown in Figure 3.2 and Eq. (3.5) indicate that Eq. (3.4) can be effectively used to develop a model to estimate the bearing capacity of unsaturated soils since the shear strength behavior with respect to matric suction is similar to that of bearing capacity [i.e. Curve (ii) in Figure 3.1]. Extending this concept, Vanapalli and Mohamed (2007) proposed a model to estimate the variation of bearing capacity of surface footings on unsaturated coarse-grained soils with respect to matric suction based on the model footing test results in an unsaturated sand to overcome the disadvantage of Eq. (3.3) [see Eq.(3.6)]. This model uses the effective shear strength parameters for saturated condition (i.e. c' and ϕ') and the *SWCC* along with a fitting parameter, ψ.

$$q_{ult(unsat)} = \begin{bmatrix} c' + (u_a - u_w)_b \left(1 - S^{\psi} \tan\phi'\right) \\ + (u_a - u_w)_{AVR} S^{\psi} \tan\phi' \end{bmatrix} N_c \xi_c + 0.5 B\gamma N_\gamma \xi_\gamma \tag{3.6}$$

where $q_{ult(unsat)}$ = ultimate bearing capacity for unsaturated soils, c' and ϕ' = effective cohesion and internal friction angle, respectively, $(u_a - u_w)_b$ = air-entry value, $(u_a - u_w)_{AVR}$ = average matric suction value (This is discussed in greater detail in a later section), S = degree of saturation, γ = soil unit weight, ψ = fitting parameter with respect to bearing capacity (ψ = 1 for I_p = 0%), B = width of footing, N_c, N_γ = bearing capacity factor from Terzaghi(1943) and Kumbhokjar (1993), respectively, and $\xi_c \left\{ = \left[1.0 + \left(\frac{N_q}{N_c}\right)\left(\frac{B}{L}\right) \right] \right\}$, ξ_γ $\left\{ = \left[1.0 - 0.4\left(\frac{B}{L}\right) \right] \right\}$ = shape factors from Vesić (1973)

Vanapalli and Mohamed (2007) extended Eq. (3.6) to unsaturated fine-grained soils and suggested a relationship between ψ and I_p after analyzing five sets of data [i.e. three sands (Mohamed and Vanapalli 2006, Steensen-Bach et al. 1987] and silt and till (Oloo 1994) as below.

$$\psi = -0.0031(I_p)^2 + 0.3988(I_p) + 1 \tag{3.7}$$

However, Eq. (3.6) may not be applicable to the unsaturated fine-grained soils because, as discussed earlier, the bearing capacity of unsaturated fine-grained soils converges to a certain value when matric suction approaches residual state condition. In other words, the bearing capacity values estimated using Eq. (3.6) can be underestimated for the suction values greater than residual suction value.

3.3 Estimation of Bearing Capacity of Unsaturated Fine-Grained Soils extending Total Stress Approach (TSA)

3.3.1 Limitations of the ESA and MESA

The bearing capacity equation originally proposed by Terzaghi (1943) was developed based on drained loading condition assuming general shear failure criteria. This implies that it is reasonable to interpret the bearing capacity of unsaturated coarse-grained soils using the *MESA* since (i) both the pore-air and the pore-water in unsaturated coarse-grained soils are in drained condition during loading stages and (ii) the general failure can be expected for relatively high density coarse-grained soils (Vanapalli and Mohamed 2007). However, the drainage condition in unsaturated fine-grained soils during in-situ plate load tests cannot be clearly defined since each load on a plate is maintained for a short period or until the settlement has ceased or the rate of settlement becomes uniform. In addition, previous studies also showed that well defined general shear failure mode is not observed for model footing or in-situ plate load tests in unsaturated fine-grained soils from the stress versus settlement relationships (Oloo 1994, Schnaid et al. 1995, Consoli et al. 1998, Costa et al. 2003, Rojas et al. 2007). These observations contributed to proposing various approaches in interpreting the in-situ plate load tests in unsaturated fine-grained soils as below.

(i) reduction factors approach without considering the influence of suction (Schnaid et al. 1995, Consoli et al. 1998)
(ii) *MESA* using constant ϕ^b [Eq. (3.3)] (Oloo 1994, Costa et al. 2003)
(iii) *MESA* using non-linear variation of ϕ^b [Eq.(3.6)] (Vanapalli and Mohamed 2007)
(iv) *MESA* using non-linear variation of ϕ^b combined with reduction factors approach

3.3.2 Modified Total Stress Approach (MTSA)

The in-situ plate load tests results in unsaturated fine-grained soils show that the failure mechanism in unsaturated fine-grained soils below a shallow foundation is governed more by punching shear failure mode rather than general shear failure (Oloo 1994, Schnaid et al. 1995, Consoli et al. 1998, Costa et al. 2003, Rojas et al. 2007). For punching failure condition, (i) well defined failure is not observed from the stress versus settlement behavior, (ii) no heave is observed on the soils outside the loaded areas, and (iii) the vertical displacement of a footing is caused mainly by the compression of the soil directly below the footing as well as the vertical shearing of the soil around the footing perimeter (Vesić 1963, 1973). This characteristic behavior can be simplified as Figure 3.3. Yamamoto et al. (2008) proposed a model to predict the bearing capacity of compressible sand based on the fact that there is quasi-linear relationship between applied stress and settlement (up to 10% of the diameter of footing). Their study suggests that the bearing capacity of sand (i.e. coarse-grained soil) can also be governed by its compressibility during loading stages.

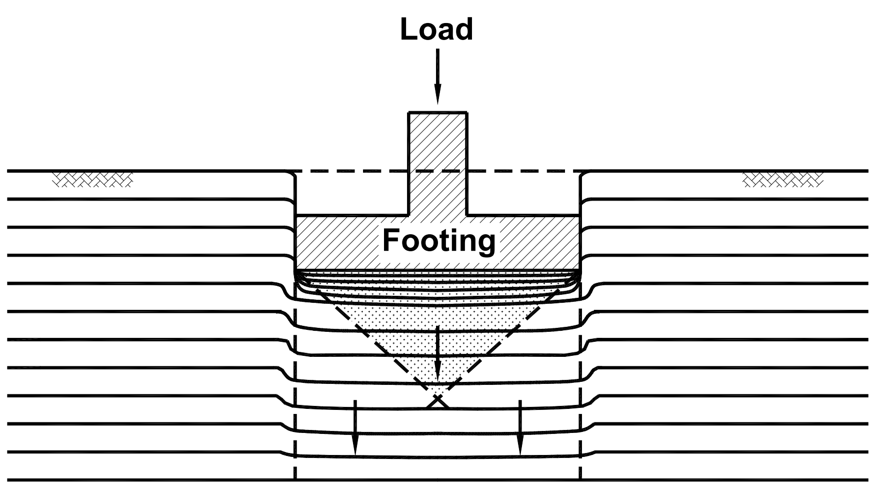

Figure 3.3 Punching shear failure mechanism in unsaturated fine-grained soils below a footing.

If it is assumed that the bearing capacity of unsaturated fine-grained soils is more dependent on the compressibility characteristics of the soil below a footing, the constant water content test can be regarded as the most reasonable test method to simulate the loading and the drainage condition for the unsaturated fine-grained soils. However, the constant water content test is time-consuming and requires elaborate equipment (Rahardjo et al. 2004). Due to this reason, in this research, unconfined compression tests results for the unsaturated fine-grained soil were used to estimate the bearing capacity of unsaturated fine-grained soils extending the conventional *TSA*. This can be justified based on the following facts and reasonable assumptions summarized below:

(i) The drainage conditions for both the constant water content and unconfined compression tests are similar.

(ii) The shear strength obtained from the unconfined compression tests typically provides conservative estimates due to the zero confining pressure.

The above discussion implies that the bearing capacity of a surface footing on unsaturated fine-grained soils can be represented as Eq. (3.8). It is of interest to note that the form of Eq. (3.8) is the same as Skempton (1948)'s equation for interpreting the bearing capacity of saturated fine-grained soils assuming undrained conditions.

$$q_{ult(unsat)} = s_{unsat} \times \xi_{c(unsat)} \times N_{c(unsat)} \tag{3.8}$$

where $q_{ult(unsat)}$ = ultimate bearing capacity of an unsaturated fine-grained, s_{unsat} = shear strength of an unsaturated fine-grained soil based on unconfined compressive strength, ξ_{unsat} = shape factor, $N_{c(unsat)}$ = bearing capacity factor, and subscript unsat = unsaturated condition

In this case, soil suction measurement is not required since the influence of soil suction on the compressive strength is included in s_{unsat} [Eq. (3.9)].

$$s_{(unsat)} = \left[s_{(sat)} + f\left(u_a - u_w\right) \right] = \left(\frac{q_{u(unsat)}}{2} \right) \tag{3.9}$$

where $s_{(unsat)}$ = shear strength of an unsaturated fine-grained soil based on unconfined compression test, $f(u_a - u_w)$ = increment of strength due to suction, $q_{u(unsat)}$ = unconfined compressive strength for an unsaturated fine-grained soil

Substituting Eq. (3.9) into Eq. (3.8) yields

$$q_{ult(unsat)} = \left[\frac{q_{u(unsat)}}{2} \right] \left[1 + 0.2\left(\frac{B}{L} \right) \right] N_{unsast} \tag{3.10}$$

The shape factor, $\xi_{c(unsat)}$ = [1+0.2(B/L)] (B = width, L = length) proposed by Meyerhof (1963) and Vesić (1973) for undrained condition is used in this study. Eq. (3.10) shows that the bearing capacity of unsaturated fine-grained soils can be simply estimated using the unconfined compressive strength of unsaturated fine-grained soils. The *TSA* such as Eq. (3.10) that were modified for estimating the bearing capacity of unsaturated fine-grained soils are termed as '*Modified Total Stress Approach'* (*MTSA*) to distinguish it from the conventional total stress approach (*TSA*) for saturated soils

3.4 Model Footing Tests in an Unsaturated Fine-Grained Soils

In this section, details of the model footing test results are provided to examine the validity of Eq. (3.10) (i.e. *MTSA*) and to determine the bearing capacity factor $N_{c(unsat)}$ for unsaturated fine-grained soils.

3.4.1 Modeling Footing Test Equipment

Model footing (50 mm × 50 mm) tests were conducted in a cylindrical high strength plastic tank (300 mm in diameter × 300 mm in height × 12.7 mm in thickness; hereafter referred to as plastic tank) on a statically compacted fine-grained soil (i.e. Indian Head till). The plastic tank was chosen because it is lighter compared to a steel tank and easy to handle during the experimental program. Three clamps were wrapped around the plastic tank to eliminate possible strain on the plastic tank during compaction of the sample and while conducting the model footing tests. Preliminary tests with two strain gauges installed on the outer surface of the plastic tank confirmed no strain during compaction and model footing tests. Three holes were drilled in the plastic tank to place conventional Tensiometers for monitoring the variation of the matric suction with depth in the compacted soil. A metal plate was attached at the top edge of the plastic tank to place a linear variable differential transformer (*LVDT*) and measure the displacement of the footing during loading. The soil in the plastic tank was statically compacted using a specially designed compactor that consists of two concentric circular plates placed on each other and a solid aluminum cylindrical bar. Four holes were drilled through the larger circular plate to allow drainage (Figure 3.4). The ratio of the diameter, D of the plastic tank to the width, *B* of footing (i.e. *D*/*B* = 6) was determined according to the previous studies as summarized in Table 3.1.

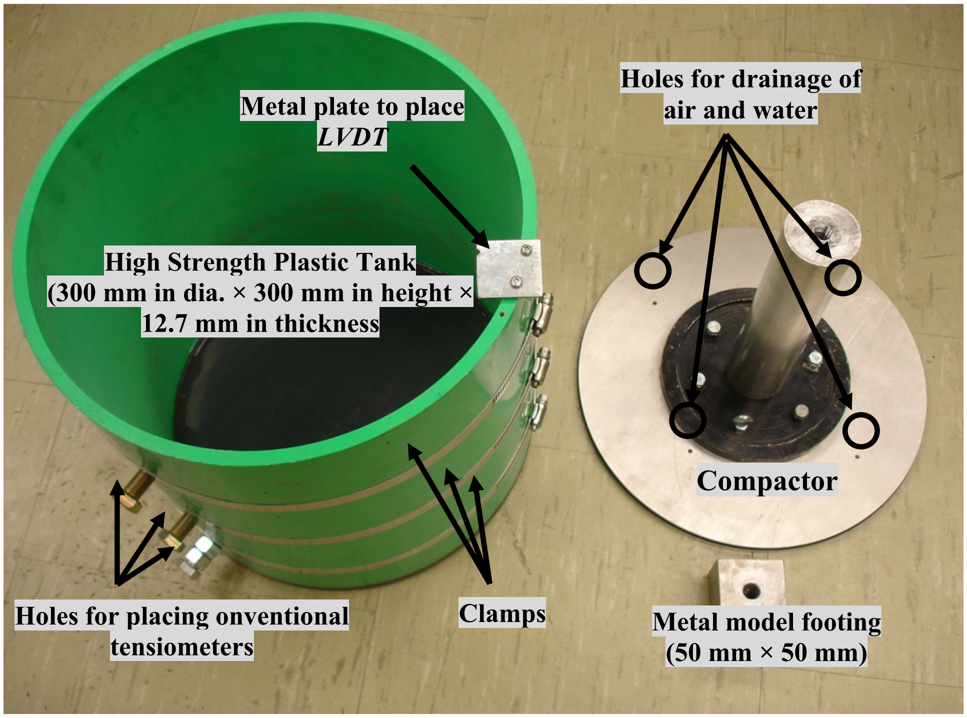

Figure 3.4 Equipments used in the study for conducting model footing tests.

Table 3.1 Summary of the ratio of the width of model footing test box to the footing size from the studies in the literature.

Box size (mm) ($W' \times L' \times H'$) [1)]	Footing size (mm) ($B \times L$) [2)] or D [3)]	Ratio $W'/(B \text{ or } D)$	Reference
5400×6900×6000	910	5.93	Adams and Collin (1997)
1000×1000×1250	160	6.25	Hanna and Abdel-Rahman (1998)
900×900×600	150	6.00	Dash et al. (2003)
600×600×400	100×100	6.00	Bera et al. (2007)

[1)] W', L', H' = width, length, and height of a model footing test box
[2)] B, L = width and length of rectangular footing
[3)] D = diameter of a circular footing

3.4.2 Sample Preparation

The same soil (i.e. Indian Head till) used in Chapter 2 was used in this chapter. Figure 3.5 shows the compaction curve for the static compaction stress of 350 kPa. Theoretically, the maximum dry density for the compaction stress of 350 kPa should be less than that of 350 kPa (one of the stresses used for the pocket penetrometer in Chapter 2). However, the maximum dry density of the soil compacted in the plastic tank (i.e. 17.3 kN/m^3 at 350 kPa) was higher than that compacted in the metal ring (i.e. 16.9 kN/m^3 at 350 kPa). This can be attributed to the difference (1) in the size of the compacted samples and (ii) grain distribution that was caused during the process of recycling the Indian Head till. From Figure 3.5, the compaction water content, w = 13.2% (γ_d = 15 kN/m^3) representing dry of optimum condition was chosen for compacting the soil and conducting the model footing tests as it is relatively easier to achieve uniform conditions and also relatively quicker to saturate the specimen.

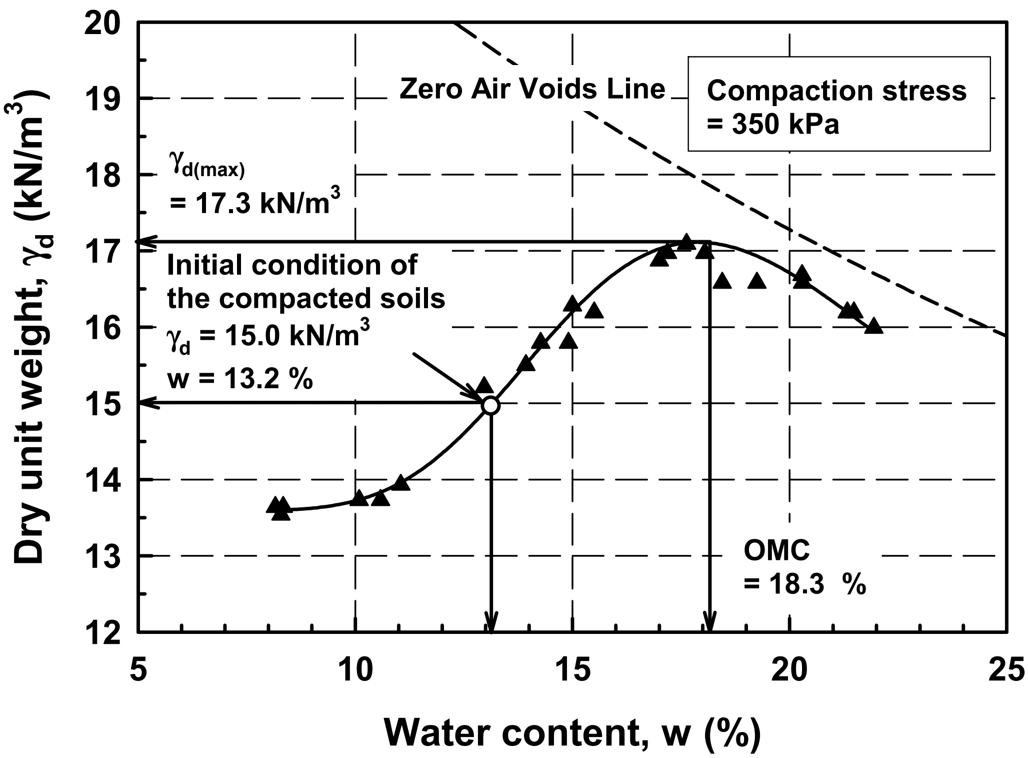

Figure 3.5 Compaction curve for the soil used.

The soil-water mixture was statically compacted in five equal layers using a compactor by applying a vertical stress of 350 kPa for each layer (Figure 3.6). The compaction stress was maintained constant until no further displacements were observed in the compacted soil. After each layer of compaction was completed, the surface was scarified and a new layer was placed. This procedure was followed to ensure continuity in all the five compacted layers. After compaction, a water reservoir was connected to the bottom of the plastic tank (Figure 3.7). The compacted soil samples in the plastic tank were first saturated by adding water in the reservoir and in the plastic tank. The water required for saturation was allowed to flow through the holes in the compactor plate (see Figure 3.4) placed on the surface of the compacted soils. During this process, the end of the aluminum bar was securely fixed to the cross bar of the loading machine to prevent any possible volume change of specimens due to swelling. When the level of water in the plastic tank was the same as that of water reservoir (i.e. indirect indication of fully saturation) the plastic tank was submerged in the water for 3 days to ensure full saturation conditions (Figure 3.8). No swelling was observed during and after the saturation process.

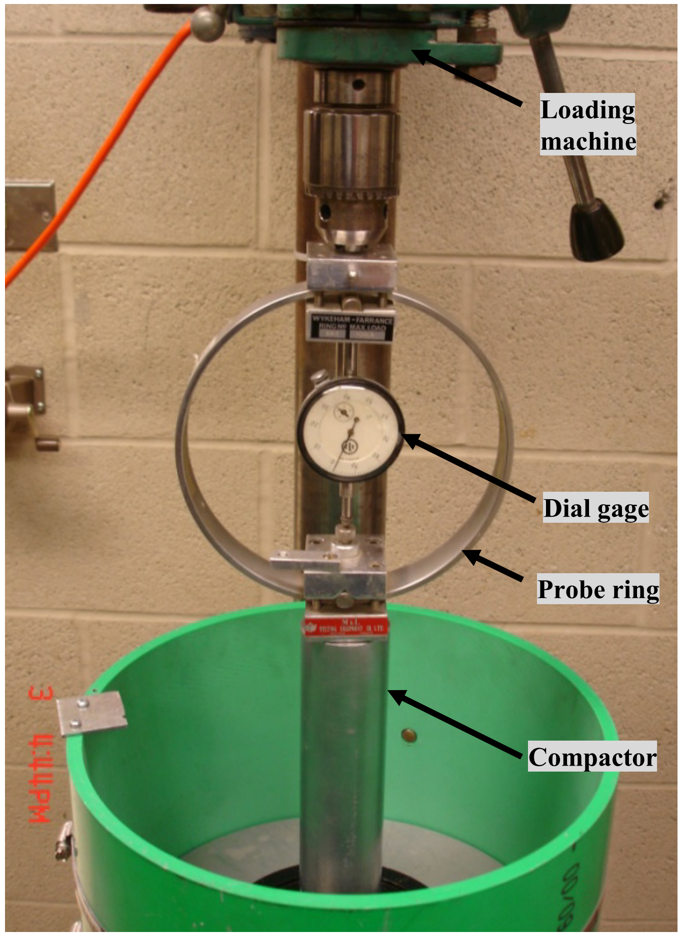

Figure 3.6 Static compaction of soils in the high strength plastic tank.

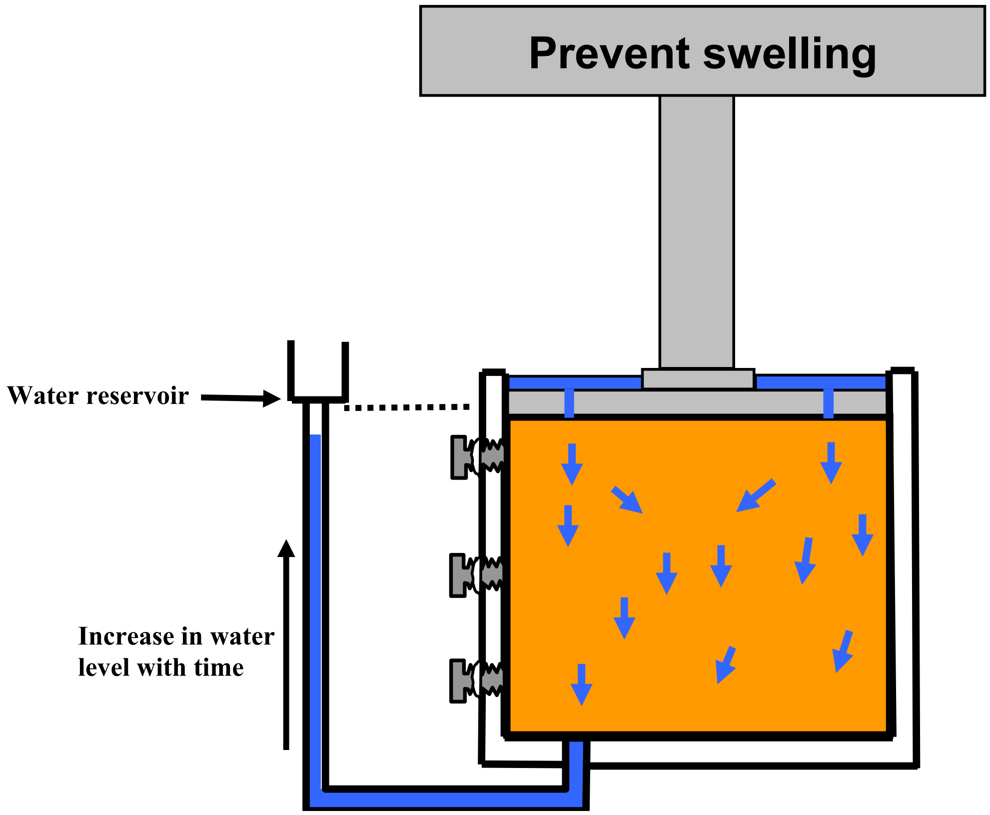

Figure 3.7 Saturation of compacted soil samples.

Figure 3.8 Compacted soil sample submerged in water.

Once the compacted soil samples in the plastic tank were saturated, the plastic tank was taken out of the water and four conventional tensiometers (Figure 3.9) were installed at the depths of 10, 40, 80, and 120 mm from the surface to monitor the variation of matric suction in the compacted soil samples (Figure 3.10). Saturation condition of the compacted soil samples was confirmed using two different methods.

(i) The conventional Tensiometers installed in the compacted soils showed zero value.

(ii) The water content of the compacted soil samples after saturation procedures was equal to 32.2%. The degree of saturation calculated using volume - mass relationship based on this water content was equal to 98.3%. This degree of saturation is close to saturation condition.

The saturated compacted soils were then subjected to air-drying for varying time periods to achieve different degrees of unsaturated conditions. However, after a certain period of air-drying, the matric suction values of the upper most layers of the compacted soil samples were significantly high (i.e. air bubbles were observed in the conventional tensiometers close to the soil surface). Hence, when the desired matric suction distribution profiles with depth were achieved, the plastic tank was securely wrapped and kept in a sealed chamber for at least 14 days to minimize the difference in the matric suction values between the upper most and bottom layer (Figure 3.11). More details of obtaining the targeted matric suction distribution profile with depth are provided in a later section.

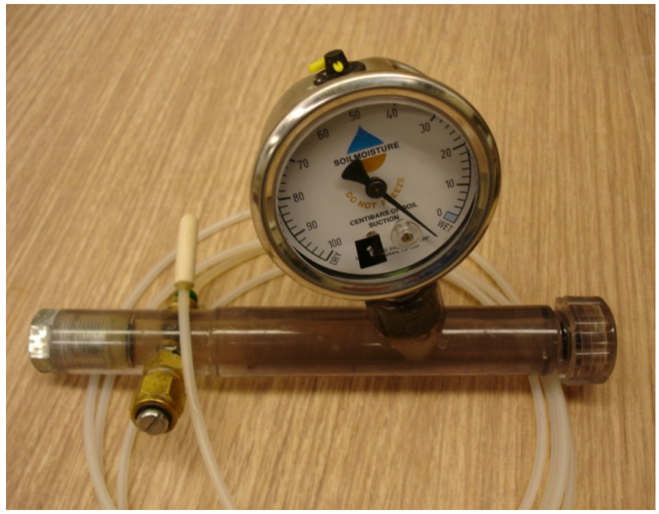

Figure 3.9 Conventional tensiometer used in the study.

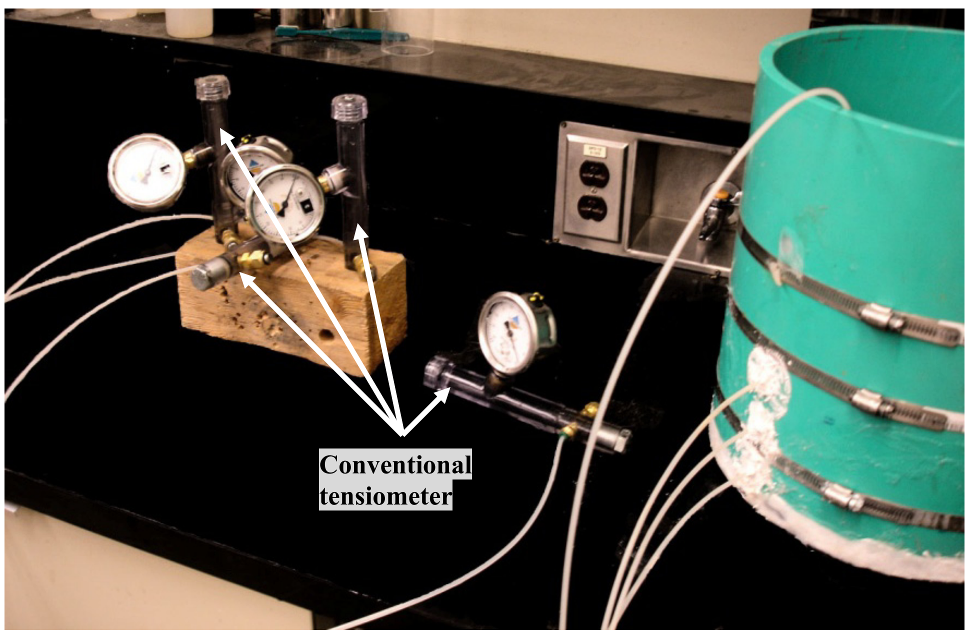

Figure 3.10 Installation of four conventional tensiometers.

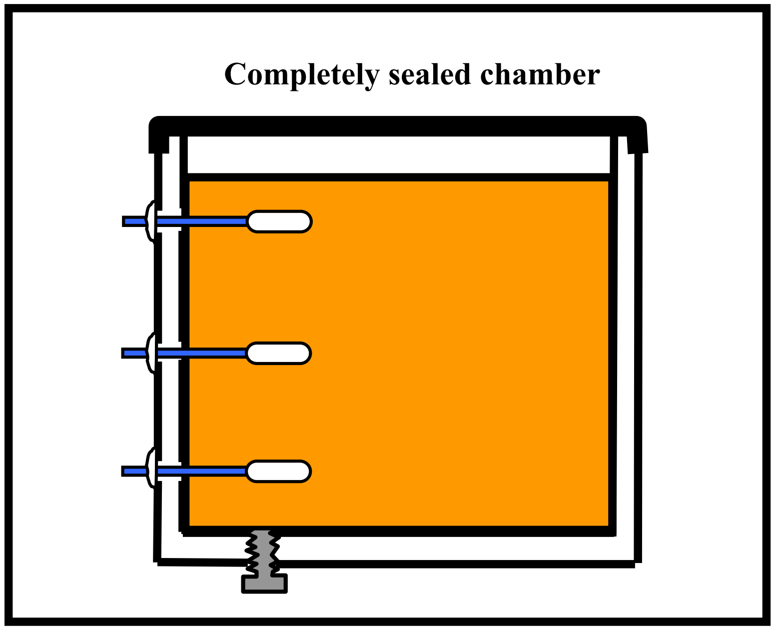

Figure 3.11 Securing the compacted soil samples in a sealed chamber to minimize the difference in the matric suction values between the upper most and bottom layer.

3.4.3 Model Footing and Unconfined Compression Tests

The plastic tank was taken out of the sealed chamber and model footings were subjected to loading at a rate of 1.14 mm/min (0.045 ins/min). The load and displacement during model footing tests were measured using a load cell and a *LVDT*, respectively and the data was automatically recorded by a data acquisition system (Figure 3.12). The same system was used for the unconfined compression tests. Additional model footing test was also conducted on a compacted soil sample that did not experience saturation-desaturation processes (i.e. as-compacted condition).

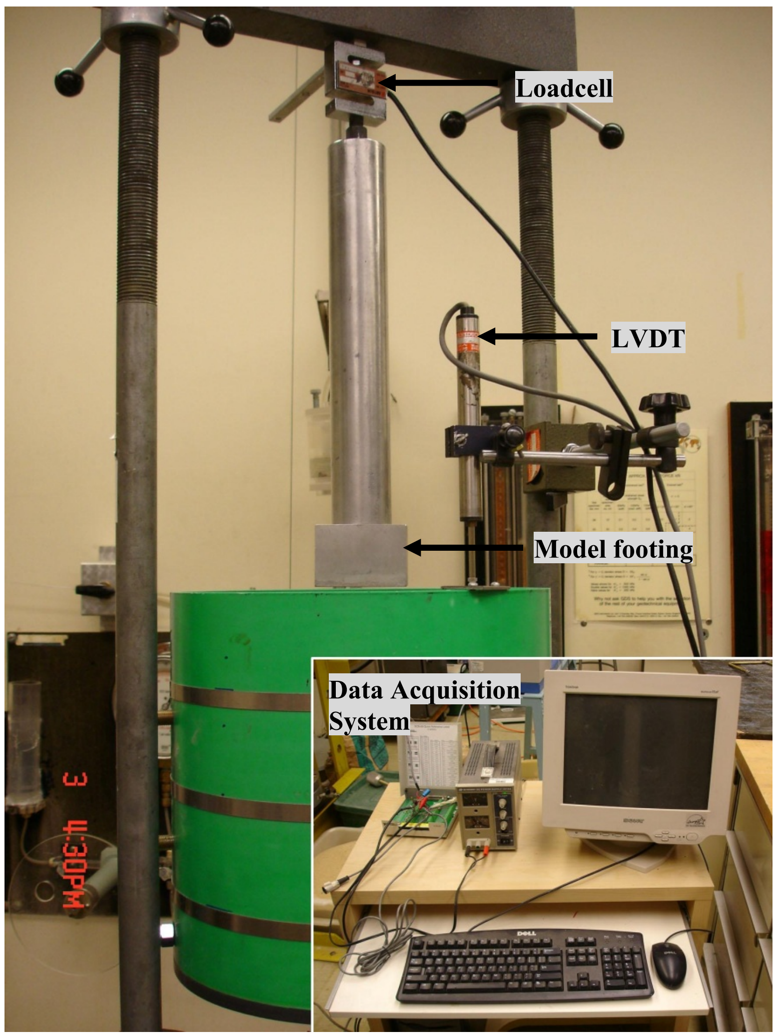

Figure 3.12 Equipment set-up for conducting model footing tests.

It was not possible to obtain soil specimens for conducting unconfined compression tests that have as close suction distribution as the air-dried compacted samples due to air-drying process. Hence, the specimens for unconfined compression tests were collected from the compacted soils at the locations outside the stress bulb using stainless steel thin-wall tubes (50 mm in diameter × 120 mm in length from the surface of compacted soils; Figure 3.13) after the model footing tests. The specimens extracted from the thin-wall tubes were trimmed into regular specimens of dimensions (50 mm in diameter × 100 mm in height) to perform unconfined compression tests. The specimens were then sheared at a rate of 1.14 mm/min that is the same rate as the model footing tests. However, for the model footing test conducted on the as-compacted soil, the unconfined compression tests were carried for the separately compacted soil specimens (50 mm in diameter × 100 mm in height) prepared at the same water content and compaction stress using the apparatus shown in Figure 2.2.

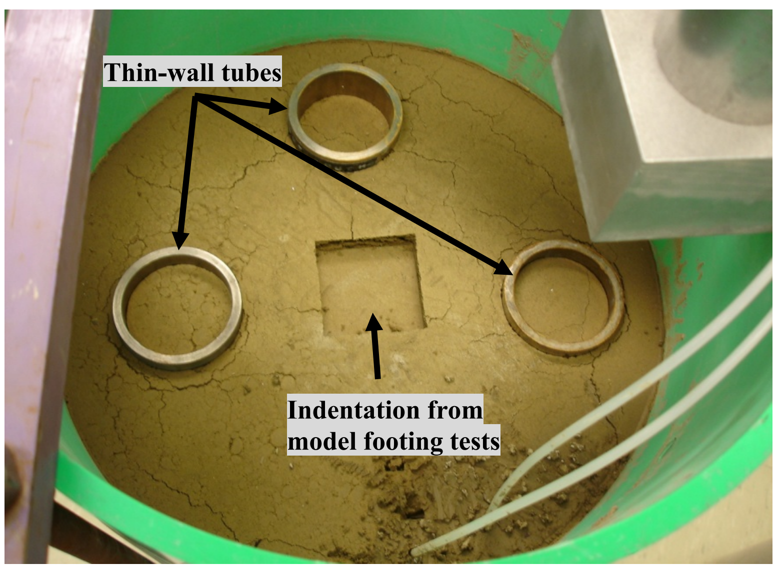

Figure 3.13 Collecting soil specimens for unconfined compression test using thin-wall tubes.

3.5 Test Results

3.5.1 SWCC and Matric Suction Distribution Profile with Depth

The *SWCC* was established using pressure plate test for identical compacted specimens (50 mm in diameter × 20 mm in thickness, ASTM D2325-68 2000) with the compaction stress of 350 kPa (Figure 3.14). The compacted specimens were first allowed to imbibe distilled water for 2 days in a pressure plate apparatus to saturate the specimens (see section 2.3.5 for more details). The saturation condition was verified from mass-volume relationships. The air-pressures were then applied to the specimens to obtain the targeted matric suction values using axis-translation technique. The mass of the specimens were regularly measured and the equilibrium conditions with respect to matric suction were confirmed when there is no change in the mass overnight (typically 12 hours or greater). The best-fit curves of the *SWCC* were established using the models proposed by Brooks and Corey (1964) [(3.11)] and van Genuchten (1980) [Eq. (3.12)].

$$\Theta = \left[\frac{1}{1 + \left(\alpha_v \Psi \right)^{n_v}} \right]^{m_v} \tag{3.11}$$

where Θ = normalized water content [= $(\theta - \theta_r)/(\theta s - \theta_r)$] , θ = volumetric water content, θ_r = residual water content, θ_s = saturated water content, and α_v, m_v, n_v = three different soil properties

$$\Theta = \left[\frac{\left(u_a - u_w \right)_b}{\Psi} \right]^{\lambda} \tag{3.12}$$

where $(u_a - u_w)_b$ = air-entry value, ψ = suction, and λ = pore size distribution index

According to the best-fit curve using Brooks and Corey (1964) model, the air-entry value is estimated to be 7.5 kPa. The residual suction value can be approximately estimated to be 420 kPa using the approach proposed by Vanapalli et al. (1999) based on the best-fit curve established using the van Genuchten (1980) model.

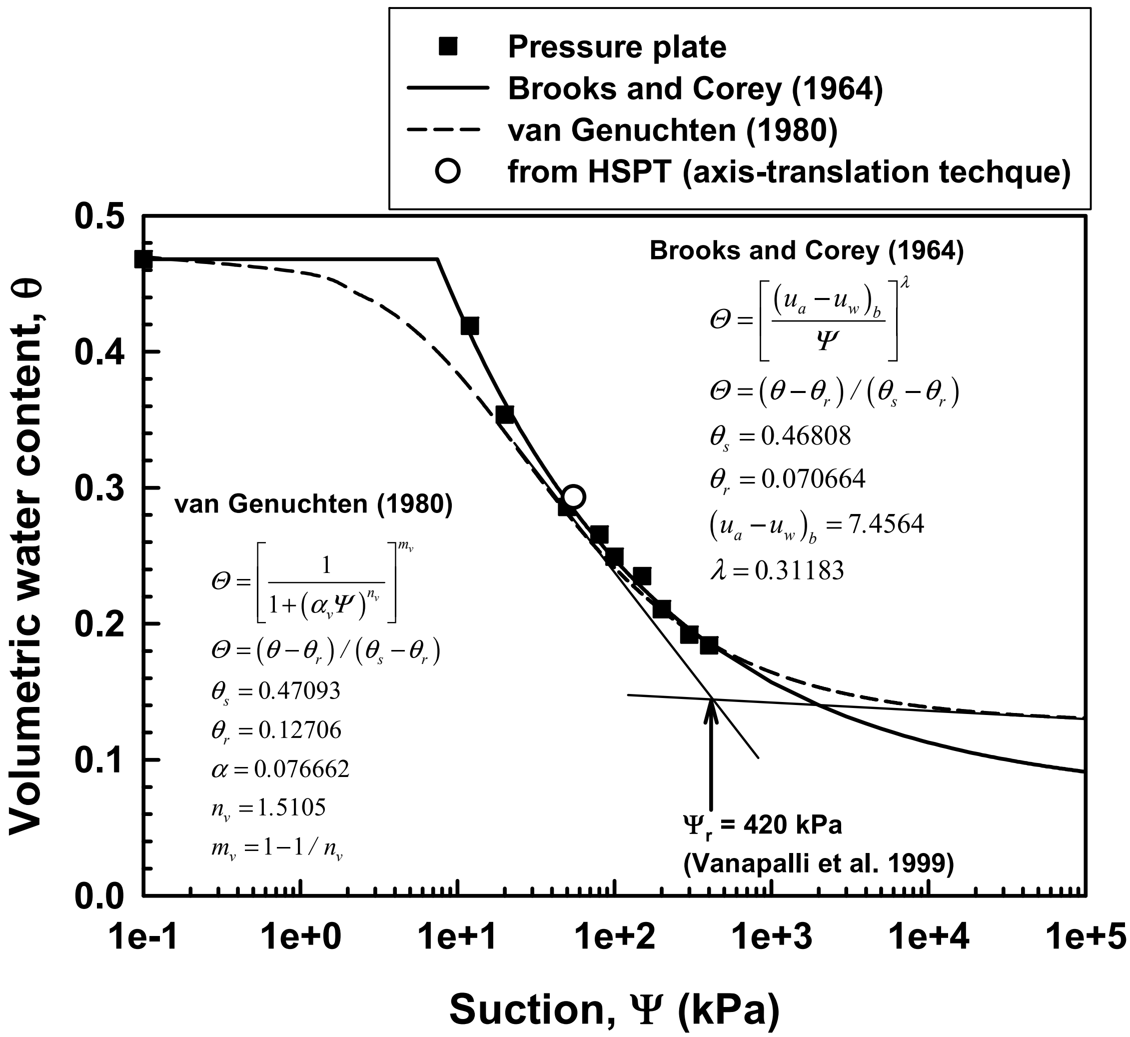

Figure 3.14 *SWCC* for the Indian Head till used in the study.

Figure 3.15 summarizes the variation of matric suction with depth in the plastic tank for five different matric suction distribution profiles, which are designated as *SAT* (saturated condition), *UNSAT1*, *UNSAT2*, *UNSAT3* (saturation-desaturation processes), and *ASCOMPAC* (as compacted condition without saturation-desaturation processes). The matric suction value of the *ASCOMPAC* was separately measured using the axis-translation technique. The matric suction distribution profiles in Figure 3.15 were obtained based on the *SWCC* using measured water contents with depth by following the procedures. After the first model footing test was completed (i.e. *UNSAT1* in Figure 3.15), axis-translation technique (Power and Vanapalli 2011, Vanapalli and Oh 2011) was performed on a specimen (50 mm in diameter × 20 mm in thickness) collected at a depth of 120 mm from the surface of the compacted soil samples in the plastic tank to cross-check the matric suction measurements from the conventional tensiometers. The specimen from this depth (i.e. 2.4 times the width of the footing) or below will not be significantly influenced by the applied loading on the model footing. This is because the depth region of 0 to 1.5*B* (Agarwal and Rana 1987, Vanapalli and Mohamed 2007, Oh et al. 2009, Oh and Vanapalli 2011) or 2*B* (Poulos and Davis 1974) (*B* is width of a footing) is the depth in which the stresses due to loading are predominant. The matric suction value for the specimen measured using the axis-translation technique was 55 kPa, which was 12 kPa higher than the value from a conventional tensiometer. This difference can be attributed to the disturbance of the compacted soil samples around the ceramic cup during installation of the conventional tensiometers. The measured matric suction (i.e. 55 kPa) and water content (i.e. 20.6%; volumetric water content, $\theta = 0.293$) fall on the measured *SWCC* (Figure 3.14). This result suggests that the matric suction value can be estimated based on the water content value using the *SWCC*. This technique was also useful to estimate the matric suction values of the upper layer of the compacted soil samples where the matric suction values were close to or greater than 100 kPa.

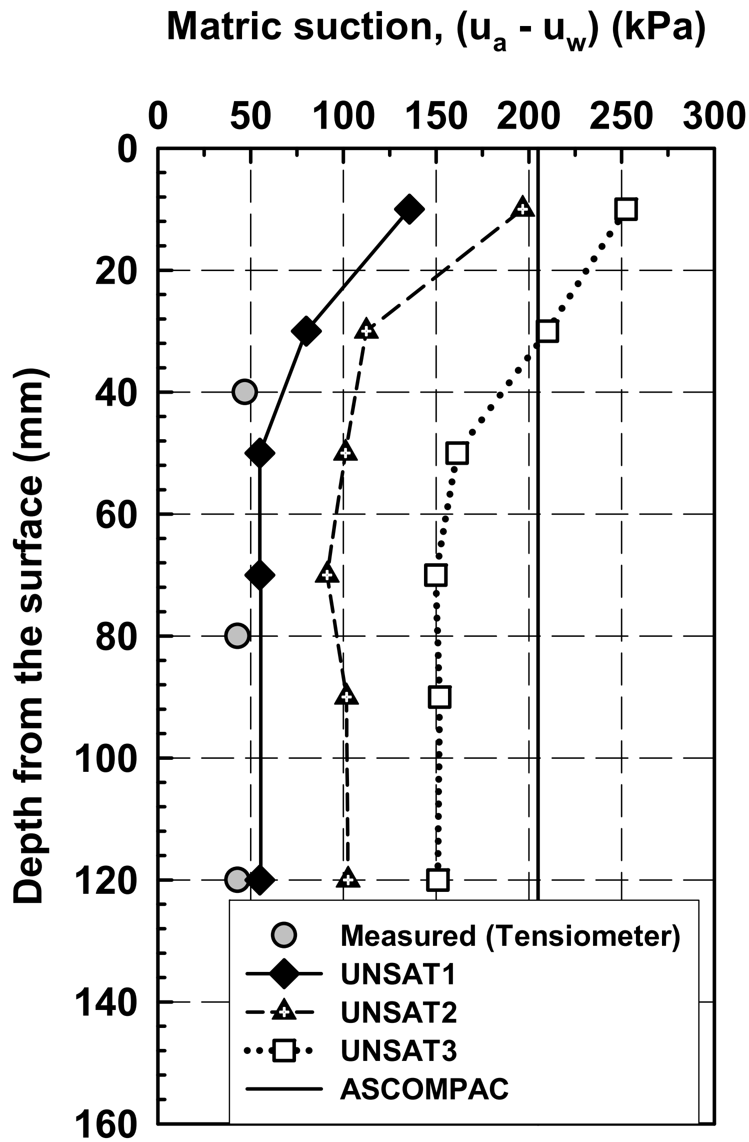

Figure 3.15 Matric suction values with depth for different matric suction distribution profiles.

3.5.2 Average Matric Suction Value and Size Effect of Footings

As explained earlier, the measurement of matric suction value is not required in the proposed *MTSA*. On the contrary, the matric suction value is key information required to estimate the bearing capacity of unsaturated soils using the *MESA*. However, as shown in Figure 3.15, the matric suction distribution profile with depth is not uniform for *UNSAT1*, *UNSAT2*, and *UNSAT3*. Hence, in this study, the concept of '*average matric suction*' is adopted as a representative matric suction value, which is defined as the matric suction value at the centroid of the matric suction distribution diagram in the stress bulb zone from surface to a depth of $1.5B - 2.0B$. Figure 3.16 shows the technique used for estimating the average matric suction value based on the measured matric suction distribution diagram. The measured non-linear matric suction profiles were simplified as two straight lines. The average matric suction values estimated using both $1.5B$ and $2.0B$ are summarized in Table 3.2.

Table 3.2 Average matric suction values for different matric suction distribution profiles.

Case	Average matric suction value, $(u_a - u_w)_{AVR}$	
	$1.5B$	$2.0B$
SAT	0	0
UNSAT1	80	55
UNSAT2	100	100
UNSAT3	197	160
ASCOMPAC	205	205

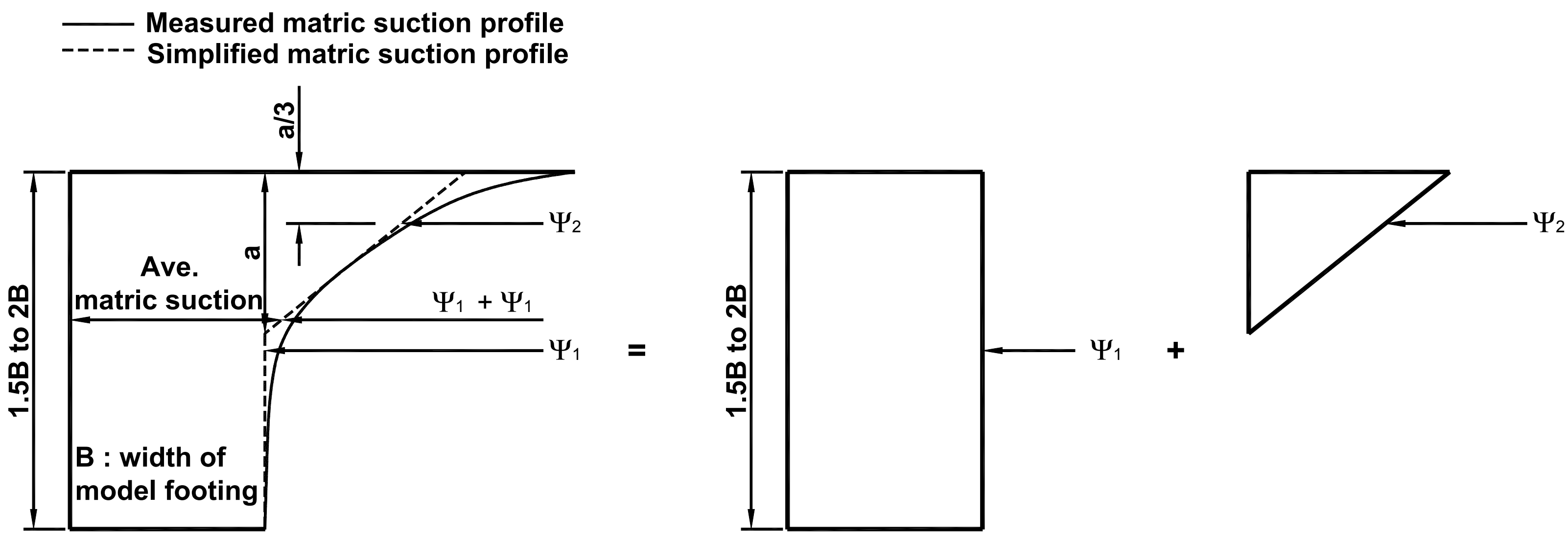

Figure 3.16 Estimation of average matric suction value based on matric suction distribution diagram.

The sizes of stress bulbs are different when loads are applied on two different sizes of footings. The resulting stress bulb for the smaller footing is shallower in comparison to that of the larger footing. If the matric suction distribution profile is uniform with depth the average matric suction value is the same regardless of footing size. However, if the matric suction distribution profile is non-uniform, the average matric suction value is dependent on the footing size. For example, in Figure 3.17, if the level of ground water table is at the location of *GWT1*, the average matric suction value for the footing B_1 (i.e. Ψ_1) is greater than that of B_2 (i.e. Ψ_2). However, if the ground water table drops to *GWT2* for only the footing B_2, the average matric suction values for both footings can be approximately the same. Hence, when the *MTSA* is used, it is suggested that the bearing capacity of an unsaturated fine-grained soil for non-uniform matric suction distribution profile be estimated using the unconfined compression test result for a specimen taken from a depth corresponding to the average matric suction.

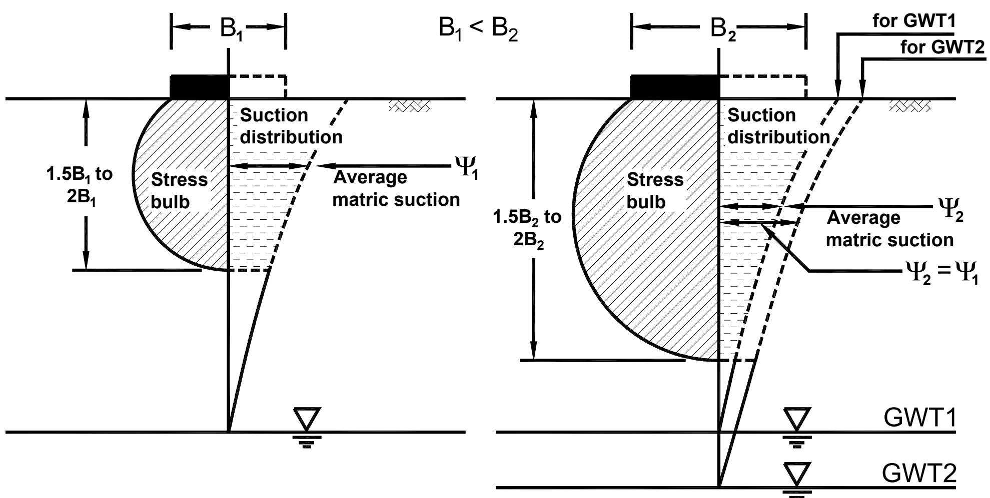

Figure 3.17 Average matric suction values for different footing sizes under idealized non-uniform matric suction distribution profile.

3.5.3 Model Footing and Unconfined Compression Test Results

Figure 3.18 shows model footing test results for both the saturated and the unsaturated soil samples. The stress versus settlement behaviors and the indentation from the model footing tests (Figure 3.19) demonstrate punching shear failure mode. This observation is consistent with the discussions provided by Vesić (1963, 1973) and the assumption made in developing the *MTSA* [i.e. Eq. (3.10)] in this chapter. In the case where well-defined failure is not observed, the ultimate bearing capacity (q_{ult}) can be estimated as the stress corresponding to either (i) a settlement equal to 10% of the width of the footing (hereafter referred to as 0.1B settlement method) (Cerato and Lutenegger 2007) or (ii) the intersection of the tangents to the initial and final portions of the stress versus displacement behaviors (hereafter referred to as graphical method) (Steensen-Bach et al. 1987, Consoli et al. 1998, Costa et al. 2003, Xu 2004).

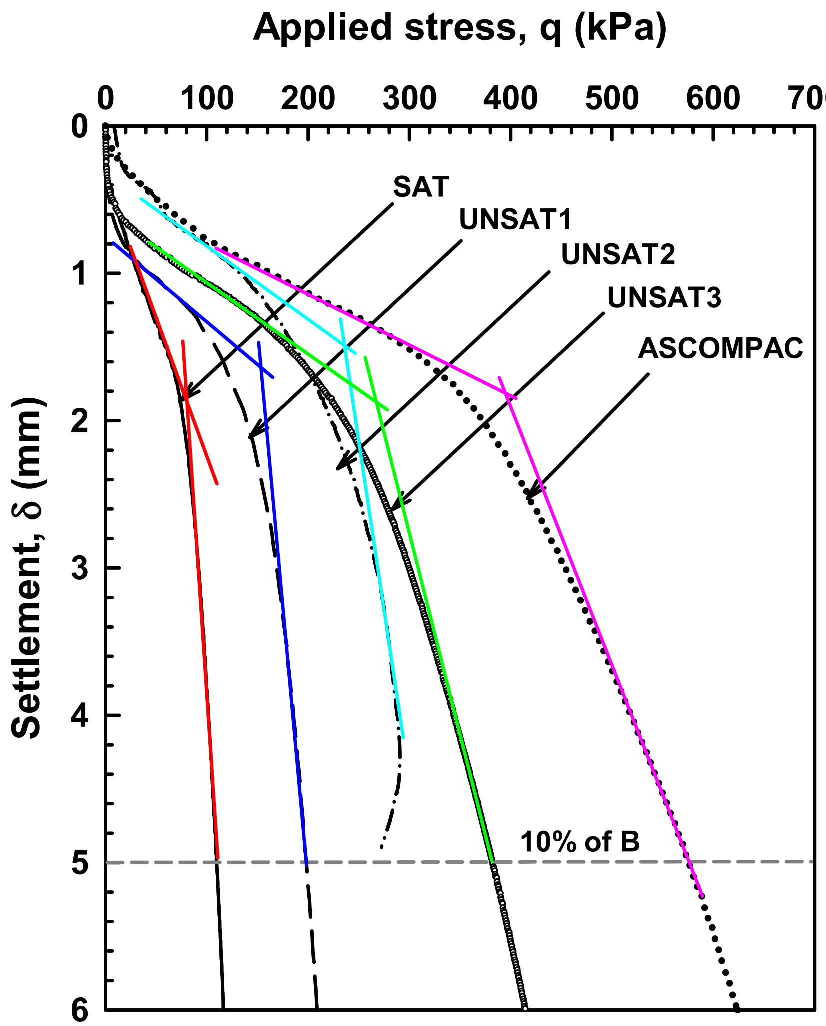

Figure 3.18 Model footing tests results.

Figure 3.19 Indentation from model footing tests.

The unconfined compression tests were carried out using two identical specimens for each matric suction distribution profile. The behavior of post-peak softening is more pronounced for specimens with higher matric suction values as shown in Figure 3.20.

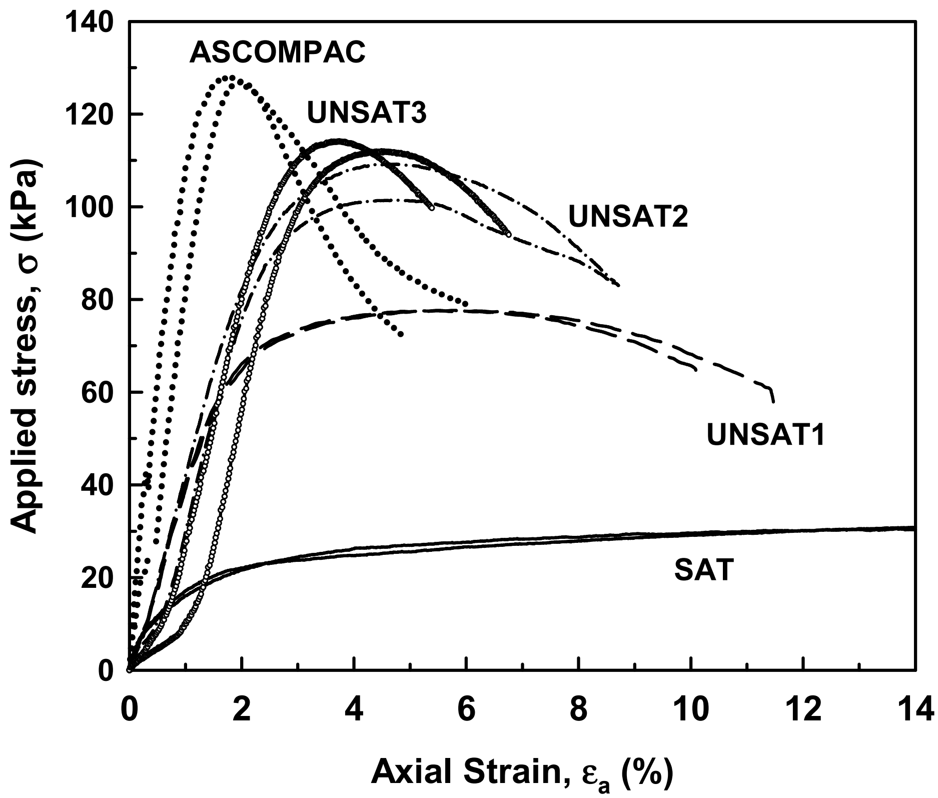

Figure 3.20 Unconfined compression tests results.

3.6 Analyses of the Experiment Results

Table 3.3 summarizes the measured bearing capacity values and those estimated using the proposed *MTSA* [i.e. Eq. (3.10)]. The bearing capacity for the *ASCOMPAC* is 1.5 times greater than *UNSAT3*, which means it is reasonable to estimate the average matric suction values based on '2.0*B*' rather than '1.5*B*' (i.e. the average matric suction values for both *UNSAT3* and *ASCOMPAC* are approximately the same if 1.5*B* is used). Based on the measured bearing capacity values, $N_{c(unsat)}$ was back-calculated for each suction distribution profile. The average $N_{c(unsat)}$ values back-calculated using Eq. (3.10) was 5.93 and 4.28 when the bearing capacity values were determined using 0.1*B* settlement and graphical method, respectively. The difference between the back-calculated $N_{c(unsat)}$ values and the value of 5.14 (i.e. originally proposed by Skempton (1948) for estimating the bearing capacity of saturated fine-grained soils under undrained loading conditions) is small.

Table 3.3 Comparison between the measured and the estimated bearing capacity values.

CASE	$(u_a - u_w)_{AVR}$ [1] (kPa)	$q_{u(unsat)}/2$ [2] (kPa)	0.1B settlement method		Graphical method		Estimated BC [5] (kPa)
			Measured BC (kPa)	$N_{c(unsat)}$ [3]	Measured BC (kPa)	$N_{c(unsat)}$ [4]	
SAT	0	13.1	109	6.93	80	5.09	80.8
UNSAT1	55	33.3	198	4.95	153	3.83	205.4
UNSAT2	100	52.7	290	4.59	233	3.68	325.1
UNSAT3	160	56.5	382	5.63	257	3.79	348.5
ASCOMPAC	205	63.7	576	7.54	384	5.02	392.9
Average				5.93		4.28	

[1] average matric suction value
[2] shear strength obtained from unconfined compression test
[3],[4] back-calculated $N_{c(unsat)}$ using the proposed *MTSA* [i.e. Eq.(3.10)]
[5] estimated bearing capacity using the proposed *MTSA* i.e. Eq.(3.10)] with $N_{c(unsat)}$ = 5.14

Figure 3.21 shows the comparison between the measured bearing capacity values and those estimated using the *MTSA* with $N_{c(unsat)}$ = 5.14. For unsaturated soil samples, the best agreement were observed for the *ASCOMPAC* samples when the bearing capacity values were estimated using the graphical method. This is because the *ASCOMPAC* samples for the unconfined compression tests were prepared by compacting in a mould separately (i.e. no external factors affected the unconfined compression test results). The q_{ult} value of *ASCOMPAC* sample determined using 0.1*B* settlement method was 1.5 times higher compared to the estimated bearing capacity. Hence, it may be postulated that the graphical method is more reasonable to determine the bearing capacity values for this study. The estimated bearing capacity values using $N_{c(unsat)}$ = 5.14 were about 1.4 times greater than the measured bearing capacity values using the graphical method for *UNSAT1*, *UNSAT2*, and *UNSAT3*. This can be attributed to the penetration of the thin-wall tubes into the compacted soils and extracting samples from the thin-wall tubes. This process contributed to a decrease in the volume (i.e. decrease of the space occupied by the pore-air), which resulted in an increase in the unconfined compressive strength. This phenomenon was not observed for the *SAT* sample due to the low friction between the soil sample and the thin-wall tube (i.e. negligible volume change).

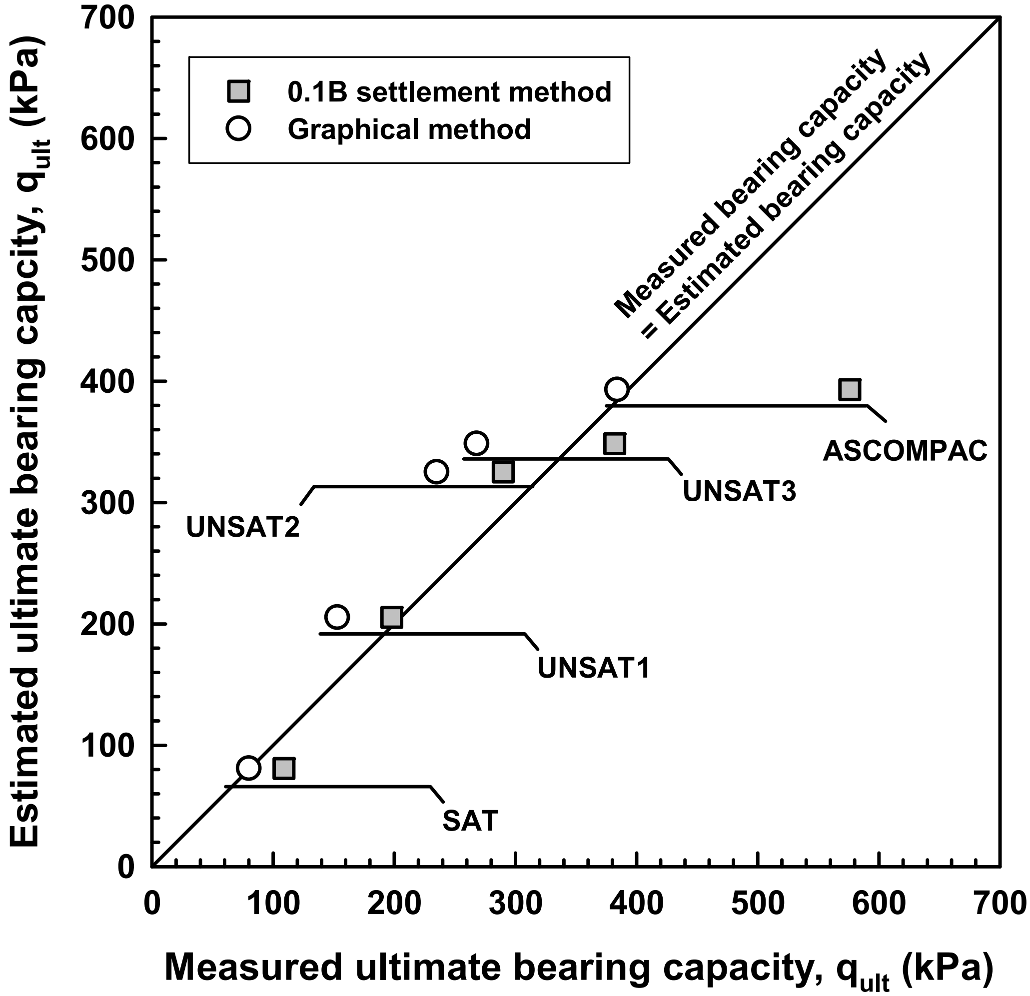

Figure 3.21 Comparison between the measured bearing capacity values and those estimated using the proposed *MTSA*.

Figure 3.22 shows the variation of measured bearing capacity values and those estimated using (i) *MTSA* [Eq. (3.10)], (ii) *MESA* using non-linear variation of ϕ^b [Eq.(3.6)], and (iii) *MESA* using non-linear variation of ϕ^b combined with reduction factors approach. The effective shear strength parameters used for the *MESA* were measured from direct shear tests with a shear rate of 10^{-5} mm/min. Table 3.4 summarizes the parameters and factors required for the *MESA*. The bearing capacity values estimated using the *MESA* combined with reduction factors approach were significantly underestimated. The *MESA* overestimated the bearing capacity values for *UNSAT1*, *UNSAT2* and *UNSAT3* but underestimated the bearing capacity for the *ASCOMPAC*. It is because the net contribution of matric suction towards the shear strength started decreasing as matric suction value approaches residual state (Vanapalli et al. 1996), which resulted in reduced contribution to the bearing capacity after a certain matric suction value. The *MTSA* provided good estimates for *SAT* and *ASCOMPAC*; however, overestimated for other cases due to the reasons described earlier (i.e. friction between soils and thin-wall tubes). Hence, the *MTSA* can be expected to be the most reasonable approach to estimate the bearing capacity of unsaturated fine-grained soils if the samples for the unconfined compression tests are obtained by general procedures being used in engineering practice.

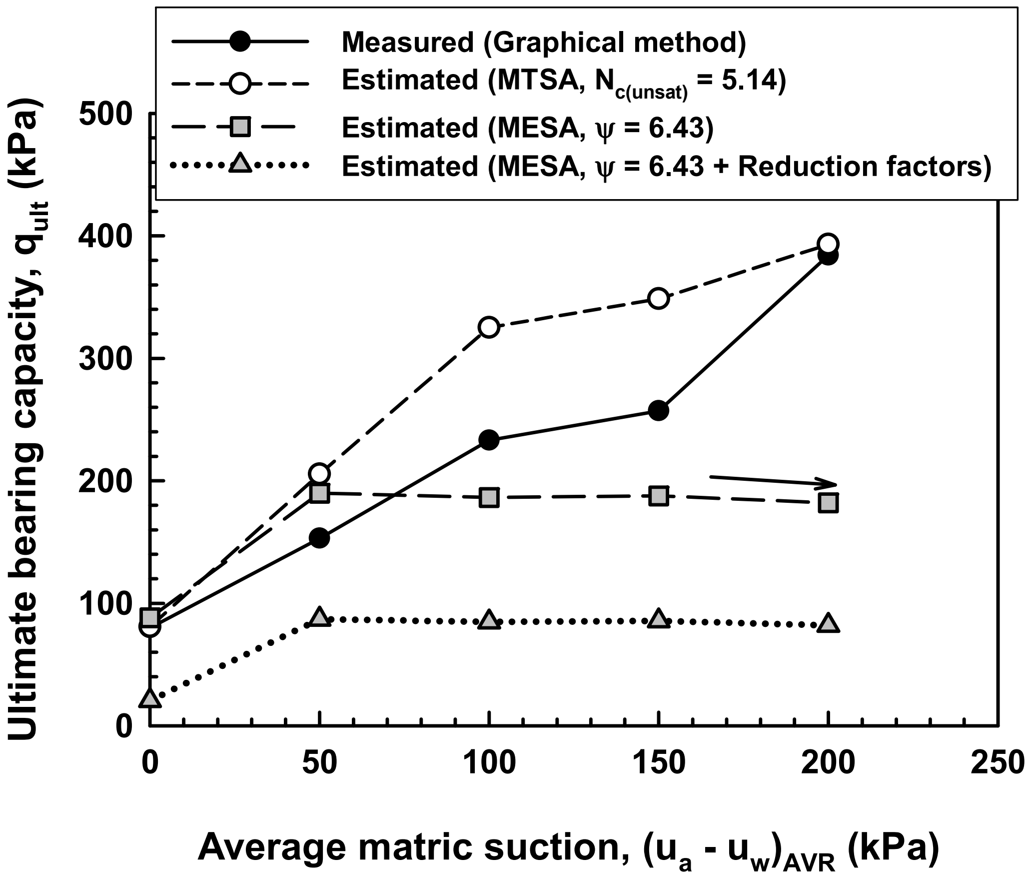

Figure 3.22 Comparison between the measured bearing capacity values and those estimated using different approaches.

Table 3.4 Summary of the parameters and factors required for the modified effective stress approach (*MESA*).

$(u_a - u_w)$ [1) (kPa)	S [2) (%)	γ [3) (kN/m^3)	c' [4) (kPa)	ϕ' [5) (°)	ψ [6) (kPa)
0	98.3	18.5	3.5	21	6.43
55	60.0	17.2			
100	52.3	16.8			
160	49	16.5			
205	44	16			

[1)]matric suction, [2)]degree of saturation, [3)]unit weight of soils
[4)]effective cohesion, [5)]effective internal friction angle
[6)]fitting parameter for bearing capacity in Eq. (3.6)

3.7 Application of the MTSA to the In-Situ Plate Load Tests in Unsaturated Fine-Grained Soils

Consoli et al. (1998) conducted in-situ plate load tests in an unsaturated residual homogeneous, cohesive soil (I_p = 20%) using three steel circular plates (i.e. 0.3 m, 0.45 m, and 0.6 m; *PLT*) and three concrete square footings (i.e. 0.4 m, 0.7 m, and 1.0 m; *FLT*). The bearing capacity value estimated using the *MTSA* [i.e. Eq. (3.10)] is 155 kPa (average unconfined compressive strength was estimated to be 50.2 kPa). Figure 3.23 shows the comparison between the measured bearing capacity values determined using both graphical and 0.1*B* settlement method and those estimated using the *MTSA*. The bearing capacity values determined using 0.1*B* settlement method was approximately 2 times higher than those determined using the graphical method. These results also suggest that the graphical method is more reasonable to determine the bearing capacity values from the stress versus settlement behavior. For smaller footings, the *MTSA* significantly underestimated the bearing capacity values. However, this discrepancy between the measured (graphical method) and the estimated bearing capacity values (i.e. 155 kPa) decreases as the footing size increases. The best agreement between them then observed for the 1.0 m × 1.0 m square footing. This result is attributed to the reason that the measured average unconfined compressive strength corresponds to the average matric suction value for the 1.0 m × 1.0 m square footing. In other words, the *MTSA* underestimated the bearing capacity values for the smaller footings since the average suction values for the smaller footings are greater than that of the 1.0 m × 1.0 m square footing, which required higher representative unconfined compressive strength values for better estimates.

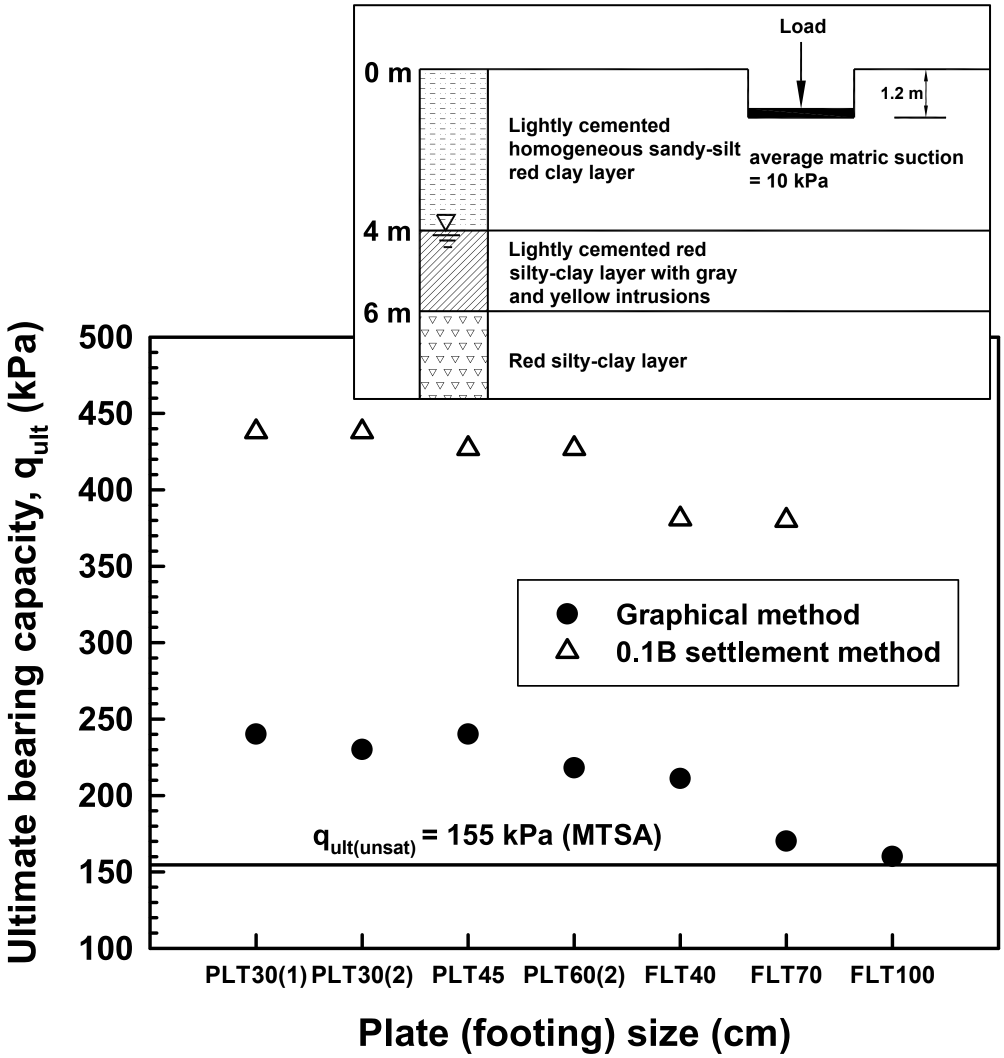

Figure 3.23 Comparison between the measured bearing capacity values and those estimated using MESA and MTSA using the in-situ plate load tests results in unsaturated fine-grained soils [data by Consoli et al. (1998)]

3.8 Model to Estimate the Variation of Bearing Capacity of Unsaturated Fine-Grained Soils with respect to Matric Suction

As mentioned earlier, the bearing capacity of unsaturated fine-grained soils can be reliably estimated using only the shear strength from the unconfined compression test results (a half the unconfined compressive strength, $q_{u(unsat)}/2$; *MTSA*). This indicates that if the variation of shear strength of an unsaturated fine-grained soil with respect to matric suction can be estimated the variation of bearing capacity of unsaturated fine-grained soil can also be estimated as well. Extending this concept, in this chapter, a semi-empirical model is proposed to estimate the variation of bearing capacity of unsaturated fine-grained soils. The proposed model required the undrained shear strength derived from unconfined compression test results for saturated condition and the Soil-Water Characteristic Curve (*SWCC*) along with two fitting parameters, υ and μ [Eq. (3.13)].

$$c_{u(unsat)} = c_{u(sat)}\left[1 + \frac{(u_a - u_w)}{(P_a/101.3)}\left(S^{\upsilon}\right)/\mu\right] \tag{3.13}$$

where $c_{u(sat)}$, $c_{u(unsat)}$ = undrained shear strength under saturated and unsaturated condition, respectively, P_a = atmospheric pressure (i.e. 101.3 kPa), and υ and μ = fitting parameters.

In Eq. (3.13), the terms, S^{υ} controls the nonlinear variation of shear strength with respect to matric suction. The term (P_a/101.3) was used to maintain consistency with respect to the dimensions and units on both sides of the equation. Combining Eq. (3.10) with Eq. (3.13), the variation of bearing capacity of unsaturated fine-grained soils can be calculated using Eq. (3.14).

$$\begin{aligned} q_{ult(unsat)} &= \left[\frac{q_{u(unsat)}}{2}\right]\left[1 + 0.2\left(\frac{B}{L}\right)\right]N_{CW} \\ &= c_{u(sat)}\left[1 + \frac{(u_a - u_w)}{(P_a/101.3)}\left(S^{\upsilon}\right)/\mu\right]\left[1 + 0.2\left(\frac{B}{L}\right)\right]N_{CW} \end{aligned} \tag{3.14}$$

The fitting parameter, $\upsilon = 2$ can be used for fine-grained soils. To obtain the fitting parameter, μ, six sets of unconfined compression tests results for unsaturated fine-grained soils reported in the literature [(1) Chen 1984, (2) Ridley 1993, (2) Vanapalli et al. 2000, (3) Babu et al. 2005, (4) Pineda and Colmenares 2005, (5) Present study (section 3.5.3)] were analyzed.

The basic properties of soils used for the analysis are summarized in Table 3.5.

Table 3.5 Basic properties of the soils used for the analysis.

Soil properties	(1)	(2)	(3)	(4)	(5)	(6)
G_s	2.88	2.61	2.68	2.7	2.61	2.72
I_p (%)	38	32	8	60	38	15.5
OMC (%)	-	-	-	32.5	35	18.3
$\gamma_{d(max)}$ (kN/m^3)	-	-	-	15.35	12.16	17.3

(1) Chen (1984)
(2) Ridley (1993)
(3) Vanapalli et al. (2000)
(4) Babu et al. (2005)
(5) Pineda and Colmenares (2005)
(6) present study (section 3.5.3)

Figure 3.24 shows the *SWCC*s for the soils used in the analysis. For the data by Chen (1984), the *SWCC* could not be provided since the experiments were conducted for the specimens compacted at different compaction water contents with the same dry density. Nonetheless, the unconfined compressive strength under saturated condition for each specimen was the same, which implies the effect of the soil structure on the shear strength can be negligible.

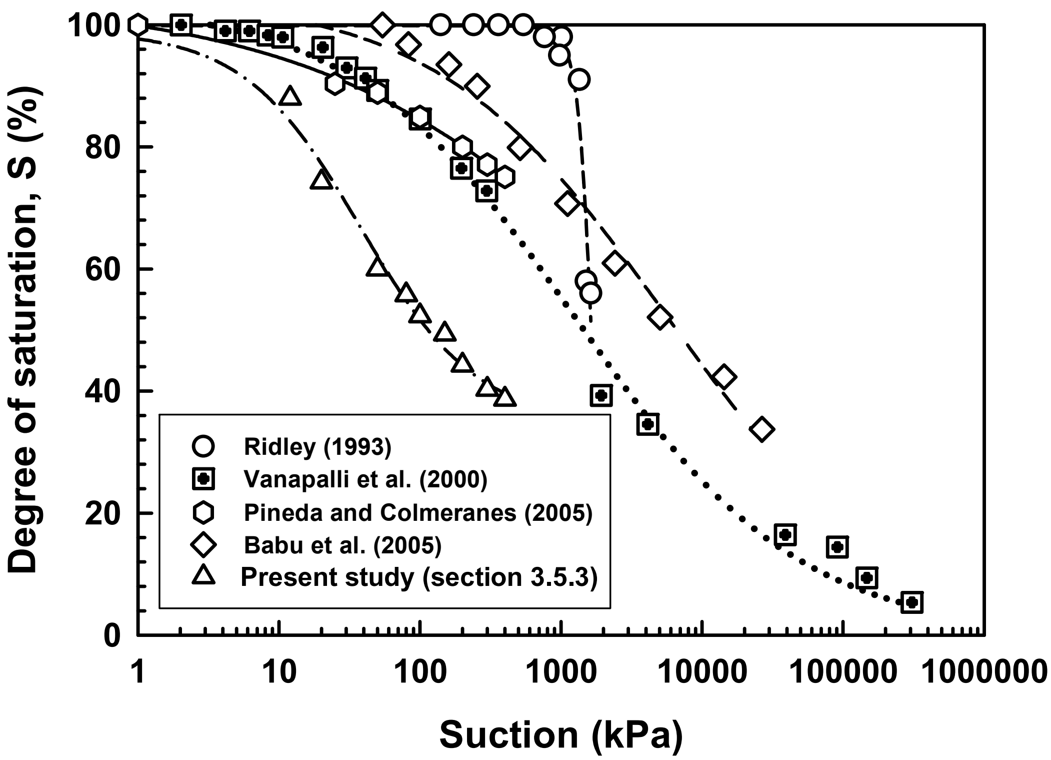

Figure 3.24 *SWCC* for the soils used in the analysis

3.8.1 Analysis of the Results

3.8.1.1 Comparison between the Measured and the Estimated Shear Strength

Figure 3.25 to Figure 3.30 show the comparisons between the measured shear strength from the unconfined compression tests and those estimated using the proposed model [i.e Eq. (3.13)]. As can be seen, good agreement was observed between the measured and the estimated shear strength values. Explanation with respect to the disagreement for the two points '(a)' and '(b)' in Figure 3.26 is provided in a later section.

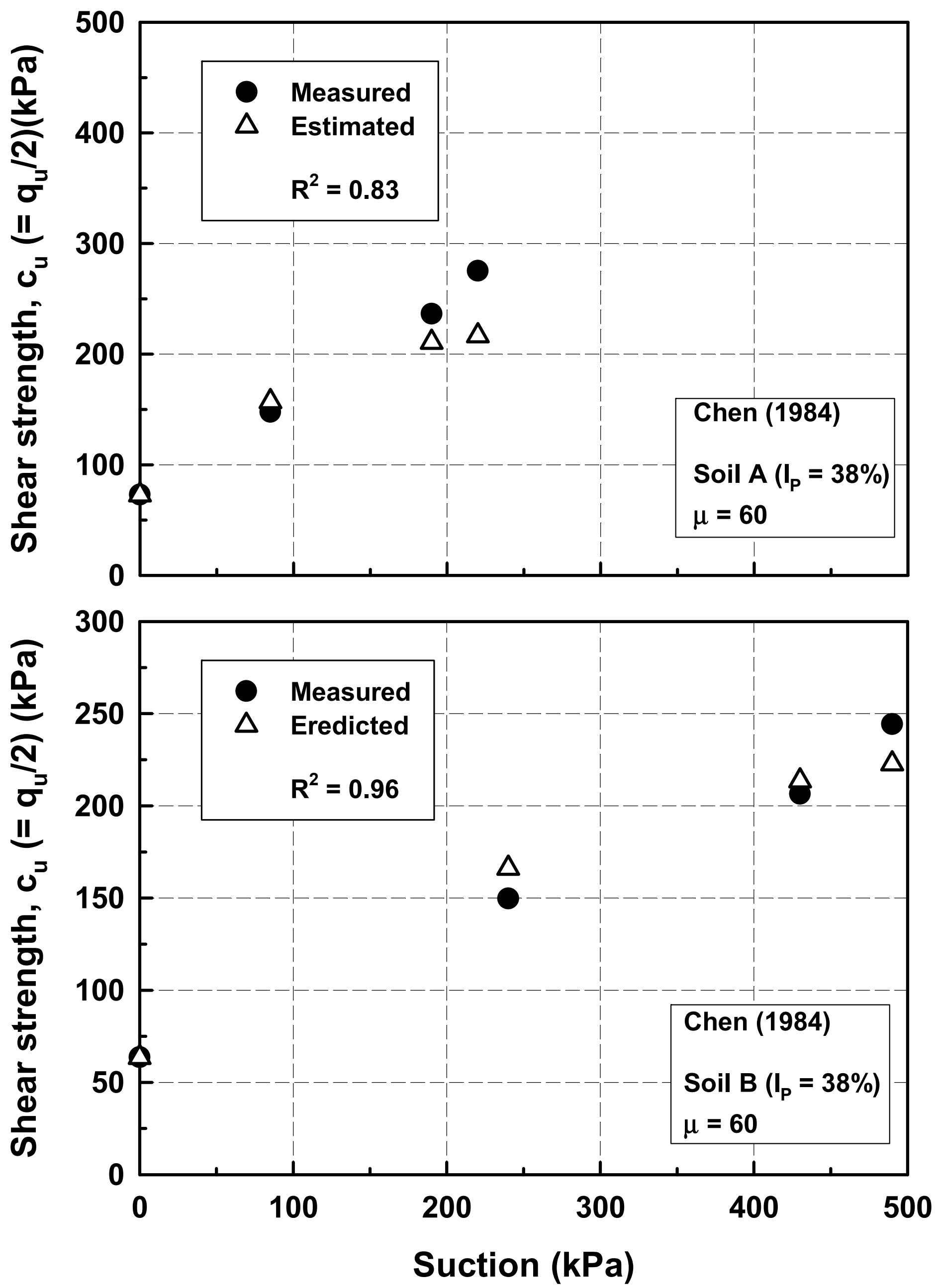

Figure 3.25 Comparison between the measured and the estimated shear strength [data from Chen (1984)].

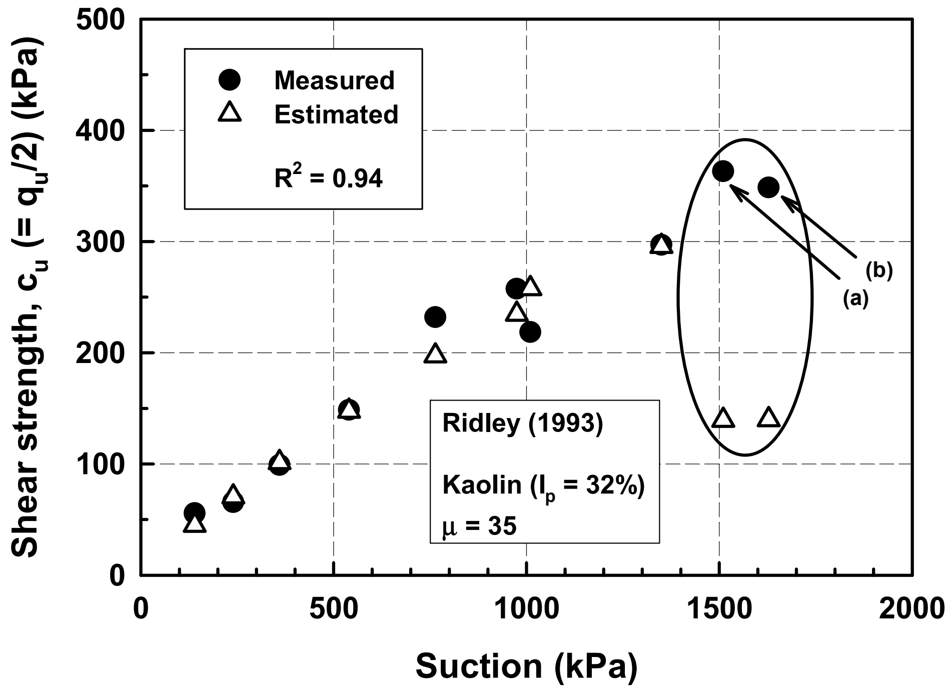

Figure 3.26 Comparison between the measured and the estimated shear strength [data from Ridley (1993)].

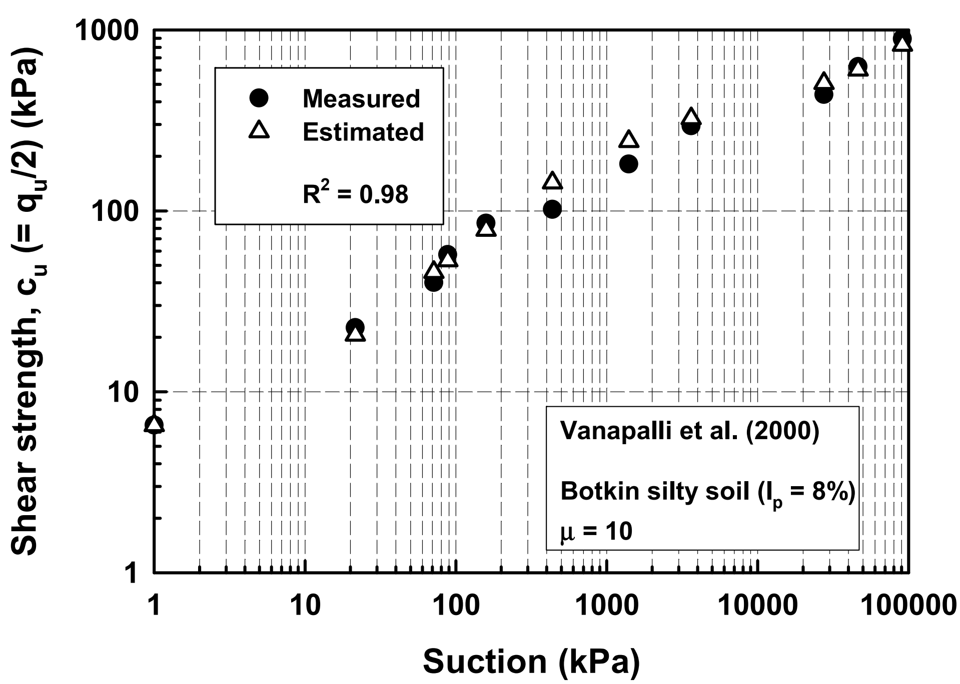

Figure 3.27 Comparison between the measured and the estimated shear strength [data from Vanapalli et al. (2000)].

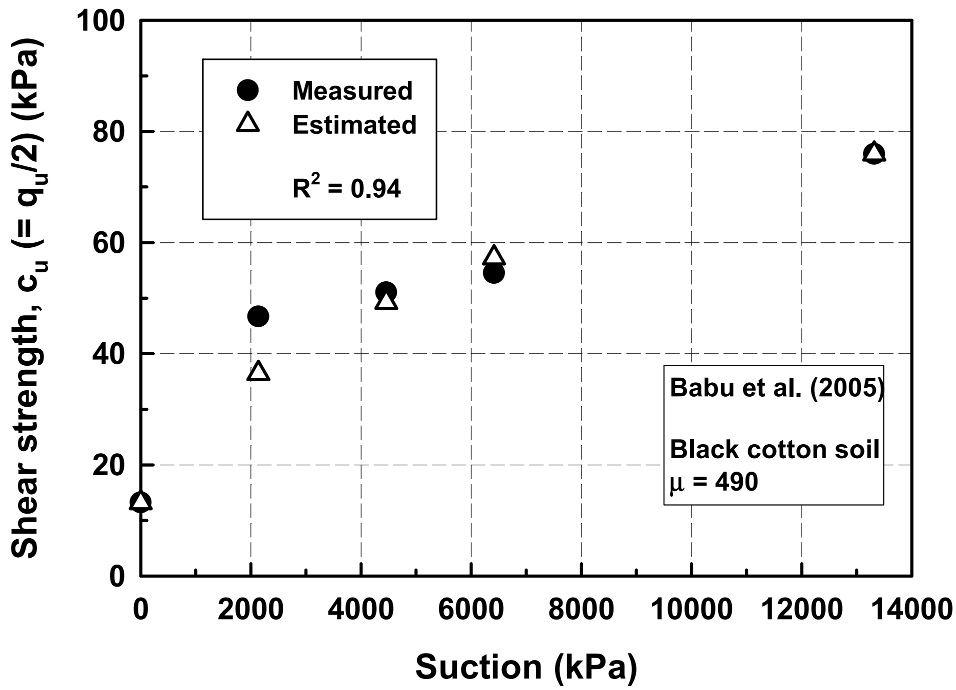

Figure 3.28 Comparison between the measured and the estimated shear strength [data from Babu et al. (2005)].

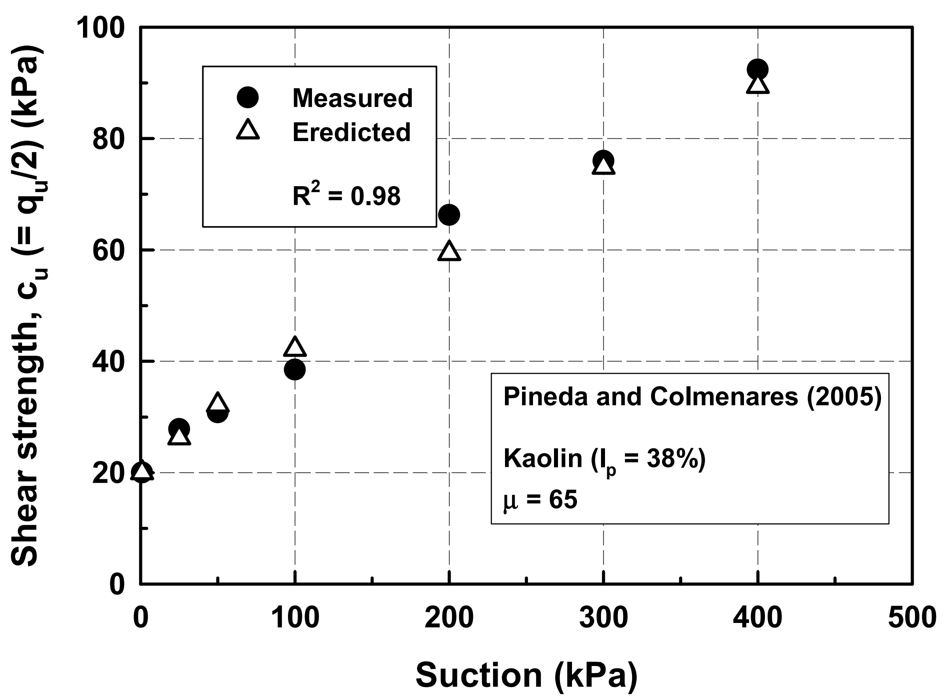

Figure 3.29 Comparison between the measured and the estimated shear strength [data from Pineda and Colmenares (2005)].

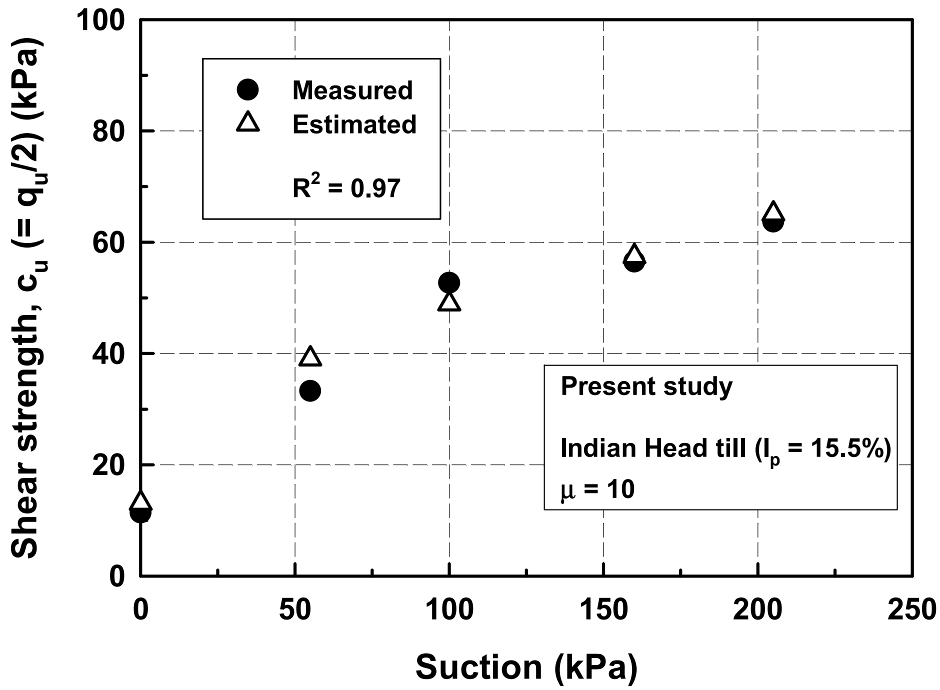

Figure 3.30 Comparison between the measured and the estimated shear strength (data from section 3.5.3).

3.8.1.2 Relationship between the Fitting Parameter, μ and Plasticity Index, I_p.

The fitting parameter, μ in Eq. (3.13) derived for each data set is summarized in Table 3.6 and plotted on semi-logarithmic scale against the plasticity index, I_p in Figure 3.31. The fitting parameter, μ was found to be constant with a value of '10' for the soils that have I_p values in the range of 8% and 15.5%. The value of μ, however, then starts increasing linearly on semi-logarithmic scale with increasing I_p [Eq. (3.15)]. The data from Chen (1984) was not taken into account in developing Eq. (3.15) due to the reason discussed above.

$$\begin{cases} \mu = 10 & for\ \ 8 \le I_p(\%) \le 15.5 \\ \mu = 2.3298 \cdot e^{0.0872(I_p)} & for\ \ 15.5 \le I_p(\%) \le 60 \end{cases} \tag{3.15}$$

Unsaturated fine-grained soils desaturate over wide range of suction in comparison to unsaturated coarse-grained soils. This phenomenon becomes more predominant as plasticity index increases. In other words, the shear strength of highly plastic unsaturated fine-grained soils can be significantly overestimated if calculated using Eq.(3.15) with lower value of μ. As a result, higher values of the fitting parameter, μ should be used to obtain better estimates for high plastic unsaturated fine-grained soils.

Table 3.6 Fitting parameter, μ for the soils used in the analysis.

References	I_p (%)	μ
Vanapalli et al. (2000)	8	10
Present study (section 3.5.3)	15.5	10
Ridley (1993)	32	35
Chen (1984)	38	60
Pineda and Colmenares (2005)	38	65
Babu et al. (2005)	60	490

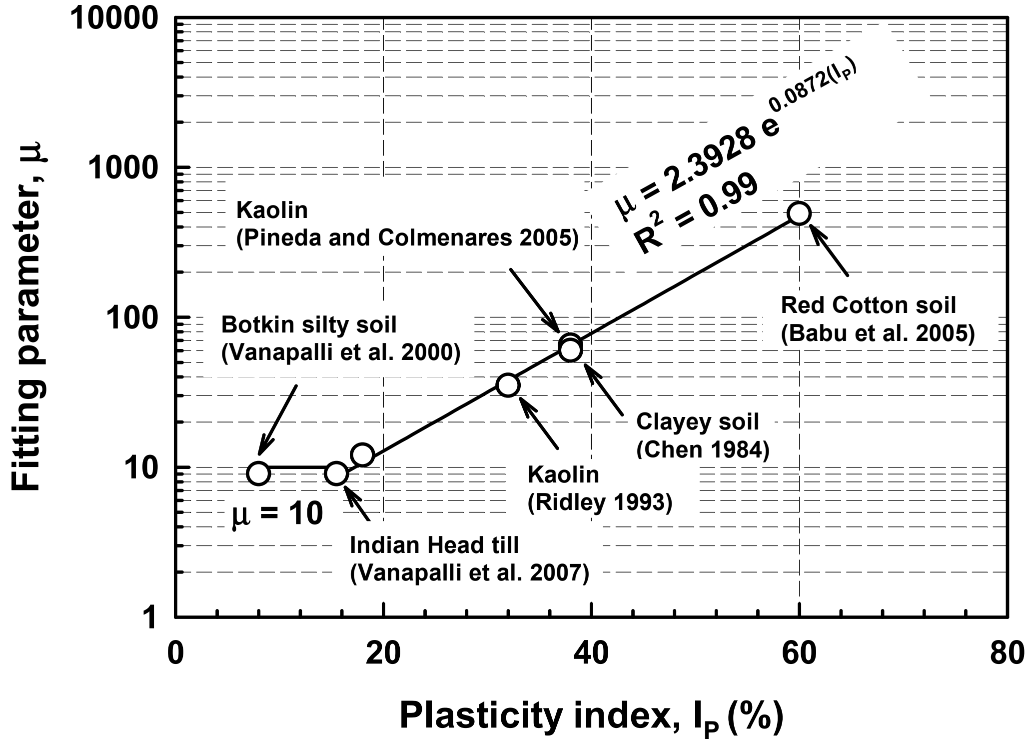

Figure 3.31 Relationship between plasticity index and the fitting parameter, μ.

3.8.2 Limitations of the Proposed Method

There are two main limitations of the proposed model for estimating the variation of bearing capacity of unsaturated fine-grained soils with respect to suction as follows:

(i) The relationship between the fitting parameter, μ and plasticity index, I_p shown in Figure 3.31 and Eq. (3.15) is developed with limited data (i.e. five data sets) for a certain range of I_p values (i.e. $8 \leq I_p$ (%) ≤ 60). The proposed model can be used in geotechnical engineering practice with greater confidence as more supporting data becomes available.

(ii) The results by Ridley (1993) in Figure 3.26 show that there is a discrepancy between the measured and the estimated shear strength values after a certain suction value (i.e. greater than 1,500 kPa in this case). This behavior can be explained using the differential form of Eq. (3.13) as shown in Eq. (3.16).

$$\frac{dc_{u(unsat)}}{d\left(u_a-u_w\right)}=\frac{c_{u(unsat)}}{\mu}\left[\left(S^{\upsilon}\right)+\left(u_a-u_w\right)\frac{d\left(S^{\upsilon}\right)}{d\left(u_a-u_w\right)}\right] \tag{3.16}$$

It can be seen that Eq. (3.16) is similar in form to the differential form of the semi-empirical nonlinear function proposed by Vanapalli et al. (1996) and Fredlund et al. (1996) to estimate the variation of the shear strength with respect to matric [i.e. Eq. (3.4)]. Eq. (3.16) indicates that at suction values close to the residual state conditions, the net contribution of matric suction towards shear strength decreases due to the same reason as explained in section 3.2.2. In other words, the estimated shear strength using the proposed model starts decreasing at suction values close to residual suction value although the measured shear strength continues to increase. The residual suction value of the soil used by Ridley (1993) can be estimated to be approximately 1,500 kPa based on the *SWCC* (Figure 3.24) and the suction values for the point '(a)' and '(b)' are close to this residual suction value (Figure 3.26). The tests results for the Kaolin (the plasticity index for the material was not available in the literature) by Aitchison (1957) also showed the similar trend as Ridley (1993)'s data (see Figure 3.32).

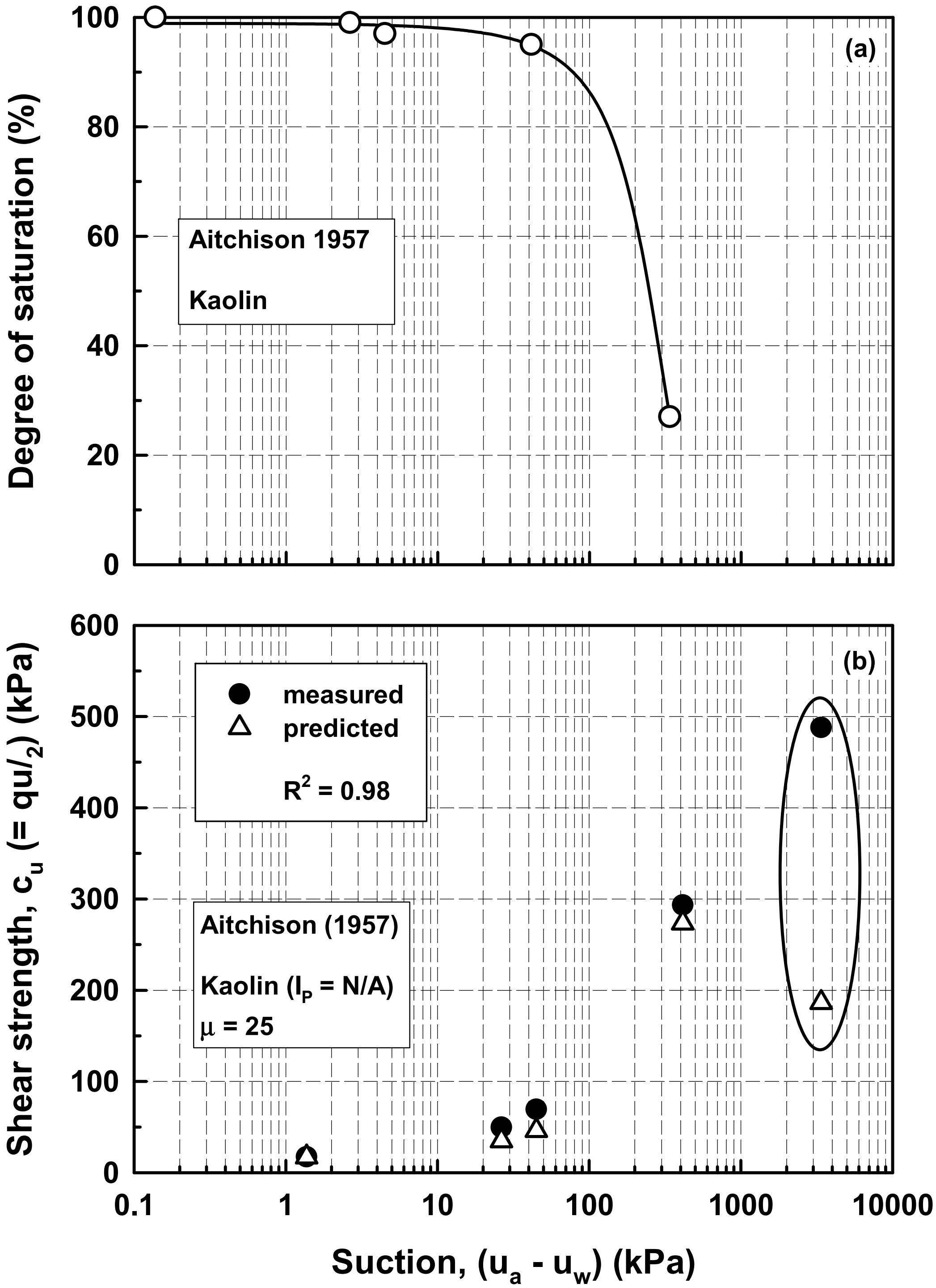

Figure 3.32 (a) *SWCC* and (b) comparison between the measured and the estimated shear strength [data from Aitchison (1957)].

3.9 Interpretation of In-Situ Plate Load Tests Results in Unsaturated Fine-Grained Soils using MESA and MTSA

In this section, an attempt is made to interpret the in-situ plate load tests results in unsaturated fine-grained soils (Costa et al. 2003, Rojas et al. 2007) using three different approaches; (i) *MESA* [i.e. Eq. (3.6)], (ii) combining *MESA* [i.e. Eq. (3.6)] with reduction factors approach [i.e. Eq. (3.1) + Eq. (3.2)] and (iii) *MTSA* [i.e. Eq. (3.10)].

Costa et al. (2003) carried out a series of in-situ plate load tests on lateritic soil deposit (i.e. clayey sand, I_p = 8%) to investigate the influence of matric suction on the bearing capacity. The matric suction values were measured using four tensiometers installed at the bottom of the test pit (1.5 m depth) besides the loading plate at depths of 0.10, 0.30, 0.60, and 0.80 m. The average value of the tensiometer readings from 0 to depth of plate size was regarded as the representative matric suction value for a certain matric suction distribution profile.

Rojas et al. (2007) performed seven in-situ plate load tests on unsaturated Lean clay (I_p = 12%). The matric suction values were measured using four tensiometers installed at depths of 0.1, 0.3, 0.6, and 0.9 m below the base of the pits (1.2 × 3.0 × 1.4 m).

Figure 3.33 shows the *SWCC*s for the two soils where the in-situ plate load tests were carried out.

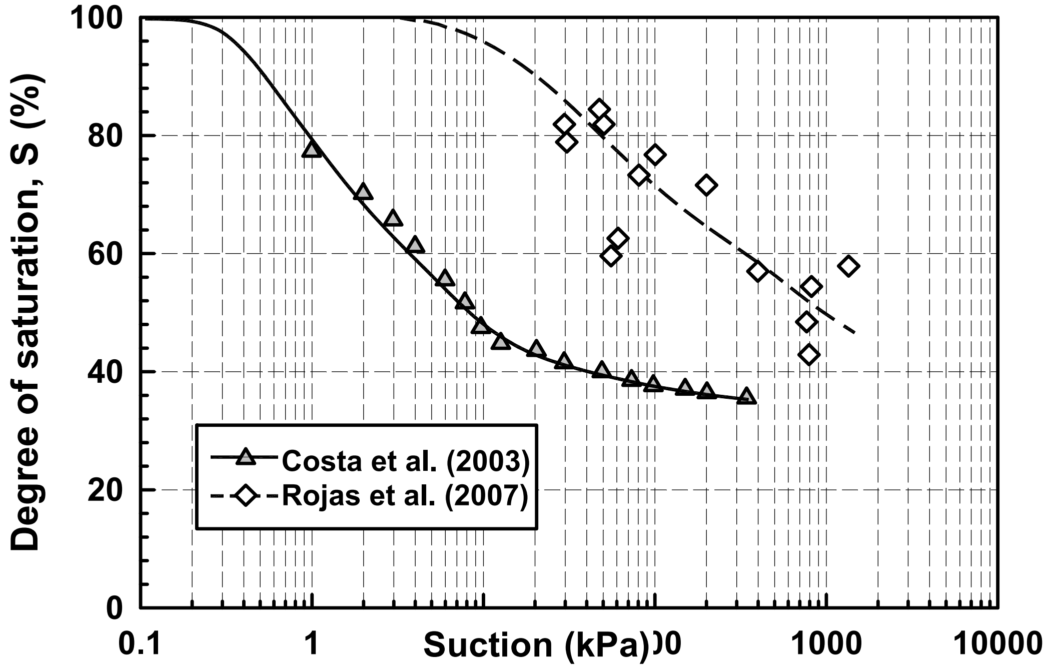

Figure 3.33 *SWCC*s for the soils where the in-situ plate load tests were conducted.

Figure 3.34 shows the comparison between the measured and the estimated bearing capacity values for the data by Costa et al. (2003). Costa et al. (2003) placed the plate at the depth of about 3.8 m below the soil surface. However, in the analysis, the influence of embedded depth on the bearing capacity was not considered since the bearing capacity values were significantly overestimated. This phenomenon indirectly justifies the assumption that was made to develop the *MTSA* (i.e. the slip surfaces below shallow foundation are typically not extended to the ground surface but instead restrict to vertical planes). The bearing capacity values estimated using the *MESA* were underestimated when the calculation is conducted with the fitting parameter, $\psi = 4$ [Eq. (3.7), $I_p = 8\%$]; therefore, $\psi = 3.5$ was used to obtain good agreement in comparison to the measured bearing capacity values. The analysis results summarized in Figure 3.34 indicate that the bearing capacity values estimated using both *MESA* with the fitting parameter, $\psi = 3.5$ and *MTSA* can provide good estimates.

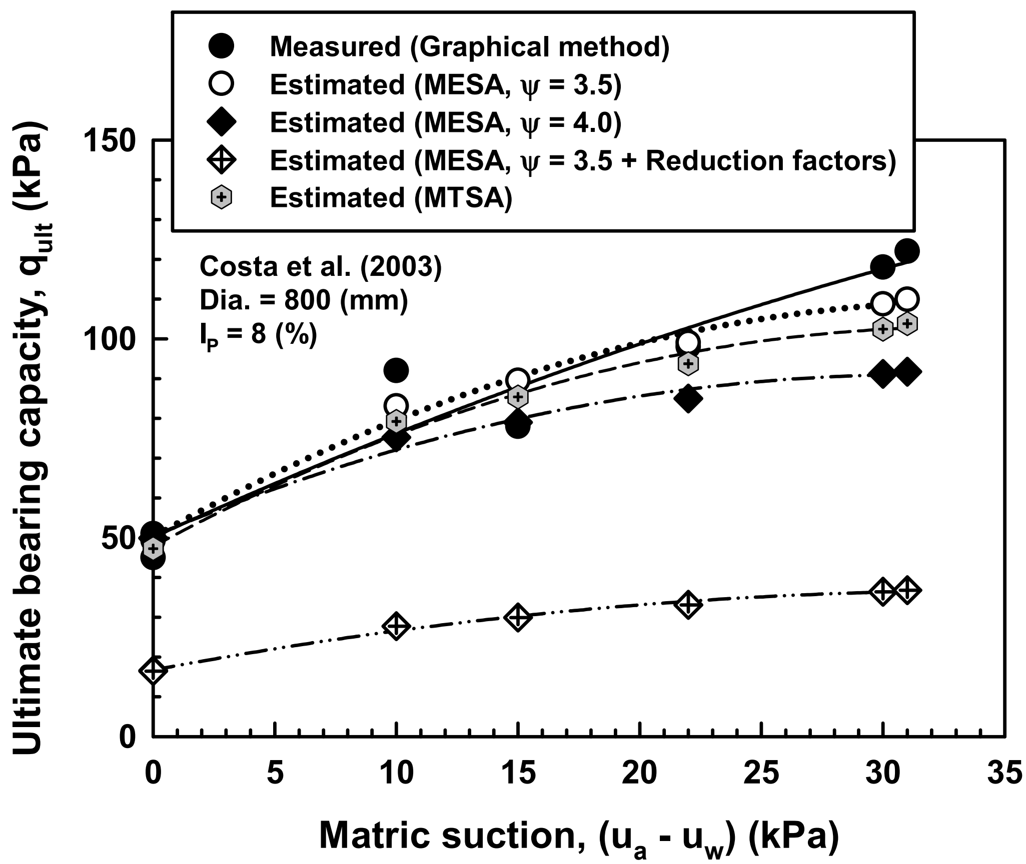

Figure 3.34 Comparison between the measured and the estimated bearing capacity values using different approaches [data from Costa et al. (2003)].

Figure 3.35 show the comparison between the measured and the estimated bearing capacity values for the data by Rojas et al. (2007). The undrained shear strength for saturated condition required to estimate the variation of bearing capacity of unsaturated fine-grained soils [i.e. Eq. (3.14)] were not available in the literature; therefore, it was back-calculated using Skempton (1948) equation and estimated to be equal to 20 kPa. This undrained shear strength for saturated condition is approximately the same as the value obtained from cone penetration tests for the Lean clay close to the ground surface under the saturated condition (Rollins et al. 2009). The bearing capacity values estimated using the *MESA* were underestimated when the calculation is conducted with the fitting parameter, $\psi = 5.34$ ($I_p = 8\%$) based on Eq. (3.7). On the contrary, good agreement was observed when the bearing capacity values were estimated using both *MESA* with $\psi = 3.5$ and *MTSA*.

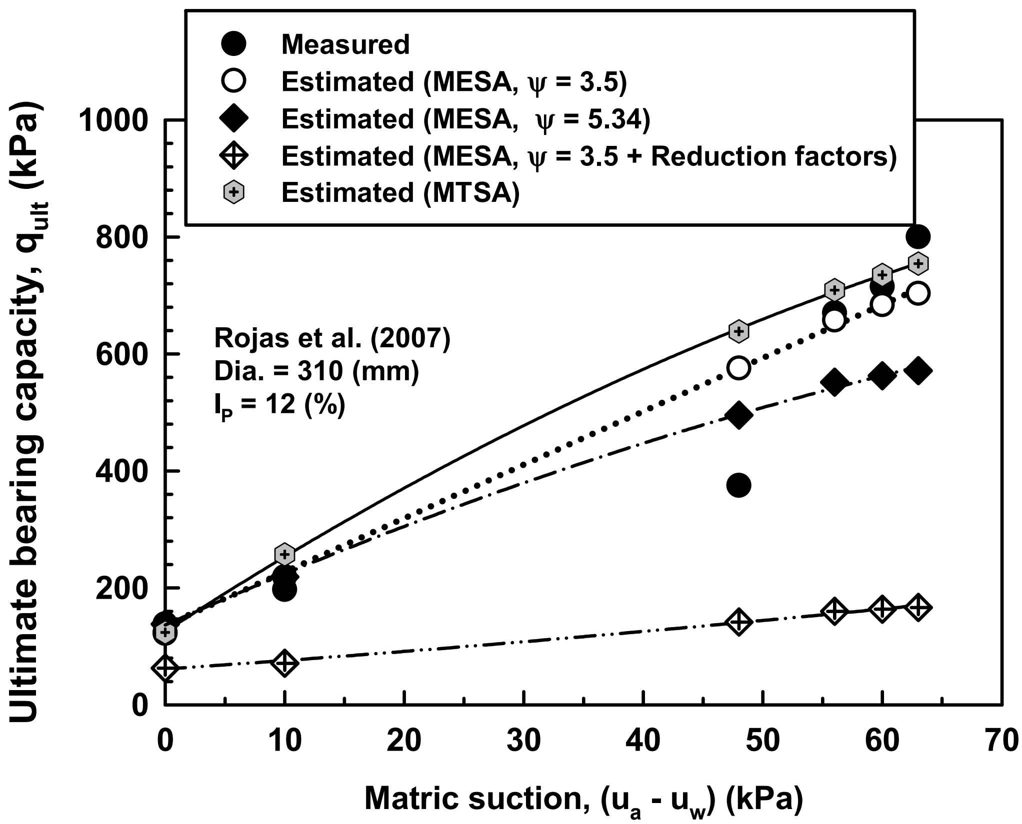

Figure 3.35 Comparison between the measured and the predicted bearing capacity values using different approaches [data from Rojas et al. (2007)].

The results in Figure 3.34 and Figure 3.35 suggest that the *MTSA* can be effectively used to estimate the bearing capacity of unsaturated fine-grained soils of various I_p values. However, the *MESA* did not provide good comparison when the bearing capacity values were calculated using the ψ values based on relationship between I_p and ψ proposed by Vanapalli and Mohamed (2007) [Eq. (3.7)]. According to Eq. (3.7), the fitting parameter, ψ increases nonlinearly with increasing I_p. However, the two new points obtained from the analysis shown in Figure 3.34 and Figure 3.35 indicates that ψ values are constant for the I_p values of 8% and 12% (Figure 3.36). This different behavioral trend in the fitting parameter, ψ can be explained offering the following two reasons. Firstly, the two hollow square points (□) in Figure 3.36 were obtained using only one data point, which means ψ values may not represent the variation of bearing capacity over a wide range of suction. Secondly, the ψ values obtained from both the previous (Vanapalli and Mohamed 2007) and present study may be considered to be reasonable as the parameter ψ may also be influenced by the drainage condition (or rate of loading). In other words, it is likely that different rates of loading can lead to different values of ψ even at the same I_p value. Hence, more studies are necessary to investigate the effect of rate of loading on the fitting parameter, ψ for various unsaturated fine-grained soils.

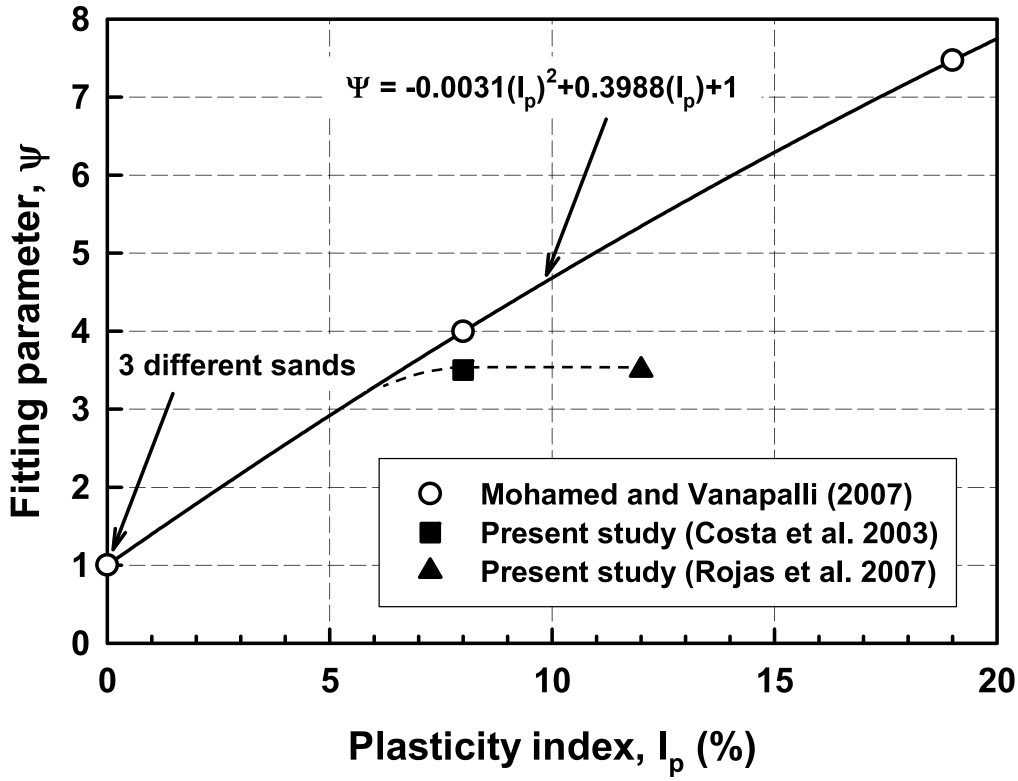

Figure 3.36 Relationship between plasticity index and the fitting parameter, ψ.

3.10 Bearing Capacity of Low Plastic Unsaturated Soils

From the studies and discussion in earlier sections, it can be seen that the bearing capacity of unsaturated coarse- (i.e. I_p = 0 %) and fine-grained soils (8 ≤ I_p (%) ≤ 60) can be more reliably estimated using the *MESA* and the *MTSA*, respectively. In this section, an attempt is made to estimate the bearing capacity of a low plastic unsaturated soil (I_p = 6%) using both the *MESA* and the *MTSA*.

3.10.1 Testing Program and Soil Properties

Oloo (1994) performed model footing (i.e. $B \times L$ = 30 mm × 30 mm and 30 mm in diameter) tests in an unsaturated fine-grained soil (Botkin silt, I_p = 6%) for five different matric suction values (i.e. 0, 25, 50, 75, 100 kPa). In this section, the model footing test results for the square footing are analyzed using both the *MESA* [Eq. (3.6)] and the *MTSA* [Eq. (3.10)] to check the validity of the two methods for low plastic unsaturated soils.

The experiments were carried out using a specially designed mould equipped with thermal conductivity sensors and ceramic disc [air-entry value, $(u_a - u_w)_b$ = 500 kPa] installed on the cylinder and on the bottom plate, respectively (Figure 3.37). The thermal conductivity sensors were used to measure matric suction values for the specimens that were statically compacted at different water contents. The specimens compacted at the same water content (i.e. 18%) and density conditions were first saturated by allowing water to flow under a small head of water in a temperature and humidity controlled room. The predetermined matric suction values were then achieved by applying air-pressure from the top of the compacted specimens extending the axis-translation technique (Hilf 1956). The model footings were loaded at a rate of 0.18 mm/min after the matric suction values in the compacted specimens reached equilibrium conditions.

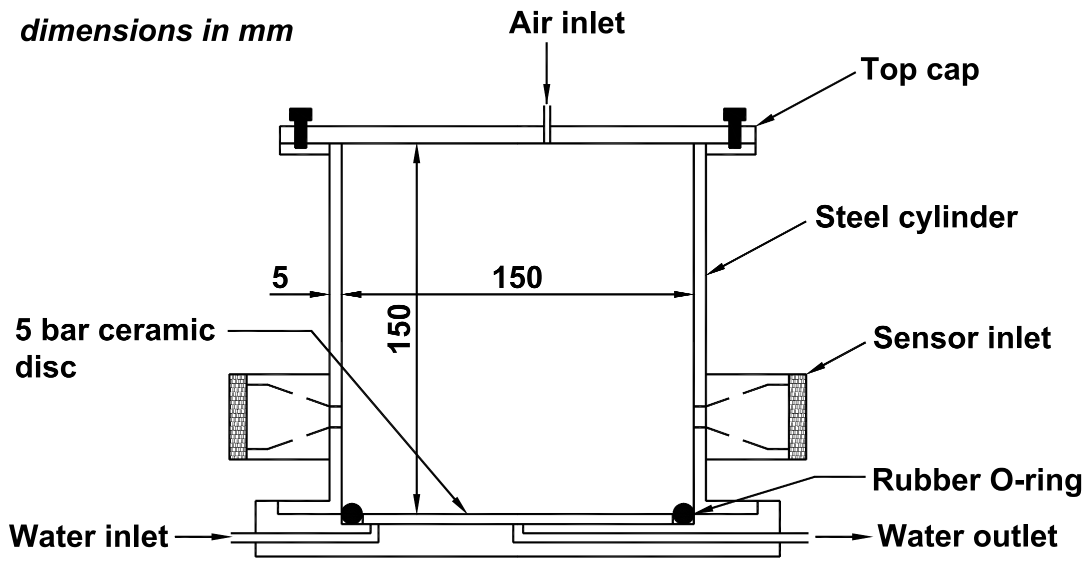

Figure 3.37 Mould used for compaction and model footing tests (Oloo 1994).

Figure 3.38 and Figure 3.39 show the grain size distribution curve and the *SWCC* for the Botkin silt used by Oloo (1994). The reasons associated with showing the grain size distribution curve and the *SWCC* for the Botkin silt used by Vanapalli et al. (2000) will be discussed later in this section. The effective shear strength parameters, c' and ϕ' were estimated to be 2.5 kPa and 28.1° from consolidated drained direct shear tests (Figure 3.40).

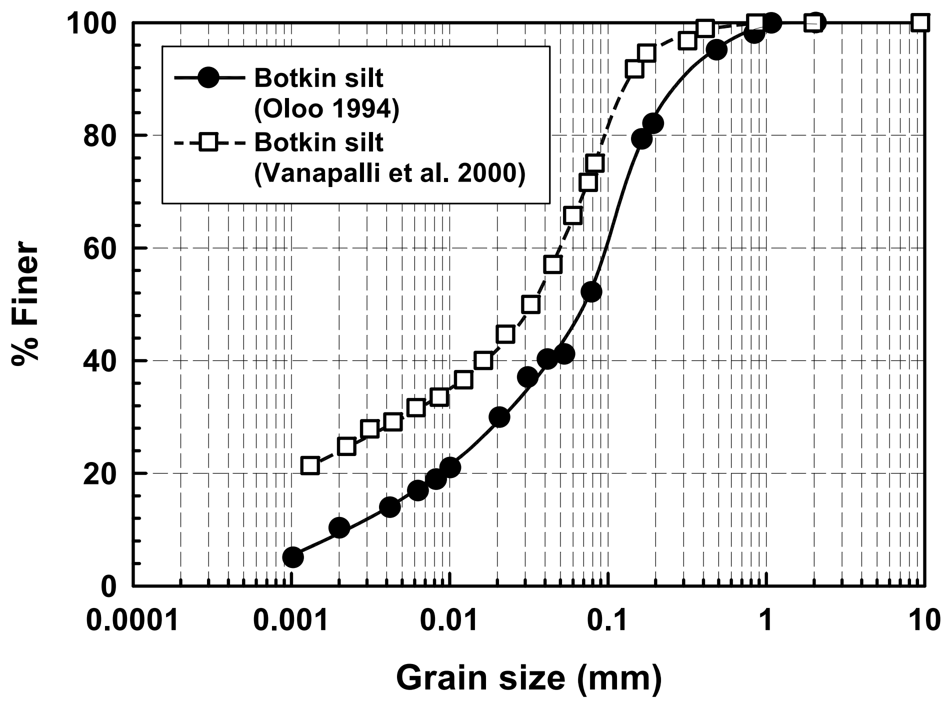

Figure 3.38 Grain size distribution curves for the Botkin silts used by Oloo (1994) and Vanapalli et al. (2000).

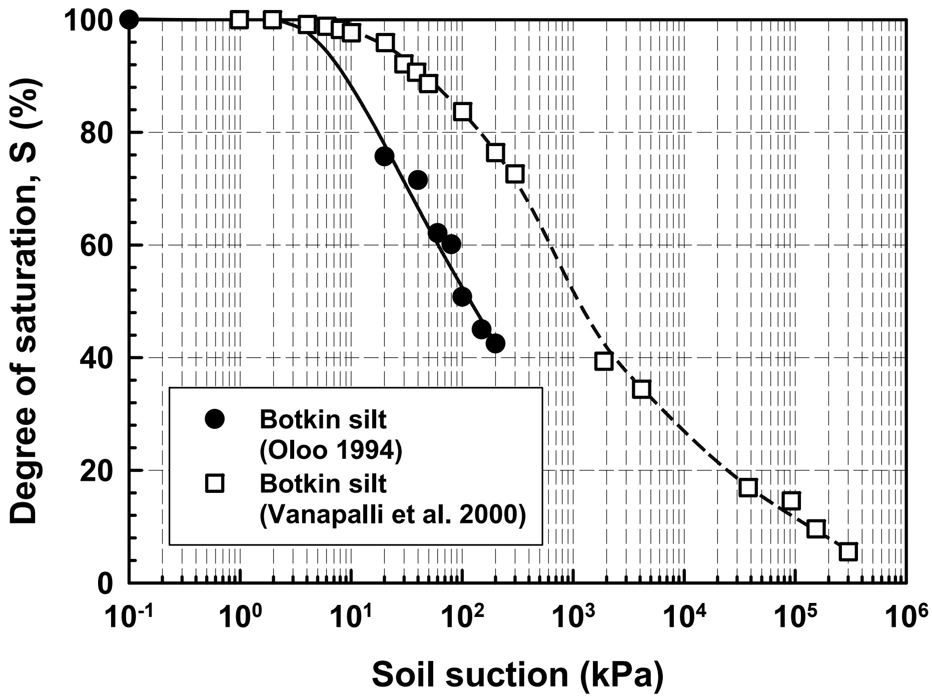

Figure 3.39 *SWCC*s for the Botkin silts used by Oloo (1994) and Vanapalli et al. (2000).

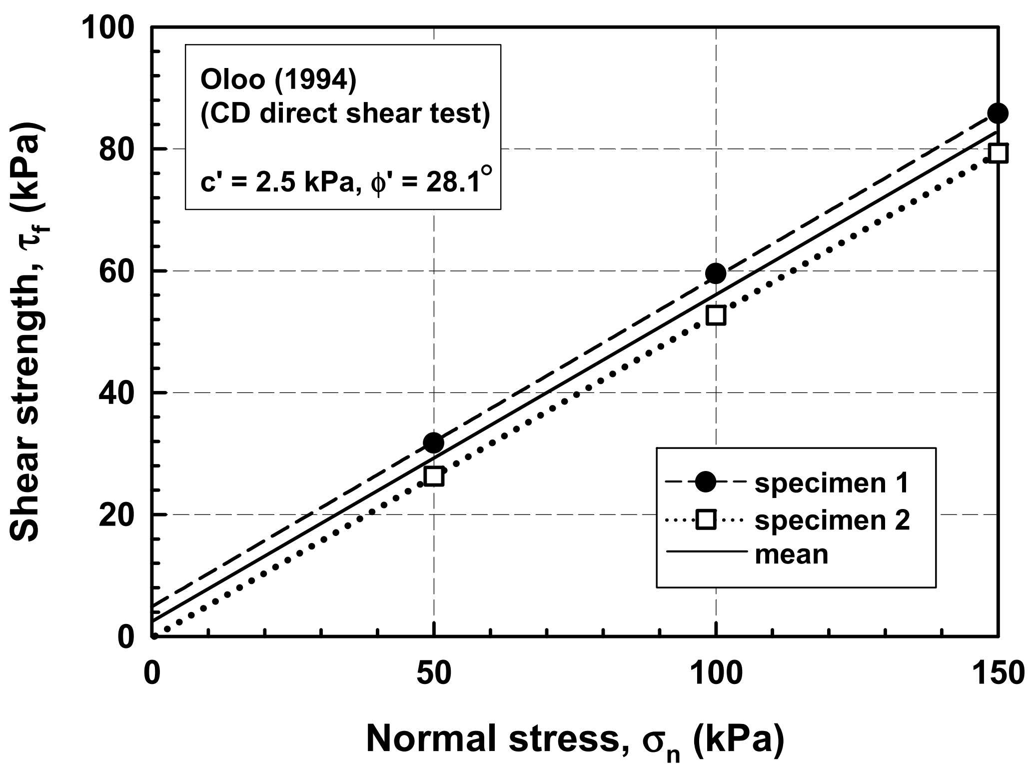

Figure 3.40 Effective shear strength envelopes for Botkin silt used by Oloo (1994).

3.10.2 Comparison between the Measured and the Estimated Bearing Capacity Values

3.10.2.1 Analysis using the Modified Effective Stress Approach

Figure 3.41 shows the comparison between the measured bearing capacity values and those estimated using the *MESA* for different ψ values assuming general shear failure mode. According to Eq. (3.7), the fitting parameter, ψ is estimated to be 3 for I_p = 6%. As can be seen, the bearing capacity values were overestimated when calculated using the ψ values less than 5. This discrepancy increases with decreasing ψ value. The details are summarized in Table 3.7.

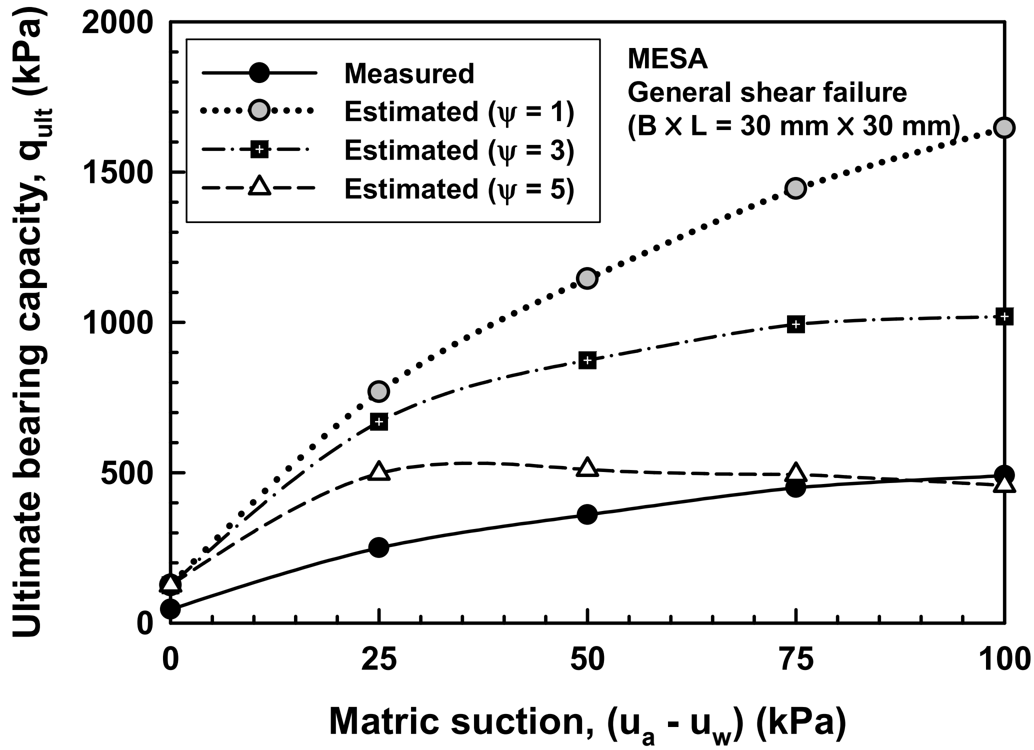

Figure 3.41 Comparison between the measured and the estimated bearing capacity values using the *MESA* assuming general shear failure mode.

Table 3.7 Measured bearing capacity (*BC*) values and those estimated using the *MESA* assuming general shear failure mode.

$(u_a - u_w)$ (kPa)	Measured *BC* (kPa)	Estimated *BC* (kPa)		
		$\psi = 1$	$\psi = 3$	$\psi = 5$
0	45	126	126	126
25	250	769	595	498
50	360	1145	699	510
75	450	1444	733	494
100	490	1646	701	457

Figure 3.42 shows the comparison between the measured bearing capacity values and those estimated using the *MESA* for different ψ values assuming local (or punching) shear failure mode. The details are summarized in Table 3.8. Good comparison was obtained when the bearing capacity values were estimated using $\psi = 1$; on the other hand, the bearing capacity values were significantly underestimated when calculated using $\psi = 3$.

.

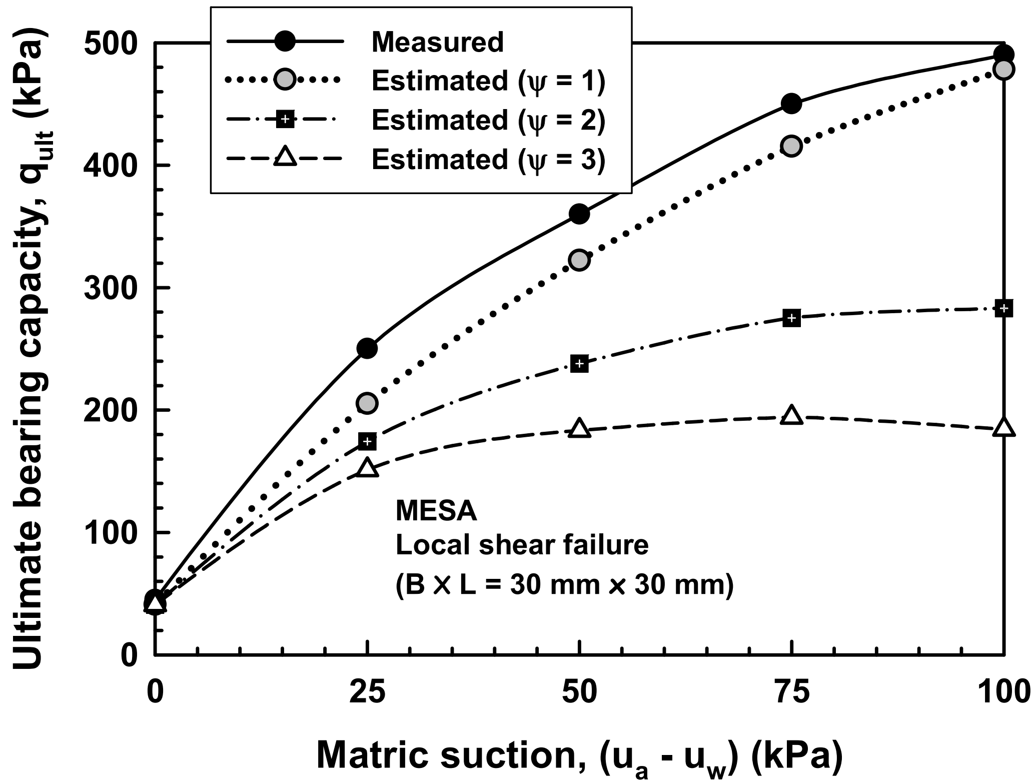

Figure 3.42 Comparison between the measured and the estimated bearing capacity values using the *MESA* assuming local shear failure mode.

Table 3.8 Measured bearing capacity (*BC*) values and those estimated using the *MESA* assuming local shear failure mode.

$(u_a - u_w)$ (kPa)	Measured *BC* (kPa)	Estimated *BC* (kPa)		
		$\psi = 1$	$\psi = 2$	$\psi = 3$
0	45	41	41	41
25	250	205	174	151
50	360	322	238	183
75	450	415	275	194
100	490	478	283	184

The results in Figure 3.41 and Figure 3.42 show that the best comparison between the measured and the estimated bearing capacity values can be obtained when the bearing capacity values are estimated using $\psi = 1$ assuming local (or punching) shear failure mode. This may be attributed to the fact that the mechanical properties of low plastic soils lie between coarse- and fine-grained soils since $\psi = 1$ is required for unsaturated coarse-grained soils and the local (or punching) shear failure is typical failure mode in unsaturated fine-grained soils.

3.10.2.2 Analysis using the Modified Total Stress Approach

The unconfined compression test results for the saturated condition [i.e. $q_{u(sat)}$] was not available in the literature (i.e. Oloo 1994); therefore, it was back-calculated using the measured bearing capacity value for the saturated condition (i.e. 14.6 kPa). The $q_{u(sat)}$ value for the Botkin silt (I_p = 8%) experimentally determined by Vanapalli et al. (2000) was 13 kPa. The variation of undrained shear strength, c_u with respect to matric suction was estimated using Eq. (3.13). As explained in section 3.8, $\upsilon = 2$ is required for fine-grained soils and $\mu = 9$ can be used for the I_p values in the range of 8% to 15.5%. However, the I_p value of the soil (i.e. I_p = 6%) used in the present study does not fall in this range. Hence, the analyses were carried out for both $\upsilon = 1$ and 2 with different μ values.

Figure 3.43 (and Table 3.9) and Figure 3.44 (and Table 3.10) provide the comparison between the measured bearing capacity values and those estimated using the **MTSA** for different μ values with $\upsilon = 1$ and 2. The best comparisons were obtained with the combinations of ($\upsilon = 1$, $\mu = 5$) and ($\upsilon = 2$, $\mu = 3$). This indicates that the bearing capacity of low plastic unsaturated fine-grained soils can be estimated using either $\upsilon = 1$ or 2 with low μ values. This may be attributed to the fact that the mechanical properties of low plasticity soils lie between coarse- and fine-grained soils. Similar trends in results were also observed from the analyses using the *MESA*.

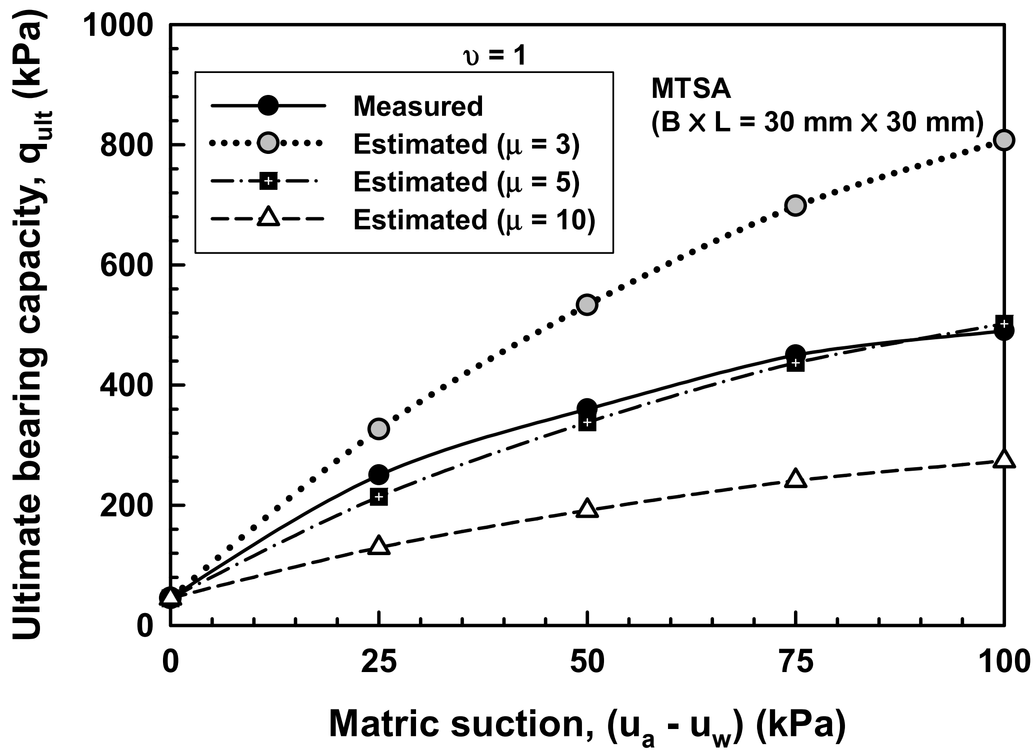

Figure 3.43 Comparison between the measured bearing capacity values and those estimated using the *MTSA* ($\upsilon = 1$ and different μ values).

Table 3.9 Measured bearing capacity (*BC*) values and those estimated using the *MTSA* ($\upsilon = 1$ and different μ values).

$(u_a - u_w)$ (kPa)	Measured *BC* (kPa)	Estimated *BC* (kPa) ($\upsilon = 1$)		
		$\mu = 3$	$\mu = 5$	$\mu = 10$
0	45	45	45	45
25	250	326	214	129
50	360	533	338	191
75	450	698	437	241
100	490	807	502	274

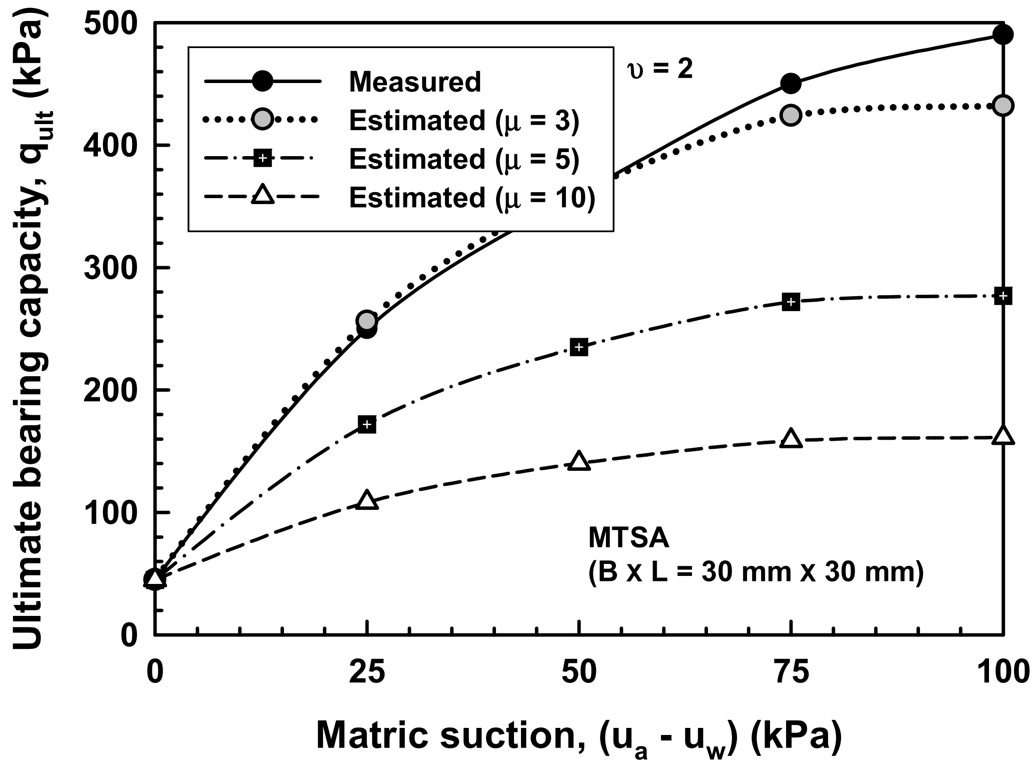

Figure 3.44 Comparison between the measured bearing capacity values and those estimated using the *MTSA* ($\upsilon = 2$ and different μ values).

Table 3.10 Measured bearing capacity (*BC*) values and those estimated using the *MTSA* ($\upsilon = 2$ and different μ values).

$(u_a - u_w)$ (kPa)	Measured *BC* (kPa)	Estimated *BC* (kPa) ($\upsilon = 2$)		
		$\mu = 3$	$\mu = 5$	$\mu = 10$
0	45	45	45	45
25	250	256	172	108
50	360	362	235	140
75	450	424	272	159
100	490	432	277	161

3.10.3 Fitting Parameters for the Bearing Capacity of Low Plastic Unsaturated Fine-Grained Soils

The fitting parameters obtained from the *MESA* and *MTSA* for the low plastic fine-grained soil are summarized in Table 3.11.

Table 3.11 Fitting parameters to estimate the bearing capacity of the unsaturated low plastic soil using the *MESA* and the *MTSA*.

Fitting parameters	*MESA* [Eq. (3.6)]		*MTSA* [Eq. (3.10)]		
	Previous study [Eq. (3.7)]	Current study	$8 \leq I_p$ (%) ≤ 60	Current study (I_p = 6%)	
ψ	3	1 (with reduction factors approach)			
υ			2	1	2
μ			$f(I_p)$ [Eq. (3.15)]	5	3

According to Vanapalli and Mohamed (2007), the fitting parameters, $\psi = 3$ [Eq. (3.7)] is required to estimated the bearing capacity using the *MESA*. However, the analyses results showed that $\psi = 1$ assuming local shear failure can provide good estimates for low plastic unsaturated fine-grained soils instead of $\psi = 3$. In case of the *MTSA*, both $\upsilon = 1$ and 2 can provide good comparisons between the measured and the estimated bearing capacity values for low plastic unsaturated fine-grained soils with μ values less than 10.

Vanapalli et al. (2000) conducted unconfined compression tests on Botkin silt (hereafter referred to as Botkin_V). The I_p value of the soil was estimated to be 8% that is 2% higher compared to the Botkin silt used by Oloo (1994) (hereafter referred to as Botkin_O). This may be attributed to the collection of samples at different periods of time and also due to the different procedures used in the preparation of the natural soil sample collected. As can be seen in Figure 3.38, the Botkin_V is finer than that of Botkin_O, which leads to higher degree of saturation at the same matric suction values (see Figure 3.39). Figure 3.45 shows the comparison between the measured undrained shear strength values and those estimated using Eq. (3.13) with $\upsilon = 2$ and $\mu = 9$ for the Botkin_V. There is a good agreement between the measured and the estimated undrained shear strength values. However, as discussed with Figure 3.44, good comparison between the measured and the estimated bearing capacity values was not observed for the Botkin_O with the same fitting parameter (i.e. $\upsilon = 2$ and $\mu = 10$). Hence, it can be concluded that the mechanical properties of unsaturated low plasticity soils lie between coarse- and fine-grained soils and the bearing capacity of low plastic unsaturated fine-grained soils can be more reliably estimated using the fitting parameters, ψ and υ proposed for coarse-grained soils.

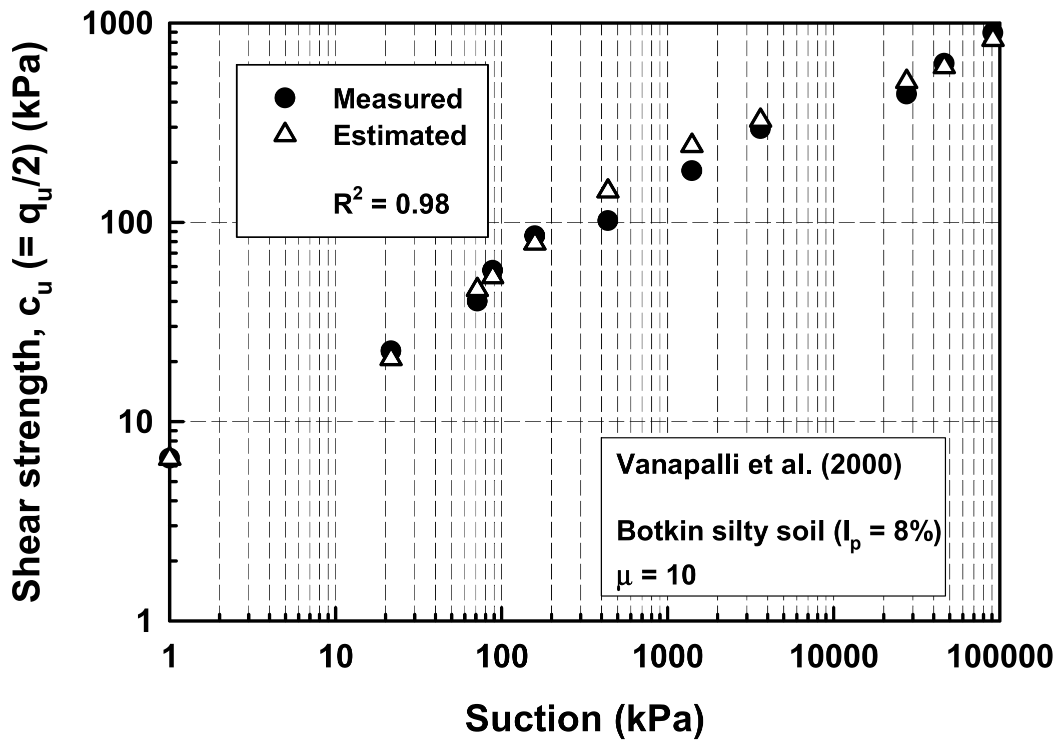

Figure 3.45 Comparison between measured and estimated unconfined compressive strength of Botkin silt used by Vanapalli et al. (2000).

3.11 Summary and Conclusions

Several researchers have attempted to interpret the in-situ plate load tests results in unsaturated fine-grained soils considering the influence of matric suction extending the effective stress approach (i.e. Modified Effective Stress Approach, *MESA*). The *MESA* can be reasonably used for the unsaturated coarse-grained soils since the drainage conditions for both pore-air and pore-water are under drained condition during loading stages. However, there are limitations to interpret the plate load tests results in unsaturated fine-grained soils using the *MESA* due to the following reasons.

(i) The drainage condition of pore-air and pore-water cannot be clearly defined during loading stages.

(ii) The constant ϕ^b value over a large suction range can lead to significant differences compared to the measured bearing capacity values.

(iii) Limitation of using constant ϕ^b value can be overcome by analyzing the in-situ plate load tests results with the model proposed by Vanapalli and Mohamed (2007). However, this model is only useful for the suction values less than residual suction value.

(iv) Reduction factors approach cannot be generalized for all types of soils and suction values.

To overcome the limitations of the *MESA* for unsaturated fine-grained soils, in this chapter, an attempt is made to interpret the model footing tests results extending total stress approach (i.e. Modified Total Stress Approach, *MTSA*). The experimental program involves conducting a series of model footing ($B \times L$ = 50 mm × 50 mm) tests on statically compacted soil for five different matric suction distribution profiles with depth. The analyses results showed that the bearing capacity of unsaturated fine-grained soils can be more reliably estimated using the *MTSA* rather than *MESA*. The justification of the *MTSA* was also tested on the in-situ plate load tests results in an unsaturated fine-grained soil (Consoli et al. 1998).

In addition, a semi-empirical model is proposed to estimate the variation of undrained shear strength of unsaturated fine-grained soils with respect to matric suction. This model can be effectively used to estimate the variation of bearing capacity of unsaturated fine-grained soils with respect to matric suction since, according to this study, the bearing capacity of unsaturated fine-grained soils is function of only shear strength.

Finally, the model footing test results in a low plastic unsaturated fine-grained soil (i.e. I_p = 6%) were analyzed using both the *MESA* and the *MTSA*. The analyses results showed that the bearing capacity of low plastic unsaturated fine-grained soils can be interpreted using both the *MESA* and the *MTSA*.

REFERENCES

Adams, M.T. and Collin, J.G. 1997. Large model spread footing load tests on geosynthetic reinforced soil foundations. *Journal of Geotechnical and Geoenvironmental Engineering*, 123(1): 66-72.

Agarwal, K.B. and Rana, M.K. 1987. Effect of ground water on settlement of footing in sand. *In* Proceedings of the 9th European Conference on Soil Mechanics and Foundation Engineering, Dublin, 751-754.

Aitchison, G.D. 1957. The strength of quasi-saturated and unsaturated soils in relation to the pressure deficiency in the pore water. *In* Proceedings of the 4th International Conference on Soil Mechanics and Foundation Engineering, London, 135-139.

ASTM D1194-94. 2003. Standard test method for bearing capacity of soil for static load and spread footings. Annual book of ASTM Standards, ASTM International, West Conshohocken, PA.

ASTM D2325-68. 2000. Standard test method for capillary-moisture relationships for coarse and medium textured soils by pressure-plate apparatus. Annual book of ASTM Standards, ASTM International, West Conshohocken, PA.

Babu, G.L.S., Rao, R.S., and Peter, J. 2005. Evaluation of shear strength functions based on soil water characteristic curves. *Journal of Testing and Evaluation*, 33(6): 461-465.

Bera, A.K., Ghosh, A. and Ghosh, A. 2007. Behavior of model footing on pond ash. *Geotechnical and Geological Engineering*, 25(3): 315-325.

Brooks, R.H. and Corey, A.T. 1964. Hydraulic properties of porous media. Hydrol. Paper 3. Colorado State Univ., Fort Collins, CO, USA.

Cerato, A.B. and Lutenegger, A.J. 2007. Scale effects of shallow foundation bearing capacity on granular material. *Journal of Geotechnical and Geoenvironmental Engineering*, 133(3): 1192-1202.

Chen, J. C. 1984. Evaluation of strength parameters of partially saturated soils on the basis of initial suction and unconfined compression strength. Asian Institute of Technology Report, Bangkok, Thailand.

Consoli, N.C., Schnaid, F. and Milititsky, J. 1998. Interpretation of plate load tests on residual soil site. *Journal of Geotechnical and Geoenvironmental Engineering*, 124(9): 857-867.

Costa, Y.D., Cintra, J.C. and Zornberg, J.C. 2003. Influence of matric suction on the results of plate load tests performed on a lateritic soil deposit. *Geotechnical Testing journal*, 2(2): 219-226.

Dash, S.K., Sireesh, S. and Sitharam, T.G. 2003. Model studies on circular footing supported on geocell reinforced sand underlain by soft clay. *Geotextiles and Geomembranes*, 21(4): 197-219.

Fredlund, D.G., Xing, A., Fredlund, M.D. and Barbour, S.L. 1996. Relationship of the unsaturated soil shear strength functions to the soil-water characteristic curve. *Canadian Geotechnical Journal*, 33(3): 440-448.

Gan, J.K-M., Fredlund, D.G. and Rahardjo, H. 1988. Determination of the shear strength parameters of an unsaturated soil using the direct shear test. *Canadian Geotechnical Journal*, 25(3): 500-510.

Garven, E. and Vanapalli, S.K. 2006. Evaluation of empirical procedures for predicting the shear strength of unsaturated soils. *In* Proceedings of the 4th International Conference on Unsaturated Soils, Carefree, 147(2): 2570–2581.

Hanna, A. and Abdel-Rahman, M. 1998. Experimental investigation of shell foundations on dry sand. *Canadian Geotechnical Journal*, 35(5): 847-857.

Hilf, J.W. 1956. An investigation of pore water pressure in compacted cohesive soils. US Bureau of Reclamation, Tech. Mem. 654, Denver: US Beuea of Reclamation.

Kumbhokjar, A.S. 1993. Numerical evaluation of Terzaghi's N_γ. *Journal of Geotechnical Engineering*, 119(3): 598– 607.

Meyerhof, G. C. 1963. Some recent research on the bearing capacity of foundations. *Canadian Geotechnical Journal*, 1(1): 16-26.

Mohamed, F.M.O. and Vanapalli, S.K. 2006. Laboratory investigations for the measurement of the bearing capacity of an unsaturated coarse-grained soil. *In* Proceedings of the 59th Canadian Geotechnical Conference, Vancouver, 219-226.

Oh, W.T. and Vanapalli, S.K. 2011. Modelling the applied vertical stress and settlement relationship of shallow foundations in saturated and unsaturated sands. *Canadian Geotechnical Journal*, 48(3): 425-438.

Oh, W.T., Vanapalli, S.K. and Puppala, A.J. 2009. A semi-empirical model for the prediction of modulus of elasticity for unsaturated soils. *Canadian Geotechnical Journal*, 46(8): 903-914.

Oloo, S.Y. 1994. A bearing capacity approach to the design of low-volume traffic roads. PhD thesis, Civil Engineering, University of Saskatchewan, Saskatoon, Canada.

Oloo, S.Y., Fredlund, D.G. and Gan, J.K-M. 1997. Bearing capacity of unpaved roads. *Canadian Geotechnical Journal*, 34(3): 398-407.

Pineda, J.A. and Colmenares, J.E. 2005. Influence of matric suction on the shear strength of compacted Kaolin under unconfined conditions: Experimental results (Part 1). *In* Proceedings of the International Symposium on Advanced Experimental Unsaturated Soil Mechanics, Trento, 215-220.

Poulos, H.D. and Davis E.H. 1974. *Elastic solutions for soil and rock mechanics*. John Wiley and Sons, NY, USA.

Power, K.C. and Vanapalli, S.K. 2010. Modified null pressure plate apparatus for measurement of matric suction. *Geotechnical Testing Journal*, 33(4): 335-341.

Rahardjo, H., Heng, O.B. and Leong, E.C. 2004. Shear strength of a compacted residual soil from consolidated drained and the constant water content tests. *Canadian Geotechnical Journal*, 41(3), 421-436.

Ridley, A.M. 1993. The measurement of soil moisture suction, PhD Thesis, University of London.

Rojas, J.C., Salinas, L.M. and Seja, C. 2007. Plate-load tests on an unsaturated lean clay. *In* Proceeding of the 2nd International Conference on Unsaturated Soils, Weimar, 445-452.

Rollins, K.M., Adsero, M.E. and Brown, D.A. 2009. Jet grouting to increase lateral resistance of pile group in soft caly. *In* Proceedings of the International Foundations Congress and Equipment Expo, ASCE, Orlando, 265-271

Schnaid, F., Consoli, N.C., Cumdani, R. and Milititsky, J. 1995. Load-settlement response of shallow foundations in structured unsaturated soils. *In* Proceedings of the 1st International Conference on Unsaturated Soils, Paris, 999-1004.

Skempton, A.W. 1948. The $\phi_u = 0$ analysis for stability and its theoretical basis. *In* Proceedings of the 2nd International Conference of Soil Mechanics and Foundation Engineering, 1, 72-77.

Steensen-Bach, J.O. and Salinas L.M. 1987. Capillary induced stresses – fact of fiction?. *In* Proceedings of the 9th European conference on Soil Mechanics and Foundation Engineering, Budapest, 83-89.

Terzaghi, K. 1943. *Theoretical Soil Mechanics*. John Wiley and Sons, New York, NY, USA.

van Genuchten, M.Th. 1980. A closed-form equation of predicting the hydraulic conductivity of unsaturated soils. S*oil Science Society of American Journal*, 44: 892-898.

Vanapalli, S.K., Fredlund, D. G., Pufahl, D. E., and Clifton, A. W. 1996. Model for the prediction of shear strength with respect to soil suction. *Canadian Geotechnical Journal*, 33(3): 379-392.

Vanapalli, S.K. and Mohamed, F.M.O. 2007. Bearing capacity of model footings in unsaturated soils. *In* Proceedings of the 2nd International Conference on Unsaturated Soils, Weimar, 483-493.

Vanapalli, S.K. and Oh, W.T. 2011. Simple techniques for the estimation of suction in compacted soils in the range of 0 to 60,000 kpa. *Geotechnical Testing Journal*, 36(6).

Vanapalli, S.K., Wright, A. and D.G. Fredlund. 2000. Shear strength of two unsaturated silty soils over the suction range from 0 to 1,000,000 kPa. *In* Proceedings of the 53rd Canadian Geotechnical Conference, Montreal, 1161-1168.

Vesić, A.B. 1963. Bearing capacity of deep foundations in sand. Highway Research Records, 39, National Academy of Sciences, National Research Council, 112-153.

Vesić A.B. 1973. Analysis of ultimate loads of shallow foundations. *Journal of the Soil Mechanics and Foundation Division*, ASCE 99(SM1): 45-73.

Xu, Y.F. 2004. Fractal approach to unsaturated shear strength. *Journal of Geotechnical and Geoenvironmental Engineering*, 130(3): 264-273.

Yamamoto, N., Randolph, M.F. and Einav, I. 2008. Simple formulas for the response of shallow foundations on compressible sands. *International Journal of Geomechanics*, ASCE, 8(4): 230-239.

CHAPTER 4

ELASTIC MODULUS OF UNSATURATED SOILS

4.1 Introduction

Bearing capacity and settlement are two key parameters that have a significant influence on the design of shallow foundations. However, it is the settlement behavior that typically governs the design of shallow foundations in comparison to the bearing capacity in several scenarios. This is particularly true for coarse-grained soils such as sands since, in sandy soils, (i) the differential settlements are predominant in comparison to clayey soils because sand deposits are typically heterogeneous in nature and (ii) the settlements occur quickly and may cause significant damages to the superstructures immediately after the construction (Maugeri et al. 1998). Foundation codes also suggest restricting the settlement of shallow foundations placed in coarse-grained soils to 25 mm and limiting their differential settlements (CFEM 2006).

Foundations are conventionally designed assuming that the soils in which they are placed are in a state of saturated condition. This implies that the concepts of conventional soil mechanics may not be valid in the estimation of elastic settlement of foundations if the soils are in a state of unsaturated conditions. Due to this reason, some investigations have been performed to study the contribution of matric suction towards the bearing capacity of unsaturated sandy soils (Steensen-Bach et al. 1987, Mohamed and Vanapalli 2006). However, there is limited information in the literature with respect to the estimation of elastic settlement behavior of shallow foundations in unsaturated sandy soils.

Elastic modulus is a key parameter in the estimation of elastic settlement of shallow foundations. This value is typically assumed to be constant both below and above the ground water table in homogeneous soil deposits. In other words, the influence of capillary or matric suction (i.e. unsaturated conditions) on the elastic modulus is not taken into account. A close examination of the experimental results of the vertically applied stress versus surface settlement (hereafter referred to as stress versus settlement) behaviors from the model footing tests conducted on soils that are in a state of unsaturated condition show that the elastic modulus is significantly influenced by matric suction (Vanapalli and Mohamed 2007).

In this chapter, a semi-empirical model is proposed to estimate the variation of initial tangent elastic modulus with respect to matric suction. The proposed model requires the *SWCC* and the initial tangent elastic modulus under saturated condition along with two fitting parameters, α and β.

4.2 Settlement of Foundations

The settlement of foundations consists of three components [Eq. (4.1)].

$$\delta = \delta_i + \delta_c + \delta_s \tag{4.1}$$

where δ = total settlement, δ_i = elastic settlement, δ_c = consolidation settlement, and δ_s = secondary settlement (or creep)

In the case of coarse-grained soils, elastic settlement occurs under drained loading conditions. The total settlement in sands is associated only with elastic settlement as there will be no (or negligible) primary or secondary consolidation settlement. The foundation settlement in sands is conventionally estimated based on the theory of elasticity using two soil parameters; modulus of elasticity, E and Poisson's ratio, ν.

The elastic modulus, E can be estimated both from laboratory and field tests. In general, the elastic modulus from conventional triaxial tests can be underestimated due to sample disturbance caused by stress relief and other mechanical disturbances. To overcome this disadvantage, Davis and Poulos (1968) suggested the use of K_0 – consolidation triaxial test results to derive elastic modulus. According to the test results by Simons and Som (1970), the elastic modulus from K_0 – consolidation triaxial tests are significantly higher than those determined from conventional undrained triaxial tests.

Plate load tests, cone penetration tests, pressuremeter tests or geophysical methods (i.e. seismic methods) are usually used to estimate in-situ elastic modulus. In case of plate load test (or model footing tests), the initial tangent elastic modulus, E_i can be calculated using Eq. (4.2) (Timoshenko and Goodier 1951). The calculation of initial tangent elastic modulus is illustrated in Figure 4.1.

$$E_i = \frac{\left(1-\nu^2\right)}{\left(\Delta\delta / \Delta q\right)} I_w B = k_{is}\left(1-\nu^2\right) I_w B \tag{4.2}$$

where E_i = initial tangent elastic modulus, k_{is} = initial tangent modulus of subgrade reaction ($=\Delta q/\Delta\delta$), Δq = increment of applied stress in elastic range, $\Delta\delta$ = increment of settlement in elastic range, ν = Poisson's ratio (a value of 0.3 was used for this study assuming drained loading conditions for the sands studied), B = width (or diameter) of plate, and I_w = influence factor (i.e. 0.79 for circular plate and 0.88 for square plate).

The initial tangent elastic modulus determined using Eq. (4.2) is representative of soils within a depth zone which is approximately 1.5B - 2.0B from the soil surface (Poulos and Davis 1974, Agarwal and Rana 1987) (see section 3.5.2 for more details).

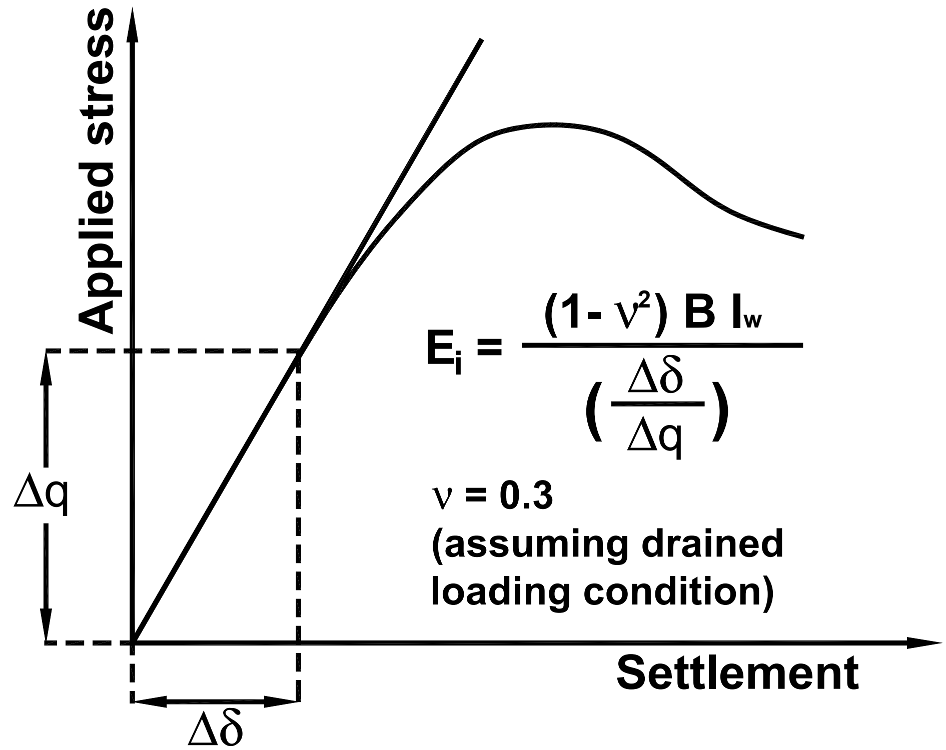

Figure 4.1 Estimation of initial tangent elastic modulus from plate load test.

4.3 Estimation of Initial Tangent Elastic Modulus with respect to Matric Suction

A simple model is proposed in this chapter that can be used to estimate the variation of initial tangent elasticity modulus, E_i with respect to matric suction. For this, first, a model is developed to estimate the variation of initial tangent modulus of subgrade reaction, k_{is} with respect to matric suction using the *SWCC* and the k_{is} under saturated condition [i.e. $E_{i(sat)}$] along with two fitting parameters, α and β as shown in Eq. (4.3). Eq. (4.3) is the same as Eq. (3.13) in form to estimate the variation of undrained shear strength of unsaturated fine-grained soils.

$$k_{is(unsat)} = k_{is(sat)}\left[1+\alpha\frac{(u_a-u_w)}{(P_a/101.3)}\left(S^{\beta}\right)\right] \tag{4.3}$$

where $k_{is(sat)}$, $k_{is(unsat)}$ = initial tangent modulus of subgrade reaction under saturated and unsaturated condition, respectively, S = degree of saturation, α, β = fitting parameters, and P_a = atmospheric pressure (i.e. 101.3 kPa)

Combining Eq. (4.2) and Eq. (4.3), the variation of the initial tangent elastic modulus with respect to matric suction can be estimated using Eq. (4.4).

$$E_{i(unsat)} = E_{i(sat)}\left[1+\alpha\frac{(u_a-u_w)}{(P_a/101.3)}\left(S^{\beta}\right)\right] \tag{4.4}$$

where $E_{i(sat)}$, $E_{i(unsat)}$ = initial tangent elastic modulus under saturated and unsaturated condition, respectively

In Eq. (4.4), the terms, S^{β} controls the nonlinear variation of the modulus of elasticity. The term (P_a/101.3) was used to maintain consistency with respect to the dimensions and units on both sides of the equation. The differential form of Eq. (4.4) [i.e. Eq. (4.5)] can be used to provide mathematical explanations with respect to the nonlinear behavior of initial tangent elastic modulus of unsaturated soils.

$$\frac{dE_{i(unsat)}}{d\left(u_a - u_w\right)} = \frac{E_{i(sat)}\alpha}{\left(P_a / 101.3\right)}\left[\left(S^{\beta}\right) + \left(u_a - u_w\right)\frac{d\left(S^{\beta}\right)}{d\left(\left(u_a - u_w\right)\right)}\right] \tag{4.5}$$

Eq. (4.5) is similar in form to the differential form of the semi-empirical model to estimate the variation of bearing capacity of unsaturated fine-grained soils with respect to matric suction [i.e. Eq. (3.14)]. Eq. (4.5) indicates that the initial tangent elastic modulus, E_i linearly increases up to the air-entry value of the soil. Beyond the air-entry value there is a nonlinear increase of E_i up to a certain matric suction value. The contribution of matric suction towards E_i then starts decreasing as matric suction approaches residual suction. This characteristic behavior is similar to the shear strength and bearing capacity of unsaturated coarse-grained soils (Figure 4.2). More details of the initial tangent elastic modulus and its influence on the elastic settlement with respect to matric suction are offered while analyzing experimental results in later sections of this chapter.

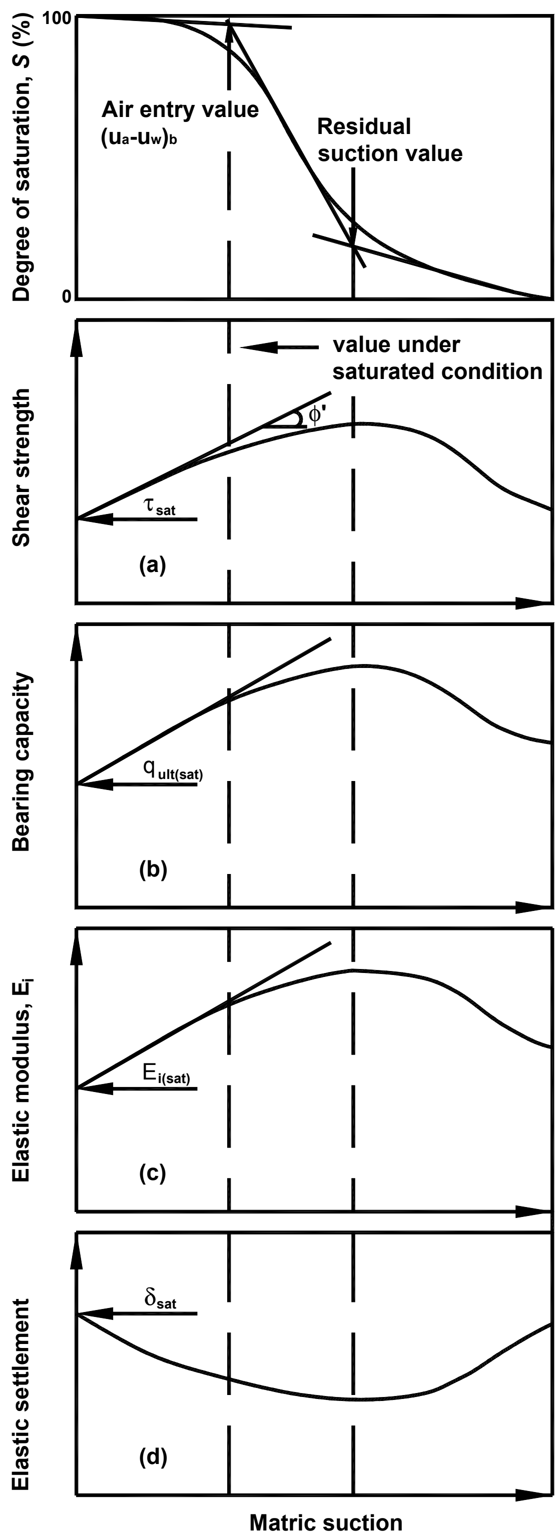

Figure 4.2 *SWCC* and the variation of (a) shear strength, (b) bearing capacity, (c) initial tangent elastic modulus and (d) elastic settlement with respect to matric suction for unsaturated coarse-grained soils.

4.4 Fitting Parameters, α and β for Unsaturated Coarse- Grained Soils

4.4.1 Fitting Parameter, β for Unsaturated Coarse-Grained Soils

A value of $\beta = 1$ can be used to provide good comparisons between measured and estimated elastic modulus for unsaturated coarse-grained soils (i.e. $I_p = 0\%$). This is consistent with the earlier concepts discussed in Chapter 3; namely, drained shear strength of unsaturated coarse-grained soils [$\kappa = 1$ in Eq. (3.4)] and bearing capacity of unsaturated coarse-grained soils [$\psi = 1$ in Eq. (3.6)].

4.4.2 Fitting Parameter, α for Unsaturated Coarse-Grained Soils

To determine the fitting parameter, α, for the unsaturated coarse-grained soils three sets of model footing test results in unsaturated sands are analyzed as follow.

4.4.2.1 Model Footing Tests and Soil Properties

Mohamed and Vanapalli (2006) carried out model footing tests in Unimin sand using two different sizes of square footings (i.e. $B \times L$ = 100 mm × 100 mm and 150 mm × 150 mm) in specially designed bearing capacity tank (width × length × height = 900 mm × 900 mm × 750 mm; University of Ottawa Bearing Capacity Equipment) which has provisions to simulate both fully saturated and unsaturated conditions (Figure 4.3). The targeted matric suction values were obtained by controlling the level of water in the bearing capacity tank. Figure 4.4 and Table 4.1 show the variation of measured matric suction values with depth and typical data from the test tank for an average matric suction value of 6 kPa.

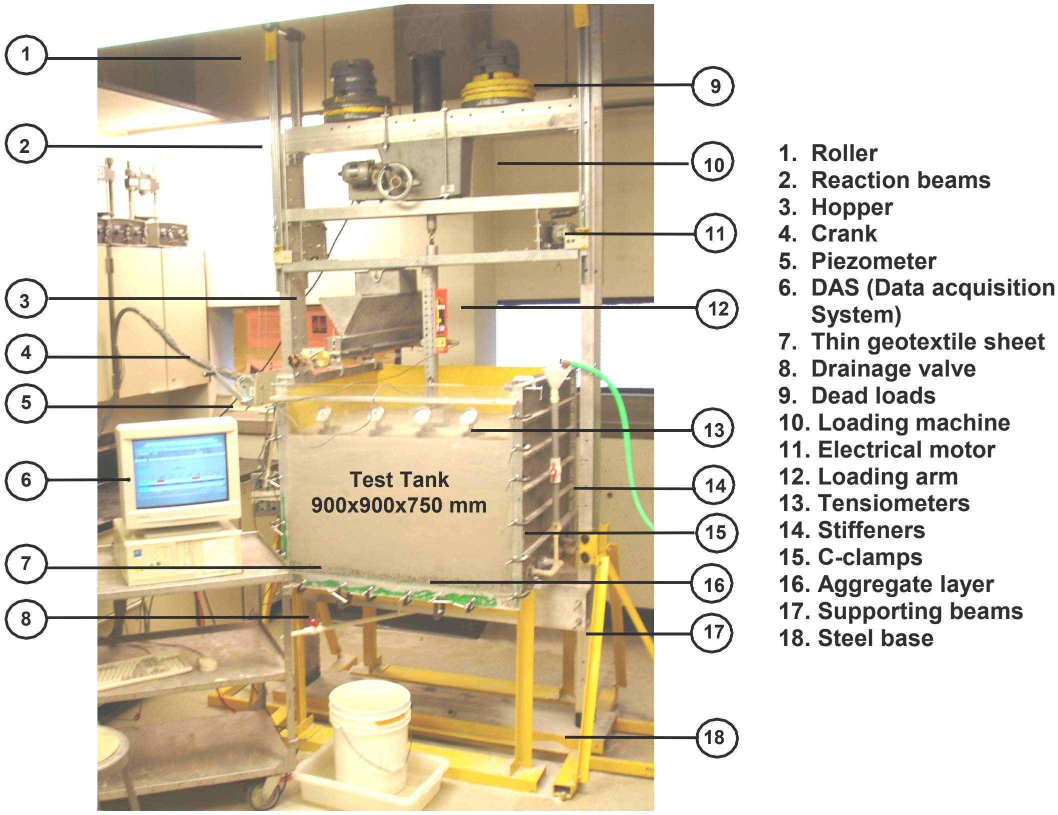

Figure 4.3 University of Ottawa Bearing Capacity Test Equipment (Mohamed and Vanapalli 2006).

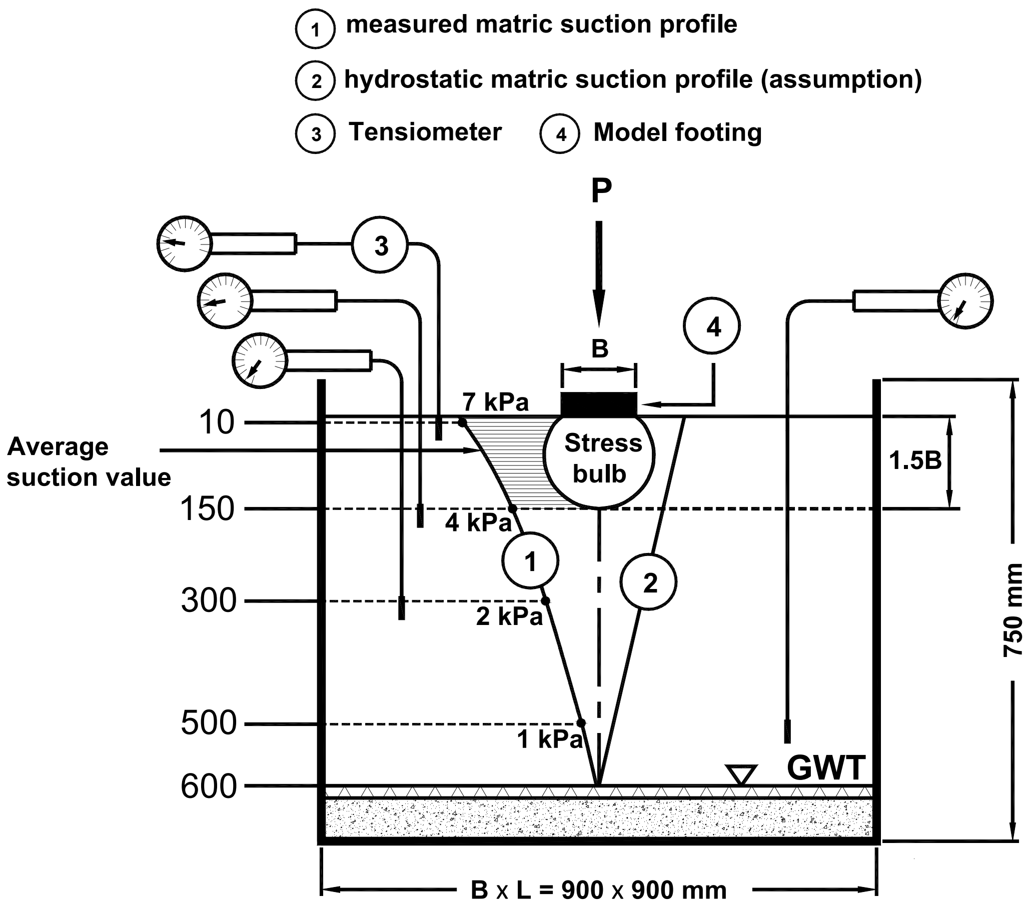

Figure 4.4 Variation of measured matric suction with depth along with hydrostatic distribution for average matric suction of 6 kPa in the stress bulb zone (Mohamed 2006).

Table 4.1 Typical data from the test tank for an average suction value of 6 kPa in the stress bulb zone.

D_f [1] (mm)	γ_t [2] (kN/m^3)	γ_d [3] (kN/m^3)	e [4]	w [5] (%)	S [6] (%)	$(u_a - u_w)$ [7] (kPa)
10	18.17	15.94	0.63	14.0	58	6
150	18.75	15.85	0.64	18.3	76	4
300	19.27	16.07	0.62	20.0	86	2
500	19.40	15.77	0.64	23.0	94	1
600	19.74	15.95	0.63	23.8	100	0

[1] depth from the surface of soil
[2] moist unit weight
[3] dry unit weight
[4] void ratio
[5] water content
[6] degree of saturation
[7] measured matric suction

Steensen-Bach et al. (1987) performed model footing (length × width × height = 22 mm × 22 mm × 20 mm) tests in Sollerod and Lund sand using a circular steel test pit (200 mm in diameter × 120 mm in height). The difference in level between the sand specimen surface and the water surface in the water reservoir was considered to be the suction values (Figure 4.5).

The basic properties of the three sands (i.e. Unimin, Sollerod, and Lund sand) and the sizes of model footings in which the tests were conducted are summarized in Table 4.2.

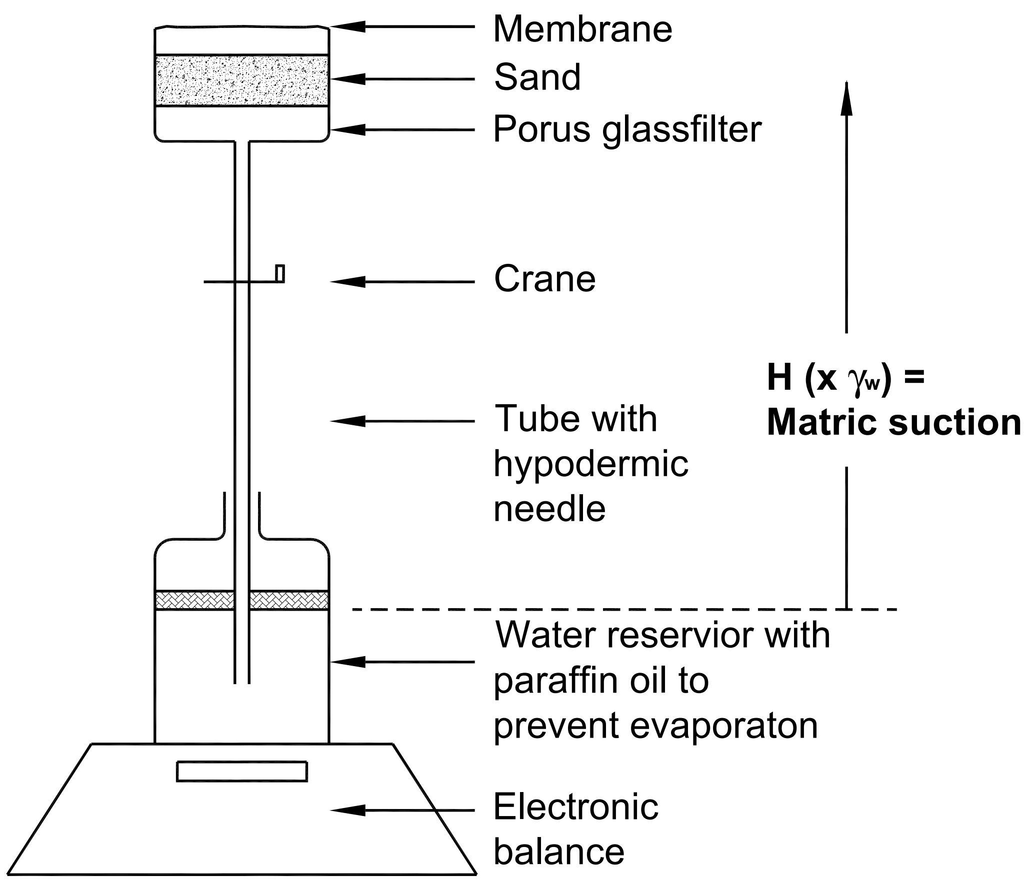

Figure 4.5 General scheme of the *SWCC* measuring equipment used by Steensen-Bach et al. (1984).

Table 4.2 Summary of the data from the three model footing tests.

	Mohamed and Vanapalli (2006)	Steensen-Bach et al. (1987)	
Soil type	Unimin sand	Sollerod sand	Lund sand
failure mode	General shear failure		
B (mm) × L (mm)	100 × 100 150 × 150	22 × 22	
c' (kPa)	0.6	0.8	0.6
ϕ' (°)	35.3	35.8	44.0
$(u_a - u_w)_b$ (kPa) [1)]	4.2	5.7	1.1

[1)] air-entry value

The *SWCC*s for the three sands described in Table 4.2 are shown in Figure 4.6. The coefficients for the equation shown in Figure 4.6 to plot the *SWCC*s and the resultant *R*-squared values are provided in Table 4.3. The *SWCC* for the Unimin sand was established using Tempe cell apparatus (Figure 4.7; Mohamed and Vanapalli 2006). In case of the apparatus shown in Figure 4.5, the variation of degree of saturation due to the drainage of water from a saturated sand specimen or the imbibition into an unsaturated sand specimen was monitored by means of an electronic balance. The capillary rise occurs through flexible, volume constant tubes connecting the specimen in the cup and a hypodermic needle embedded in a reservoir on the balance.

From the *SWCC*s shown in Figure 4.6, it can be seen that, at the same degree of saturation, Sollerod sand shows the highest suction value followed by Unimin sand and Lund sand. Such a behavior can be attributed to Lund sand which offers less resistance to desaturation due to relatively low percentage of fines. In other words, the pore spaces in Lund sand are relatively larger than the other two sands. The *SWCC*s in Figure 4.6 were established without the application of any stress. However, it can be postulated that the *SWCC* behavior of coarse-grained soils such as sands will not be influenced by the applied stress since the volume change in sands due to applied stress can be negligible.

The grain size distribution curves of the three sands are shown in Figure 4.8.

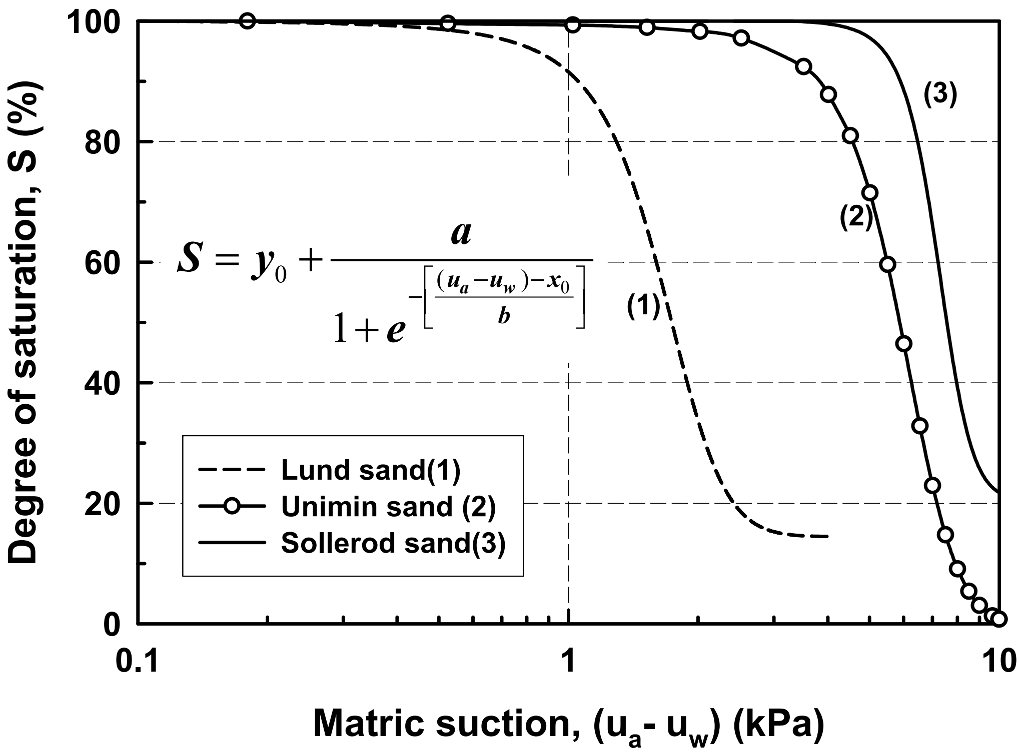

Figure 4.6 *SWCC*s of the three sands studied.

Table 4.3 The coefficients for the equation shown in Figure 4.6 to plot the *SWCC*s and the resultant *R*-squared values.

Soil	a	b	x_0	y_0	R^2
Lund sand	85.98	-0.294	1.635	14.46	1
Sollerod sand	78.91	-0.6631	7.212	20.68	0.998
Unimin sand	100.43	-0.942	5.888	-0.517	0.994

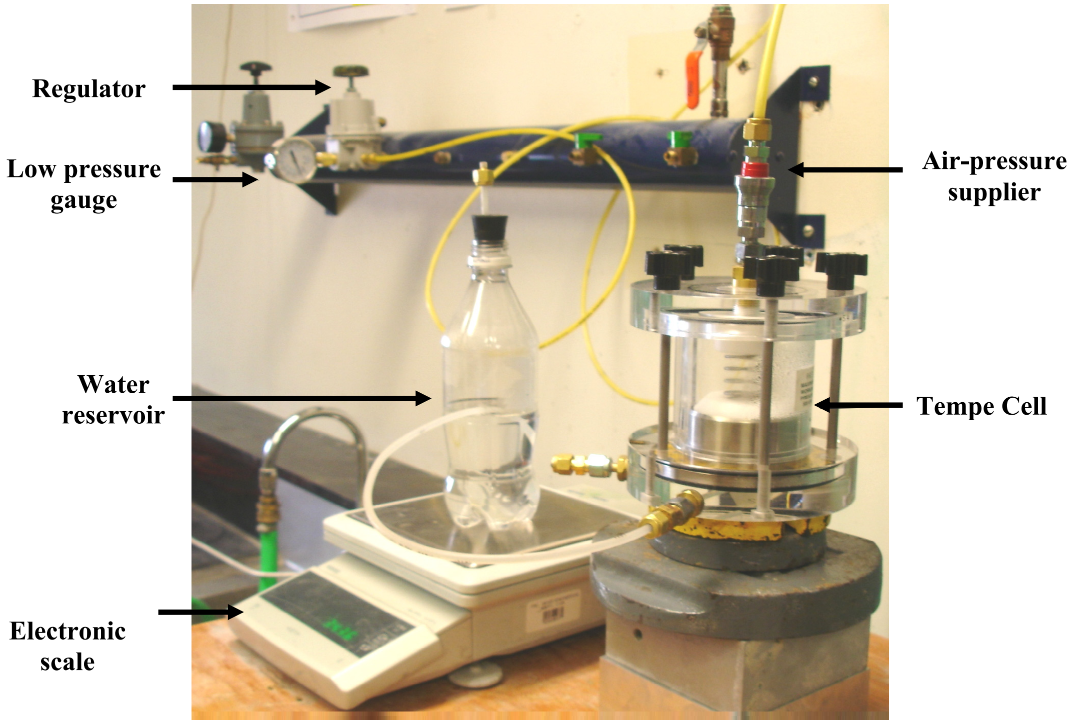

Figure 4.7 Tempe cell apparatus for establishing the *SWCC* for Unimin sand (Mohamed and Vanapalli 2006).

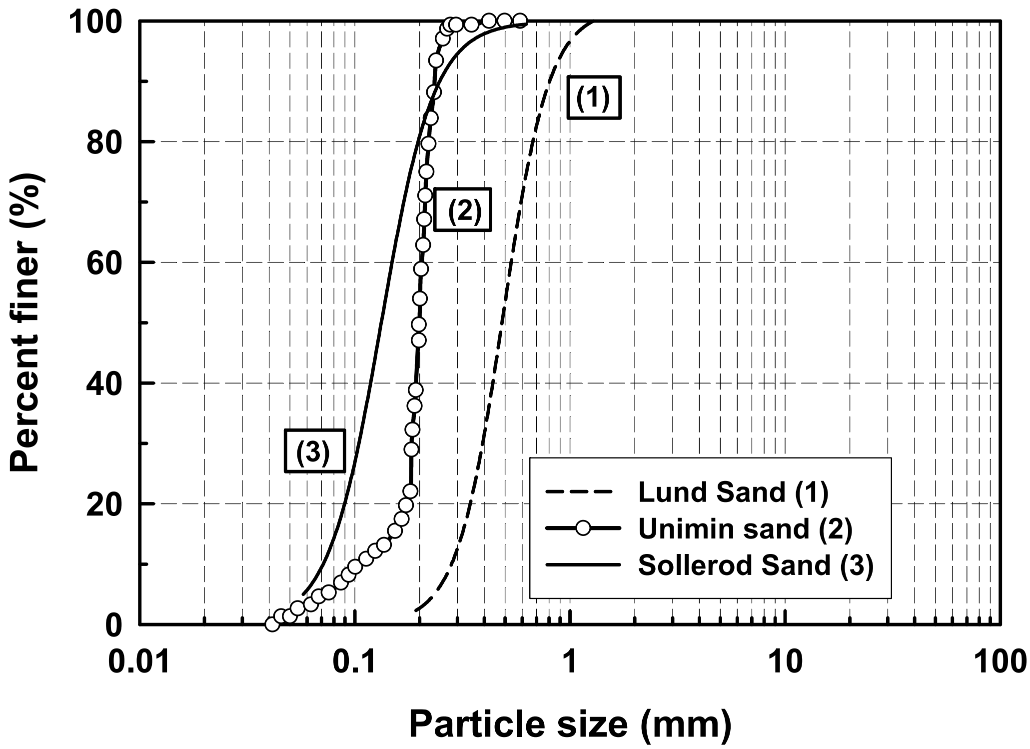

Figure 4.8 Grain size distribution curves of the three sands studied.

4.4.2.2 Model Footing Tests Results

The tests results in Unimin sand for the footings of 100 mm × 100 mm and 150 mm × 150 mm are shown in Figure 4.9 and Figure 4.10, respectively for different matric suction values. The model footing tests results for Sollerod and Lund sand for different matric suction values are shown in Figure 4.11 and Figure 4.12, respectively.

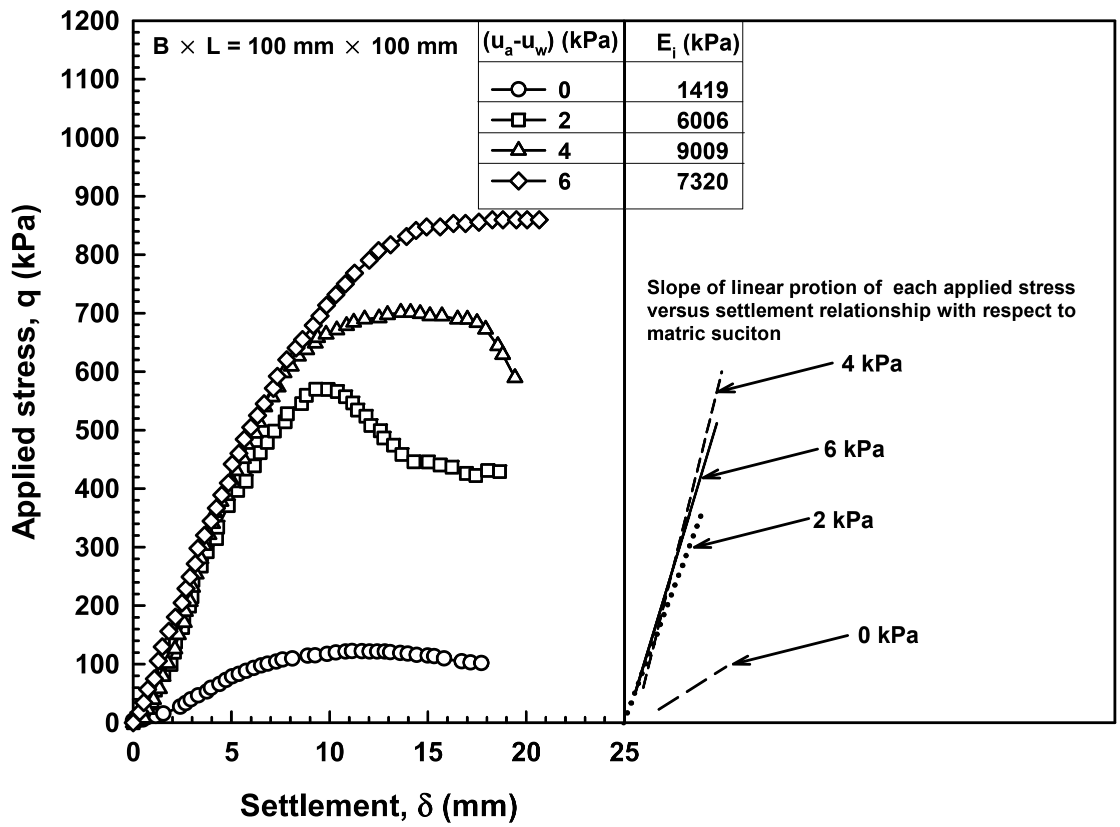

Figure 4.9 The relationship between the applied stress versus settlement in Unimin sand ($B \times L$ =100 mm × 100 mm) [data from Mohamed and Vanapalli (2006)].

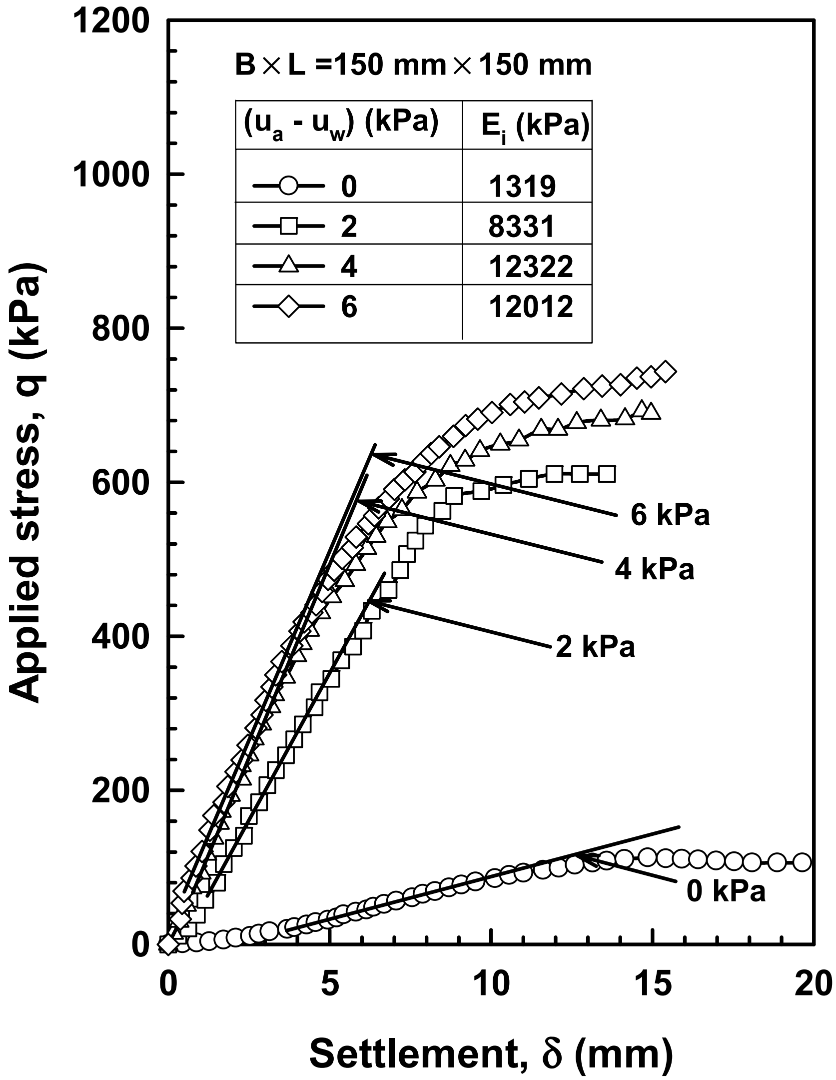

Figure 4.10 The relationship between the applied stress versus settlement in Unimin sand ($B \times L$ =150 mm × 150 mm) [data from Mohamed and Vanapalli (2006)].

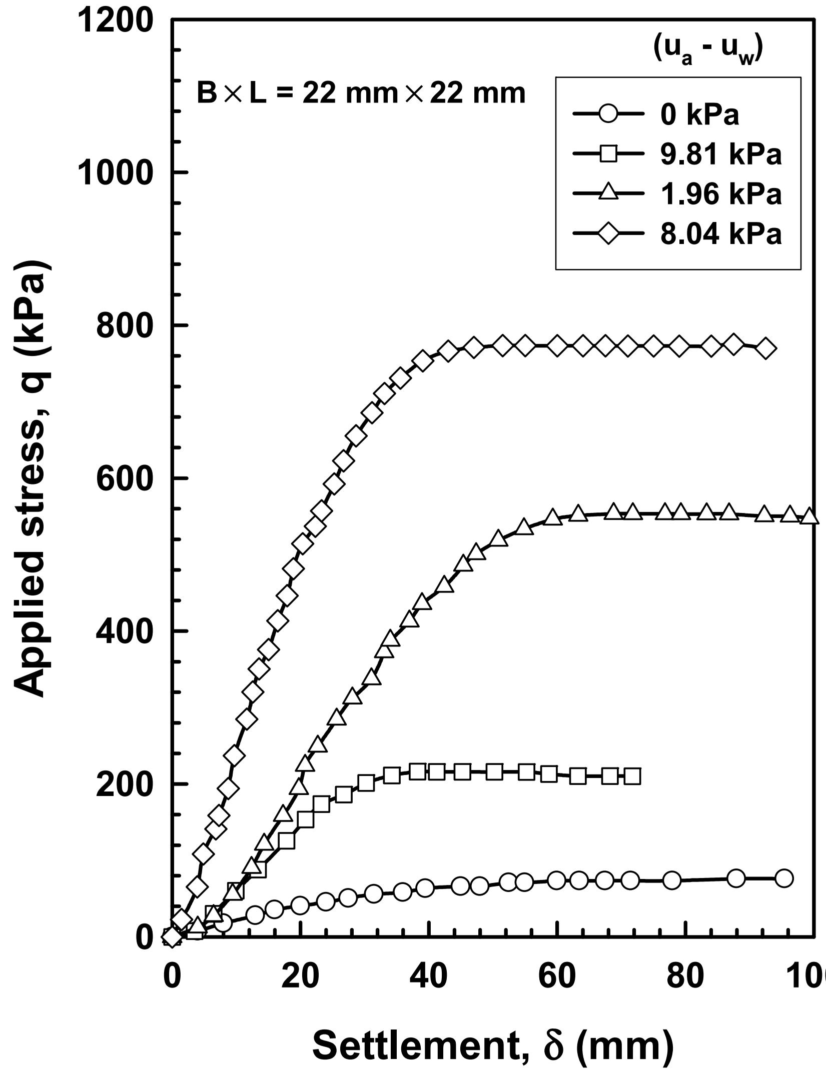

Figure 4.11 The relationship between the applied stress versus settlement in Sollerod sand [data from Steensen-Bach et al. (1987)].

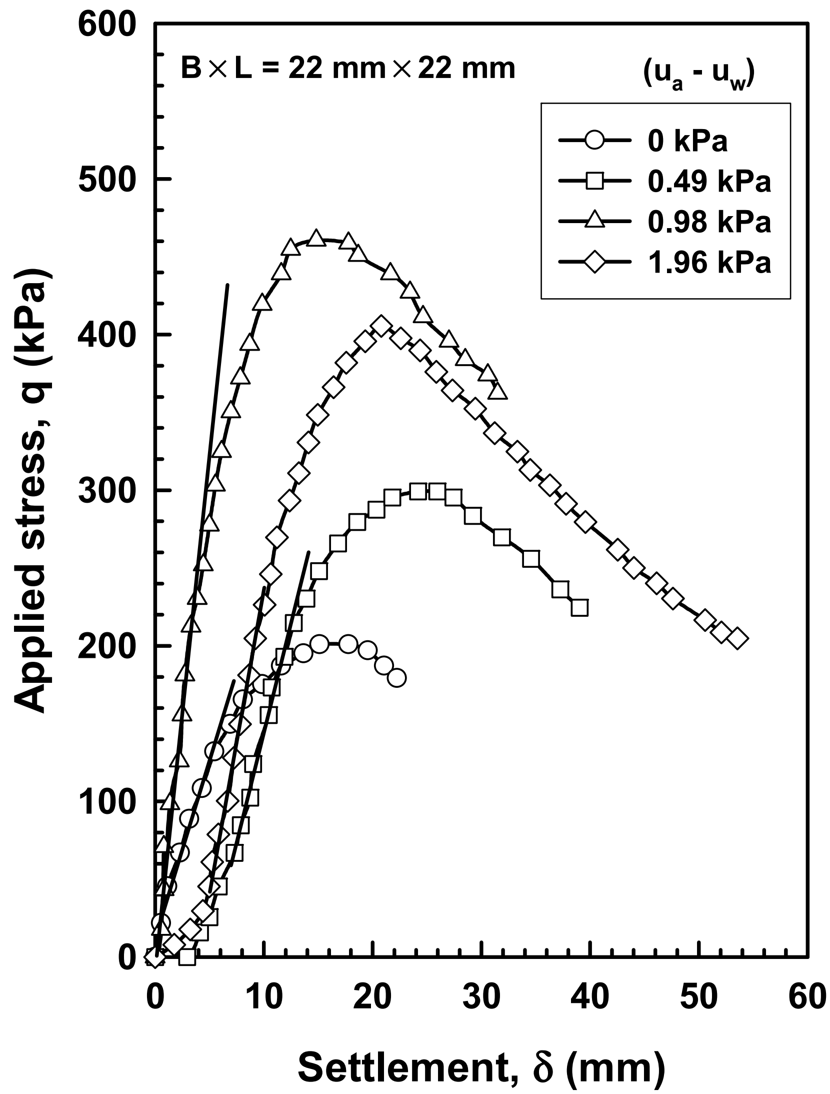

Figure 4.12 The relationship between the applied stresses versus settlement in Lund sand [data from Steensen-Bach et al. (1987)].

4.4.2.3 Analysis of the Model Footing Tests Results

Figure 4.13, Figure 4.14, and Figure 4.15 show the *SWCC*s, the variation of initial tangent elastic modulus and elastic settlement with respect to matric suction from the model footing tests conducted in Unimin, Sollerod and Lund sand, respectively. The initial tangent elastic modulus values were calculated using Eq. (4.2) based on the linear portion of the stress versus settlement behaviors. The initial tangent elastic modulus values for Sollerod and Lund sand are low in comparison to Unimin sand due to the relatively small size of the model footings used for testing. Elastic settlements were estimated for the applied stress of 40 kPa since all three sands exhibited elastic behavior below this stress level.

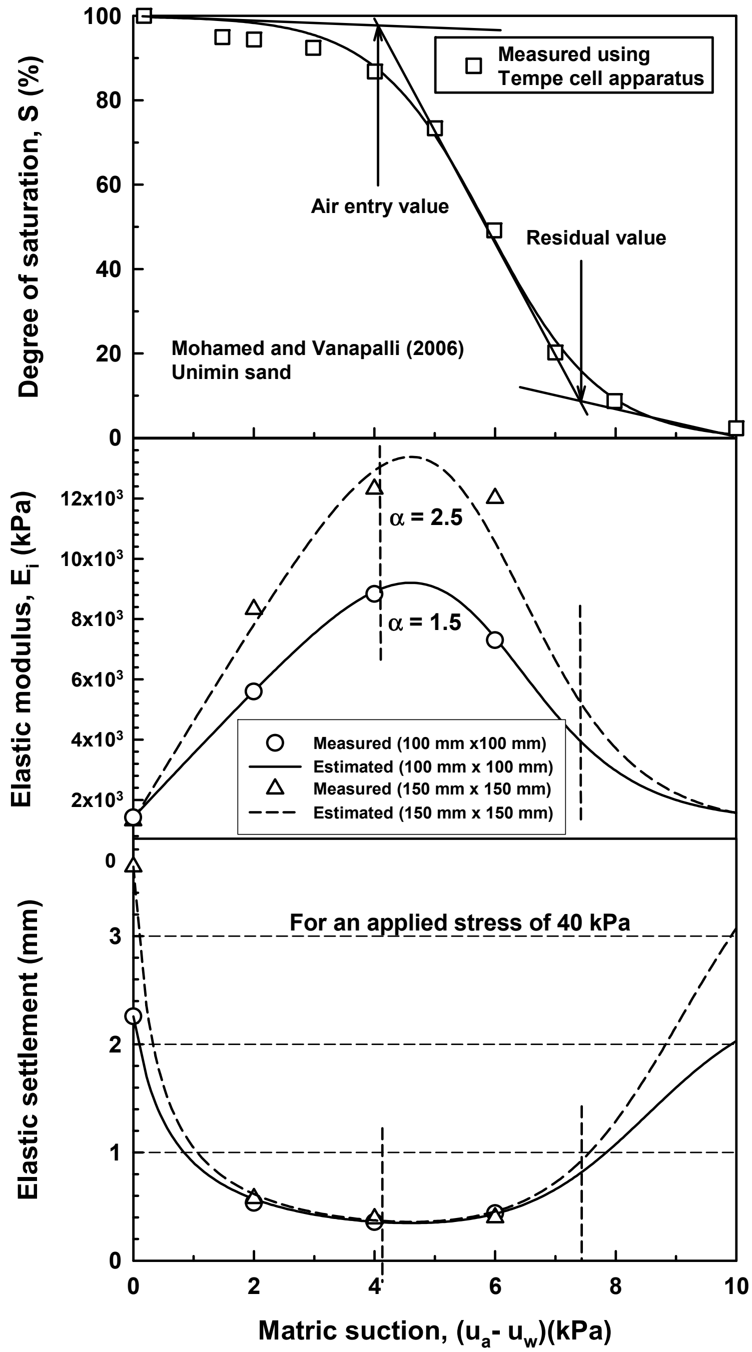

Figure 4.13 *SWCC* and the variation of initial tangent elastic modulus and elastic settlement with respect to matric suction for the model footing tests in Unimin sand [data from Mohamed and Vanapalli (2006)].

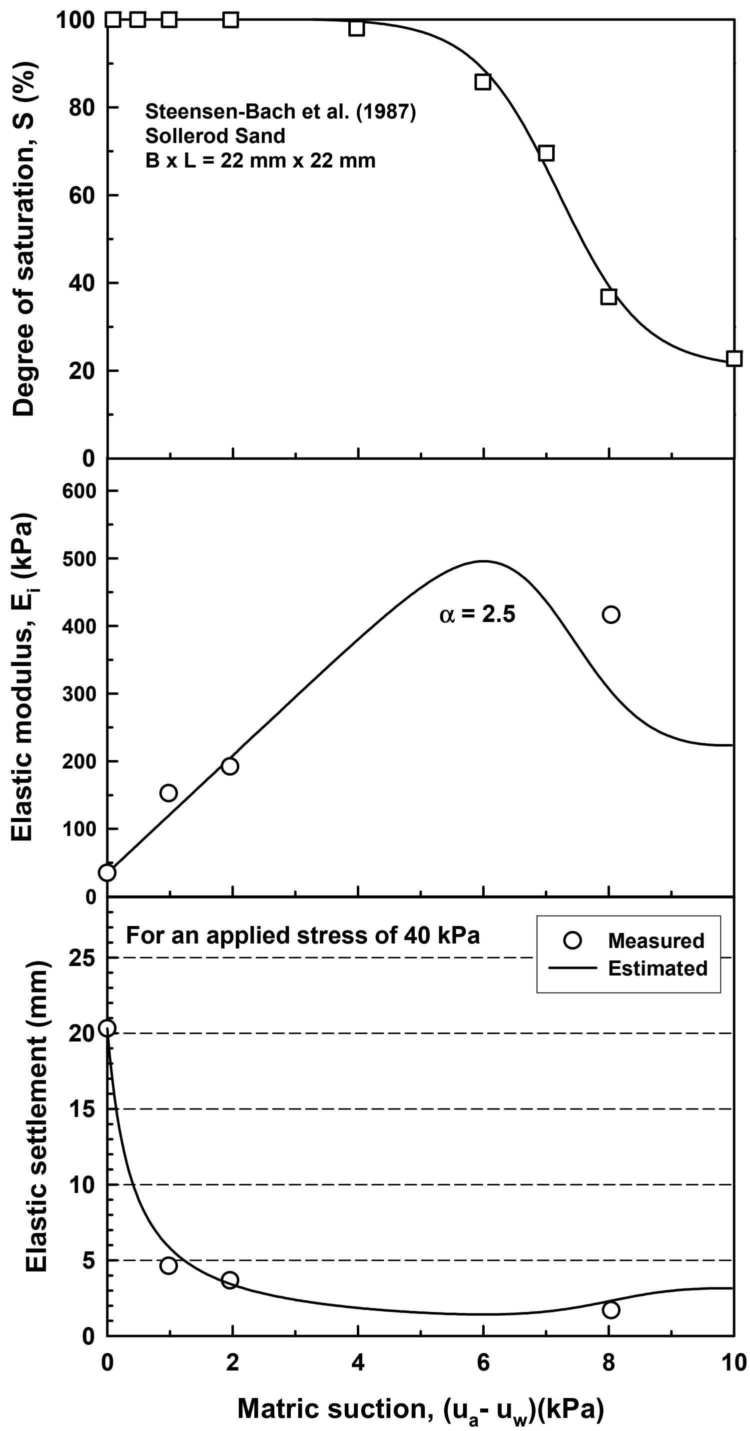

Figure 4.14 *SWCC* and the variation of initial tangent elastic modulus and elastic settlement with respect to matric suction for the model footing tests in Sollerod sand [data from Steensen-Bach et al. (1987)].

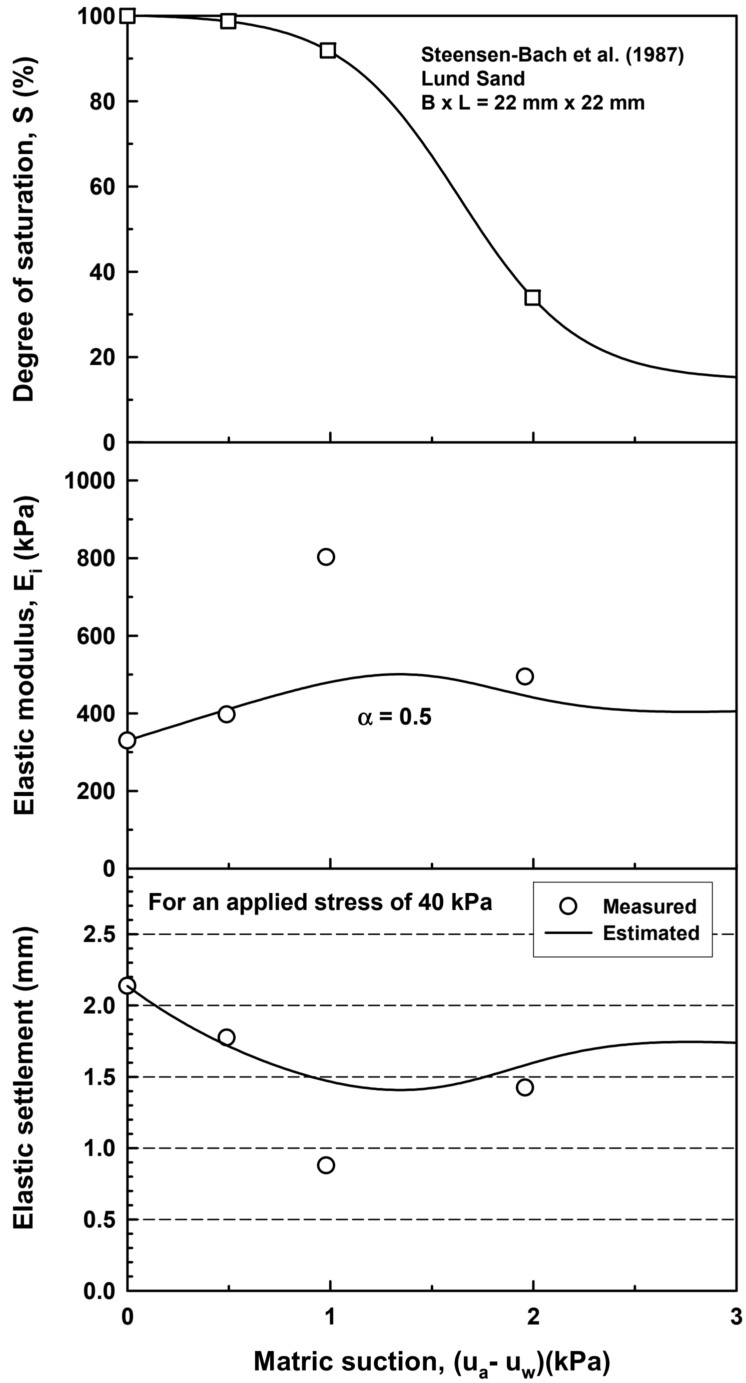

Figure 4.15 *SWCC* and the variation of initial tangent elastic modulus and elastic settlement with respect to matric suction for the model footing tests in Lund sand [data from Steensen-Bach et al. (1987)].

The fitting parameter, α in Eq. (4.4) used for the three different sands are summarized in Table 4.4. The fitting parameter, α = 2.5 was required for Unimin sand (tested with 150 mm × 150 mm model footing) and Sollerod sand (tested with 22 mm × 22 mm model footing). On the other hand, α = 0.5 and 1.5 were required for Lund sand (tested with 22 mm × 22 mm model footing) and Unimin sand (tested with 150 mm × 150 mm model footing), respectively. These results show no defined trend or relationship between α and the size of the footing for the three different sands analyzed. Such a behavior can be attributed to the model footing tests carried out on Sollerod and Lund sands with relatively small sizes of model footings in a relatively low suction range. More explanations are offered with respect to this behavior in later sections.

Table 4.4 Fitting parameter, α for each test.

Soil	α
Coarse-grained sand	
100 mm × 100 mm	1.5
150 mm × 150 mm	2.5
Sollerod sand	
22 mm × 22 mm	2.5
Lund sand	
22 mm × 22 mm	0.5

Figure 4.16 and Figure 4.17 show the variation of initial tangent elastic modulus and elastic settlement with respect to the fitting parameter, α, respectively, for the footing of 150 mm × 150 mm in Unimin sand. The results show that the use of the fitting parameter, α between 1.5 and 2 provide conservative initial tangent elastic modulus values for sandy soils. The elastic settlements associated with these initial tangent elastic modulus values also provided conservative estimates.

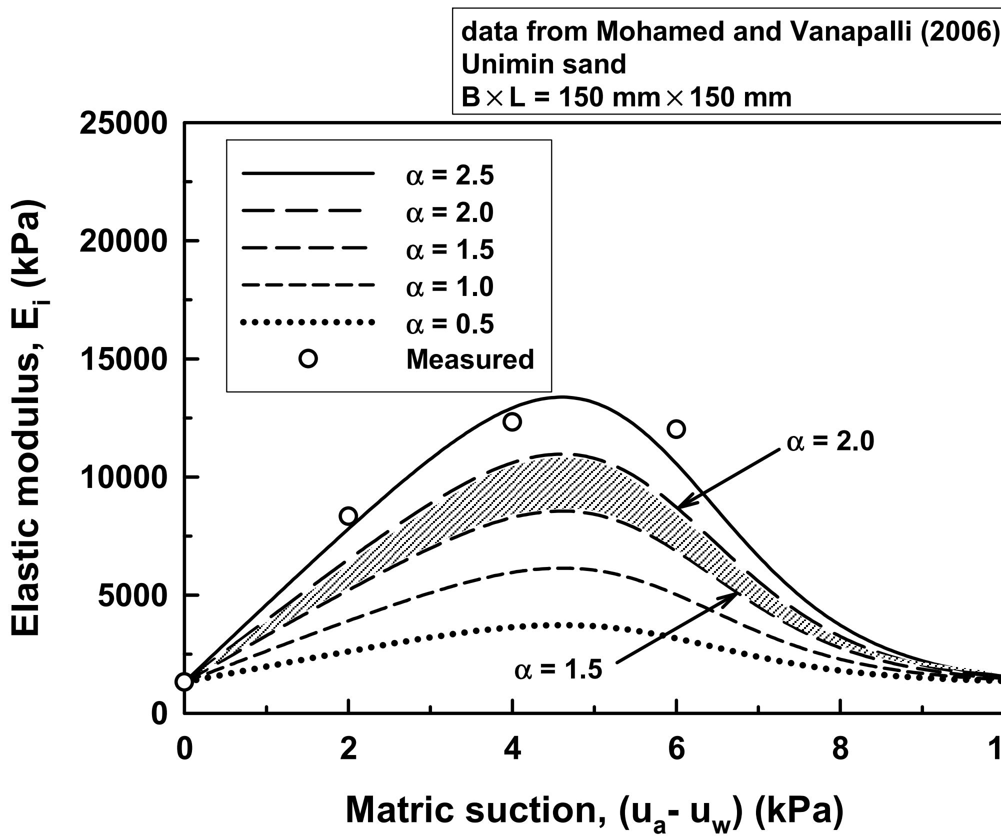

Figure 4.16 Variation of initial tangent elastic modulus with respect to the fitting parameter, α for 150 × 150 mm footing loaded in Unimin sand.

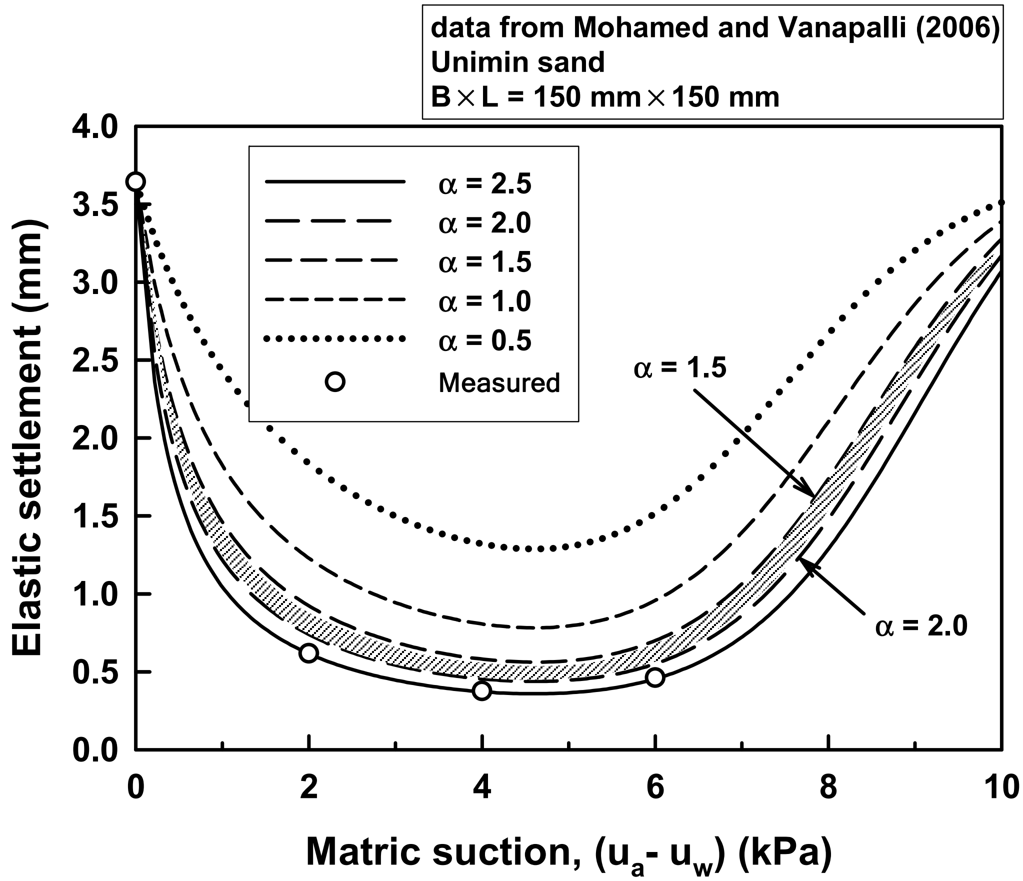

Figure 4.17 Variation of elastic settlement with respect to the fitting parameter, α for 150 × 150 mm footing loaded in Unimin sand.

Figure 4.18 shows the variation of elastic settlement with respect to matric suction for different applied stress values in the range of 40 to 400 kPa for 100 mm × 100 mm model footing tested in Unimin sand. For the applied stress of 400 kPa, the minimum elastic settlement is 3.50 mm at a matric suction value of 5 kPa. This elastic settlement value is the same as the value measured for an applied stress of 100 kPa at matric suction value of 0.5 kPa.

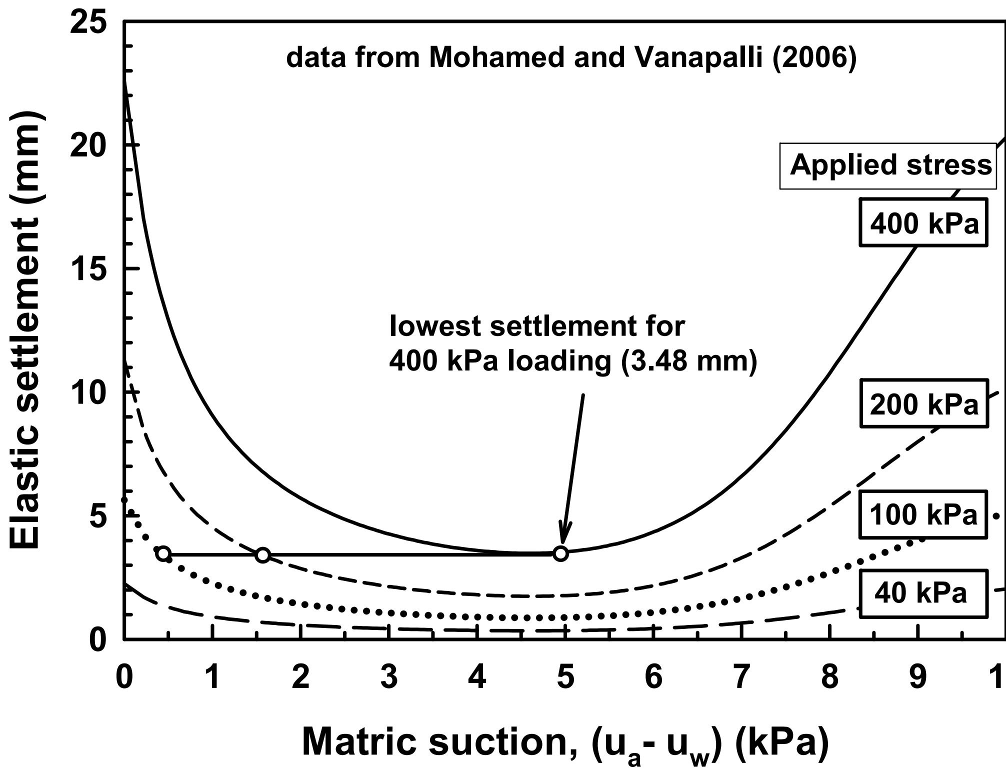

Figure 4.18 Variation of elastic settlement for various applied stresses for 100 × 100 mm model footing loaded in Unimin sand.

4.4.2.4 Variation of the Fitting Parameter, α with respect to Footing Size for Unsaturated Sands

Additional investigations were carried out to better understand the influence of the model footing size on the fitting parameter, α using a new series of model footing tests results provided by Li (2008) on Unimin sand. Figure 4.19 and Figure 4.20 show the model footing ($B \times L$ = 37.5 mm × 37.5 mm) test results and comparisons between the measured and the estimated initial tangent elastic modulus values. As can be seen in Figure 4.20, there is good comparison between the measured initial tangent elastic modulus values and those estimated with $\alpha = 0.5$.

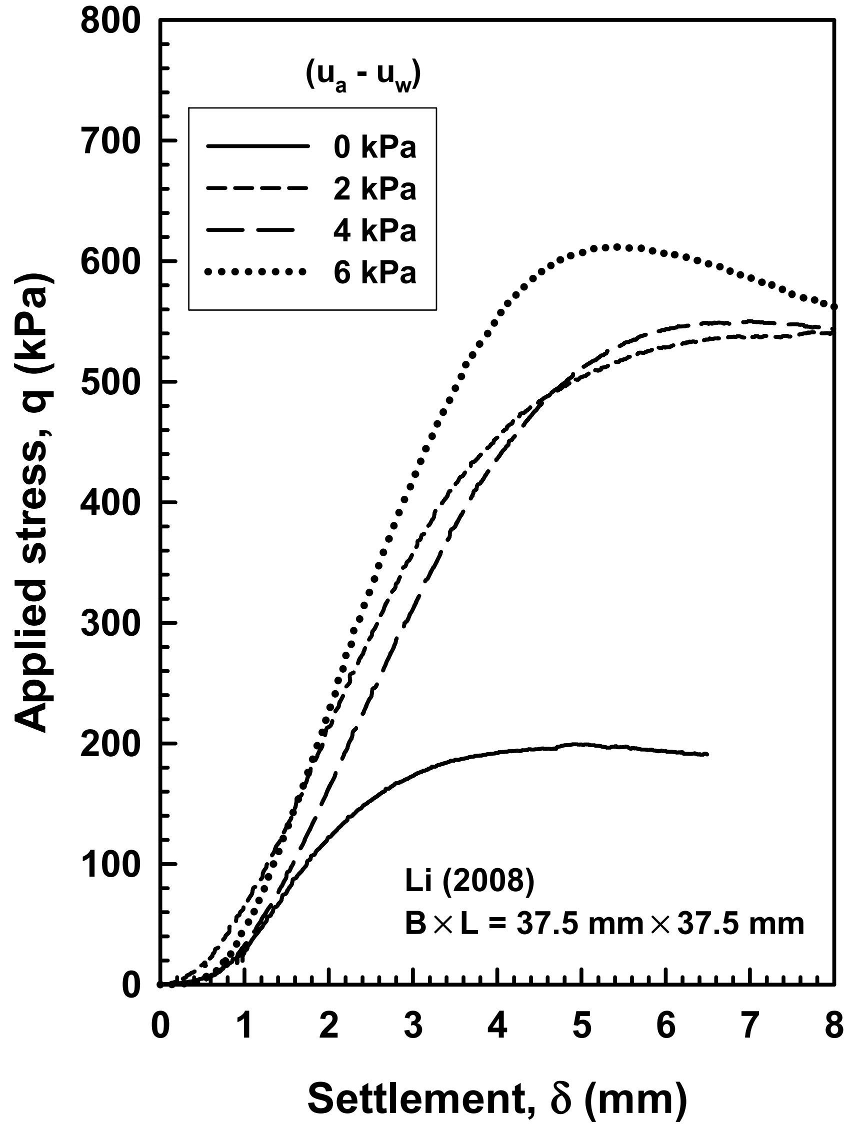

Figure 4.19 Applied stress versus settlement behavior in Unimin sand ($B \times L$ =37.5 mm × 37.5 mm) [data from Li (2008)].

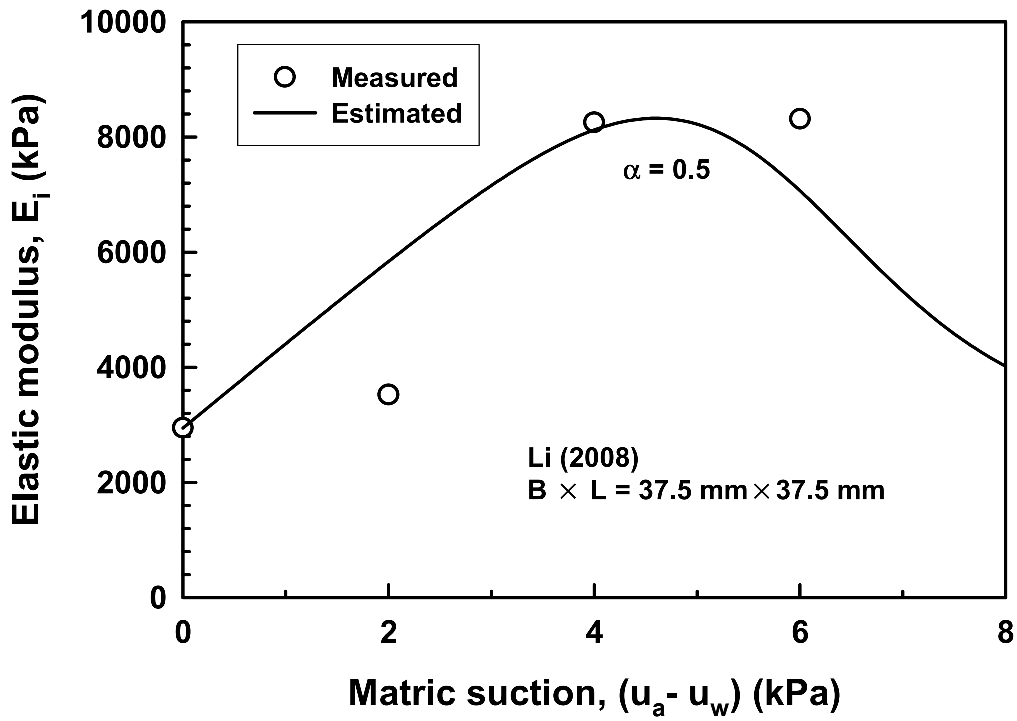

Figure 4.20 Comparison between the measured and the estimated initial tangent elastic modulus for 37.5 mm × 37.5 mm model footing in Unimin sand [data from Li (2008)].

Figure 4.21 shows the variation of the fitting parameter, α with respect to the width of model footing for the model footing tests results in Unimin sand (i.e. 37. 5 mm, 100 mm and 150 mm). This result suggests that fitting parameter, α decreases nonlinearly with decreasing model footing size.

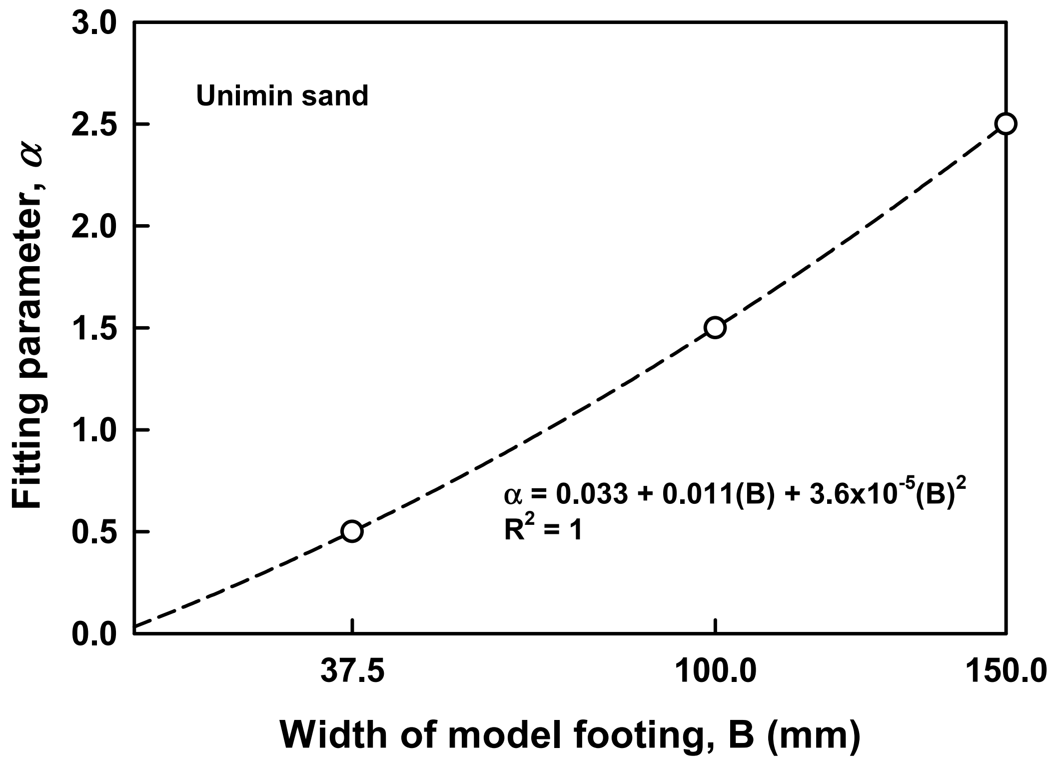

Figure 4.21 Variation of the fitting parameter, α with respect to the width of model footing for Unimin sand.

The more defined trend may be explained using the ratio of the model footing size to the size of soil particles (i.e. particle size scale effect) (Figure 4.22). The size of the soil particles in Figure 4.22(a) and (b) are shown to be constant since the grain size distribution curve for all the sands used for the analyses fall in a narrow band and are approximately uniform in nature. However, the footing sizes used in the testing program are different.

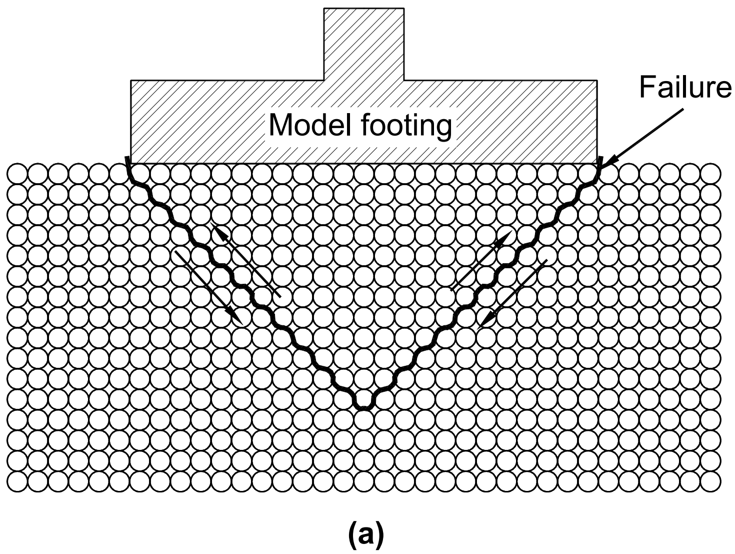

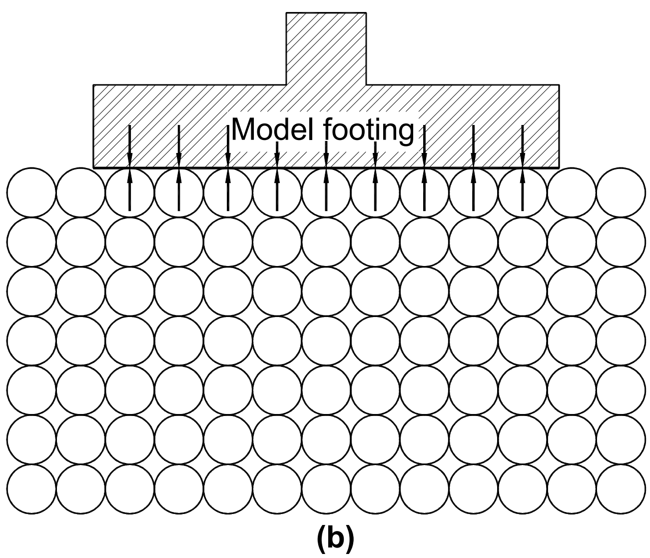

Figure 4.22 Resistance mechanism of unsaturated soils under a model footing with respect to the size of soil particles.

When a footing size is relatively large compared to the soil particle sizes, the resistance in a soil is typically developed along a well-defined failure plane [Figure 4.22(a)]. However, when a footing size is relatively small, the load applied on the model footing is mostly carried by the individual soil particles and not due to the frictional resistance arising between the soil particles [Figure 4.22(b)]. In this scenario, the contribution of matric suction towards initial tangent elastic modulus is also less as the soil particles are relatively large in comparison to size of the model footing [i.e. Figure 4.22(b)]. Due to this reason, the parameter, α for the 150 mm × 150 mm footing is greater than that of 37.5 mm × 37.5 mm footing. This behavior can also be extended to explain the result of 100 × 100 mm footing behavior which is in between the Figure 4.22(a) and (b).

The above observations can also be extended for the experimental results on Sollerod and Lund sand. The particle sizes of the Lund sand are larger than those of Sollerod sand for the whole range of percent finer. Hence, the contribution of matric suction towards initial tangent elastic modulus is less for Lund sand when the model footing tests are performed with the same model footing size (i.e. 0.5 for Lund sand and 2.5 for Sollerod sand).

4.4.3 Behavior of Initial Tangent Elastic Modulus and Elastic Settlement in Unsaturated Coarse-Grained Soils

From Figure 4.13, Figure 4.14, Figure 4.15 and Figure 4.20, it can be seen that the behavior of initial tangent elastic modulus is different in the three stages of desaturation; that is boundary effect zone, transition zone and residual zone (Vanapalli et al. 1999).

(i) ***Boundary effect zone***: the initial tangent elastic modulus linearly increases up to air-entry value

(ii) ***Transition zone***: the initial tangent elastic modulus nonlinearly increases up to a certain matric suction value then gradually decreases.

(iii) ***Residual zone***: the initial tangent modulus of elasticity decreases and approaches constant value.

This nonlinear behavior of initial tangent elastic modulus indicates that the proposed semi-empirical models in Eq. (4.4) is useful to estimate the variation of initial tangent elastic modulus of unsaturated sandy soils in all the three different zones of the *SWCC*.

The elastic settlement of model footing gradually decreases with an increase in initial tangent elastic modulus as matric suction increases in the boundary effect zone. In the transition zone, decreasing trends of elastic settlements can be observed in the lower suction region. However, elastic settlements start gradually increasing as the suction approaches the residual zone. Such a behavior can be attributed to the gradual decrease of initial tangent elastic modulus in this zone. The elastic settlements in the residual zone remain almost constant irrespective of further increase in matric suction values. It is of interest to note that the elastic settlement at zero matric suction (i.e. saturated condition) and 10 kPa (i.e. residual condition) values are almost the same for the model footing tests results in Unimin sand (see Figure 4.18).

4.5 Fitting Parameters, α and β for Unsaturated Fine-Grained Soils

4.5.1 Fitting Parameter, β for Unsaturated Fine-Grained Soils

The preliminary study showed that a value of β = 2 can be used to provide good comparisons between the measured and the estimated initial tangent elastic modulus for unsaturated fine-grained soils.

4.5.2 Fitting Parameter, α for Unsaturated Fine-Grained Soils

To determine the fitting parameter, α for unsaturated fine-grained soils two sets of in-situ plate load tests results in unsaturated fine-grained soils are analyzed along with the model footing tests results provided in Chapter 3.

4.5.2.1 Model footing and In-Situ Plate Load Test Results used in the Analyses and Soil Properties

Costa et al. (2003) carried out a series of in-situ plate load tests on lateritic soil deposit (i.e. clayey sand) to investigate the influence of matric suction on the bearing capacity under unsaturated conditions. The matric suction values were measured using four tensiometers installed at the bottom of the test pit (1.5 m depth) besides the loading plate at depths of 0.10, 0.30, 0.60, and 0.80 m. The average value of the tensiometer readings from 0 to *B* depth was regarded as the representative matric suction value.

Rojas et al. (2007) performed seven plate load tests on unsaturated Lean clay. The matric suction values were measured using four tensiometers installed at the depths of 0.1, 0.3, 0.6, and 0.9 m below the base of the pits (1.2 × 3.0 × 1.4 m).

Details of the model footing tests on a statically compacted Indian head till are presented in Chapter 3.

Some key details of the model footing and in-situ plate load tests in the three fine-grained soils are summarized in Table 4.5. The stresses versus settlement behaviors for each soil are shown in Figure 4.23, Figure 4.24, and Figure 4.25. Figure 4.26 shows the *SWCC*s for the three fine-grained soils.

Table 4.5 Summary of the bearing capacity and shape factors used in the study for calculating the bearing capacity.

Author	Soil type	I_p	Suction Measurement	Plate base [1] (mm)	Remark [2]
Steensen-Bach et al. (1987)	Sollerod and Lund sand	NP	Capillary height	22□	C
Mohamed and Vanapalli (2007)	Unimin sand	NP	Tensiometer	100□ 150□	C
Li (2008)	Unimin sand	NP	Tensiometer	37.5□	C
Costa et al. (2003)	Clayey sand	8	Tensiometer	80*	N
Rojas et al. (2007)	Lean clay	12	Tensiometer	310*	N
Oh (from Chapter 3)	Glacial till	15.5	Tensiometer, Axis-tranlastion technique	50□	C

[1](□) Square footing, (*) Circular footing
[2]C – compacted soil (laboratory test), N – Natural soil (field test)

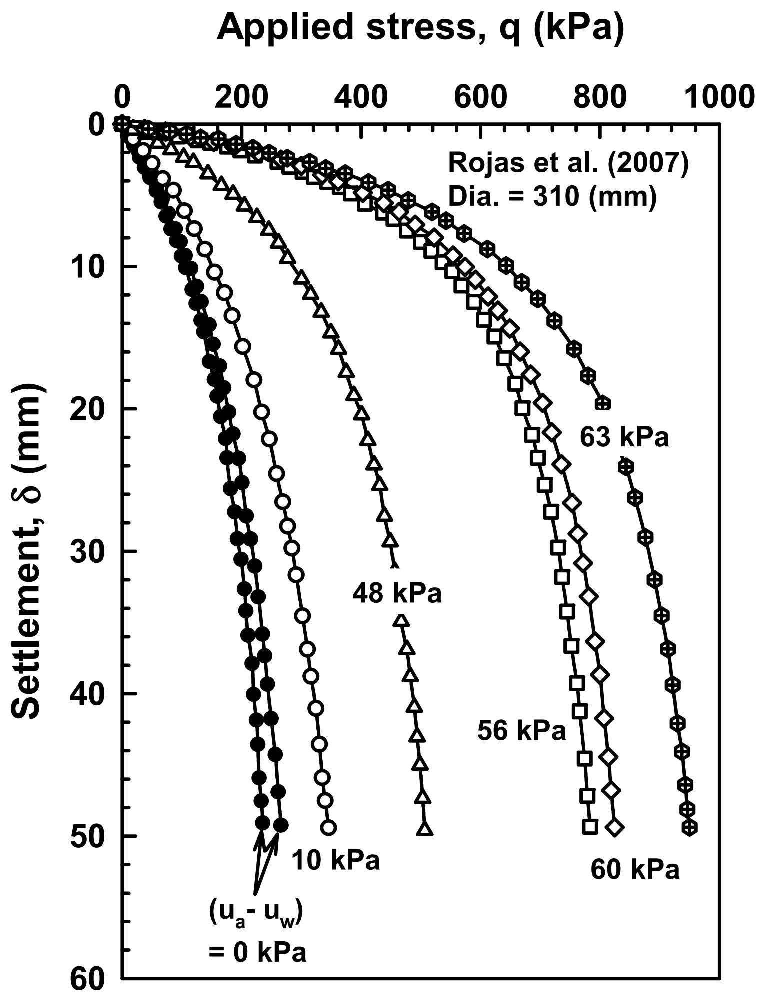

Figure 4.23 In-situ plate load test results by Costa et al. (2003).

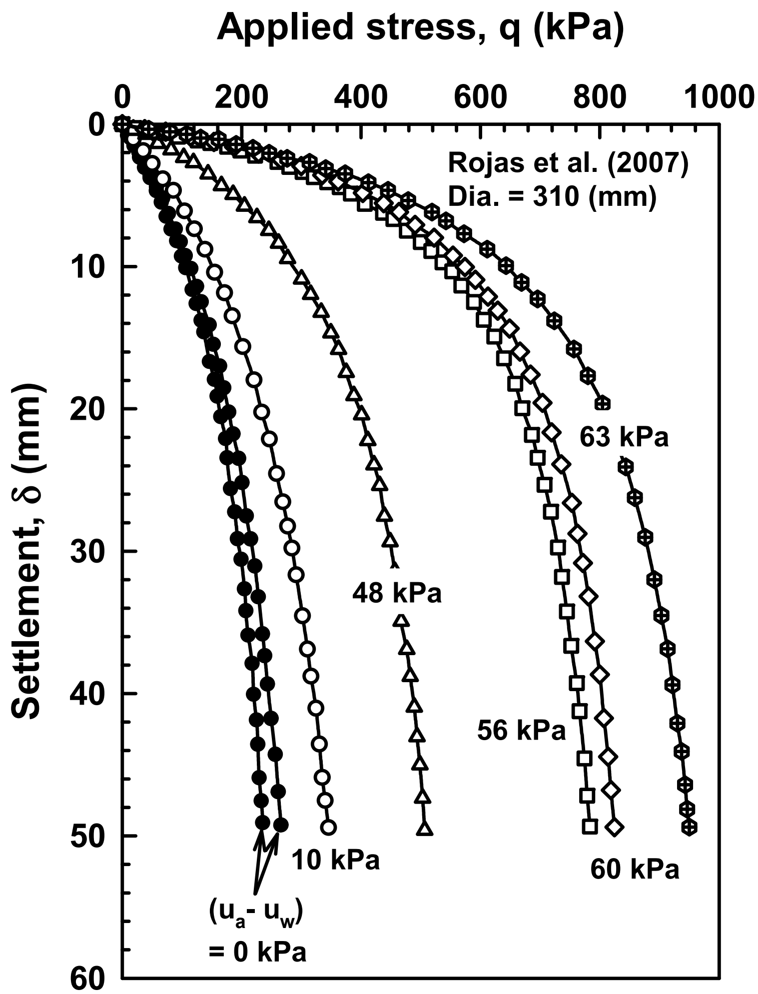

Figure 4.24 In-situ plate load test results by Rojas et al. (2007).

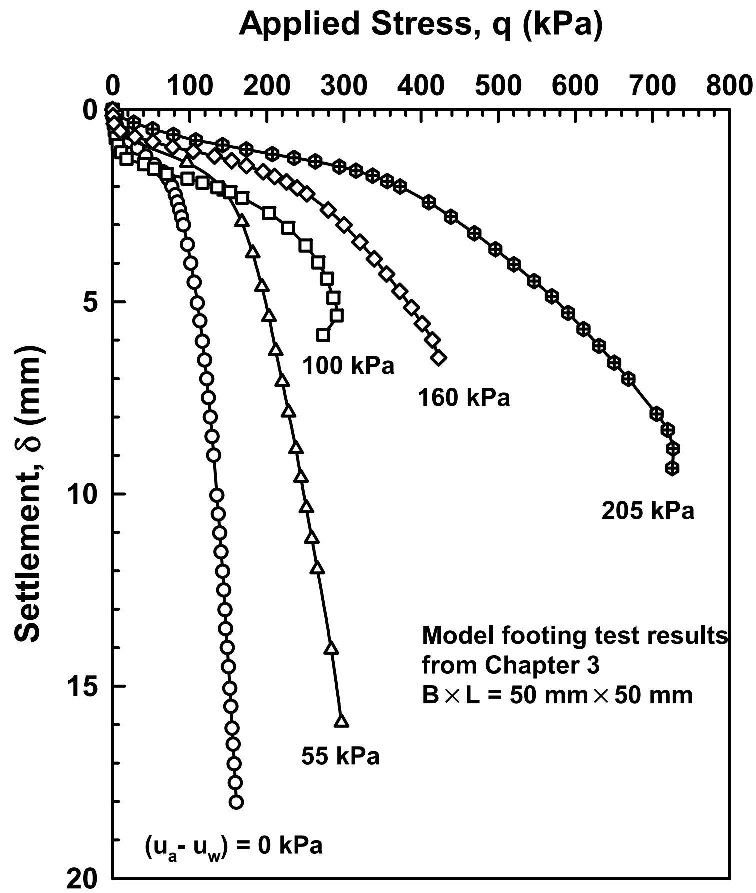

Figure 4.25 Model footing test results (from Chapter 3).

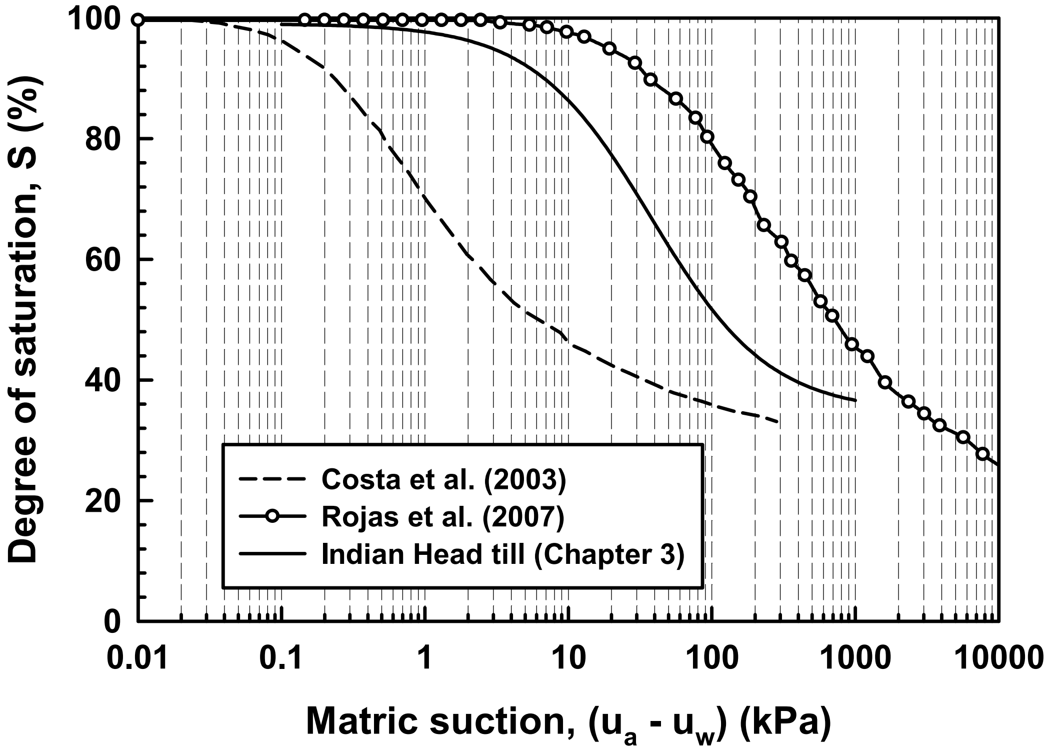

Figure 4.26 *SWCC*s for the three fine-grained soils used in the analysis.

4.5.2.2 Analysis of the Tests Results

Figure 4.27 provides the comparison between the measured and the estimated initial tangent elastic modulus values for the in-situ plate load test results by Costa et al. (2003). The fitting parameter $\beta = 2$ was used for fine-grained soils regardless of the value of plasticity index, I_p as explained earlier. The fitting parameter, α was estimated to be between 1/10 and 1/3.2 depending on the matric suction values. Extending the same procedure, α was estimated to be between 1/20 and 1/6.5 for the results by Rojas et al. (2009) (Figure 4.28). Figure 4.29 shows the comparison for the model footing tests in Indian Head till provided in Chapter 3 with the fitting parameter, $\alpha = 1/10$.

The comparisons for the results by Costa et al. (2003) and Rojas et al. (2007) indicate that lower values of α are required for relatively low matric suction values. This implies that the contribution of matric suction towards the initial tangent elastic modulus is less when the matric suction values are low. This phenomenon was not observed for the model footing tests results in Indian Head till (Chapter 3) since the lowest matric suction value used for the experiments was greater than 50 kPa (i.e. approximately 5 times greater than the air-entry value).

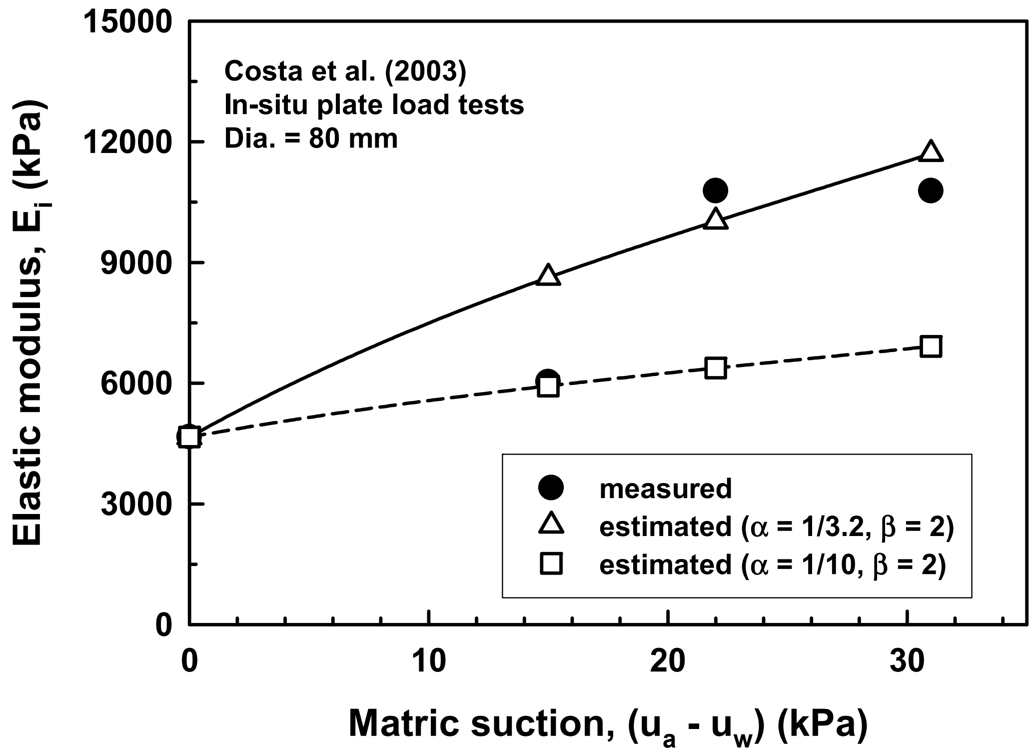

Figure 4.27 Comparison between measured and estimated initial tangent elastic modulus for the in-situ plate load test results by Costa et al. (2003).

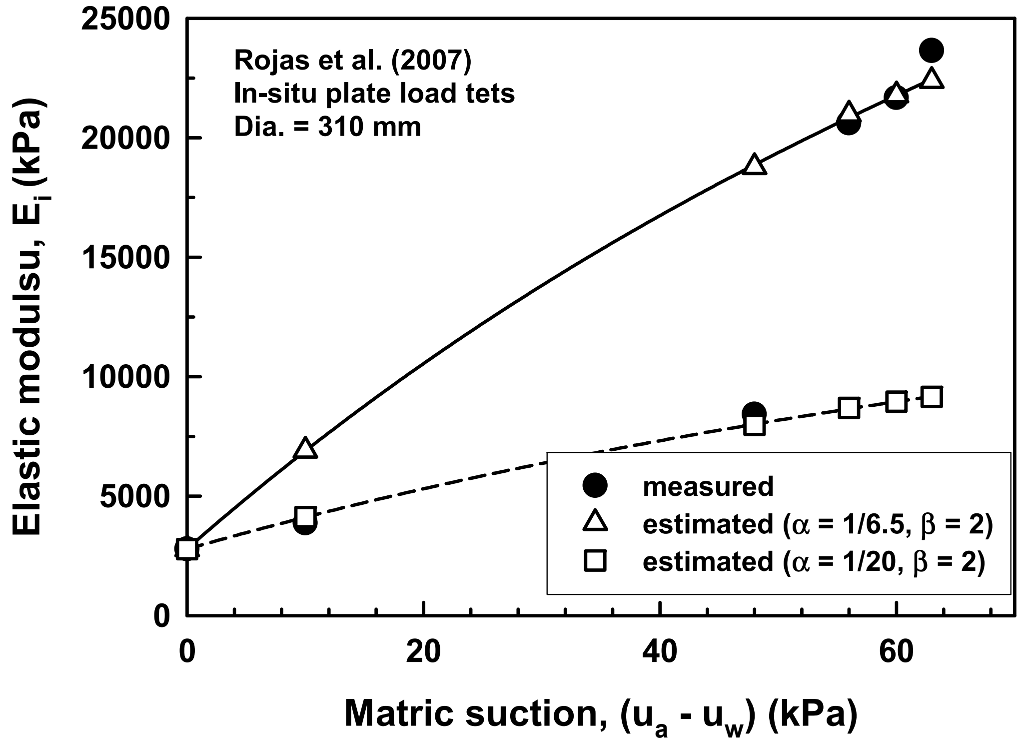

Figure 4.28 Comparison between measured and estimated modulus of elasticity for the in-situ plate load test results by Rojas et al. (2007).

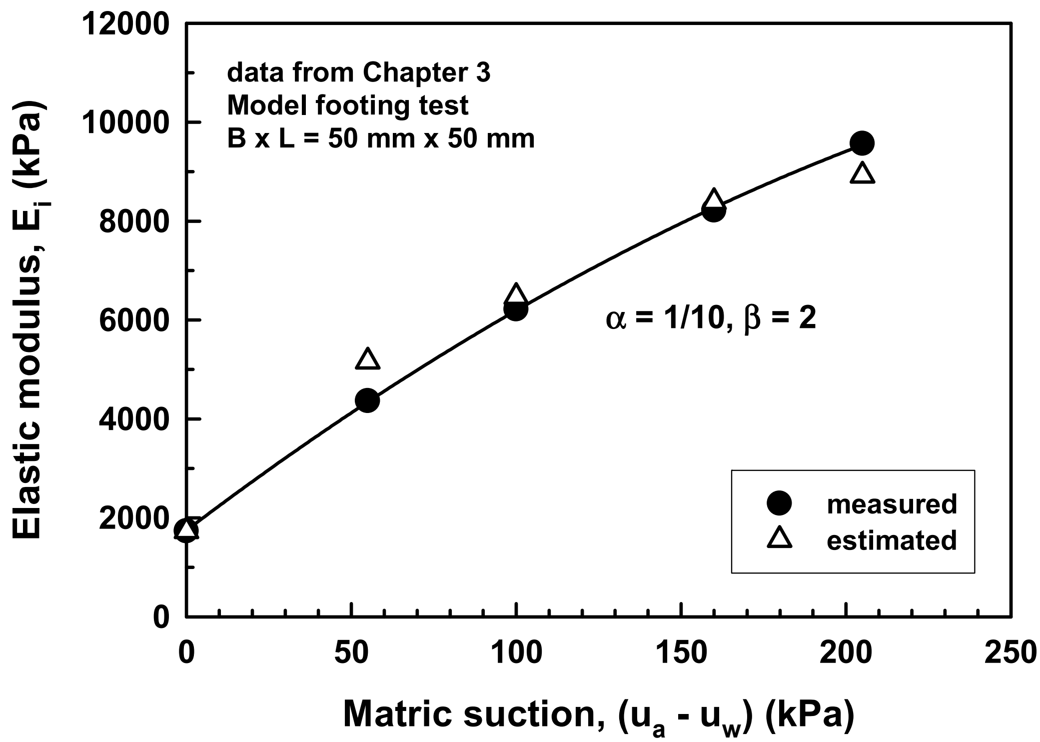

Figure 4.29 Comparison between measured and estimated initial tangent elastic modulus using the data presented in Chapter 3.

4.6 Relationship between Plasticity Index and Fitting Parameters, α and β

The fitting parameters, α and β for both coarse- and fine-grained soils used in this study are summarized in Table 4.6. Based on the values for the fitting parameters, α shown in Table 4.6, a relationship is developed between ($1/\alpha$) and plasticity index, I_p using upper [Eq. (4.6)] and lower [Eq. (4.7)] boundaries as shown in Figure 4.30. The relationship shows that the inverse of α (i.e. $1/\alpha$) nonlinearly increases with increasing I_p. The upper and lower boundary relationship can be used for low and high suction values respectively at a certain I_p.

$$(1/\alpha) = 0.5 + 0.312(I_p) + 0.109(I_p)^2 \qquad (0 \le I_p(\%) \le 12) \tag{4.6}$$

$$(1/\alpha) = 0.5 + 0.063(I_P) + 0.036(I_P)^2 \qquad (0 \le I_P(\%) \le 16) \tag{4.7}$$

Table 4.6 Summary of the fitting parameters, α and β with respect to plasticity index.

Author	Soil type	I_p	α	β
Steensen-Bach et al. (1987)				
Mohamed and Vanapalli (2007)	Coarse-grained soils	NP	1.5	1
Li (2008)				
Costa et al. (2003)		8	1/4	
Rojas et al. (2007)	Fine-grained soils	12	1/6.5	2
data from Chapter 3		15.5	1/10	

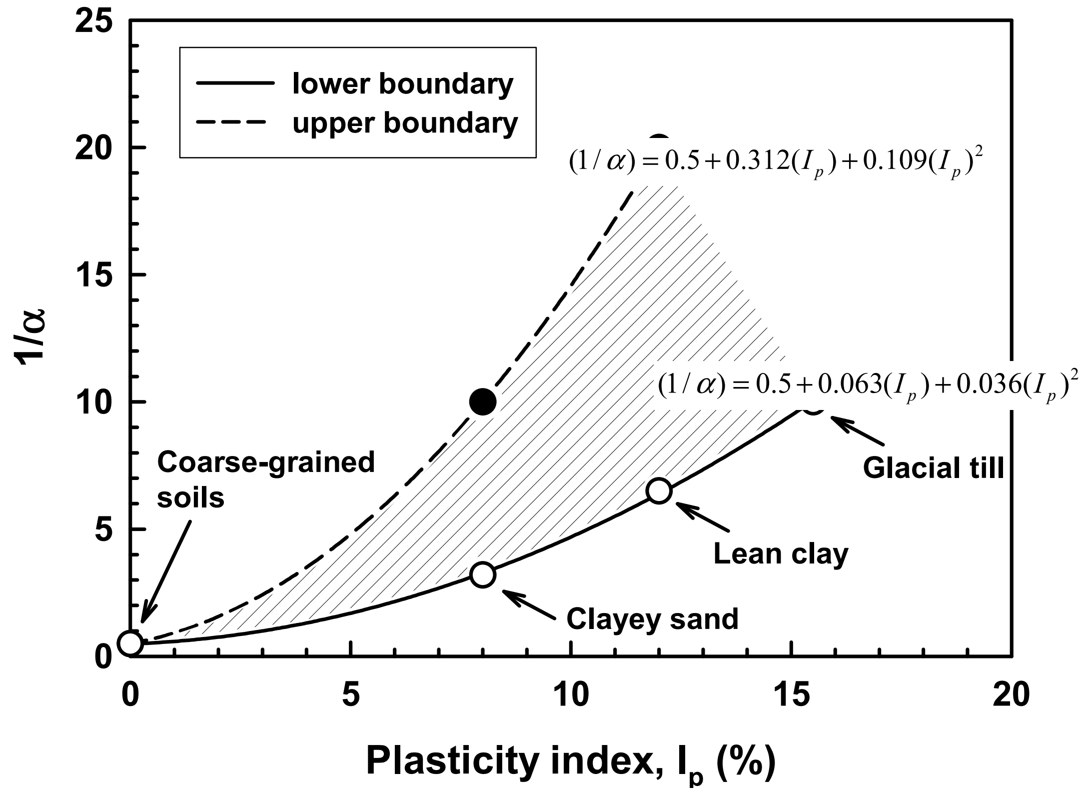

Figure 4.30 The relationship between $(1/\alpha)$ and plasticity index.

4.7 Influence of the Fitting Parameters, α and β on the Estimated Initial Tangent Elastic Modulus

The *SWCC* extends only over a narrow range of matric suction value for coarse-grained soils such as sandy soils (Figure 4.6). Due to this reason, the mechanical properties of unsaturated sandy soils; namely, shear strength (Donald 1956, Vanapalli and Lacasse 2009), bearing capacity (Steensen-Bach et al. 1987; Vanapalli and Mohamed 2007, Lins et al. 2009), initial tangent elastic modulus (this study), and shear modulus (Qian et al. 1993) also rapidly vary in this narrow range of matric suction. The net contribution of matric suction towards increase in mechanical properties starts decreasing as matric suction approaches residual suction value in coarse-grained soils. Hence, the variation of mechanical properties with respect to matric suction for coarse-grained soils is typically 'bell shape'.

Figure 4.31 shows the influence of the fitting parameter, α on the estimated initial tangent elastic modulus versus matric suction relationship in coarse-grained soils. The initial tangent elastic modulus values estimated using Eq. (4.4) are underestimated when $\alpha = 1$ is used since the whole range of *SWCC* distributes over a narrow range of matric suction value for coarse-grained soils. This results in low value of the term, $(u_a - u_w)S^{\beta}$. Hence, the fitting parameter, α greater than '1' is required to obtain reasonable values of initial tangent elastic modulus for coarse-grained soils.

The *SWCC*s for fine-grained soils are typically distributed over a wide range of suction values. The initial tangent elastic modulus sharply increases at the beginning of desaturation and then gradually increases as suction reaches residual value. The initial tangent elastic modulus values estimated using Eq. (4.4) with α = 1 are typically overestimated since the suction range for fine-grained soils is relatively large, which results in higher value of the term, $(u_a - u_w)S^{\beta}$. Hence, the fitting parameter, α less than '1' is required to obtain reasonable values of initial tangent elastic modulus for fine-grained soils (Figure 4.31).

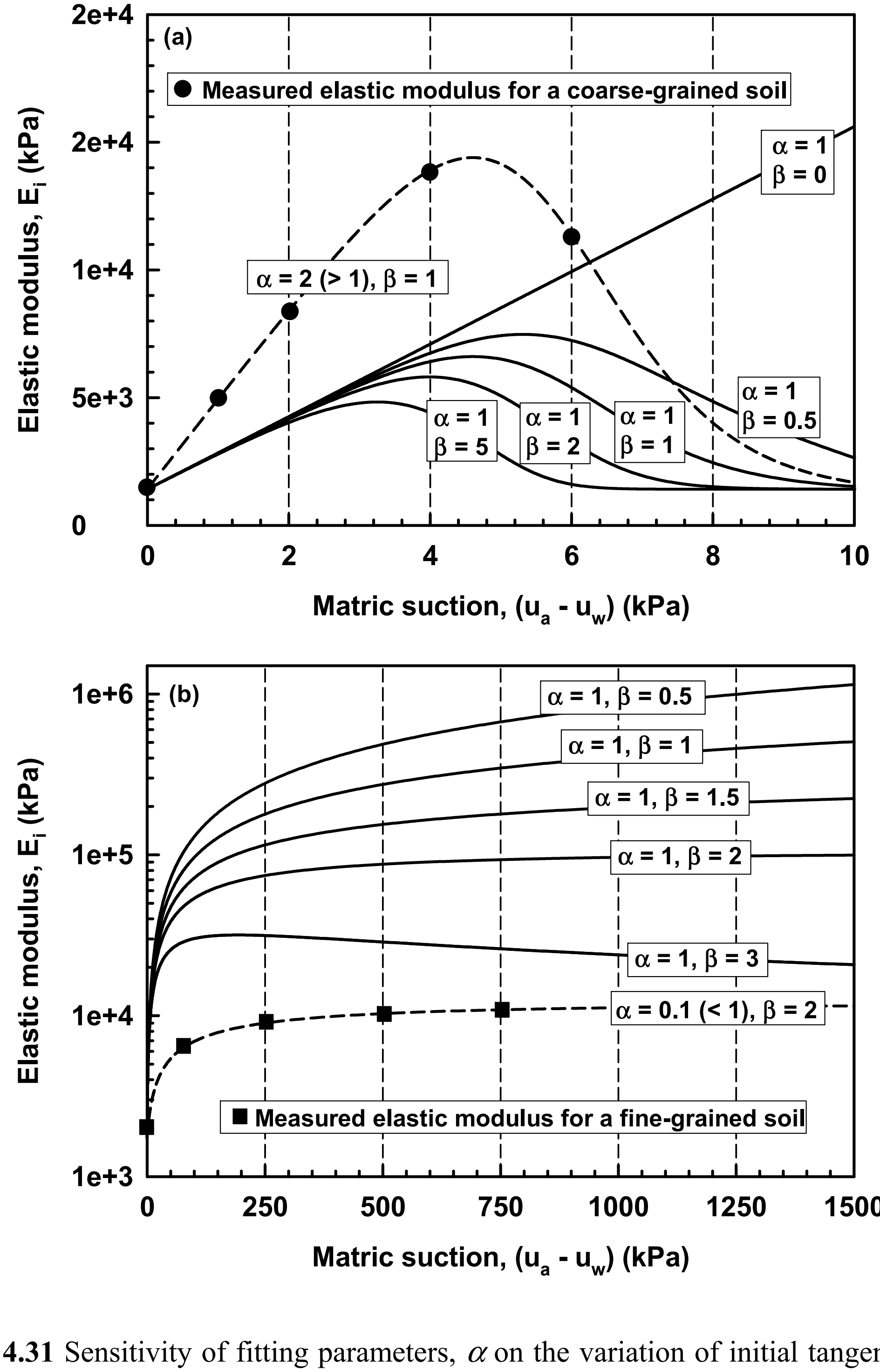

Figure 4.31 Sensitivity of fitting parameters, α on the variation of initial tangent elastic modulus with respect to matric suction for (a) coarse- and (b) fine-grained soils.

4.8 Summary and Conclusions

A semi-empirical model is proposed in this chapter for estimating the variation of the initial tangent elastic modulus with respect to matric suction for unsaturated soils. The conclusions obtained from this study are as follows.

(i) The estimated initial tangent elastic modulus and elastic settlement values using the proposed model are approximately the same as model footing test results in sands. The proposed model is useful to estimate the variation of initial tangent elastic modulus of unsaturated soils in all the three zones of the *SWCC* (i.e. boundary effect, transition, and residual zone).

(ii) The fitting parameters, α = 2.5 and β = 1 are expected to provide reasonable estimation of initial tangent elastic modulus of unsaturated sands in modeling the stress versus elastic settlement behavior of model footing tests. In addition, it is also expected that the value of α between 1.5 and 2 provides conservative elastic settlements in engineering practice (i.e. large sizes of footings).

(iii) For the model footing tests in Unimin sand, the elastic settlement behavior under saturated condition is approximately the same as unsaturated condition in the case where the matric suction value is greater than residual suction value.

(iv) Elastic settlements of shallow foundations in unsaturated sandy soils can be significantly reduced even if low matric suction values are maintained in the soils.

(v) The proposed model has been successfully extended to estimate the variation of initial tangent elastic modulus of unsaturated fine-grained soils. In this case, the fitting parameter, β = 2 is required and the fitting parameter, α can be estimated using the relationship between α and plasticity index, I_p [the inverse of α (i.e. $1/\alpha$) non-linearly increases with increasing I_p].

More test results both in the laboratory and in-situ conditions using different footing sizes taking account of the influence of embedment depth of footings into the soil would be valuable. The fitting parameter, α versus plasticity index, I_p relationship developed in this chapter is based on limited data (i.e. the plasticity index values ranging from 0 to 16%). Hence, more studies on (i) model footing or in-situ plate load tests using different sizes of footings for the same soils (i.e. same I_p to interpret the effect of footing size on the fitting parameter α) and (ii) soils with higher plasticity index [i.e. I_p (%) > 16] are necessary. The technique presented in this paper is encouraging for modeling studies and practicing engineers to predict immediate or elastic settlement of shallow foundation in unsaturated soils with a reasonable degree of accuracy.

REFERENCES

Agarwal, K.B. and Rana, M.K. 1987. Effect of ground water on settlement of footing in sand. *In* Proceedings of the 9th European Conference on Soil Mechanics and Foundation Engineering, Dublin, 751-754.

Costa, Y.D., Cintra, J.C. and Zornberg J.C. 2003. Influence of matric suction on the results of plate load tests performed on a lateritic soil deposit. *Geotechnical Testing Journal*, 26(2): 219- 226.

Davis, A.G. and Poulos, H.G. 1968. The use of elastic theory for settlement prediction under three dimensional conditions. *Géotechnique*, 18(1): 67-91.

Donald, I.B. 1956. Shear strength measurements in unsaturated non-cohesive soils with negative pore pressures. *In* Proceedings of the 2nd Australia-New Zealand Conference on Soil Mechanics and Foundation Engineering: 200-205.

Li, X. 2008. Laboratory studies on the bearing capacity of unsaturated sands. M.A.Sc. thesis, University of Ottawa, Canada.

Lins, Y., Schanz, T. and Vanapalli, S. K. 2009. Bearing capacity and settlement behavior of a strip footing on an unsaturated coarse-grained soil. *In* Proceedings of the 4th Asia-Pacific Conference on Unsaturated Soils, , New Castle, 443-448.

Maugeri, M., Castelli, F., Massimino, M.R. and Verona, G. 1998. Observed and computed settlements of two shallow foundations on sand. *Journal of Geotechnical and Geoenvironmental Engineering*, 124(7): 595-605.

Mohamed, F.M.O. and Vanapalli, S.K. 2006. Laboratory investigations for the measurement of the bearing capacity of an unsaturated coarse-grained soil. *In* Proceedings of the 59th Canadian Geotechnical Conference, Vancouver.

Poulos, H.D. and Davis, E.H. 1974. *Elastic solutions for soil and rock mechanics*. John Wiley and Sons, New York.

Qian, X., Gray, D.H. & Woods, R.D. 1993. Void and granulometry: effects and shear modulus of unsaturated soils. *Journal of Geotechnical Engineering*, 119(2): 295-314.

Rojas, J.C., Salinas, L.M. and Seja, C. 2007. Plate-load tests on an unsaturated lean clay. Springer Proceedings in Physics 112: 445-452.

Simons, N.E. and Som, N.N. 1970. Settlement of structures on clay with particular emphasis on London clay. Constr. Industry Research Institute Assoc. Report 22: 51.

Steensen-Bach, J.O., Foged, N. and Steenfelt, J.S. 1987. Capillary induced stresses–fact of fiction?. *In* Proceedings of the 9th European Conference on Soil Mechanics and Foundation Engineering, Budapest, 83-89.

Timoshenko, S., and Goodier, J.N. 1951. *Theory of elasticity*. McGraw-Hill, New York.

Vanapalli, S.K, and Mohamed, F.M.O. 2007. Bearing capacity of model footings in unsaturated soils. *In* Proceedings of the 2nd International Conference on Unsaturated Soils, Weimar, 483-493.

Vanapalli, S.K., Fredlund, D. G., Pufahl. 1999. The influence of soil structure and stress history on the soil-water characteristics of a compacted till. *Géotechnique*, 49(2): 143-159.

Vanapalli, S.K. and Lacasse, F. 2009. Comparison between the measured and predicted shear strength behavior of unsaturated sands. *In* Proceedings of the 4th Asia-Pacific Conference on Unsaturated Soils, Newcastle, 739-744.

CHAPTER 5

MODELLING THE STRESS VERSUS SETTLEMENT BEHAVIOR OF SHALLOW FOUNDATIONS IN UNSATURATED COARSE-GRAINED SOILS

5.1 Introduction

The initial tangent of elastic modulus is a key parameter (more discussions in Chapter 4), to estimate the elastic settlement of shallow foundations in coarse-grained soils. However, in the case of shallow foundations, it is necessary to interpret the range of stresses corresponding to the elastic settlements to reliably estimate the elastic settlements for different matric suction values. This can be obtained by estimating the variation of applied stress versus surface settlement (hereafter referred to as stress versus settlement) behavior of shallow foundations in unsaturated soils.

In this chapter, two methodologies are proposed for estimating the stress versus settlement behavior of model footing tests in unsaturated sands. In the first method (i.e. *Method I*), the stress versus settlement behavior is simplified using elastic-perfectly plastic behavior. In other words, the relationship was idealized using two straight lines, which represent elastic and perfectly plastic behavior, respectively. The elastic line is estimated using the semi-empirical model proposed in Chapter 4 [i.e. Eq. (4.3)] to estimate the variation of the initial tangent modulus of subgrade reaction (k_{is}) with respect to matric suction. The plastic line is established using the semi-empirical model introduced in Chapter 3 to estimate the variation of bearing capacity with respect to matric suction [i.e. Eq. (3.6), Vanapalli and Mohamed 2007]. In the second method (i.e. *Method II*), finite element analysis (hereafter referred to as *FEA*) is carried out using elastic-perfectly plastic model with Mohr-Coulomb yield criterion (Chen and Zhang 1991). The *FEA* is undertaken using the *SIGMA/W* (Krahn 2007), a software product of *GEO-SLOPE* (i.e. Geostudio 2007). The validity of the proposed methodologies (i.e.

Method I and *Method II*) is tested using the model footing tests results in unsaturated sand provided by Mohamed and Vanapalli (2006).

In addition, *Method II* (i.e. *FEA*) is also extended to simulate the stress versus settlement behavior of in-situ footing load tests results in unsaturated sand provided by Briaud and Gibbens (1994). These load test results are also used to explain the scale effect of footing size in unsaturated soils. Unlike saturated soils, investigating the scale effect in unsaturated soils is difficult since it is a function of both the footing size and matric suction. This difficulty can be overcome by conducting the model footing tests in an unsaturated soil that has uniform matric suction distribution profile with respect to depth. Hence, in this study, details of a Large Tempe Cell that can be used to achieve uniform matric suction distribution profile with depth are also presented in the Appendix.

5.2 Background

5.2.1 Bearing Capacity of Unsaturated Sandy Soils

The variation of bearing capacity of surface footings on unsaturated soils can be calculated using the semi-empirical model [Eq. (5.1)] proposed by Vanapalli and Mohamed (2007) as explained in Chapter 3 [i.e. Eq. (3.6)].

$$q_{ult(unsat)} = \begin{bmatrix} c' + (u_a - u_w)_b \left(1 - S^{\psi} \tan\phi'\right) \\ + (u_a - u_w)_{AVR} S^{\psi} \tan\phi' \end{bmatrix} N_c \xi_c + 0.5 B \gamma N_\gamma \xi_\gamma \qquad (5.1)$$

where $q_{ult(unsat)}$ = ultimate bearing capacity for unsaturated soils, c', ϕ' = effective cohesion and internal friction angle, respectively, $(u_a - u_w)_b$ = air-entry value, $(u_a - u_w)_{AVR}$ = average matric suction value, S = degree of saturation, γ = soil unit weight, ψ = fitting parameter with respect to bearing capacity (ψ = 1 for coarse-grained soils), B = width of footing, N_c, N_γ = bearing capacity factor from Terzaghi(1943) and Kumbhokjar (1993), respectively, and $\xi_c \left\{ = \left[1.0 + \left(\frac{N_q}{N_c}\right)\left(\frac{B}{L}\right) \right] \right\}$, $\xi_\gamma \left\{ = \left[1.0 - 0.4\left(\frac{B}{L}\right) \right] \right\}$ = shape factors from Vesić (1973)

The average matric suction value, $(u_a - u_w)_{AVR}$ in Eq. (5.1) is defined as the matric suction value at the centroid of the matric suction distribution diagram in the stress bulb zone from surface to a depth of 1.5B - 2B (where B = width of model footing). More details of average matric suction value are described in Section 3.5.2.

The original bearing capacity equation proposed by Terzaghi (1943) was based on assuming plane strain condition for continuous footings. Hence, the effective internal friction angle, ϕ' obtained from the conventional laboratory tests such as triaxial shear test or direct shear test need to be modified taking account of the difference between plane strain and axisymmetric conditions in the conventional triaxial compression tests. It is known that ϕ' obtained under plane strain condition (i.e. ϕ'_{PS}) is typically higher than that obtained under axisymmetric condition (i.e. ϕ'_{AS}) (Marachi et al. 1981, Alshibli et al. 2003, Wanatowski and Chu, 2007).

Wanatowski and Chu (2007) showed that the difference in the measured ϕ' values from plane and axisymmetric condition increases with decreasing void ratio. The minimum ratio of ϕ'_{PS}/ ϕ'_{AS} was approximately 1.1 for the void ratio range they studied (i.e. 0.654 - 0.969). The Danish Code of Practice (*DS* 415) (1984) suggested 1.1 as a ratio of ϕ'_{ps}/ ϕ'_{AS}. In addition, another relationship is also suggested in the Danish code in terms of relative density, I_D as below.

$$\phi'_{PS} = \phi'_{AS}(1 + 0.163 I_D) \tag{5.2}$$

where ϕ'_{PS}, ϕ'_{AS} = effective internal friction angle under plane and axisymmetric strain condition, respectively, and I_D = relative density

The study by Steensen-Bach et al. (1987) showed that there was good comparison between the measured and the computed bearing capacity values when the effective internal friction angle, ϕ' was increased by 10 to 15 %.

These previous studies suggest that increasing the ϕ' values by 10% can provide good estimates of bearing capacity values calculated using the Terzaghi (1943) bearing capacity theory. Hence, in this chapter, the analyses were carried out using two different effective internal friction angles; namely ϕ' (i.e. 35.3°) and 1.1 ϕ' (i.e. 39°), for both computation of bearing capacity using Eq. (5.1) and the *FEA* for comparison purposes. The ratio of $\phi'_{PS}/\ \phi'_{AS}$ estimated using Eq. (5.2) based on the average relative density (i.e. 63.76%) for the sand used by Mohamed and Vanapalli (2006) also estimated to be 1.1.

The bearing capacity factors, N_c and N_q proposed by Terzaghi (1943) are commonly used in engineering practice. However, there is no consensus in the literature with respect to the use of appropriate values of N_γ. There are significant differences in N_γ values proposed by various investigators for effective internal friction angles, ϕ' greater than 30°; however, the differences are negligible for ϕ' values less than 30° (Budhu 2006).

As can be seen in Eq. (5.1), the bearing capacity equation for surface footings in unsaturated soils proposed by Vanapalli and Mohamed (2007) adopts N_c (along with N_q) suggested by Terzaghi (1943), N_γ by Kumbhokjar (1993) and shape factors by Vesić (1973). The variation of the bearing capacity factors with effective internal friction angle, ϕ' is shown in Figure 5.1.

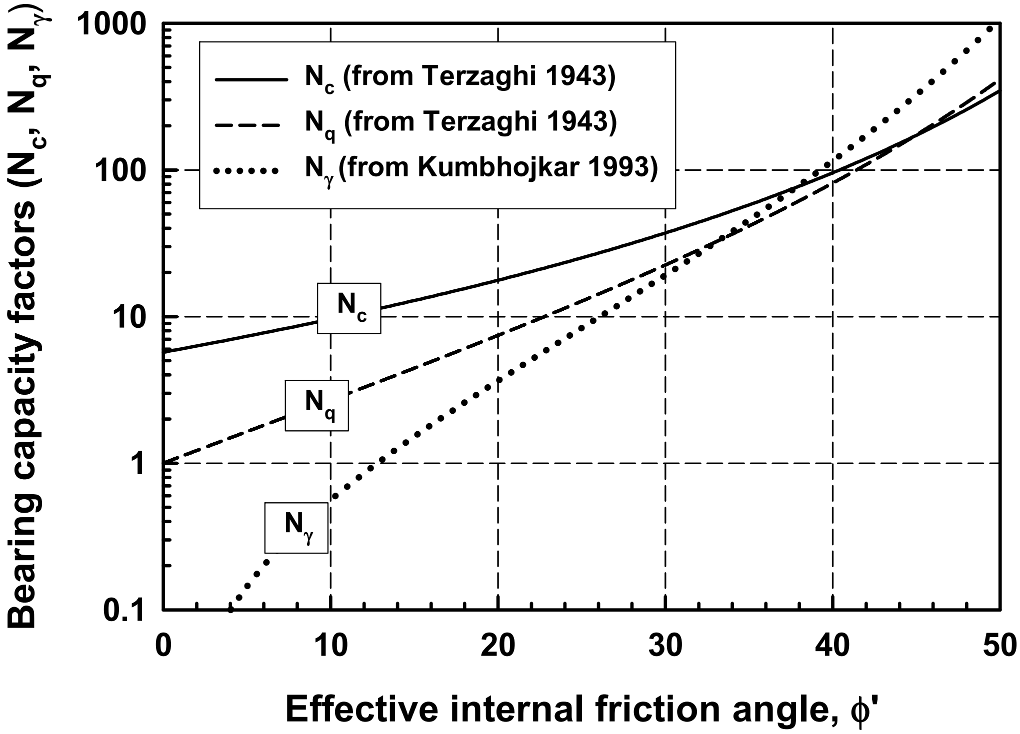

Figure 5.1 Variation of bearing capacity factors with respect to effective internal friction angle used in the bearing capacity equation proposed by Vanapalli and Mohamed (2007).

To investigate the reliability of the bearing capacity factors used by Vanapalli and Mohamed (2007) [i.e. N_c from Terzaghi (1943) and N_γ from Kumbhokjar (1993) in Eq. (5.1)], the bearing capacity values from the model footing tests under saturated condition [Steensen-Bach et al. (1987) and Mohamed and Vanapalli (2006)] were compared with those estimated using different bearing capacity equations proposed by Terzaghi (1943), Meyerhof (1963), Vesić (1973) and Vanapalli and Mohamed (2007). Table 5.1 provides a summary of the bearing capacity and shape factors used by several investigators. Figure 5.2(a) and (b) show the comparison between the measured and the calculated bearing capacity values for the model footing tests results by Steensen-Bach et al. (1987) and Mohamed and Vanapalli (2006), respectively. The calculated bearing capacity values using Eq. (5.1) are the closest to those from the model footing tests.

Table 5.1 Summary of the bearing capacity and shape factors used by several investigators.

	$q_{ult} = cN_c\xi_c + 0.5B\gamma N_\gamma \xi_\gamma$: Bearing capacity of surface footing			
Author	N_c	N_γ	ξ_c	ξ_γ
Terzaghi (1943)	$(N_q - 1)\cot\phi'$	$\frac{\tan\phi'}{2}\left(\frac{K_p}{\cos^2\phi} - 1\right)$	1.3 (square)	0.8 (square)
Meyerhof (1963)	$(N_q - 1)\cot\phi'$	$(N_q - 1)\tan(1.4\phi')$	$1 + 0.2K_p\left(\frac{B}{L}\right)$	$1 + 0.1K_p\left(\frac{B}{L}\right)$
Vesić (1973)	Meyerhof (1963)	$2(N_q + 1)\tan\phi$	$1 + \left(\frac{N_q}{N_c}\right)\left(\frac{B}{L}\right)$	$1 - 0.4\left(\frac{B}{L}\right)$
Vanapalli and Mohamed (2007)	Terzaghi (1943)	Kumbhojkar (1973)	Vesić (1973)	Vesić (1973)

K_p: passive earth pressure coefficient
N_c, N_g = bearing capacity factors
ζ_c, ξ_c = shaper factors
c', ϕ' = effective cohesion and internal friction angle
B, L = width and length of a footing

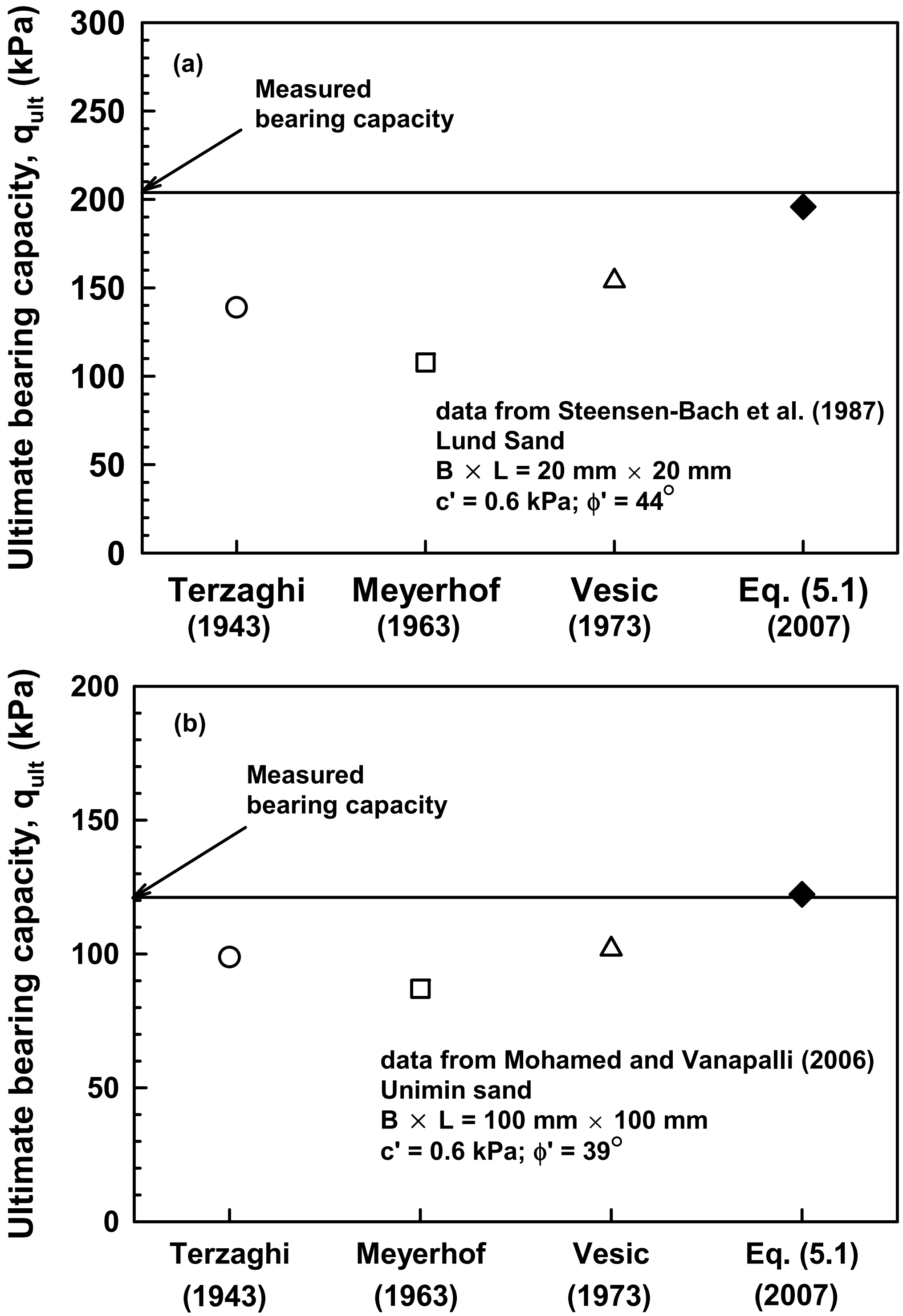

Figure 5.2 Comparison between the measured bearing capacity values and those estimated for saturated condition using different bearing capacity equations for the data by (a) Steensen-Bach et al (1987) and (b) Mohamed and Vanapalli (2006).

5.2.2 Influence of Air-Entry Value on the Estimated Bearing Capacity Values

Unlike fine-grained soils, the *SWCC*s of coarse-grained soils distribute in a narrow range of matric suction values. Many sands rapidly desaturate from saturated conditions to close to dry conditions over a matric suction range of 0 to 10 kPa. This indicates that even low matric suction values such as 1 kPa in coarse-grained soils can lead to significant differences in estimated bearing capacity values. Due to this reason, in this chapter, the air-entry value of the sand on which the model footing tests were conducted was estimated using three different methods.

5.2.3 Initial Tangent Elastic Modulus of Unsaturated Sands

In Chapter 4, a semi-empirical model was proposed to estimate the variation of initial tangent modulus of subgrade reaction, k_{is} with respect to matric suction as shown in Eq. (5.3) [Eq. (4.3) in Chapter 4]. The details of the fitting parameter, α and β are described in Chapter 4.

$$k_{is(unsat)} = k_{is(sat)} \left[1 + \alpha \frac{(u_a - u_w)}{(P_a / 101.3)} \left(S^{\beta} \right) \right] \tag{5.3}$$

where $k_{is(sat)}$, $k_{is(unsat)}$ = initial tangent modulus of subgrade reaction under saturated and unsaturated condition, respectively, S = degree of saturation, α, β = fitting parameters, and P_a = atmospheric pressure (i.e. 101.3 kPa)

Based on Eq. (5.3), the variation of the modulus elasticity with respect to matric suction can be estimated using Eq. (5.4) [Eq. (4.4) in Chapter 4].

$$E_{unsat} = E_{sat} \left[1 + \alpha \frac{(u_a - u_w)}{(P_a / 101.3)} \left(S^{\beta} \right) \right] \tag{5.4}$$

where $E_{i(sat)}$, $E_{i(unsat)}$ = initial tangent elastic modulus under saturated and unsaturated condition, respectively

5.3 Proposed Methodologies to Estimate the Applied Vertical Stress versus Surface Settlement Behavior of Model Footing Tests in Unsaturated Sands

The model footing tests results provided by Mohamed and Vanapalli (2006) were used in this study to simulate the stress versus settlement behavior of model footing tests in unsaturated sand. The details of model footing tests (i.e. dimension of the bearing capacity test tank, soil properties, procedure of saturation and desaturation of the sand, and estimation of the average matric suction value) and soils properties are detailed in Chapter 4.

5.3.1 Method I

In this method, the stress versus settlement behavior was assumed to consist of two straight lines, *L1* (elastic line) and *L2* (plastic line) as shown in Figure 5.3 assuming elastic-perfectly plastic behavior. The line, *L1* in Figure 5.3 represents linear elastic behavior which has a slope equal to initial tangent modulus of subgrade reaction, k_{is}. The k_{is} value for a certain matric suction values can be calculated using Eq. (5.3). The line, *L2* represents unrestricted perfectly plastic settlement behavior under constant stress, which can be drawn based on the bearing capacity value estimated using Eq. (5.1).

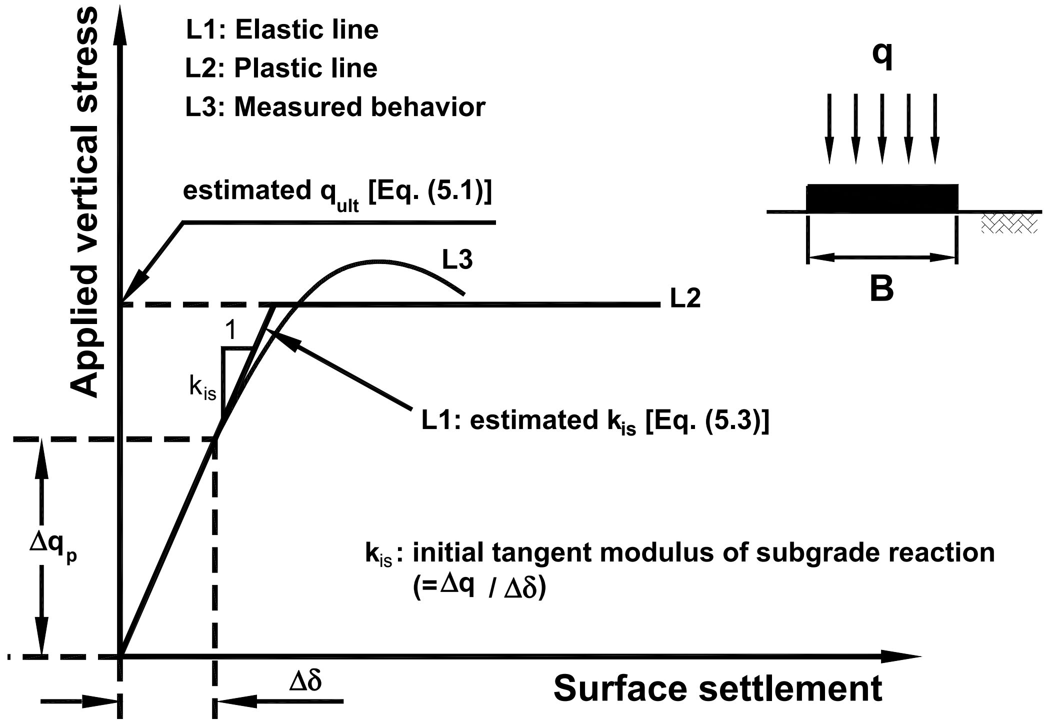

Figure 5.3 Measured (*L3*) and simplified (*L1* and *L2*) stress versus settlement behavior from model footing tests.

5.3.2 Method II (Finite Element Analysis)

5.3.2.1 Finite Element Analysis (FEA) in Unsaturated Sandy soils

The second method uses the finite element analysis (*FEA*) to obtain the stress versus settlement behaviors by simulating the model footing tests in unsaturated sand using the Mohr-Coulomb yield criterion. In this study, the analyses were carried out using the commercial finite element software, *SIGMA/W* (a software product of *GEO-SLOPE*; Geostudio 2007) with the yield function of elastic-perfectly plastic model [Chen and Zhang 1991, Eq. (5.5)].

$$F = \sqrt{J_2}\sin\left(\bar{\theta} + \frac{\pi}{3}\right) - \sqrt{\frac{J_2}{3}}\cos\left(\bar{\theta} + \frac{\pi}{3}\right)\sin\phi' - \frac{I_1}{3}\sin\phi' - c\cos\phi' \tag{5.5}$$

where J_1 = first stress invariant, J_2 = second deviatoric stress invariant, J_3 = third deviatoric stress invariant, and $\bar{\theta}$ $\left[= \frac{1}{3}\cos^{-1}\left(\frac{3\sqrt{3}}{2}\frac{J_3}{J_2^{3/2}}\right)\right]$ = lode angle

It is well known that two independent stress state variables (i.e. matric suction and net normal stress) are necessary to reasonably interpret the mechanical properties of the unsaturated soils. Due to this reason, conventional elasto-plastic models for unsaturated soils use matric suction as a primary stress variable along with the net normal stress (Alonso et al.1990, Cui and Delage 1996, Wheeler and Sivakumar 1995). These constitutive models indicate that the variation of volumetric deformations (i.e. swelling-shrinkage) or net normal stress which results in change in degree of saturation should be taken into account to estimate the behavior of unsaturated soils. Gallipoli et al. (2003) proposed a simple elasto-plastic model using a single yield surface taking account of volumetric hardening based on the assumption that the e_{unsat}/e_{sat} at the same average skeleton stress is a unique function of bonding variable, ξ_G [$= f(s)(1-S_r)$] [where e_{sat}, e_{unsat} = void ratio in saturated and unsaturated condition, respectively at the same average net normal stress, $f(s)$ = function of suction, and $(1-S_r)$ = degree of saturation of air].

The development of elasto-plastic models for unsaturated soils has reduced the number of tests required to determine the parameters for the models; however, there are still difficulties in conducting the tests for unsaturated soils as they require elaborate testing equipments. Hence, in this chapter, the elastic-perfectly plastic model developed for saturated soils was used. The variation of suction value of the unsaturated soils below the model footing due to loading and specific volume change associated with desaturation was not taken into in the *FEA* account since the model footing tests were conducted on unsaturated sand in a relatively short period of time.

The *FEA* was performed as an axisymmetric problem with equivalent area although the model footing test results used in the present study were obtained for a square footing. This can be justified based on the following experimental and numerical studies published in the literature. For example, Cerato and Lutenegger (2006) conducted model footing tests on a sand with both square and circular footings (width and dia. = 102 mm). The bearing capacity values using a square footing was higher than those using a circular footing by a mean value of 1.25 times. This is attributed to using a square footing whose width was equal to the diameter of the circular footing (i.e. not equivalent area). Gourvenec et al. (2006) showed that the bearing capacity of a square footing is less than that of an equivalent circular footing by 3% based on the *FEA* results.

5.3.2.2 Estimation of Soil Properties for the FEA

Total Cohesion and Internal Friction Angle

In *SIGMA*/*W* (Geostudio 2007), the variation of pore-water pressure with depth can be simulated by defining an initial water table and maximum negative pressure head assuming that pore-water pressure varies hydrostatically with distance above and below the initial water table as shown in Figure 5.4 (Krahn 2007). For instance, if maximum negative pressure head is lower than the height of unsaturated soil layer (i.e. $H_{max} < H_{unsat}$) the negative pore-water pressure is constant up to ground surface beyond maximum negative pressure head. On the other hand, if maximum negative pressure head is greater than the height of unsaturated soil layer (i.e. $H_{max} > H_{unsat}$) the negative pore-water pressure hydrostatically increases up to ground surface.

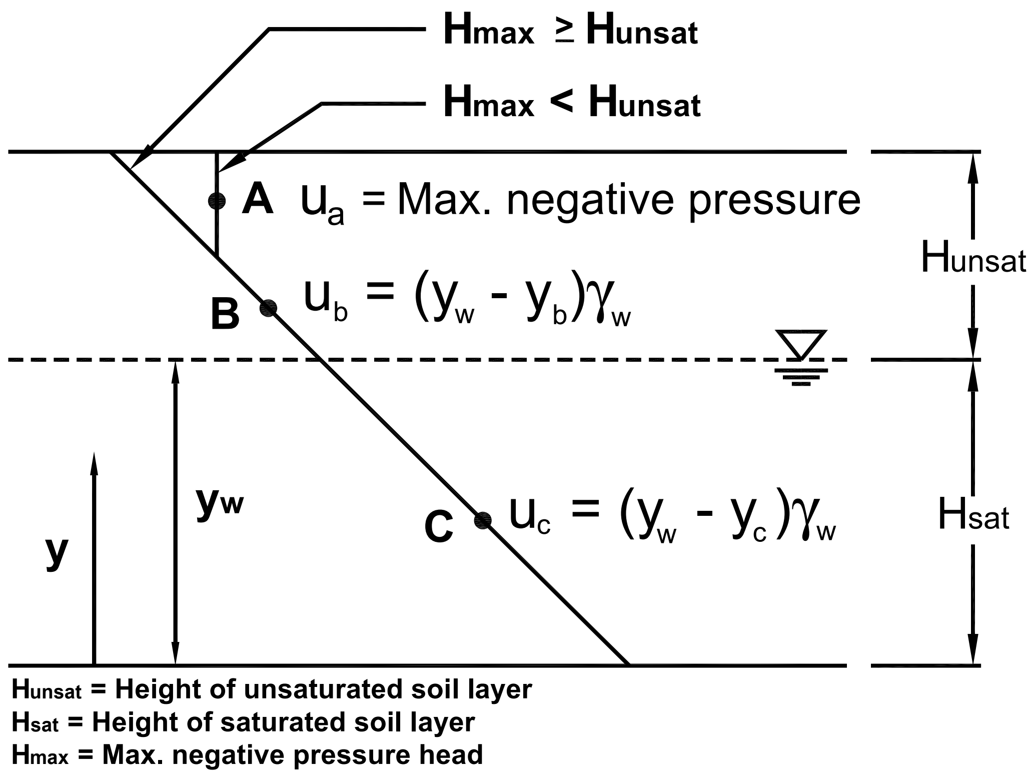

Figure 5.4 Estimation of positive and negative pore-water pressure in *SIGMA/W*.

Based on the hydrostatic pore-water pressure distribution diagram, the contribution of matric suction, ϕ^b towards total cohesion (or apparent cohesion), c is calculated using Eq. (5.6) as given below.

$$c = c' + (u_a - u_w)\tan\phi^b \tag{5.6}$$

The ϕ^b value can be specified as an input parameter in *SIGMA/W*. However, determination of ϕ^b for unsaturated soils from laboratory tests (i.e. modified triaxial compression or modified direct shear test) is time-consuming and needs elaborate equipment. The total cohesion, c can be more easily and reliable calculated using Eq. (5.7) [Eq. (3.4) in Chapter 3] that was originally proposed by Vanapalli et al. (1996a) and Fredlund et al. (1996) to predict the variation of the shear strength with respect to matric suction using *SWCC* as a main tool. By setting the value of $(\sigma_n - u_a)$ as zero (i.e. surface footing) in Eq. (5.7) the total cohesion can be calculated using Eq. (5.8). The fitting parameter, $\kappa = 1$ is required for coarse-grained soils (i.e. I_p = 0%; Garven and Vanapalli 2006). The concept in Eq. (5.8) can be implemented in *SIGMA/W* by setting the ϕ^b value as zero and having the total cohesion c instead of c' in the *FEA*.

$$\tau_{unsat} = c' + (\sigma_n - u_a)\tan\phi' + (u_a - u_w)(S^\kappa)(\tan\phi') \tag{5.7}$$

$$c = c' + \left(u_a - u_w\right)\left(S^\kappa\right)\tan\phi' \tag{5.8}$$

In case of the effective internal friction angle, ϕ', constant value can be used regardless of the matric suction value since ϕ' is not influenced by the matric suction (Vanapalli et al. 1996b, Wang et al. 2002, Nishimura et al. 2007). However, in the *FEA*, two different ϕ' values were used taking account of the difference plain strain and axisymmetric conditions.

Elastic Modulus

The elastic modulus for the *FEA* is mostly estimated using the triaxial test results (except unconsolidated undrained test for saturated soils). Janbu (1963) showed that the initial tangent elastic modulus, E_i increases with increasing the confining pressure [Eq. (5.9)].

$$E_i = KP_a\left(\frac{\sigma_3}{P_a}\right)^{n_J} \tag{5.9}$$

where E_i = initial tangent elastic modulus, σ_3 = confining pressure, P_a = atmospheric pressure, K = modulus number, and n_J = exponent determining the rate of variation of E_i with σ_3

The concept in Eq. (5.9) indicates that different values of E_i should be assigned to the elements of the *FEA* meshes to obtain reasonable stress versus settlement behavior. However, conducting the triaxial tests with different confining pressures to estimate the parameters, K and n_J in Eq. (5.9) are time-consuming. Hence, in the present study, different approach is used to estimate E_i for the *FEA*.

Preliminary studies were undertaken to estimate reasonable E_i values for the *FEA*. First, the stress versus settlement behaviors were estimated using the E_i values calculated using the equation proposed by Timoshenko and Goodier (1951) [Eq. (5.10)] based on the model footing test results (Mohamed and Vanapalli 2006). However, the stresses from the *FEA* using those E_i values were significantly low in comparison to the measured stresses for entire range of settlements. This can be attributed to the reason that the influence of Poisson's ratio, ν and the model footing size, B (i.e. I_w) on the stress versus settlement behaviors is considered in the process of analysis since ν and B are included as input parameters in the *FEA*. Hence, the E_i values for the *FEA* were estimated using Eq. (5.11) without including ν and I_w.

$$E_i = \frac{\left(1-\nu^2\right) I_w}{\left(\Delta\delta / \Delta q\right)} B = k_{is}\left(1-\nu^2\right) I_w B \tag{5.10}$$

where E_i = initial tangent elastic modulus, k_{is} = initial tangent modulus of subgrade reaction (=$\Delta q/\Delta\delta$), Δq = increment of applied stress in elastic range, $\Delta\delta$ = increment of settlement in elastic range, ν = Poisson's ratio (a value of 0.3 was used for this study assuming drained loading conditions for the sands studied), B = width (or diameter) of plate (or model footing), and I_w = influence factor (i.e. 0.79 for circular plate and 0.88 for square plate).

$$E_i = \frac{B}{\left(\Delta\delta / \Delta q\right)} = \frac{\Delta q}{\left(\dfrac{\Delta\delta}{B}\right)} \tag{5.11}$$

The E_i values calculated using Eq. (5.11), however, also did not provide a good comparison between the measured and the estimated stress versus settlement behaviors in the elastic range. However, when 1.5B was used instead of B in Eq. (5.11) [i.e. Eq. (5.12)] good agreement was observed between the measured and the estimated stress versus settlement behaviors in elastic range.

$$E_i = \frac{1.5B}{(\Delta\delta / \Delta q)} = \frac{\Delta q}{\left(\dfrac{\Delta\delta}{1.5B}\right)} \tag{5.12}$$

Agarwal and Rana (1987) performed model footing tests in sands to study the influence of ground water table on settlement. The results of the study showed that the settlement behavior of relatively dry sand is similar to that of a sand with a ground water table at a depth of 1.5*B* below the model footing (Figure 5.5). These results indirectly support that the increment of stress due to the load applied on the model footing is predominant in the range of 0 to 1.5*B* below model footing. It is of interest to note that 1.5*B* in Eq. (5.12) represents the depth of which the stress below a foundation is predominant as observed by Agarwal and Rana (1987). However, as observed from the model footing tests results in an unsaturated fine-grained soil (Indian Head till) in Chapter 3, the variation of bearing capacity with respect to matric suction was well explained by using 2*B* rather than 1.5*B*.

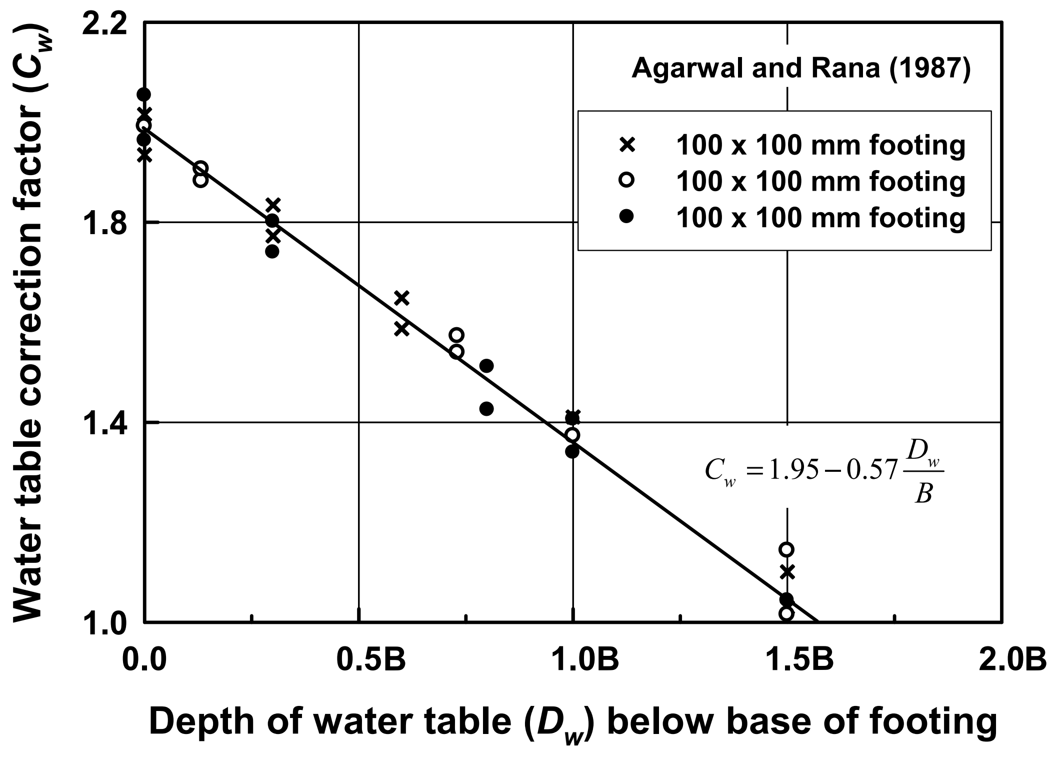

Figure 5.5 Relationship between water table correction factor (C_w) and depth of water table below base of footing (Agarwal and Rana 1987).

Air-Entry Value

The air-entry value of the sand in the bearing capacity tank was estimated based the *SWCC* using two different methods.

(i) Matric suction value corresponding to the point at which the initial constant slope portion terminates on the *SWCC* (*AEV* 1 in Figure 5.6)

(ii) Matric suction value corresponding to the intersection of the first two linear slope segments of the *SWCC* (*AEV* 2 in Figure 5.6) using the procedures detailed in Vanapalli et al. (1999).

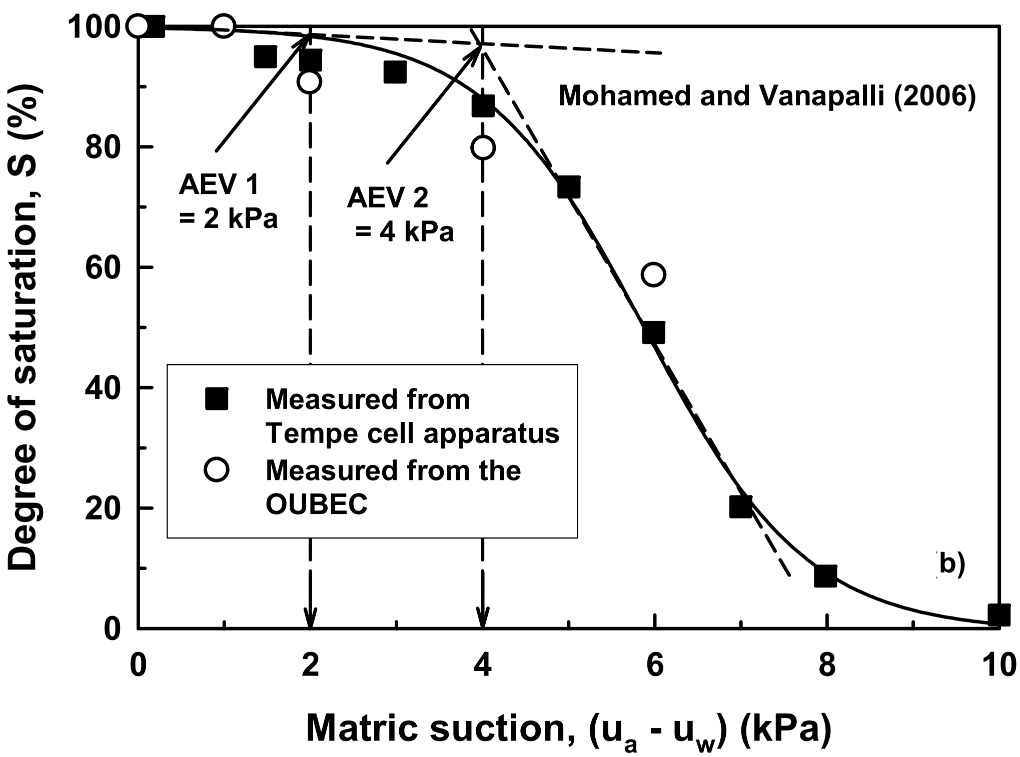

Figure 5.6 *SWCC* for the tested sand with air-entry values measured using two different procedures [data from Mohamed and Vanapalli (2006)].

The parameters such as effective and total cohesion, effective internal friction angle, initial tangent modulus of subgrade reaction and initial tangent elastic modulus used for the two different methods (i.e. *Method I* and *Method II*) proposed in this chapter are summarized in Table 5.2.

Table 5.2 Summary of the soil properties used for the analysis.

$(u_a - u_w)_{AVR}$ (kPa)	c' or c 1) (kPa)	ϕ' (°)	$1.1\phi'$ (°)	k_{is}_1 3) (kN/m^3)	k_{is}_2 4) (kN/m^3)	E_i 5) (kPa)	E_i 6) (kPa)
0	0.60	35.3	39.0	17,726	17,726	2,659	2,659
2	2.56			75,000	69,840	11,250	10,476
4	4.08			112,500	110,255	16,875	16,538
6	3.36			91,410	91,111	13,711	13,667

1)effective cohesion
2) total cohesion estimated using Eq. (5.8)
3),5) measured k_{is} and E_i, respectively
4),6) estimated k_{is} [Eq. (5.3)] and E_i [Eq. (5.4)], respectively

5.3.2.3 Procedures to Model the Model Footing Tests on Unsaturated Sandy Soils in the FEA

The procedures used in the present study for modelling the model footing tests on unsaturated sands in the *FEA* can be summarized as below.

(i) Determine the average matric suction value (i.e. matric suction value corresponding to the centroid of the matric suction distribution profile) based on the matric suction distribution diagram using the procedures described in section 3.5.2.

(ii) Model the soil on which the model footing test is conducted as a single soil layer with the average matric suction.

(iii) Calculate the total cohesion, c corresponding to the average matric suction value using Eq. (5.8) (set the value of ϕ^b zero in *SIGMA/W*).

(iv) Calculate the initial tangent elastic modulus for saturated condition, $E_{i(sat)}$ using Eq. (5.12) and also estimate the variation of initial tangent elastic modulus with respect to suction [i.e. $E_{i(unsat)}$] using and Eq. (5.4).

(v) Apply appropriate boundary conditions to the meshes.

The procedure of modelling is schematically illustrated in Figure 5.7.

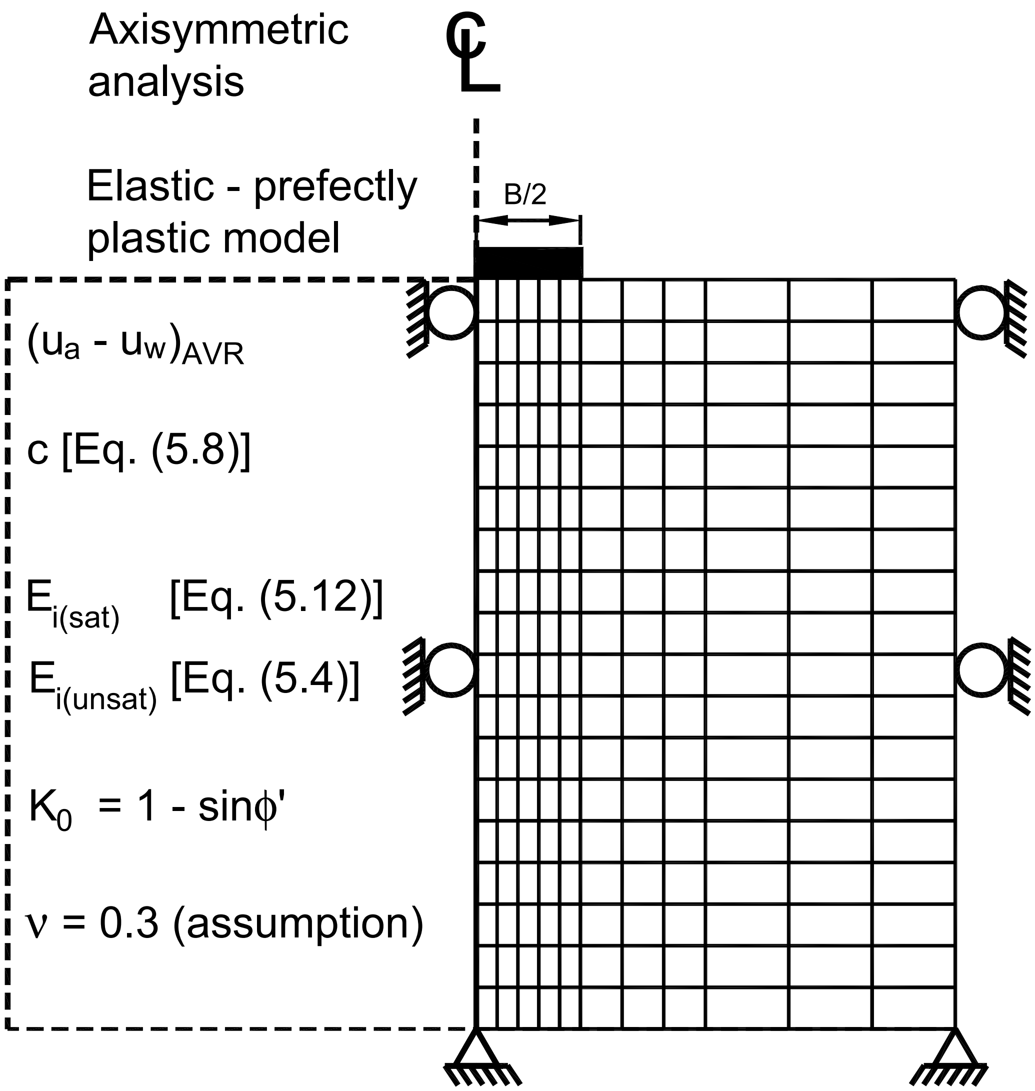

Figure 5.7 Soil properties and boundary conditions for the *FEA*.

5.4 Analysis Results

5.4.1 Comparison between the Measured and the Estimated Stress versus Settlement Behavior

As can be seen in Table **5.2**, good agreement was observed between the measured and the estimated k_i values. This indicates that the reliability of the *Method I* is dependent on the estimated bearing capacity values that can be calculated using Eq. (5.1). In case of the unsaturated coarse-grained soils, the estimated bearing capacity values can be significantly influenced by air-entry values. Due to this reason, in this study, three different air-entry values; namely, *AEV* 1 (2 kPa), *AEV* 2 (4 kPa) (see Figure 5.6) and average air-entry value, *AEV* 3 (3 kPa) [= (*AEV* 1 + *AEV* 2)/2] were considered to study the sensitivity of the air-entry value on the estimated stress versus settlement behaviors. In addition, the influence of effective internal friction angle, ϕ' on the stress versus settlement behavior was also studied using two different effective internal friction angles (i.e. ϕ' and $1.1\phi'$) as discussed earlier.

Table 5.3 and Figure 5.8 show the measured and the estimated bearing capacity values obtained using Eq. (5.1) for different matric suction values with three different air-entry values (i.e. *AEV* 1, *AEV* 2 and *AEV* 3) and two effective internal friction angles (i.e. ϕ' and $1.1\phi'$).

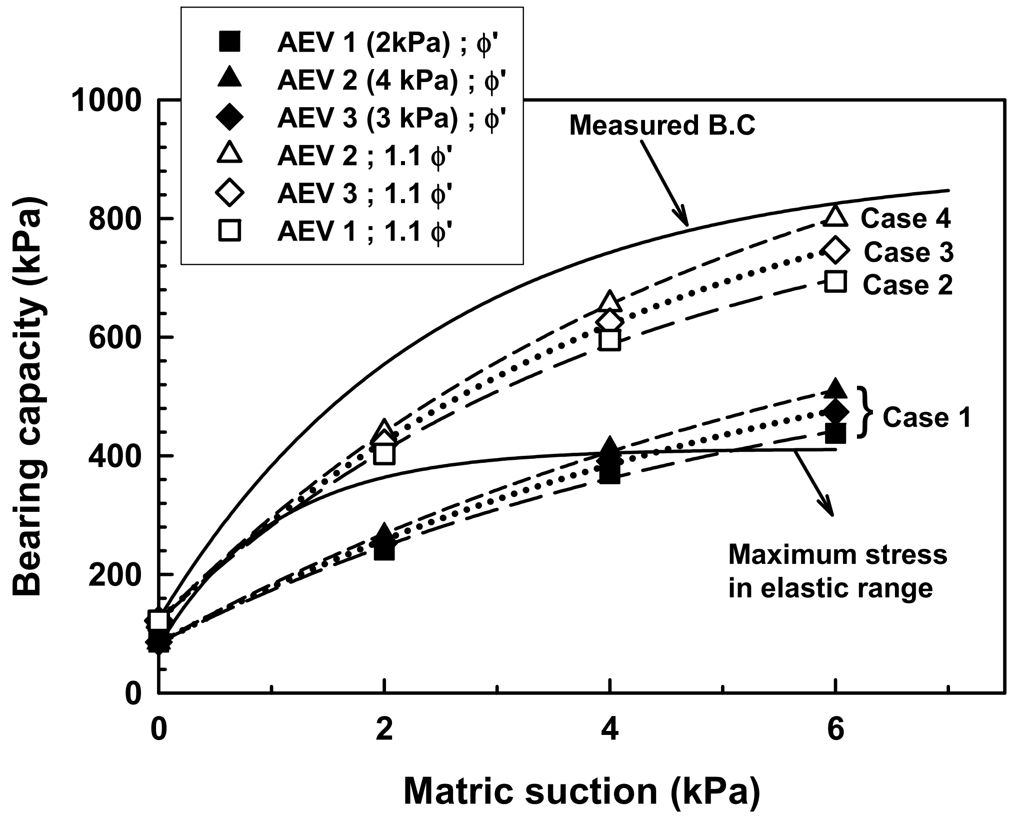

Figure 5.8 Measured bearing capacity values and those estimated using Eq. (5.1) for different air-entry values and effective friction angles.

Table 5.3 Comparison between the measured and estimated bearing capacity (*BC*) values for different average matric suction and air-entry values (*AEV*) and effective internal friction angles.

			Estimated *BC*					
			AEV 1 (2kPa)		*AEV* 2 (4 kPa)		*AEV* 3 (3 kPa) [(*AEV* 1 + *AEV* 2)/2]	
$(u_a - u_w)_{AVR}$ (kPa)	Measured *BC* (kPa)	Maximum stress [1)] (kPa)	ϕ' (Case 1)	1.1 ϕ' (Case 2)	ϕ' (Case 1)	1.1 ϕ' (Case 4)	ϕ' (case 1)	1.1 ϕ' (case 3)
0	121	79	86	122	86	122	86	122
2	570	370	241	403	265	439	253	421
4	715	378	370	595	411	656	391	625
6	840	431	438	694	509	800	474	747

[1)] maximum stress in the elastic range of stress versus settlement behavior

The estimated bearing capacity values obtained using *AEV* 2 and 1.1 ϕ' are closest to the measured values. However, the bearing capacity values obtained using ϕ' are underestimated regardless of the *AEV*. From these results, two important observations can be made as follows.

(i) The methodology of estimating air-entry value (i.e. *AEV* 1, *AEV* 2 and *AEV* 3) can lead to recognizable differences in the bearing capacity values estimated using Eq. (5.1) for the sand used in the present study. For instance, the estimated bearing capacity with *AEV* 2 was 15 % higher than that of *AEV* 1 at the matric suction of 6 kPa (i.e. highest matric suction value) even though the difference in the air-entry value was only 2 kPa.

(ii) The estimated bearing capacities are more reasonable when 1.1ϕ' is used

The results in Figure 5.8 were grouped into four categories (Case 1 to Case 4) based on the comparisons between the measured and the estimated bearing capacity values. Each case can be interpreted with the aid of Figure 5.9 as follows.

(i) ***Case 1*** (air-entry value = *AEV* 1, *AEV 2* and *AEV* 3 and effective internal friction angle = ϕ'): The bearing capacity values are significantly underestimated compared to the measured values, which can lead to uneconomical design of foundations.

(ii) ***Case 2*** (air-entry value = *AEV* 1 and effective internal friction angle = 1.1ϕ'): The estimated settlement is close to the measured value, but the bearing capacity is underestimated. This case is also not reasonable from an engineering practice point of view as it results in uneconomical design of foundations.

(iii) ***Case 3*** (air-entry value = *AEV* 3 and effective internal friction angle = 1.1ϕ'): This case can be considered to be more reasonable since both the estimated bearing capacity and settlement are close to the measured values but are on the conservative side.

(iv) ***Case 4*** (air-entry value = *AEV* 2 and effective internal friction angle = 1.1ϕ'): The estimated bearing capacity is close to the measured value, but the settlement is overestimated.

In summary, using the average air-entry value, *AEV* 3 [= (*AEV* 1 + *AEV* 2)/2] and 1.1ϕ' provides the most reasonable stress versus settlement behaviors (i.e. ***Case 3***). Hence, in the present study, the average air-entry value (*AEV* 3 = 3 kPa) and two different effective internal friction angles (i.e. ϕ' and 1.1ϕ') were used for the comparison between the measured stress versus settlement behaviors and those estimated using the *Method II* (i.e. *FEA*).

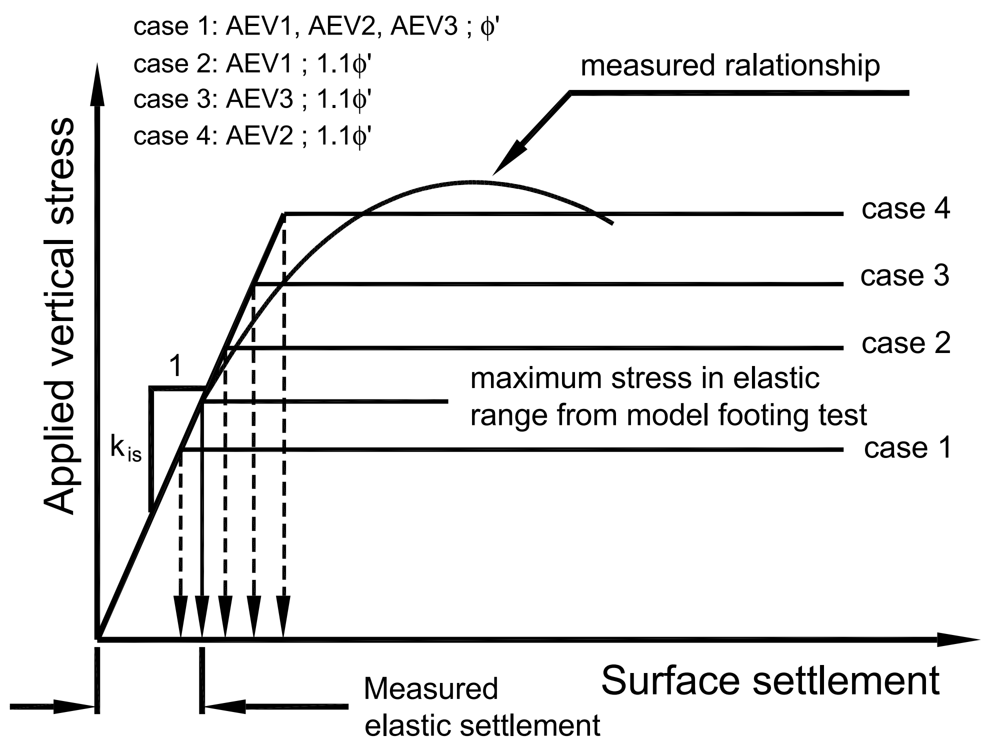

Figure 5.9 Different scenarios of the estimated applied vertical stress versus surface settlement relationship obtained using the proposed method.

Figure 5.10 shows the comparison between the measured stress versus settlement behaviors and those estimated using the *Method I* and the *Method II*. The bearing capacity values using the *Method II* with ϕ' shows good agreement compared with the measured values, while those obtained with $1.1\phi'$ are significantly overestimated. These results imply that it may not be necessary to consider the effect of stress-strain condition (i.e. plain strain and axisymmetric condition) on ϕ' in the *FEA*. This behavior can be attributed to the difference in failure mechanism between Eq. (5.1) (limit equilibrium approach) and the *FEA* (Mohr-Coulomb criterion).

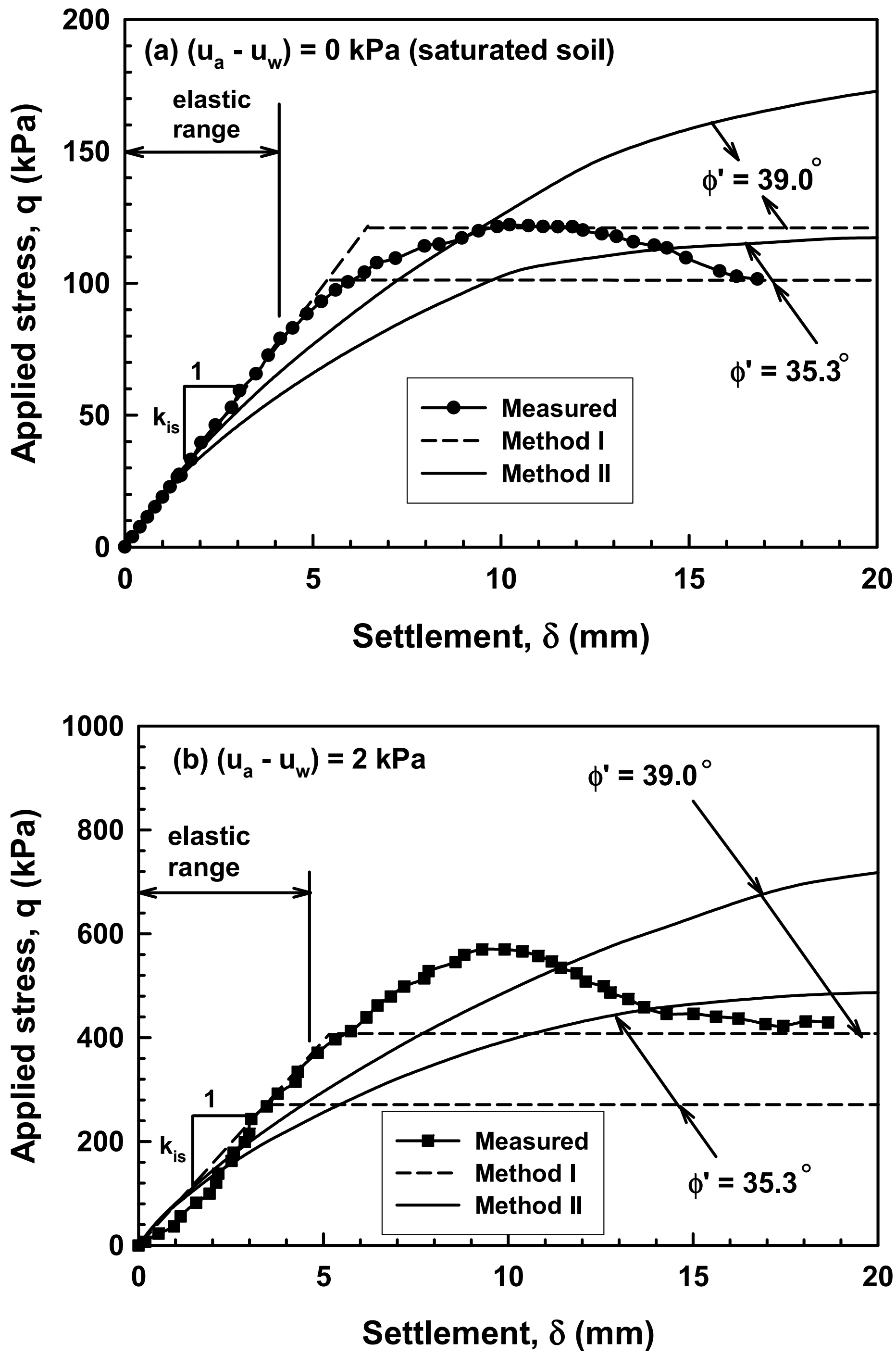

Figure 5.10 Comparison between the measured stress versus settlement behaviors and those estimated using the *Method I* (i.e. idealized behavior) and the *Method II* (*FEA*) for the matric suction value of (a) 0 kPa and (b) 2 kPa.

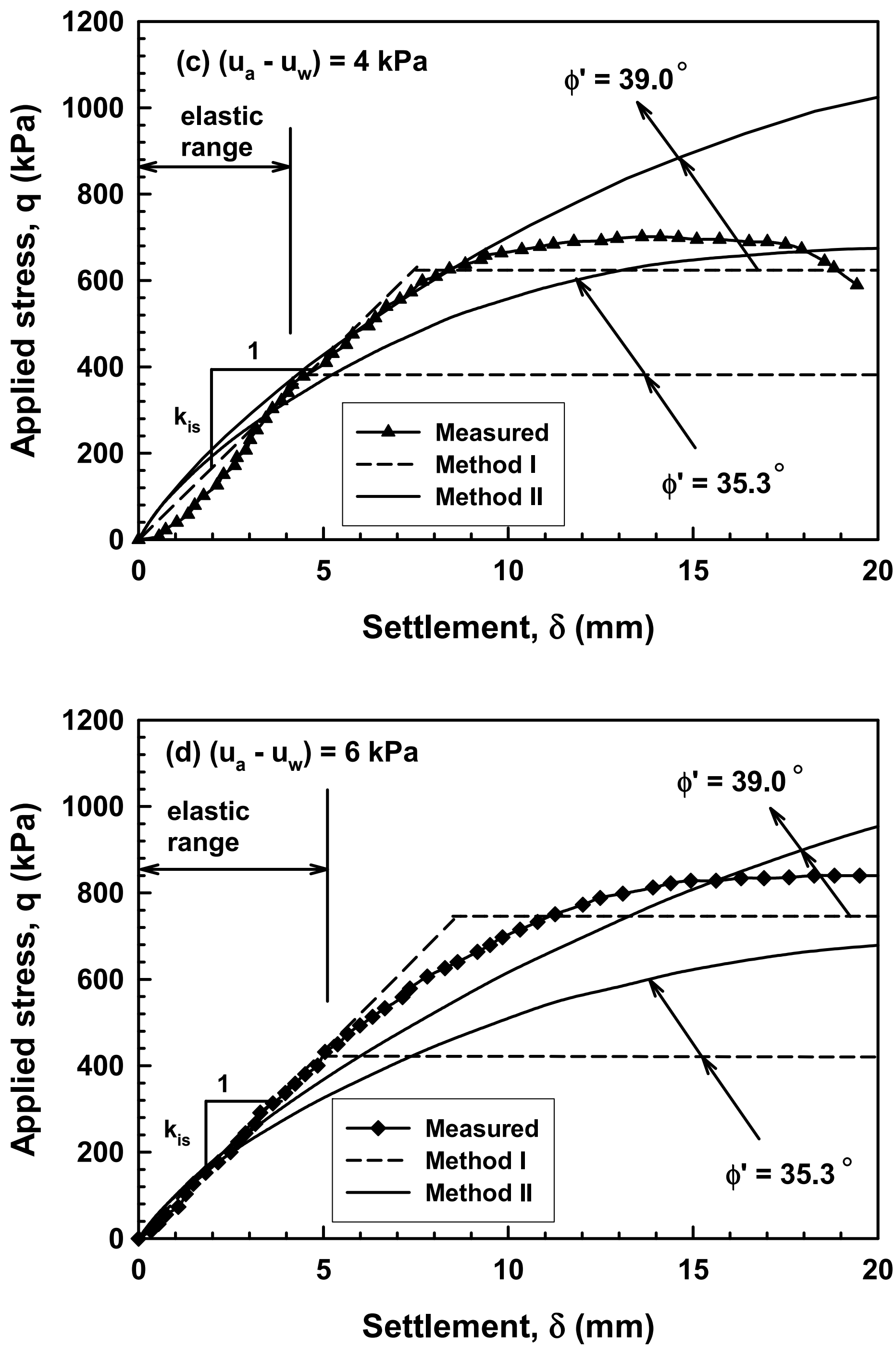

Figure 5.10 Comparison between the measured stress versus settlement behaviors and those estimated using the *Method I* (i.e. idealized behavior) and the *Method II* (*FEA*) for the matric suction value of (c) 4 kPa and (d) 6 kPa.

5.4.2 Comparison between the Measured and the Estimated Bearing Capacity and Elastic Settlement

Figure 5.11 shows the comparison between the measured bearing capacity values and those estimated using the two different methods (i.e. *Method I* and *Method II*). As explained in section 5.4.1 '*Comparison between the Measured and the Estimated Stress versus Settlement Behavior*', the bearing capacity values estimated using *Method I* with internal friction angle of 1.1ϕ' and *Method II* with ϕ' shows good agreement in comparison to the measured values.

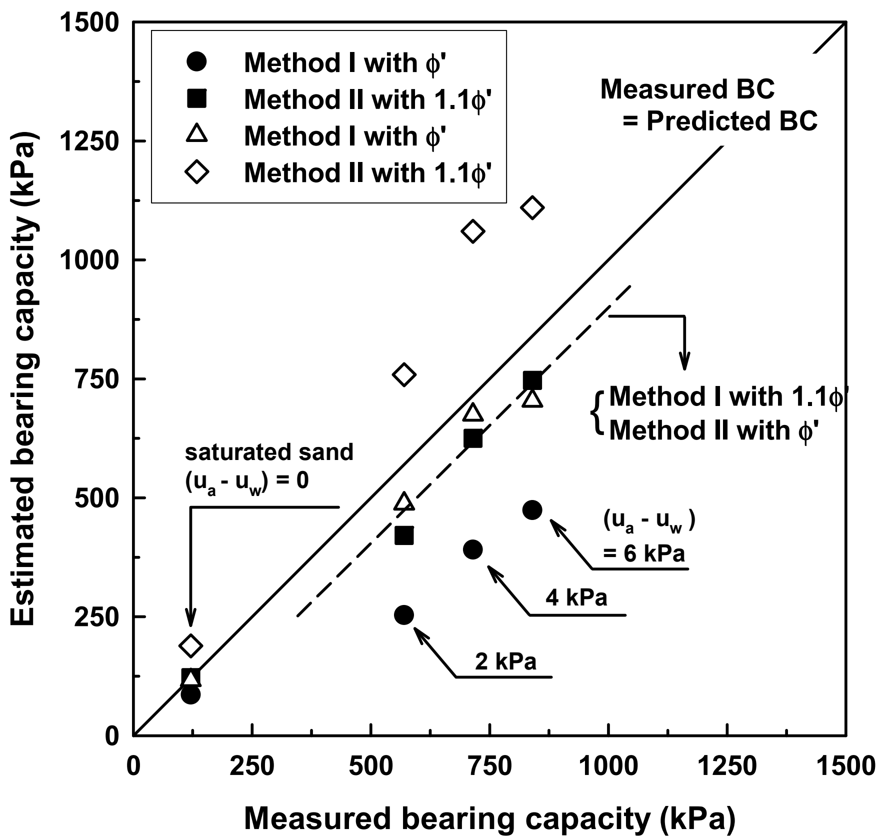

Figure 5.11 Comparison between the measured and the estimated bearing capacity values.

The elastic settlements using *Method I* with 1.1ϕ' were overestimated, while those estimated using *Method I* and *Method II* with ϕ' were underestimated as shown in Figure 5.12. This phenomenon can be explained using Figure 5.9 which shows the elastic settlement for the *Case 3* (*Method I* with 1.1ϕ') is overestimated whereas for the *Case 1* (*Method I* with ϕ') is underestimated. Hence, it can be expected that the best-fit curve (i.e. short-dash line in Figure 5.12) using the estimated elastic settlements from both '*Method I* with ϕ'' and '*Method I* with 1.1ϕ'' can provide reasonably good elastic settlement estimates.

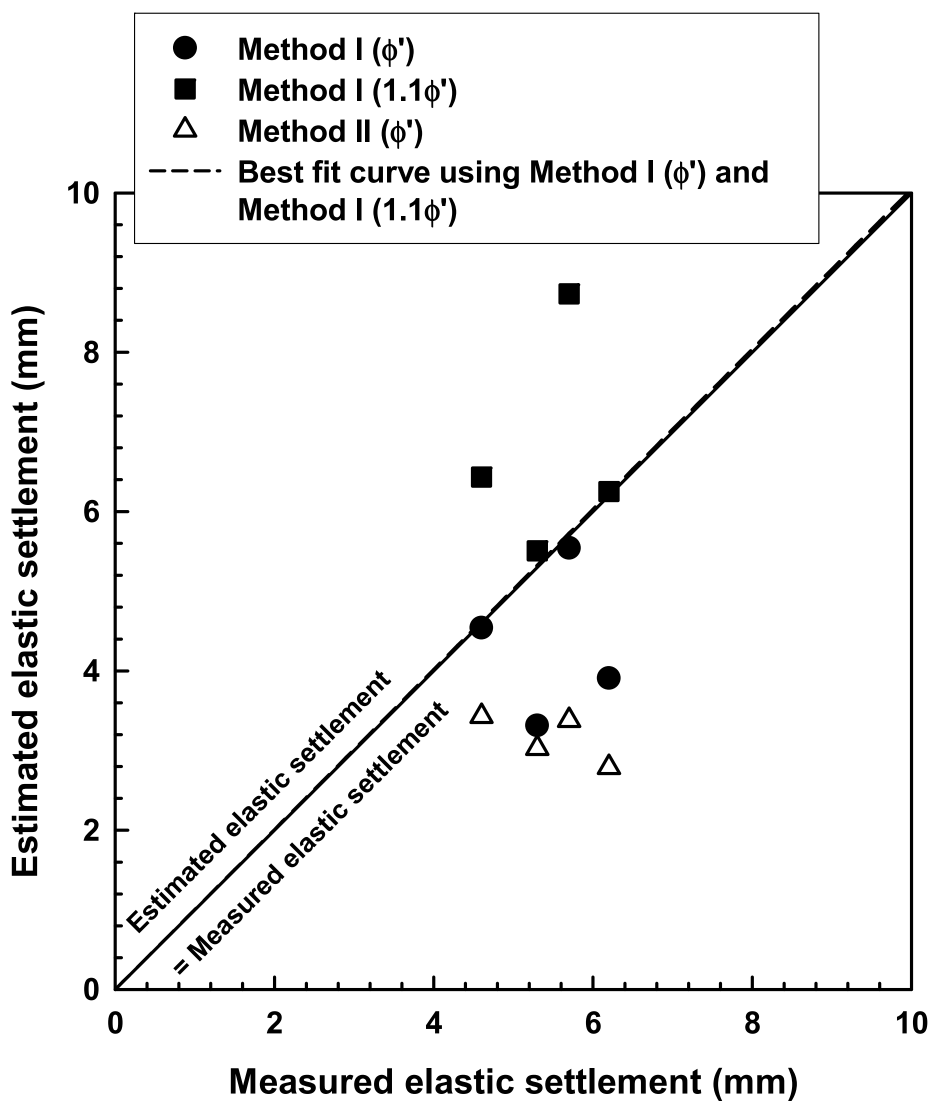

Figure 5.12 Comparison between the measured and the estimated elastic settlements.

5.5 Estimation of Applied Vertical Stress versus Surface Settlement Behavior of In-Situ Footing Load Tests in Unsaturated Sands

In this section, *Method II* (i.e. *FEA*) has been extended to simulate the stress versus settlement behavior of in-situ footing ($B \times L$ = 1 m × 1 m) load tests in unsaturated sand.

5.5.1 Settlement Prediction Symposium for Spread Footings on Sand

Shallow foundations are typically less expensive compared to deep foundations (Briaud 1992). However, practicing engineers, especially highway bridge engineers, prefer deep foundations mainly due to the following two reasons: (i) the deep foundations are more reliable and safer than shallow foundations and (ii) there are uncertainties associated with the design and analysis of shallow foundations.

The Federal Highway Administration (*FHWA*) has encouraged investigators to study the performance of shallow foundations by providing research funding. As part of this research project, several series of in-situ footing load tests were conducted on sandy soils along with other field and laboratory tests. These studies were summarized in a symposium held at Texas A&M University in 1994 (Briaud and Gibbens 1994). In this section, some of the research work undertaken through this project is used in the simulations of stress versus settlement behavior of in-situ footing load tests in unsaturated sands.

5.5.1.1 Site Description and Soil Properties

The site selected for the in-situ footing load tests was predominantly sand (mostly medium dense silty sand) from 0 to 11 m overlain by hard clay layer (Figure 5.13). The ground water table was observed at a depth of 4.9 m. Figure 5.14 shows the grain size distribution curves for the soil samples collected from three different depths (i.e. 1.4 m - 1.8 m, 3.5 m - 4.0 m, and 4.6 m - 5.0 m). The grain size distribution curve of the Sollerod sand (Steensen-Bach et al. 1987) shown in Figure 5.14 is similar to the sand sample collected at the depth of 1.4 m to 1.8 m. The reasons associated with showing the grain size distribution curve of Sollerod sand will be discussed later. The soil properties used in the analysis are summarized in Table 5.4.

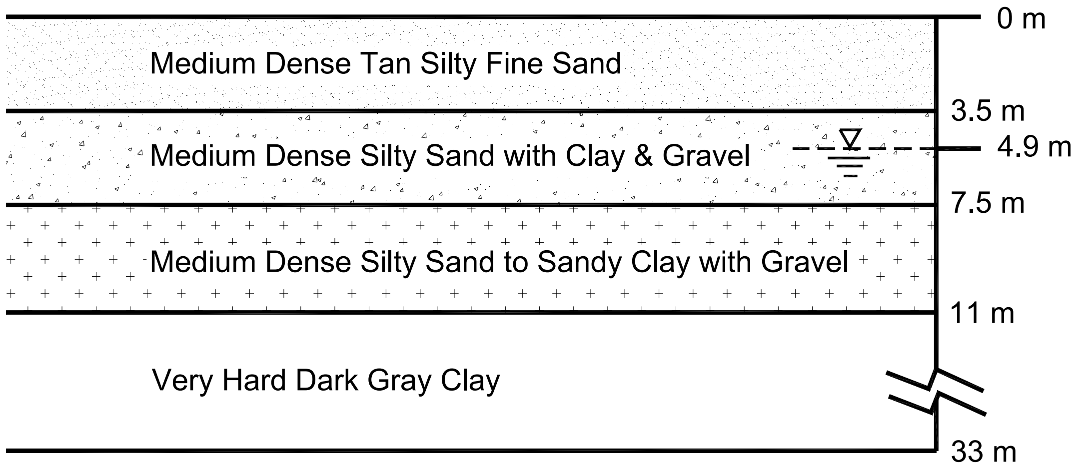

Figure 5.13 The average soil profile at the test site (Briaud and Gibbens 1994).

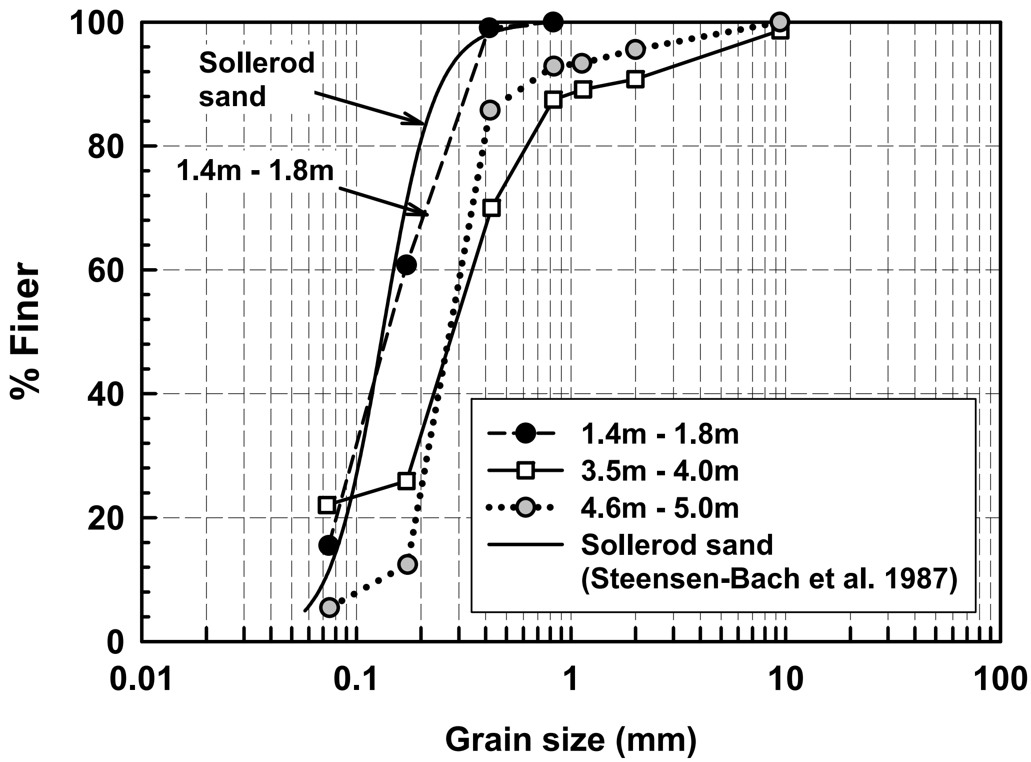

Figure 5.14 Grain size distribution curves of the soil samples collected from three different depths and Sollerod sand.

Table 5.4 Summary of the soil properties of the site for the in-situ footing load tests.

Property	Sand (0.6 m)	Sand (3.0 m)
Specific gravity, G_s	2.64	2.66
Water content, w (%)	5.0	5.0
Void ratio, e	0.78	0.75
Effective cohesion, c' (kPa)	0.0	0.0
Effective internal friction angle, ϕ' (°)	35.5	34.2

5.5.1.2 In-situ Footing Load Tests

Five sets of in-situ footing load tests were carried out using four different sizes of square footings (i.e. 1 m, 1.5 m, 2.5 m, and 3 m). Figure 5.15 and Figure 5.16 show the 'load versus settlement' and 'stress versus settlement' behaviors from the load tests, which were established using the envelope of the 30 minutes readings. The load test results for the 1 m × 1 m footing were used for the *FEA*. The remainder of the tests was used to interpret the scale effect of shallow foundations in unsaturated sandy soils.

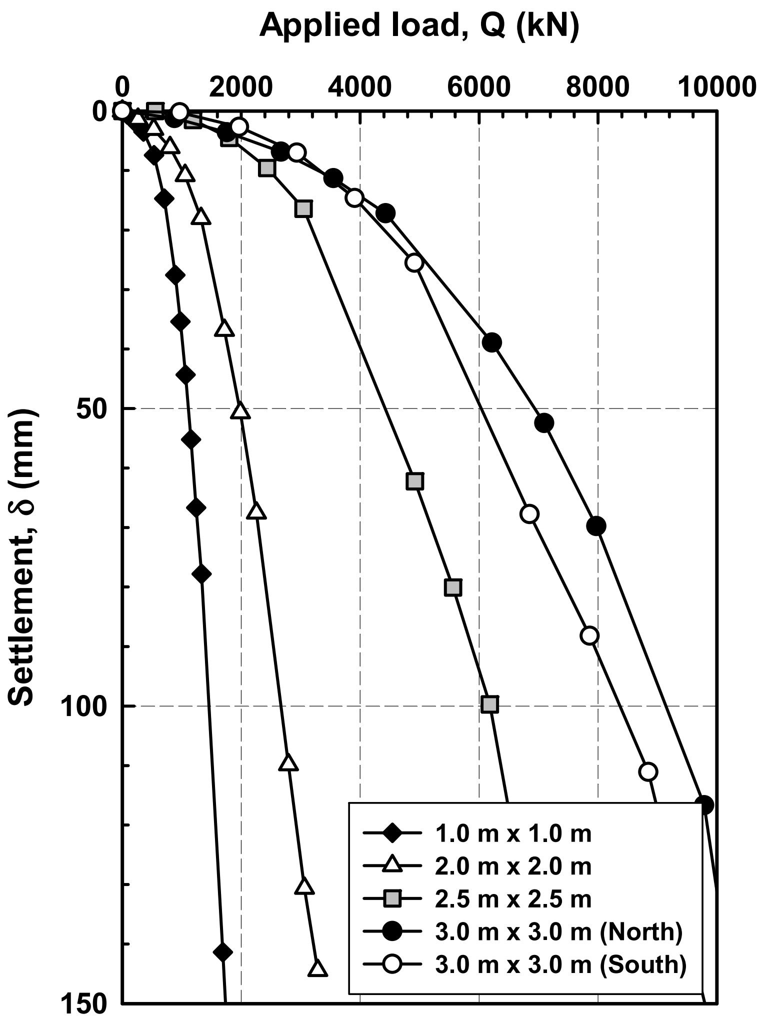

Figure 5.15 Applied load versus settlement behavior from in-situ footing load tests (Briaud and Gibbens 1994).

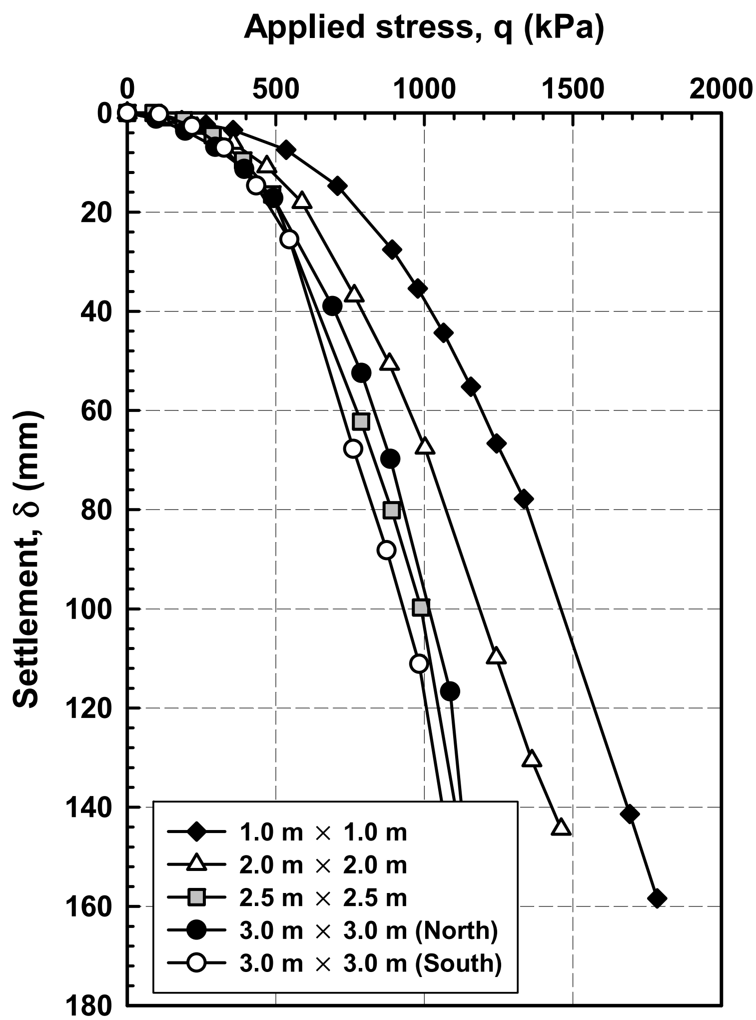

Figure 5.16 Applied stress versus settlement behavior from in-situ footing load tests (Briaud and Gibbens 1994).

5.5.2 Modelling the Stress versus Settlement Behavior of In-Situ Footing Load Test

The commercial finite element software, *SIGMA/W* (Geostudio 2007; Krahn 2007) was used to simulate stress versus settlement behavior of in-situ footing ($B \times L$ = 1 m × 1 m) load tests. The *FEA* was performed using elastic-perfectly plastic model extending the methodology described in section 5.3.2. The square footing was modeled as a circular footing with an equivalent area (i.e. 1.13 m in diameter; axisymmetric problem).

5.5.2.1 Soil-Water Characteristic Curve

The grain size distribution curves for the soil samples collected from three different depths vary (see Figure 5.14). Hence, in this study, the grain size distribution curve for the range of depth, 1.4 m - 1.8 m was chosen as the representative grain size distribution curve since the stress below the 1 m × 1 m footing is predominant in the range of 0 to 1.5 m (or 2 m) (i.e. 1.5B or 2B) below the footing. The *SWCC* for the soil, however, in this range of depth was not available in the literature. Due to this reason, the *SWCC* for Sollerod sand (Figure 5.17) measured by Steensen-Bach et al. (1987) was used in the analysis since both the collected soil samples from the depth of 1.4 m – 1.8 m and Sollerod sand have similar grain size distribution curves and shear strength parameters (i.e. c' = 0.8 kPa and ϕ' = 35.8^{o} for Sollerod sand) (see Table 5.4). The air-entry [i.e. $(u_a - u_w)_b$] and residual suction [i.e. $(u_a - u_w)_r$] values were estimated to be 5.8 kPa and 8.5 kPa, respectively from the *SWCC*.

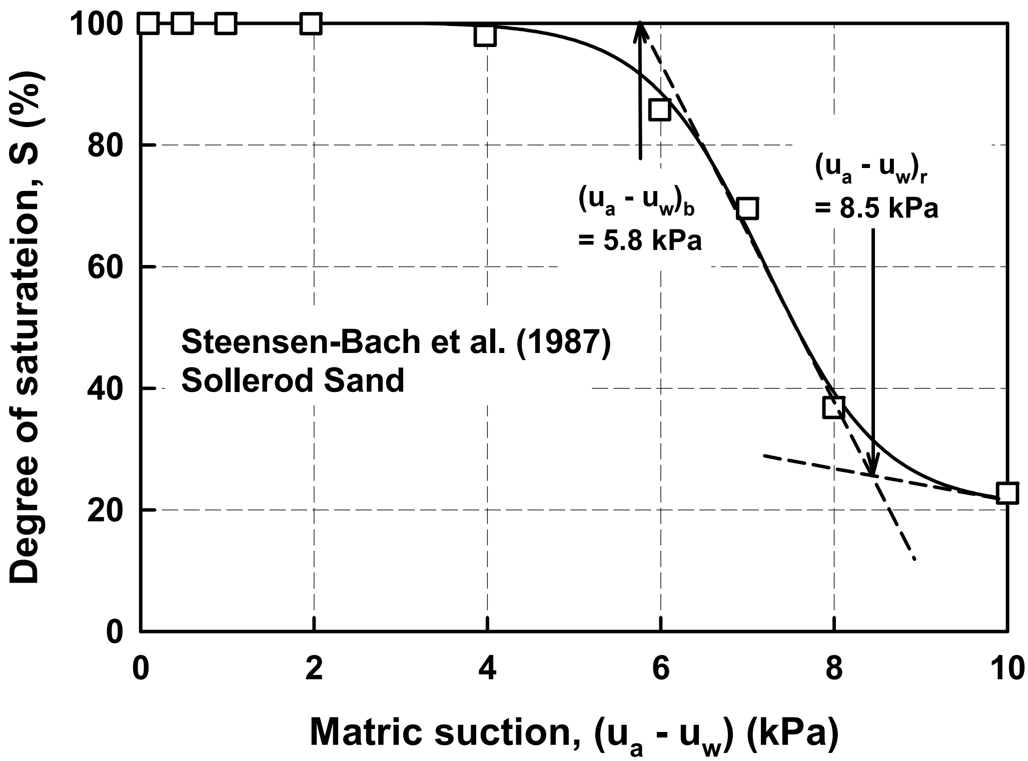

Figure 5.17 *SWCC* used for the analysis [data from Steensen-Bach et al. (1987)].

5.5.2.2 Soil Properties used for the FEA

As shown in Table 5.4, the water content values at the depths of both 0.6 m and 3.0 m are the same (i.e. 5%). This indicates that the matric suction value can be assumed to be constant in this range of depth for the *FEA*. The degree of saturation calculated using the information shown in Table 5.4 is 22.8%. The corresponding matric suction value for this degree of saturation is 10 kPa from the *SWCC*. This field matric suction distribution profile is consistent with the typical matric suction distribution profile above ground water table for the coarse-grained soils, which increases gradually (which is close to hydrostatic conditions) up to residual matric suction value and thereafter remains close to constant conditions. The total cohesion, c is estimated to be 1.56 kPa [Eq. (5.8)] and the initial tangent elastic modulus, E_i is estimated to be 125,000 kPa (125 MPa) and 187,500 kPa (187.5 MPa) using Eq. (5.11) and Eq. (5.12), respectively for field conditions [i.e. $(u_a - u_w) = 10$ kPa].

5.5.3 Analysis Results

5.5.3.1 Comparison between the Measured and the Estimated Stress versus Settlement Behavior

Figure 5.18 shows the comparison between the measured stress versus settlement behavior and those estimated using the *FEA*. The stress versus settlement behavior using the E_i based on B [i.e. Eq. (5.11); hereafter referred to as $E_{i(B)}$] provides reasonably good agreement for a wide range of displacement. The results obtained based on 1.5B [i.e. Eq. (5.12); hereafter referred to as $E_{i(1.5B)}$], however, generally underestimated the displacement. To further investigate the measured and the estimated stress versus settlement behaviors, the results in Figure 5.18 were re-plotted for the settlements in the range of 0 to 25 mm (i.e. permissible settlement in the design of shallow of foundations in sandy soils) as shown in Figure 5.19. The results showed that there is a better agreement for the settlements less than 10 mm when $E_{i(1.5B)}$ is used. The results in Figure 5.18 and Figure 5.19 indicates that the *Method II* can be reliably extended to in-situ footing load tests (i.e. relatively large size footings) based on reasonable estimation of matric suction value in fields.

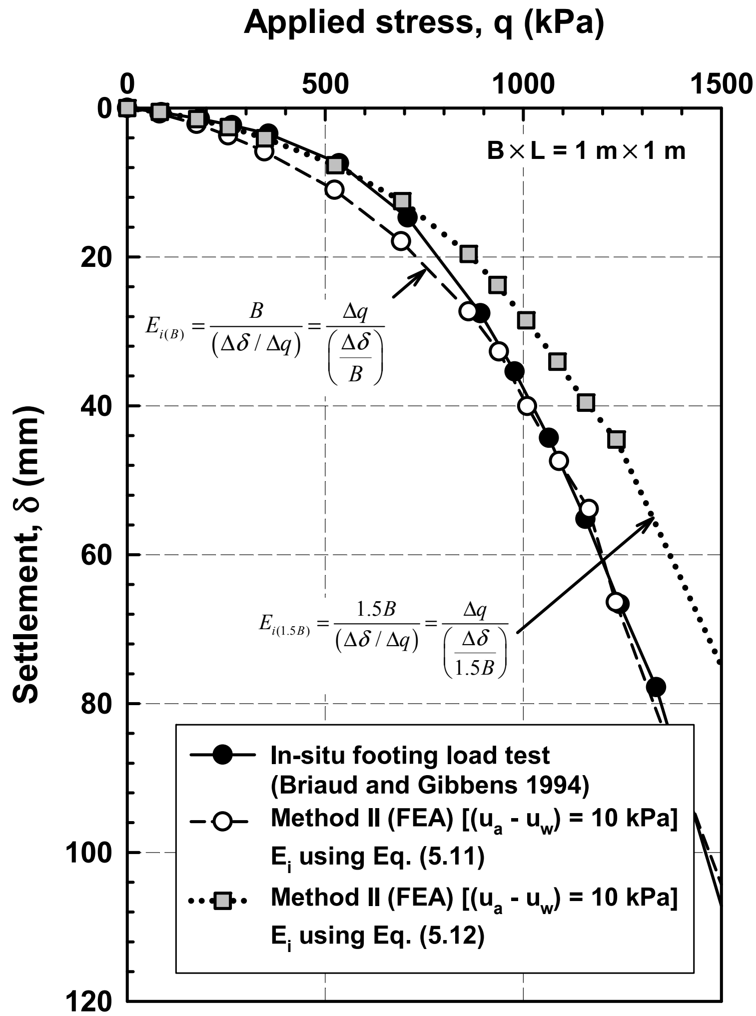

Figure 5.18 Comparison between the measured stress versus settlement behaviors and those estimated using *Method II* (*FEA*) for a wide range of displacement [data from Briaud and Gibbens (1994)].

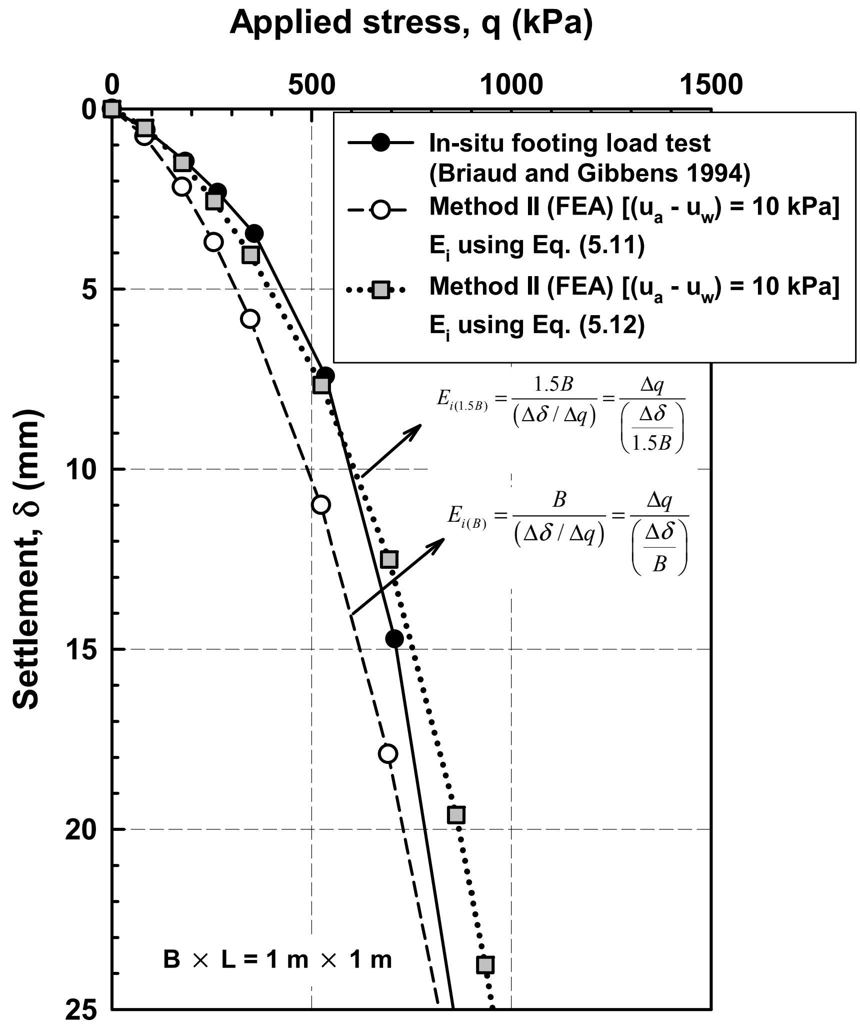

Figure 5.19 Comparison between the measured stress versus settlement behaviors and those estimated using *Method II* (*FEA*) for the settlements in the rage of 0 to 25 mm [data from Briaud and Gibbens (1994)].

.

5.5.3.2 Variation of Stress versus Settlement Behavior with respect to Matric Suction

When a shallow foundation is placed on unsaturated soils the stress versus settlement behavior can be substantially influenced by the variation of matric suction associated with water infiltration into the soils. In other words, the estimation of the variation of stress versus settlement behavior with respect to matric suction is a key factor that should be considered in the design of shallow foundations placed in unsaturated soils. Hence, an attempt is made to estimate the variation of stress versus settlement behaviour of the in-situ footing with respect to matric suction by performing *FEA* for different matric suction values.

As a first step, the variation of c and E_i with respect to matric suction value was estimated. The E_i value estimated using Eq. (5.11) [i.e. $E_{i(B)}$] was used in this analysis since the stress versus settlement behavior using $E_{i(B)}$ provided conservative settlements in the range of 0 to 25 mm. It should be noted that the $E_{i(B)}$ value for the saturated condition was back-calculated using Eq. (5.4) with $\alpha = 2$ and $\beta = 1$.

Figure 5.20 shows the variation of stress versus settlement behavior with respect to matric suction obtained suing the *FEA*. The results in Figure 5.20 are analyzed with more focus on the 25 mm displacement. Figure 5.21(a) shows the variation of the applied stress corresponding to the displacement of 25 mm (CFEM 2006) with respect to matric suction. The applied stress increases up to the air-entry value and then starts decreasing as the matric suction approaches residual matric suction value. Figure 5.21(b) shows the variation of settlement under the applied stress of 310 kPa with respect to matric suction. The stress 310 kPa is chosen since the settlement for saturated condition at this stress is 25 mm. The stress corresponding to 25 mm of settlement decreases by 1.5 times as the soil approaches saturation condition (i.e. from 10 kPa to 0 kPa). The settlement at the matric suction of 10 kPa (i.e. field condition) is approximately 5 mm and then increases up to 25 mm (i.e. permissible settlement) as the soil approaches saturation condition under constant stress [Figure 5.21(b)]. The results in Figure 5.21 imply that unexpected problems associated with displacement are likely due to decrease in matric suction. It is also of interest to note that such a problem can be alleviated if the soil remains in unsaturated condition with a matric suction value of 2 kPa.

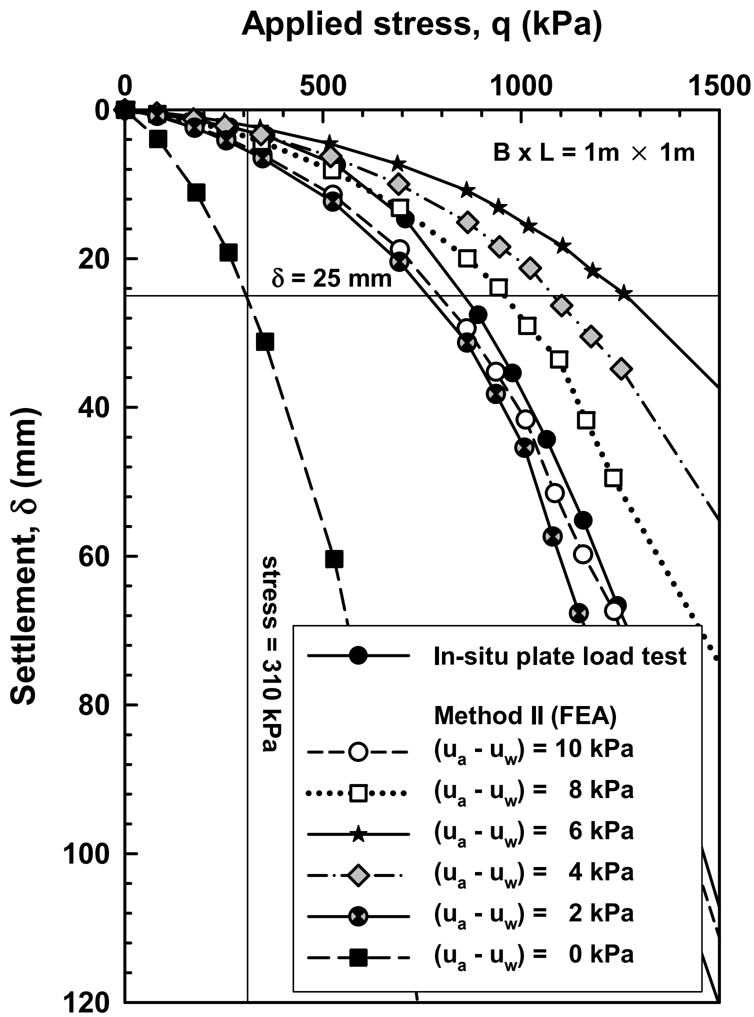

Figure 5.20 Variation of stress versus settlement behavior with respect to matric suction obtained using *Method II* (*FEA*) [data from Briaud and Gibbens (1994)].

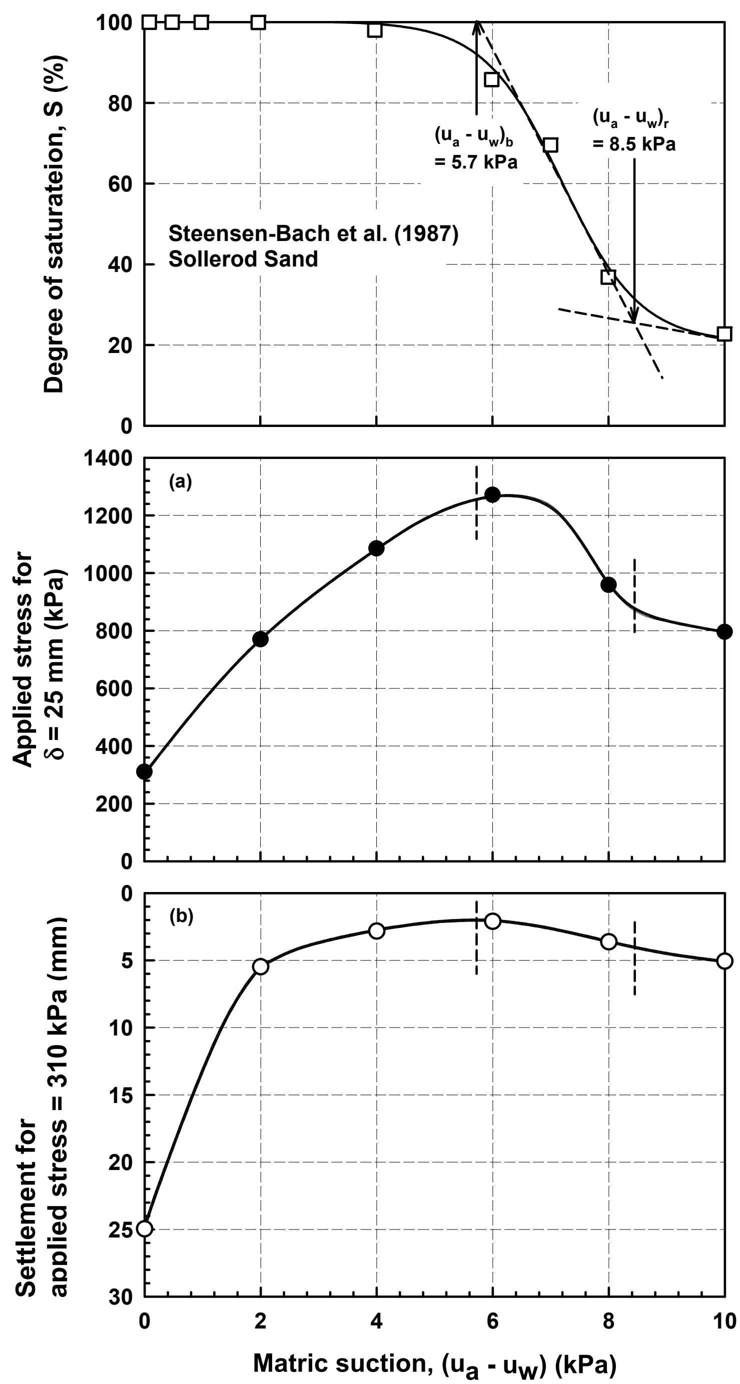

Figure 5.21 *SWCC* and the variation of (a) stress corresponding to the displacement of 25 mm and (b) settlement under constant stress (i.e. 310 kPa) with respect to matric suction [data from Briaud and Gibbens (1994)].

5.6 Scale Effect of Shallow Foundation in Unsaturated Sands

As shown in Figure 5.16, the stress versus settlement behavior of the in-situ footing load tests for different footing sizes (i.e. 1, 2, 2.5, and 3 m) show different settlements under a certain stress. This behavior indicates that the stress versus settlement behavior is dependent on the footing size (i.e. scale effect).

Briaud (2007) suggested that scale effect can be eliminated by plotting the stress versus settlement behaviors as 'applied stress' versus 'settlement/width of footing' (i.e. δ/B) curves [i.e. normalized settlement; Eq. (5.13)]. Similar trends of results were reported by Osterberg (1947) and Palmer (1947).

$$\frac{\delta}{B}=\frac{q\left(1-\nu^{2}\right)}{E}I_{w} \tag{5.13}$$

where E = elastic modulus, ν = Poisson's ratio, δ, q = settlement and corresponding stress, B = width (or diameter) of plate, and I_w = factor involving the influence of shape and flexibility of loaded area

According to the report published by *FHWA* (Briaud and Gibbens 1997), this behavior can be explained using triaxial test analogy (Figure 5.23). If triaxial tests are conducted for identical sand samples under the same confining pressure where the top platens are different sizes of footings the stress versus strain behaviors for the samples are unique regardless of the diameter of the samples (i.e. the same stress for the same strain). This concept is similar to relationship between applied stress versus δ/B from plate load tests since the term, δ/B can be regarded as strain.

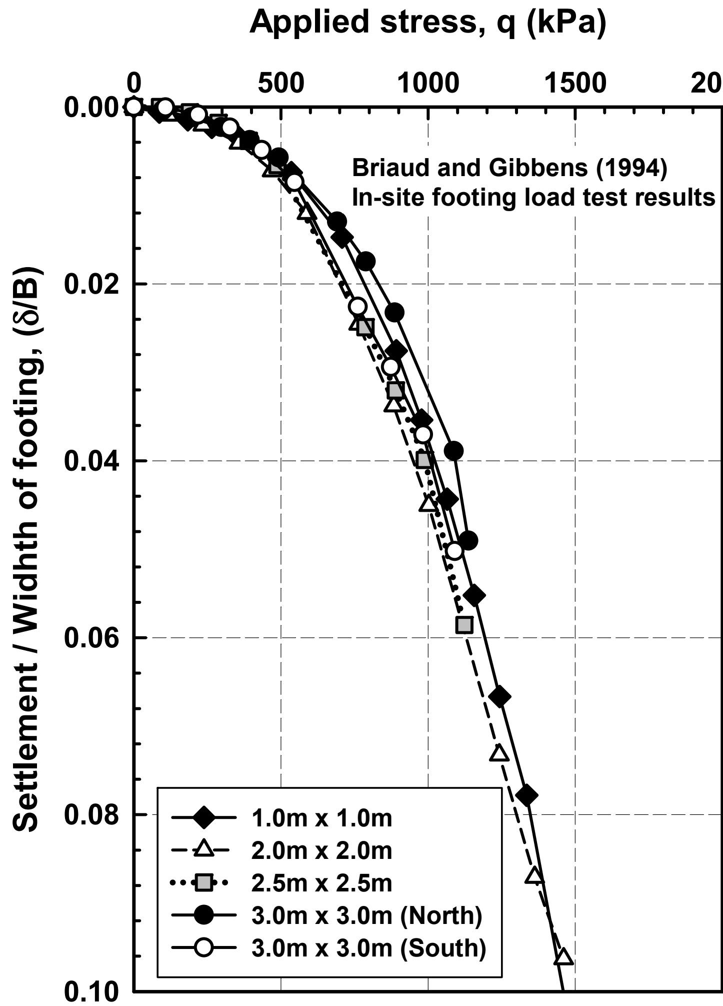

Figure 5.22 Normalized in-situ footing load test results [Briaud (2007)].

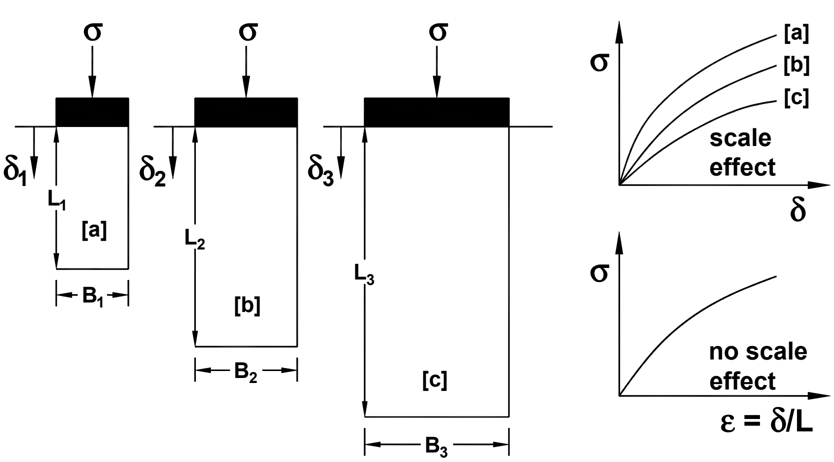

Figure 5.23 Triaxial test/shallow foundation analogy [*FHWA* (1997)].

Consoli et al. (1998) suggested that the scale effect of the in-situ plate and footing load test results (Figure 5.24) can be eliminated when the applied stress and settlement are normalized with unconfined compressive strength, q_u and footing width, B respectively [Eq. (5.14), Figure 5.25]. They also analyzed the plate load test results available in the literature (D'Appolonia et al. 1968, Ismael 1985) and showed that the concept in Eq. (5.14) can be extended to the plate load test results in sandy soils as well.

$$\left(\frac{q}{q_u}\right)=\left\{\frac{C_d}{q_u C_s}\right\}\left(\frac{\delta}{D}\right) \tag{5.14}$$

where q = applied stress, q_u = unconfined compressive strength at the depth of embedment, δ = settlement, D = width of footing, C_s = coefficient involving shape and stiffness of loaded area [I_w in Eq. (5.10)], and C_d = coefficient of deformation [= $E/(1-\nu^2)$].

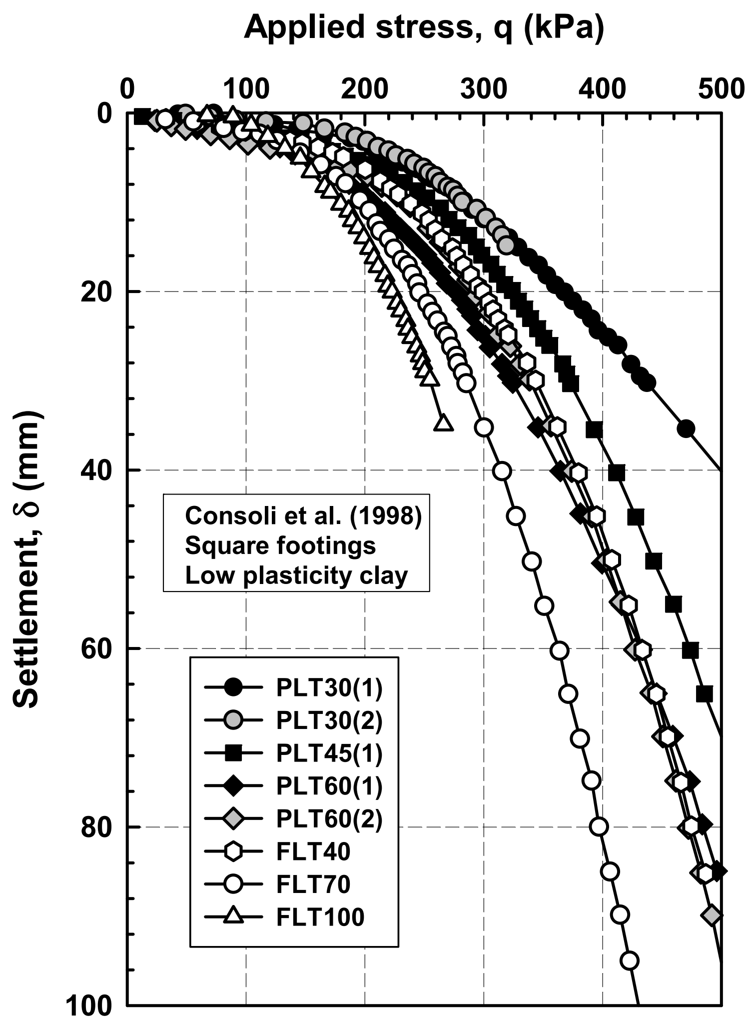

Figure 5.24 Stress versus settlement behaviors from in-situ plate (*PLT*) and footing (*FLT*) load tests (Consoli et al. 1998).

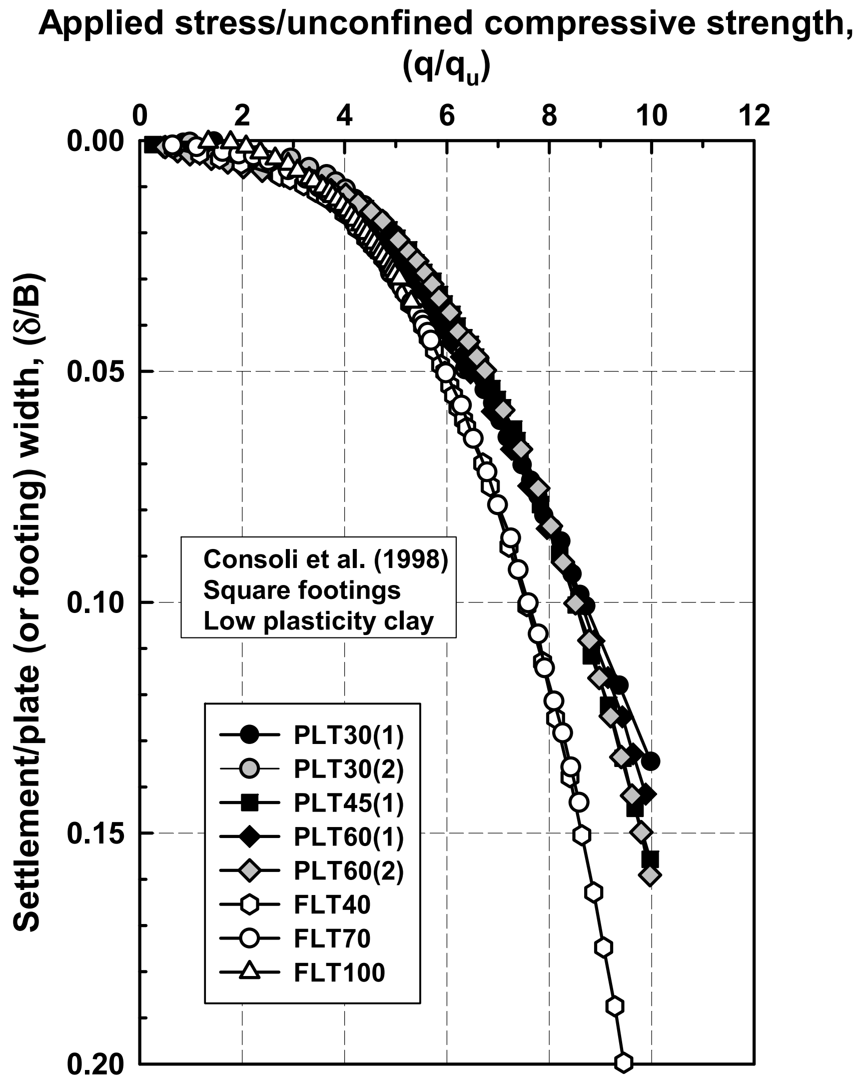

Figure 5.25 Normalized in-situ footing load test results [data from Consoli et al. (1998)]

The elimination of the scale effect of plate size using normalization procedure can be effectively used for the case where the distribution of matric suction profile is relatively uniform with depth in unsaturated soils. For example, the sites where the in-situ footing load tests were conducted (i.e. Briaud and Gibbens 1994, Consoli al. 1998), the variation of matric suction with depth is negligible up to a certain depths (i.e. matric suction distribution (1) in Figure 5.26), which results in approximately the same average matric suction value regardless of the sizes of footings used. On the other hand, the average matric suction value for each footing can be different when non-uniform matric suction distribution profile is considered below the footings (i.e. matric suction distribution (2) in Figure 5.26). In this case, the concept in Eq. (5.13) and Eq. (5.14) cannot be valid since the elastic modulus is a function of not only the footing width, *B* but also matric suction.

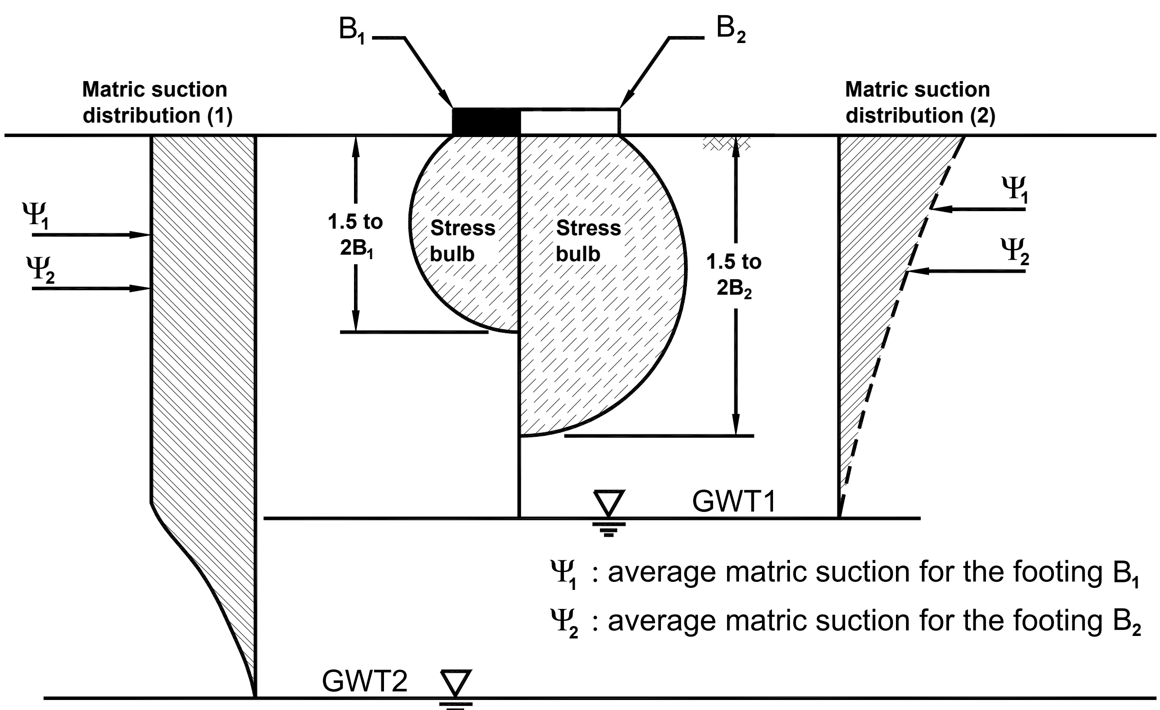

Figure 5.26 Average matric suction values for different sizes of footings under uniform and non-uniform matric suction distribution profiles.

5.7 Summary and Conclusions

In this chapter, two methodologies are proposed to estimate the applied vertical stress versus surface settlement behavior of both saturated and unsaturated sands based on the assumption that its behavior is elastic-perfectly plastic. In the first method (i.e. *Method I*) the stress versus settlement behavior was established as segments of two straight lines; (i) the first segment is the linear elastic line which has a slope (i.e. initial tangent modulus of subgrade reaction, k_{is}) obtained using Eq. (5.3), and (ii) the second segment is the plastic line which is parallel to the settlement axis and starts on the elastic line with a value equal to the bearing capacity computed using Eq.(5.1). The lines for unsaturated conditions can be estimated using the values under saturated condition; namely, liner elastic line using $k_{is(sat)}$ and plastic line using $q_{ult(sat)}$ along with *SWCC*. In the second method (i.e. *Method II*), finite element analysis (*FEA*) is carried out to show how the stress versus settlement relationship in unsaturated sands can be simulated using the elastic-perfectly plastic model.

The results show that *Method I* can provide good comparison between the measured and the estimated bearing capacity and settlement behavior of sands both under saturated and unsaturated. The estimated bearing capacity values can be conservative in comparison to the measured values when calculated using average air-entry value, *AEV* 3[= (*AEV* 1 + *AEV* 2)/2]. The best-fit curve for the settlements obtained using *Method I* with both ϕ' and 1.1 ϕ' shows good agreement in comparison to the measured settlements. The bearing capacity values obtained using *Method II* show good agreement with measured values, while settlements were underestimated.

Three important observations from this study are summarized below.

(i) The methodology of estimating air-entry value (i.e. *AEV* 1, *AEV* 2 and *AEV* 3) can lead to recognizable differences in the estimated bearing capacity values for the coarse-grained soils.

(ii) The bearing capacities can be estimated with greater reliability when effective internal friction angle, ϕ' is increased by 10%.

(iii) A different form of equation [Eq. (5.12)] should be used for estimating elastic modulus from model footing tests for the *FEA* instead of the conventional equation proposed by Timoshenko and Goodier (1951) [Eq. (5.10)].

To check the validity of the methodologies, *Method II* has been extended to the in-situ footing ($B \times L$ = 1 m × 1 m) load test results in unsaturated sand (Briaud and Gibbens 1994). The results showed that the stress versus settlement behaviors estimated using $E_{i(B)}$ (E_i based on the width of footing, B) provides reasonably good agreement in comparison to those from in-situ footing load test for especially large displacement (i.e. greater than 25 mm). On the other hand, the stress versus settlement behavior estimated using $E_{i(1.5B)}$ (E_i based on the 1.5 times the width of footing) provided better agreement when the range of displacement was small (i.e. less than 10 mm). *Method II* can also be reliably used to estimate the variation of stress versus settlement behaviors with respect to matric suction.

The scale effect can be significantly reduced by re-plotting the stress versus settlement behaviors as "stress versus displacement/width of footing" curves. Such a behavior, however, can be more valid when the soil at the site is homogeneous and isotropic in nature. If non-uniform matric suction distribution exists below the footings, the homogeneous conditions of the sand layer are not assured because the elastic modulus is a function of not only the footing width, B but also is dependent on the matric suction. The scale effect of plate size in unsaturated soils can be investigated more effectively by conducting the model footing tests in a Large Tempe Cell that can be used to simulate uniform matric suction distribution profile with depth.

REFERENCES

Agarwal, K.B., and Rana, M.K. 1987. Effect of ground water on settlement of footing in sand. *In* Proceedings of the 9th European Conference on Soil Mechanics and Foundation Engineering, Dublin, 751-754.

Alonso, E.E., Gens, A. and Josa, A. 1990. A constitutive model for partially saturated soils. *Géotechnique*, 40(4): 405–430.

Alshibli, A.K., Batiste, S.N. and Sture, S. 2003. Strain localization in sand: plane strain versus triaxial compression. *Journal of Geotechnical and Geoenvironmental Engineering*, ASCE, 129(6): 484-494.

Briaud, J.-L. (1992). *The Pressuremeter*. Balkema, Rotterdam, The Nederlands.

Briaud, J.-L., 2007. Spread footings in sand: load settlement curve approach. *Journal of Geotechnical and Geoenvironmental Engineering*, 133(8): 905-920.

Briaud, J.-L. and Gibbens, R.M. 1994. Test and prediction results for five large spread footing on sand. *In* Proceedings of the FHWA spread Footing Prediction Symposium, ASCE, Geotechnical Special Publication 41.

Briaud, J. -L., and Gibbens, R. M. 1997. Large scale load tests and data base of spread footings on sand. FHWA-RD-97-068, Federal Highway Administration, Washington, D.C.

Budhu, M. 2006. *Soil Mechanics and Foundations*. John Wiley & Sons, NY, USA.

Canadian Foundation Engineering Manual (4th Edition). 2006. Canadian Geotechnical Society.

Cerato, A.B. and Lutenegger, A.J. 2006. Bearing capacity of square and circular footings on a finite layer of granular soil underlain by a rigid base. *Journal of Geotechnical and Geoenvironmental Engineering*, 132(11): 1496-1501.

Chen, W.F. and Zhang, H. 1991. *Structural plasticity: theory, problems, and CAE software*. Springer-Verlag.

Consoli, N.C., Schnaid, F. and Milititsky, J. 1998. Interpretation of plate load tests on residual soil site. *Journal of Geotechnical and Geoenvironmental Engineering*, 124(9): 857-867.

Cui, Y.J. and Delage, P. 1996. Yielding and plastic behavior of an unsaturated compacted silt. *Géotechnique*, 46(2): 291–311.

DS 415. 1984. The Danish code of practice for foundation engineering. Danish Society of Civil Engineering.

D'Appolonia, D.J., D'Appolonia, E. and Brisette, R.F. 1968. Settlement of spread footings on sand. *Journal of Soil Mechanics and Foundations Division*, ASCE, 3: 735-760.

Fredlund, D.G., Xing, A., Fredlund, M.D. and Barbour, S.L. 1996. Relationship of the unsaturated soil shear strength to the soil-water characteristic curve. *Canadian Geotechnical Journal*, 33(3): 440-448.

Gallipoli, D., Gens, A., Sharma, R. and Vaunat, J. 2003. An elasto-plastic model for unsaturated soil incorporating the effects of suction and degree of saturation on mechanical behavior. *Géotechnique*, 53(1): 123-135.

Garven, E. and Vanapalli, S.K. 2006. Evaluation of empirical procedures for predicting the shear strength of unsaturated soils. *In* Proceedings of the 4th International Conference on Unsaturated Soils, Carefree, 2570–2581.

Gourvenec, S., Randolph, M. and Kingsnorth, O. 2006. Undrained bearing capacity of square and rectangular footings. *International Journal of Geomechanics*, 6(3): 147-157.

Ismael, N.F. 1985. Allowable pressure from loading tests on Kuwaiti soils. *Canadian Geotechnical Journal*, 22(2): 151-157.

Janbu, N. 1963. Soil compressibility as determined by oedometer and triaxial tests. *In* Proceedings of the European Conference on Soil Mechanics and Foundation Engineering, 1: 19-25.

Krahn, J. 2007. *Stress and deformation modelling with SIGMA/W* (SIGMA/W manual). Goe-slope International Ltd: 119-120.

Kumbhokjar, A.S. 1993. Numerical evaluation of Terzaghi's N_{γ}. *Journal of Geotechnical Engineering*, ASCE, 119(3): 598– 607.

Marachi, N.D., Duncan, J.M., Chan, C.K. and Seed, H.B. 1981. Plane-strain testing of sand. Laboratory Shear Strength of Soils, ASTM STP 740, Philadelphia, PA: 294-302.

Meyerhof, G.G. 1963. Some recent research on the bearing capacity of foundations, *Canadian Geotechnical Journal*, 1(1): 16-26.

Mohamed, F.M.O. and Vanapalli, S.K. 2006. Laboratory investigations for the measurement of the bearing capacity of an unsaturated coarse-grained soil. *In* Proceedings of the 59th Canadian Geotechnical Conference, Vancouver.

Nishimura, T., Toyota, H., Vanapalli, S.K. and Oh, W.T. 2007. Evaluation of critical state parameters for an unsaturated soil. *In* Proceedings of the 60th Canadian Geotechnical Conference, Ottawa, 1029-1036.

Osterberg, J.S. 1947. Discussion in symposium on load tests of bearing capacity of soils. ASTM STP 79, ASTM, Philadelphia, PA: 128-139.

Palmer, L.A. 1947. Field loading tests for the evaluation of the wheel load capacities of airport pavements. ASTM STP 79, ASTM, Philadelphia, PA: 9-30.

Steensen-Bach, J.O., Foged, N. and Steenfelt. J.S. 1987. Capillary Induced Stresses – Fact or Fiction?. *In* Proceedings of the 9th European Conference on Soil Mechanics and Foundation Engineering, Budapest, 83-89.

Terzaghi, K. 1943. *Theoretical Soil Mechanics*. John Wiley and Sons, New York, NY, USA.

Timoshenko, S. and Goodier, J.N. 1951. *Theory of Elasticity*. McGraw-Hill, New York, USA.

Vanapalli, S.K., Fredlund, D. G., Pufahl, D. E. and Clifton, A. W. 1996a. Model for the prediction of shear strength with respect to soil suction. *Canadian Geotechnical Journal*, 33(3): 379-392.

Vanapalli, S.K., Fredlund, D.G. and Pufahl, D.E. 1996b. The relationship between the soil-water characteristic curve and the unsaturated shear strength of a compacted glacial till. *Geotechnical Testing Journal*, 19(3): 259-268.

Vanapalli, S.K., Fredlund, D.G. and Pufahl, D.E. 1999. The influence of soil structure and stress history on the soil-water characteristics of a compacted till. *Géotechnique*, 49(2): 143-159.

Vanapalli, S.K. and Mohamed, F.M.O. 2007. Bearing capacity of model footings in unsaturated soils. *In* Proceedings of the 2nd International Conference on Unsaturated Soils, Weimar, 483-493.

Vesić A.B. 1973. Analysis of ultimate loads of shallow foundations. *Journal of the Soil Mechanics and Foundation Division*, ASCE, 99(1): 45-73.

Wanatowski, D. and Chu, J. 2007. Drained behavior of Changi sand in triaxial and plane-strain compression. *Geomechanics and Geoengineering*, 2(1): 29-39.

Wang, Q, Pufahl, D.E., and Fredlund, D.G. 2002. A study of critical state on an unsaturated silty soil. *Canadian Geotechnical Journal*, 39(1): 213-218.

Wheeler S.J. and Sivakumar, V. 1995. An elasto-plastic critical state framework for unsaturated soil. *Géotechnique*, 45(1): 35–53.

CHAPTER 6

SHEAR MODULUS OF UNSATURATED SOILS

6.1 Introduction

The shear modulus, G is a key parameter used in the evaluation of dynamic response of geotechnical structures associated with earthquakes, machine vibrations and blasting. The strains in geotechnical structures due to the dynamic loads are significantly small and the shear modulus determined at small-strain (i.e. typically less than 0.001%) is referred to as the maximum conditions (i.e. G_{max}). Maximum shear modulus, G_{max} represents elastic shear modulus since at small-strains the slippage at particle contacts is negligible and the soil response is governed by elastic deformation of particle material (Hardin and Kalinski 2005).

Maximum shear modulus, G_{max} can be determined both in the field and in the laboratory using various types of tests (Table 6.1). Among these methods, the bender element and the resonant column tests are most commonly used in laboratory to determine G_{max} of unsaturated soils since the test equipment for those tests can easily be modified to determine G_{max} of both saturated and unsaturated soils (Ng and Menzies 2007). However, determination of G_{max} of unsaturated soils may require considerable amount of time to achieve equilibration conditions with respect to volume and suction of the specimens. Typically, the time required for equilibration is a couple of days for cohesionless soils; however, much longer time periods are necessary for cohesive soils. Due to this reason, several investigators proposed empirical or semi-empirical equations for estimating G_{max} taking account of the influence of compaction water content, degree of saturation or suction (Wu et al. 1984, Qian et al. 1993, Edil and Sawangsuriya 2005, Sawangsuriya et al. 2008, Cho and Santamarina 2001, Mancuso et al. 2002, Mendoza et al. 2005). However, there are limitations to extend these equations to other types of soils as the empirical constants required for these equations were developed based on experimental results on the limited number of soils.

Table 6.1 Various tests to estimate G_{max} both in the laboratory and in filed.

Test type	Test methods (References)
Field tests	• Surface wave tests (Nazarian and Stokoe 1983) • Seismic crosshole tests (Roesler 1977) • Dynamically loaded drilled shaft (Kurtulus and Stokoe 2008)
Laboratory tests	• Bender element tests (Shirley and Anderson 1975, Picornell and Nazarian 1998, Lee et al. 2007) • Resonant column tests (Seed and Idriss 1970, Kim et al. 2003, Hardin and Kalinski 2005) • Cyclic triaxial tests (Ladd and Dutko 1985) • Cyclic direct simple shear tests (Airey and Wood 1987).

In this chapter, a semi-empirical model is proposed to estimate the variation G_{max} of non-plastic sandy soils (i.e. I_p = 0%) with respect to matric suction using the Soil-Water Characteristic Curve (*SWCC*) as a tool. The proposed model uses two parameters that can be derived from grain size distribution curve.

6.2 Background

6.2.1 Determination of G_{max} for Unsaturated Soils – Bender Element and Resonant Column Test

The bender element and the resonant column tests are most commonly used to determine G_{max} of unsaturated soils ($G_{max(unsat)}$). However, the bender element test is regarded as a more conventional laboratory tool due to the following reasons; (i) its simplicity and ease of conducting tests by modifying conventional static triaxial test equipment (Ferreira et al. 2006) and (ii) unlimited number of tests can be performed on identical specimens.

Figure 6.1 shows schematic diagram of a bender element apparatus for unsaturated soils combined with pressure plate extractor used by Lee et al. (2007). The testing technique involves achieving predetermined matric suction values in the soil specimens using the axis-translation technique (Lee et al. 2007). A waveform voltage is applied to the transmitter element after achieving equilibrium conditions with respect to matric suction in the specimen used. The time, t required for the waveform voltage to reach the receiver element located on the other side of the specimen is then recorded. Maximum shear modulus, G_{max} can be calculated using Eq. (6.1) given below.

$$G_{max} = \rho \cdot V_S^{\,2} = \rho\left(\frac{d}{t}\right)^2 \tag{6.1}$$

where ρ = unit mass density of soil, V_S = shear wave velocity, d = distance between elements, and t = waveform voltage travel time

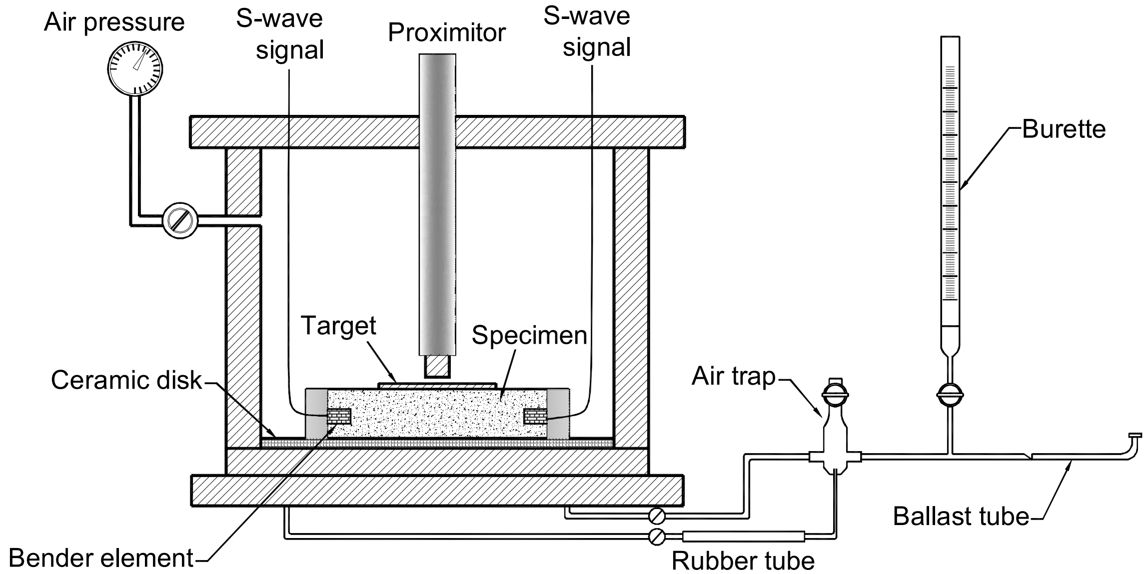

Figure 6.1 Schematic diagram of a bender element method apparatus combined with the pressure plate extractor (Lee et al. 2007).

Figure 6.2 shows a schematic diagram of a resonant column test apparatus with matric suction control system used by Kim et al. (2003). The matric suction values in the specimens are controlled by applying pore-air and pore-water pressures through the lines connected to the top and the bottom of the specimen. After the specimen reaches equilibrium condition with respect to volume and matric suction, harmonic torsional load is applied on top of the specimen by an electromagnetic loading system while the bottom of the specimen is fixed against rotation. The variation of the acceleration amplitude according to loading frequency (i.e. frequency response curve) is recorded and the maximum amplitude and corresponding frequency is determined. Maximum shear modulus, G_{max} can be estimated using Eq. (6.1) (i.e. $G_{max} = \rho V_s$) and the required shear wave velocity (i.e. V_s) can be calculated using Eq. (6.2) given below (Richart et al. 1970).

$$\frac{I}{I_o} = \frac{\omega_n L_s}{V_s} \tan\left(\frac{\omega_n L_s}{V_s}\right) \tag{6.2}$$

where I, I_o = mass polar moment of inertia of specimen and attached mass, respectively, V_s = shear wave velocity in soil column, ω_n = natural circular frequency, and L_s = length of specimen

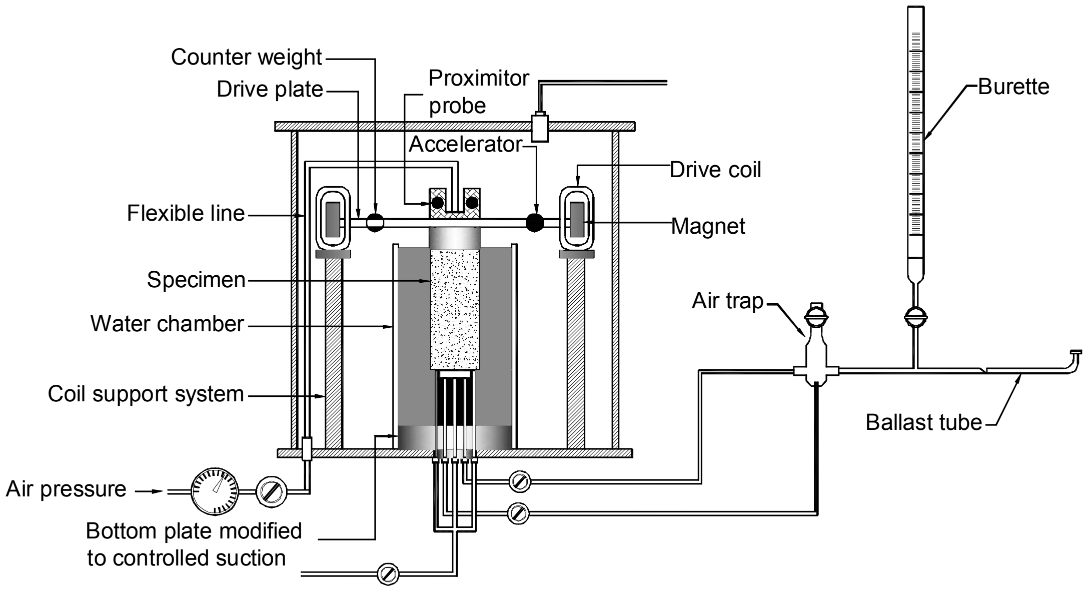

Figure 6.2 Schematic diagram of a resonant column method apparatus with a control system for matric suction application (Kim et al. 2003).

6.2.2 Determination of G_{max} for Unsaturated Soils – Empirical or Semi-Empirical Equations

Determination of G_{max} experimentally is time-consuming and cumbersome. This is especially true for unsaturated soils. Due to this reason, several researchers have been studying to develop empirical (or semi-empirical) equations (or models) that can be used to estimate G_{max} of unsaturated soils [i.e. $G_{max(unsat)}$] using certain soil properties and empirical constants. Table 6.2 summarizes the equations or models available in the literature developed using the measured $G_{max(unsat)}$ obtained from the bender element and the resonant column tests. The equations in Table 6.2 can be categorized into two groups. The first group includes the equations to estimate G_{max} of unsaturated soils compacted at different water contents (Wu et al. 1984, Sawangsuriya 2006, Sawangsuriya et al. 2008). The second group includes the equations to estimate the variation of G_{max} with respect to suction for a certain confining pressure (or overburden pressure) and void ratio (Cho and Santamarina 2001, Mancuso et al. 2002, Mendoza et al 2005, Takkabutr 2006, Hoyos et al. 2011). The typical behavior of G_{max} with respect to suction for different soil types can be summarized as Figure 6.3 based on the experiment results in the literature presented in Table 6.2.

Table 6.2 Summary of the equations to estimate G_{max} values of unsaturated soils (*BET* = Bender Element Test, *RCT* = Resonant Column Test, Typical behavior = variation of G_{max} with respect to matric suction in Figure 6.3)

Author(s)	Soil/material	Testing method	Typical behavior	Proposed equation	Remarks
Wu et al. (1984)	Fine-grained cohesionless soils	*RCT*	Curve (i)	$G_{max(S)} = [1+H(S)]G_{max(dry)}$ $H(S) = \begin{cases} (a-1)\sin\left(\dfrac{\pi S}{2S_{opt}}\right) & S \le S_{opt} \\ (a-1)H_1(S)H_2(S) & S > S_{opt} \end{cases}$ $S_{opt}(\%) = -6.5\log\left[D_{10}(mm)\right]+1.5$ $G_{max(S)}$ = G_{max} at any degree of saturation, S, $G_{max(dry)}$ = G_{max} at dry condition, a = maximum value of $G_{max(S)}/G_{max(dry)}$, and S_{opt} = optimum degree of saturation (i.e. degree of saturation at a)	• More details on the functions, $H_1(S)$ and $H_2(S)$ are available in Wu et al. (1984). • Specimens are compacted at different water contents (i.e. specimens are not identical)
Cho and Santamarina (2001)	Clean glass beads, Mixture of Kaolinite and glass beads, Granite powder, and Sandboil sand	*BET*	Curve (i) for glass beads, Curve (ii) for the remainder	$V_{s(unsat)} = V_{s(sat)}\left[1+\dfrac{2\sigma'_{eq}}{(1+K_0)\sigma'_v}\right]^{\beta_{CS}}\sqrt{\dfrac{e+G_s}{eS+G_s}}$ $V_{s(sat)}$, $V_{s(unsat)}$ = shear wave velocity under saturated and unsaturated condition, respectively, σ'_{eq} = equivalent effect stress due to suction, β_{CS} = empirical parameter, e = void ratio, G_s = specific gravity; and K_0 = coefficient of lateral earth pressure at rest	• If cohesionless soils desaturate gradually by air drying, the bonding between soil particles continuously increases up to dry condition due to the effects that are similar to cementation (Rinaldi et al. 1998). In this case the $V_{s(max)}$ can be calculated using the equation given below. $V_{s(max)}(m/sec) = 2{,}200\sqrt{D_{10}(\mu m)}$ for $(5\mu m \le D_{10} \le 300\mu m)$

Hoyos et al. (2001)	Silty sand	*BET, RCT*		$$G_{max(unsat)} = A_H\left(p - u_a\right)^{B_H}$$ $(p - u_a)$ = net confining pressure and A_H, B_H = fitting parameters	• The fitting parameter, A is the value at $(p - u_a)$ = 1 kPa and the fitting parameter, B represents how susceptible the soil stiffness is to changes in $(p - u_a)$.
Mancuso et al. (2002)	Silty sand (decomposed granite)	*RCT*	Curve (iii)	$$G_{max(unsat)} = A\left[\frac{\left(p-u_a\right)_C + \left(u_a-u_w\right)}{p_a}\right]^{n_M} OCR^{m_M}$$ $$for\ \left(u_a-u_w\right) \le \left(u_a-u_w\right)_b$$ $$G_{max(unsat)} = G_{max(s^*)}\left\{\left[1-r\right]e^{-\beta_M\left[\left(u_a-u_w\right)-\left(u_a-u_w\right)_b\right]} + r\right\}$$ $$for\ \left(u_a-u_w\right) \ge \left(u_a-u_w\right)_b$$ $G_{max(sat)}$, $G_{max(unsat)}$ = maximum shear modulus under saturated and unsaturated condition, respectively, A = stiffness index, m_M, n_M = stiffness coefficients, OCR = over consolidation ratio, $G_{max(s^*)}$ = G_{max} at air-entry value, $(u_a - u_w)_b$, β_M = parameter that controls the rate of increase of soil stiffness with respect to suction, $(p - u_a)_C$ = mean net stress and r = ratio between $G_{max(s^*)}$, and the threshold value of G_{max}.	• The effect of bulk-water on G_{max} is dominant in the boundary effect zone; therefore, the gradient of G_{max} versus $(u_a - u_w)$ relationship is the same as that of G_{max} versus p' (mean effective stress) relationship in this zone. • The effect of menisci-water becomes predominant in the residual zone as progressive shift takes place in the transition zone from bulk-water to menisci–water.
Mendoza et al. (2005)	Kaolinite clay	*BET*	Curve (ii)	$$G_{max(unsat)} = 30000\,\frac{(2.3-e)^2}{1+e}\left[\ln(u_a-u_w)\right]^{1.35}$$ $G_{max(unsat)}$ = maximum shear modulus under	• The volume of the specimens was allowed to change during both the drying and wetting paths. (i) ***Boundary effect zone***: sharp

				unsaturated condition, e = void ratio, and $(u_a - u_w)$ = suction	increase of G_{max} due to the increase in the density of the soil (ii) ***Transition zone***: gradual increase of G_{max} due to some shrinkage (iii) ***Residual zone***: sharp increase of G_{max} due to the particle displacement and rotation due to the influence of soil structure effects without major volume change
Sawangsuriya (2006)	Clayey sand, Silt, Lean clay, and Fat clay	*BET*	N/A	$G_{max(unsat)} = A_S f(e)(\sigma_0 - u_a)^{n_S} + C\Theta^{\kappa_S}(u_a - u_w)$ $G_{max(unsat)} = A_S f(e)\left[(\sigma_0 - u_a) + \Theta^{\kappa_S}(u_a - u_w)\right]^{n_S}$ A_S, C_S, κ_S, n_S = fitting parameters optimized to obtained a best-fit, e = void ratio, $f(e)$ = $[1/(0.3+0.7e^2)]$ (Hardin 1978), Θ = normalized volumetric water content and $(\sigma_0 - u_a)$ = net confining pressure.	• Initial compaction water content has significant influence on G_{max} value.

Sawangsuriya et al. (2008)	Lean clay, Silt, and Clayey sand	*BET*	N.A	$G_{max} = \left(w \frac{E}{E_{std}} \frac{w_{opt}}{w_{opt,std}} \right) (\alpha_S \log \psi - \beta_S)$ E = compaction energy achieved by enhanced or reduced Proctor effort, E_{std} = compaction energy achieved by standard Proctor effort, w = compaction water content, w_{opt} = optimum water content, $w_{opt,std}$ = optimum water content obtained from enhanced or reduced Proctor effort, ψ = soil suction and α_S, β_S = fitting parameters associated with soil composition	
Takkabutr (2006)	Sand and Clay	*BET, RCT*	Curve (i)	$\frac{G_{max(unsat)}}{\sigma_0} = A_T \sigma_0^{B_T} \left[\psi^{C_T \exp D_T \sigma_0} \right] \exp(E_T \psi)$ $G_{max(unsat)} = \left[I_T \ln \Psi + J_T \right] \exp\left[\left(L_T \Psi + M_T \right) K_0 \right]$ σ_0 = confinement (kPa) ($\geq$ 1 kPa), K_0 = K_0 stress state value, Ψ = matric suction (kPa), (A_T, B_T, C_T, D_T, E_T) and (I_T, J_T, L_T, M_T) = constants	• Influence of compaction water content, matric suction, confinement, and K_0 stress condition on G_{max}.

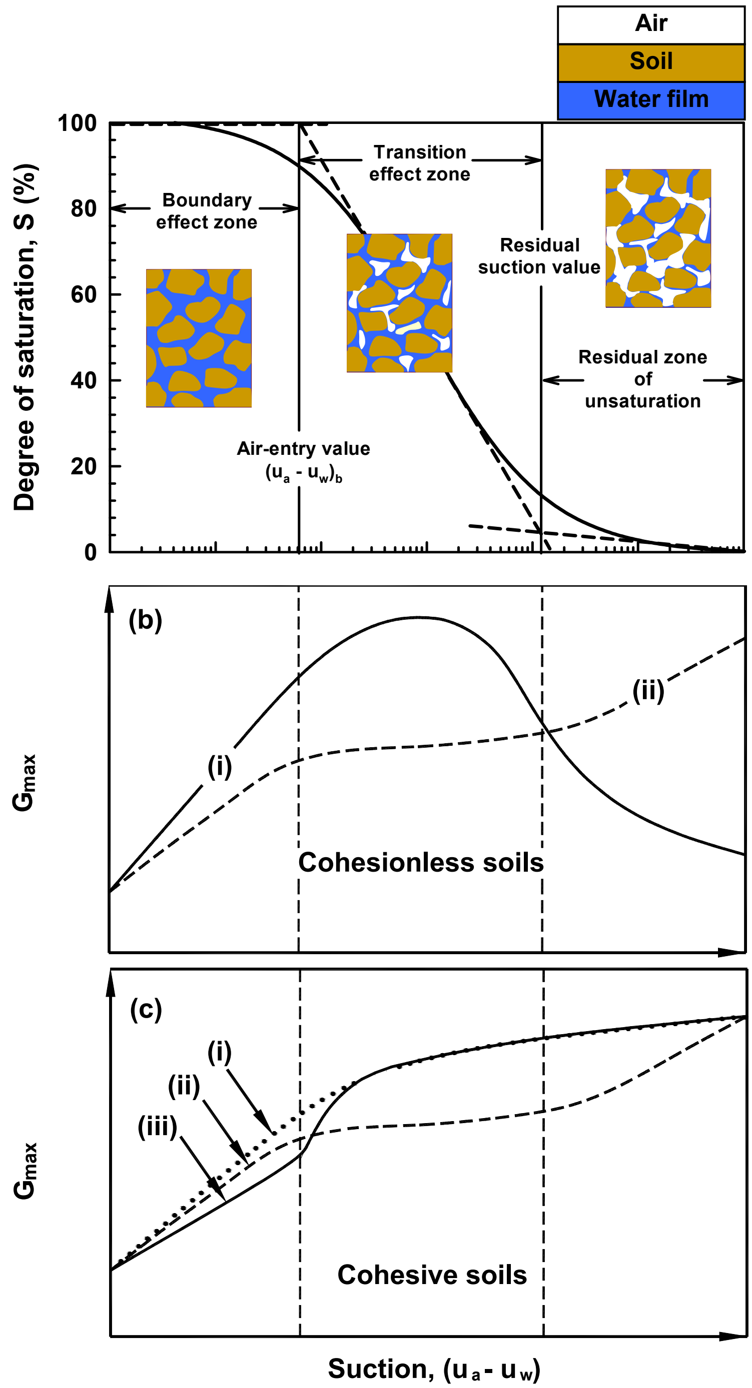

Figure 6.3 (a) Typical *SWCC* with three different stages of desaturation; and variation of maximum shear modulus, G_{max} for (b) cohesionless and (c) cohesive soils with respect to suction.

6.3 Model to Estimate the Variation of G_{max} of Unsaturated Non-Plastic Sandy Soils with respect to Matric Suction

6.3.1 Factors that Influence G_{max} of Unsaturated Soils

Maximum shear modulus, G_{max} is influenced by various factors such as soil type (i.e. plasticity index, I_p), soil fabric or structure (i.e. dry unit weight, compaction water content and void ratio), confining pressure (Qian et al. 1993, Takkabutr 2006), and stress and strain history (Hardin and Drnevich 1972, Hoyos et al. 2011). However, in the case of clean, dry, and cohesionless soils, G_{max} is governed by void ratio and confining pressure (Hardin and Richart 1963, Kokusho 1980), which can be generalized using the form shown in Eq. (6.3).

$$G_{max} = AF(e)\left(\sigma_0'\right)^n \tag{6.3}$$

where A and n = constant, $F(e)$ = function of void ratio, and σ'_0 = effective stress

In this chapter, a model is proposed that can be used to estimate the variation of G_{max} of non-plastic sandy soils with respect to matric suction that are subject to a certain confining pressure (or overburden pressure). For cohesive soils, the changes in matric suction associated with rainfall, evaporation or ground water table movement can result in subsequent changes in the soil structure. On the contrary, for cohesionless soils such as sandy soils, there is little or no influence of wetting and drying cycles on the volume change (or void ratio) (Fredlund and Rahardjo 1993, Oh and Vanapalli 2011). This means that the function of void ratio, $F(e)$ in Eq. (6.3) can be ignored in estimating the variation of G_{max} of non-plastic sandy soils with respect matric suction under a certain overburden pressure.

Asslan and Wuttke (2012) conducted bender element tests on Houston sand for two different net stresses, 50 kPa and 100 kPa. Ghayoomi and McCartney (2012) conducted bender element tests on F-75 Ottawa sand during centrifuge tests (40g) for two different depths, 3.51 cm and 11.11 cm. Figure 6.4(a) shows the normalized V_s values for the data presented by Asslan and Wuttke (2012) and Ghayoomi and McCartney (2012) using lower V_s values (i.e. the ratio of higher V_s to lower V_s at the same matric suction values).

As can be seen, the ratios are almost constant regardless of confining pressure or overburden pressure. This implies that the behaviors of G_{max} with respect to matric suction for different confining pressures are approximately parallel to each other [Figure 6.4(b)] .

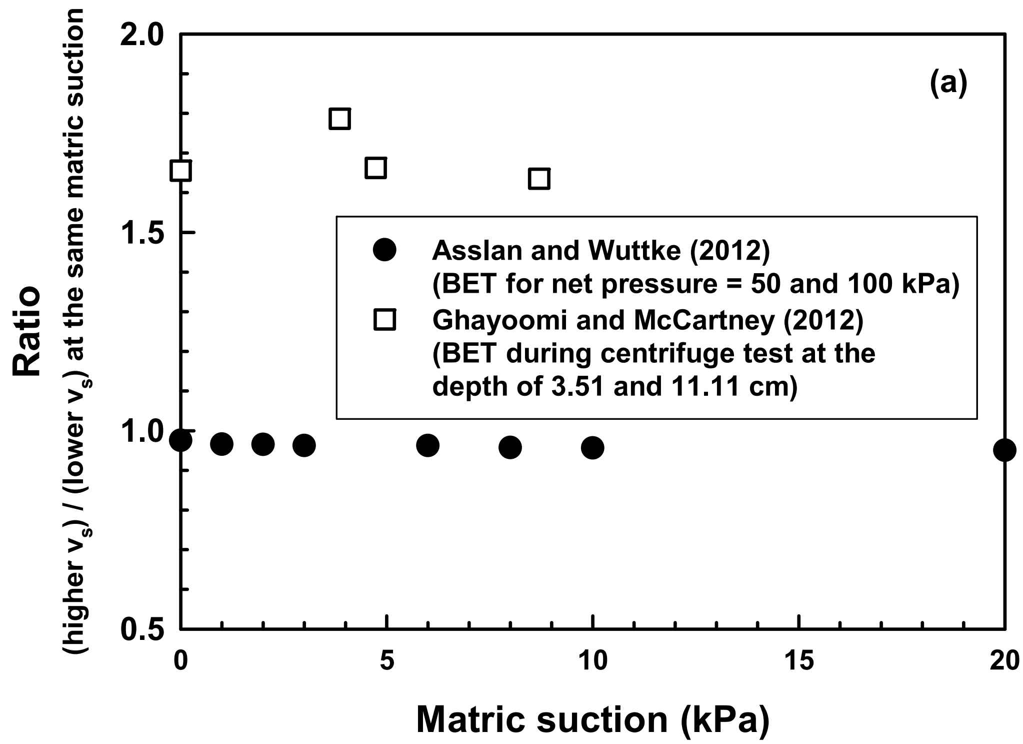

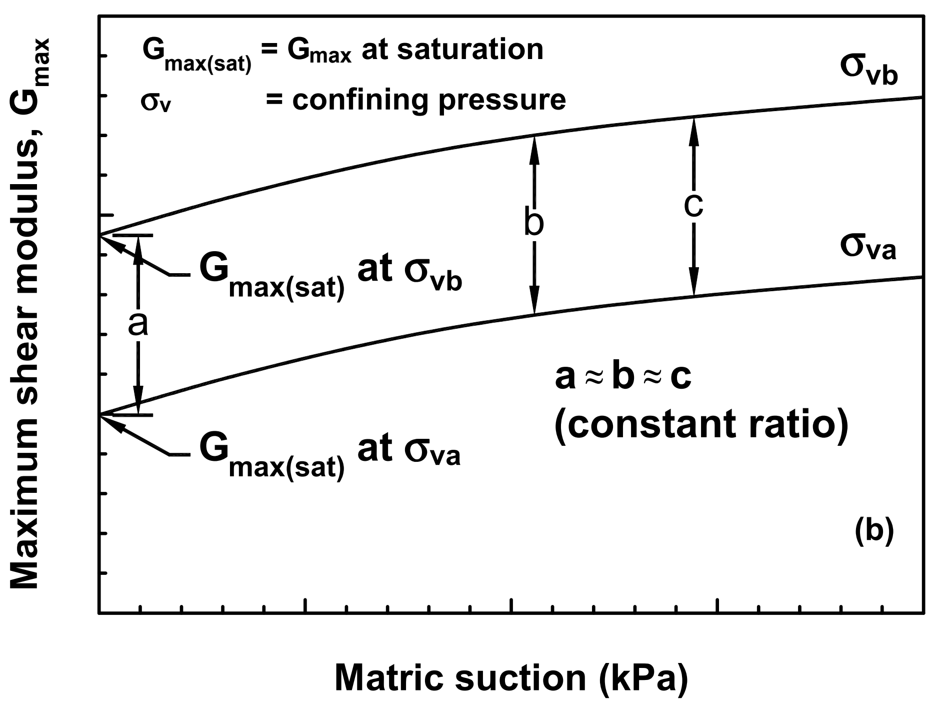

Figure 6.4 (a) Normalized shear wave velocities [data from Asslan and Wuttke (2012) and Ghayoomi and McCartney (2012)] and (b) typical behavior of G_{max} with respect to suction for cohesionless soils under different net pressures.

6.3.2 Non-Liner Variation of G_{max} with respect to Suction

In the present study, the Soil-Water Characteristic Curve (*SWCC*) is used as a tool in the proposed model to estimate the non-linear behavior of G_{max} with respect to matric suction. The *SWCC* is relatively unique for sandy soils and, according to Asslan and Wuttke (2012), the shape of *SWCC* is closely related to the variation of G_{max} with respect to matric suction. This implies that the influence of matric suction on G_{max} can be effectively represented using the *SWCC*. The *SWCC* has also been successfully used to estimate the variation of mechanical properties of unsaturated soils with respect to suction such as shear strength (Fredlund et al. 1996, Vanapalli et al. 1996), bearing capacity (Vanapalli and Mohamed 2007) and elastic modulus (Oh et al. 2009).

6.3.3 Proposed Model

Based on the discussion above, a simple model [Eq. (6.4)] is proposed to estimate the variation of G_{max} of cohesionless (i.e. non-plastic, I_p = 0%) soils with respect to matric suction extending the same philosophy proposed by Oh et al. (2009) for the elastic modulus model. The proposed model uses G_{max} at the saturated condition and the *SWCC* along with two fitting parameters, ζ and ξ. It should be noted that the proposed model does not take the influence of void ratio and effective stress on $G_{max(unsat)}$ into account due to the reasons discussed earlier.

$$G_{max(unsat)} = G_{max(sat)}\left[1+\zeta\left(\frac{(u_a-u_w)}{P_a/101.3}\right)\left(S^{\xi}\right)\right] \tag{6.4}$$

where $G_{max(sat)}$, $G_{max(unsat)}$ = maximum shear modulus under saturated and unsaturated condition, respectively, P_a = atmospheric pressure (i.e. 101.3 kPa), S = degree of saturation, and ζ, ξ = fitting parameters

6.4 Experimental Results Used in the Analysis

The bender element and resonant column tests results for various non-plastic sandy soils available in the literature are analyzed in the present study to provide the justification of the proposed model as follow.

Picornell and Nazarian (1998) studied the effect of matric suction on G_{max} using the bender element device combined with pressure plate extractor. The experiments were performed on four different reconstituted soils (i.e. coarse and fine sand, silt and clay). Only the test results for coarse sand were used in the analyses. For each matric suction value, two identical coarse sand specimens were prepared and then placed in the pressure plate extractor. When the specimens reached equilibrium conditions with respect to matric suction the bender element tests were performed on one of the specimens and the other specimen was used to measure water content (i.e. degree of saturation).

Kim et al. (2003) investigated the variation of G_{max} with respect to matric suction on a sand in the laboratory using resonant column test. The specimens were prepared by a 5-layer undercompaction method to obtained uniform density of specimens. The targeted matric suction values in the specimens were obtained by applying positive pore-air and pore-water pressures extending axis-translation technique. The confining pressure of 41 kPa was maintained throughout the tests. The experiment results for only three sand specimens were used in the analyses. They also conducted field cross-hole tests and showed that there is a good comparison between the shear moduli obtained in the laboratory and in the field.

Takkabutr (2006) studied the influence of matric suction and K_0 stress state on G_{max} for sand and clayey soils using both bender element and resonant column tests. The bender element tests were conducted in a triaxial cell to study the influence of K_0 on G_{max}. The *SWCC* was measured using a modified pressure plate extractor extending axis-translation technique for assessing the *SWCC* of unsaturated soils under anisotropic stress states. The results for only the sand obtained with the confining pressure = 17.25 kPa were used in the analyses.

Lee et al. (2007) studied the effect of matric suction on G_{max} of three types of subgrade soils (i.e. I_p = 0, 4.9 and 14.2%) using a volumetric pressure plate extractor equipped with bender element test. The targeted matric suction values were obtained by applying positive air-pressure extending axis-translation technique and the bender element tests were carried out when the specimens reached equilibrium conditions. The test results for only non-plastic soil were used in the analyses.

Ghayoomi and McCartney (2011) conducted bender element tests to study the variation of G_{max} with respect to matric suction during centrifuge tests for a sand (i.e. F-75 Ottawa sand). The degree of saturation and matric suction value of the soil in the centrifuge test was controlled using steady-state infiltration. To apply infiltration, water is first uniformly sprayed from a pressurize storage tank over the surface of the soil through a series of six fine-mist spray nozzles. During steady-state infiltration water moves towards the water table located at the bottom of a soil layer, which led to approximately uniform matric suction value throughout the soil. The *SWCC* of the sand was established using a hanging column test with controlled outflow. The test results performed under 40*g* were used for the analyses. The physical properties of the soils used for the analyses are summarized in Table 6.3.

Table 6.3 Properties of the soils used for the analyses

	Picornell and Nazarian (1998)	Kim et al. (2003)	Takkabutr (2006)	Lee et al. (2007)	Ghayoomi and McCartney (2011)
Specific gravity (G_s)	2.62	2.66	2.65	2.65	2.65
Plasticity index (I_p)	NP	NP	NP	NP	NP
Soil classification (*USCS*)	SP	SW	SP	SW	SP
Coefficient of Uniformity (C_U)	1.2	7.2	1.9	6.2	1.7
#200 passing %	0	2.5	0	1.3	0.5
OMC (%)	-	9.7	18	10.5	-
γ_{max} (kN/m^3)	-	19.7	15.35	19.91	-
Remark	PN-sand	K-sand	T-sand	L-sand	GM-sand

Figure 6.5 and Figure 6.6 show the grain size distribution curves and *SWCC*s, respectively for the soils used in the analyses. For the soil used by Picornell and Nazarian (1998), only the range of the grain sizes (i.e. between 0.85 mm and 0.425 mm) was available in the literature. The solid line in the hatched area is the assumed grain size distribution curve derived based on the range of the grain sizes reported in Picornell and Nazarian (1998). For the *SWCC* provided by Kim et al. (2003), the degree of saturation values for the initially compacted specimens were less than 100% since no efforts were made to fully saturate the compacted specimens before the process of desaturation. For the soil used by Picornell and Nazarian (1988), the number of data was not enough to establish whole range of *SWCC*. However, this is not a concern since only the measured points were used in the analyses. The *SWCC* used by Picornell and Nazarian (1998) is quite different from that of Takkabutr (2006) although both sands have similar grain size distribution curve. This is because the *SWCC* used by Takkabutr (2006) was established under the confinement of 17.25 kPa. Due to the same reason, the *SWCC* used by Ghayoomi and McCartney (2011) has lower air-entry value compared to that of Takkabutr (2006) although the air-entry value of a finer SP sand would be higher than that of a coarser SP sand. The materials used by Picornell and Nazarian (1998), Kim et al. (2003), Takkabutr (2006), Lee et al. (2007) and Ghayoomi and McCartney (2011) are hereafter referred to as PN-, K-, T-, L- and GM-sand, respectively.

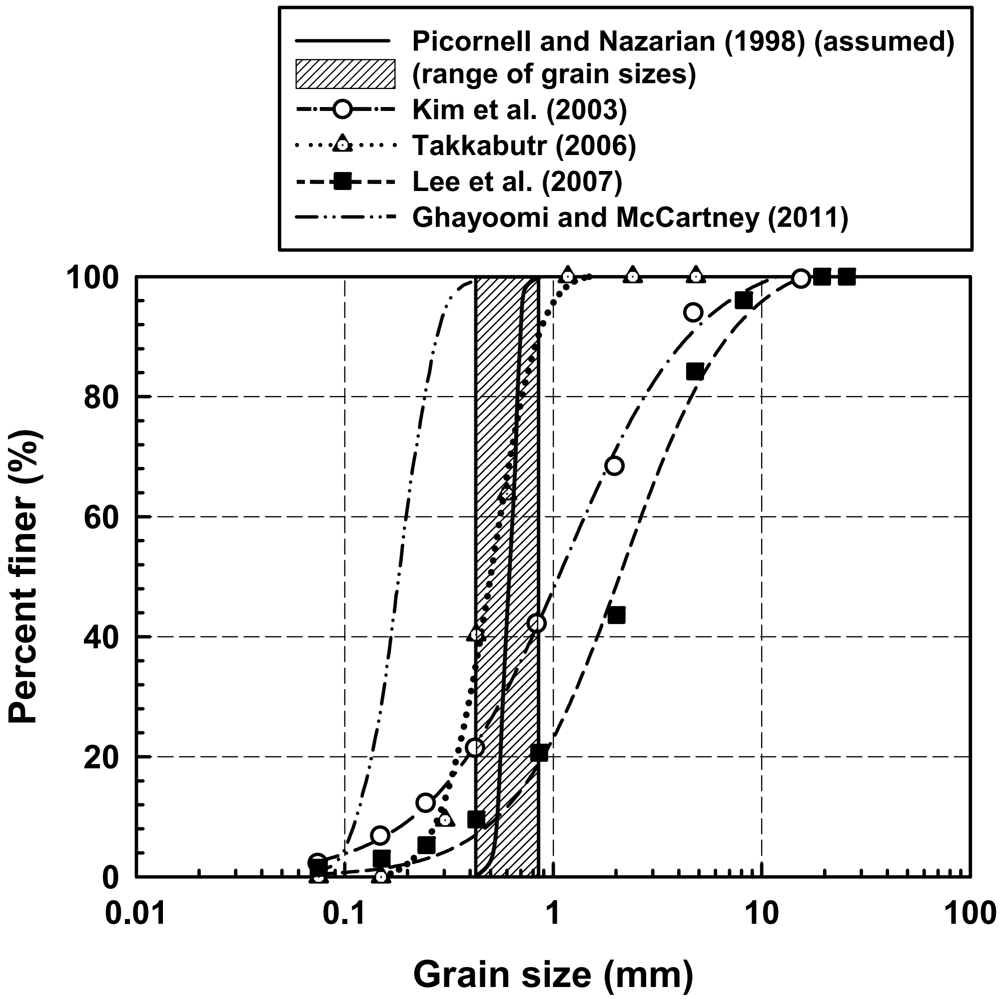

Figure 6.5 Grain size distribution curves for the non-plastic sandy soils used in the analysis.

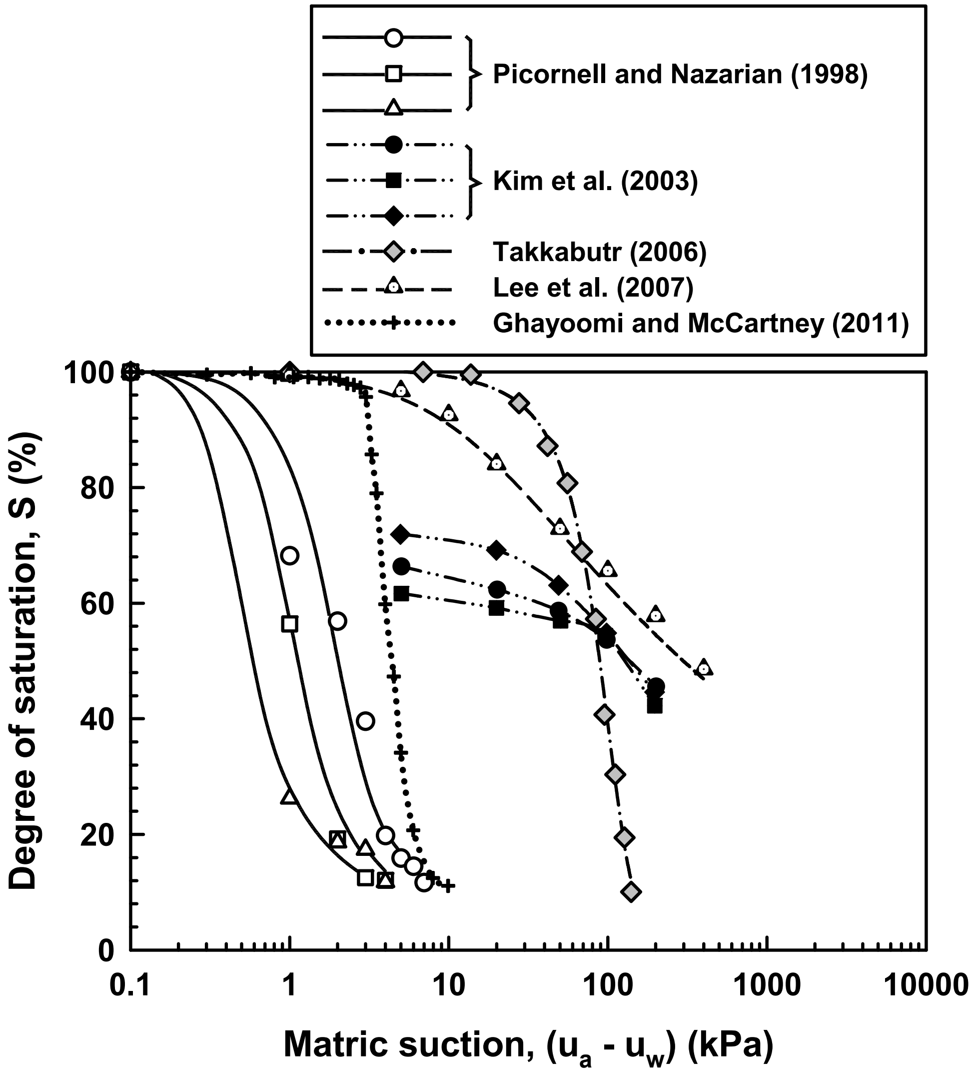

Figure 6.6 *SWCC*s for the non-plastic sandy soils used in the analysis.

6.5 Comparison between the Measured and the Estimated Shear Modulus

Figure 6.7 to Figure 6.10 provide comparisons between the measured G_{max} values and those estimated using the shear modulus model proposed in this chapter [i.e. Eq. (6.4)] for different matric suction values. The fitting parameters, ζ and ξ that provide most reasonable estimates are summarized in Table 6.4 for the five non-plastic sandy soils.

Table 6.4 Fitting parameters, ζ and ξ values for the soils studied.

Reference	*USCS*	I_p	ξ	ζ	C_U
Picornell and Nazarian (1998)	SP	NP	0.5	0.35	1.2
Ghayoomi and McCartney (2011)	SP	NP	0.5	0.2	1.7
Takkabutr (2006)	SP	NP	0.5	0.035	1.9
Kim et al. (2003)	SW	NP	1	0.025	7.5
Lee et al. (2007)	SW	NP	1	0.025	6.9

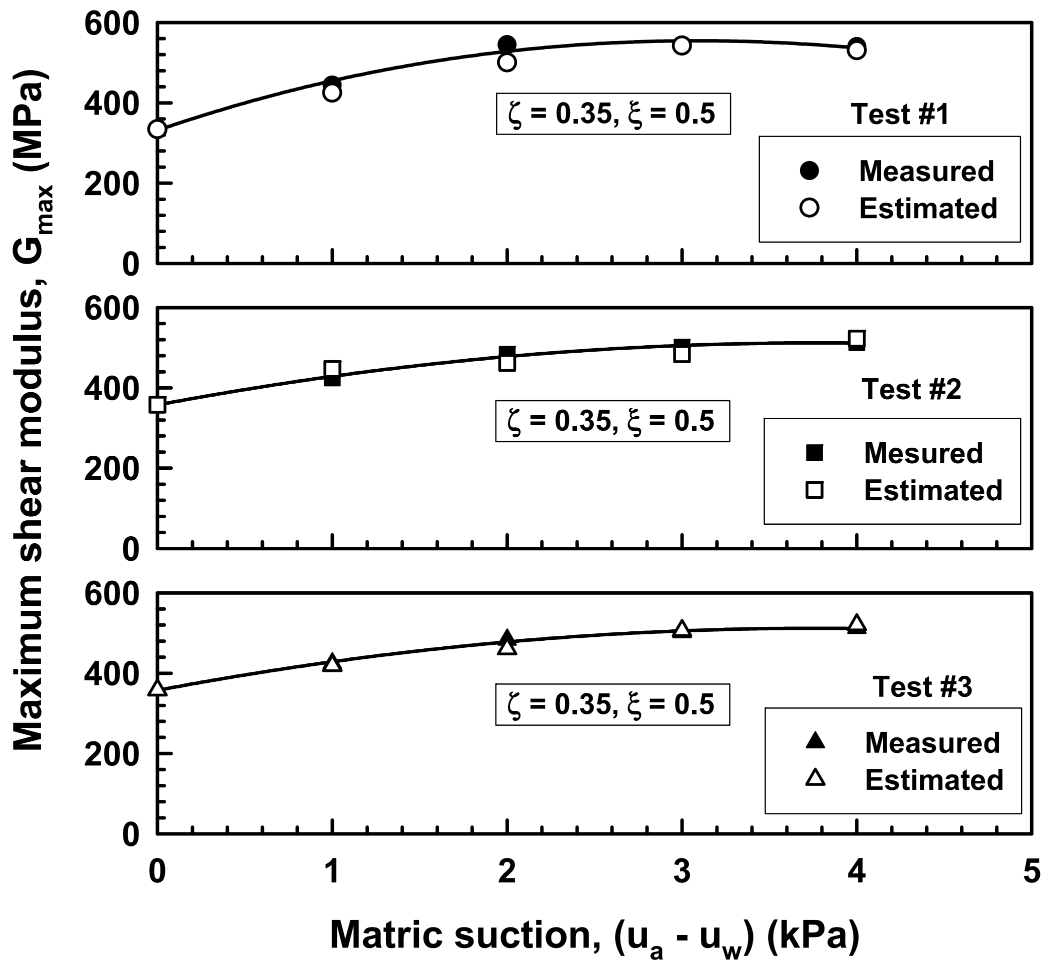

Figure 6.7 Comparison between the measured and the estimated G_{max} values for the date by Picornell and Nazarian (1998).

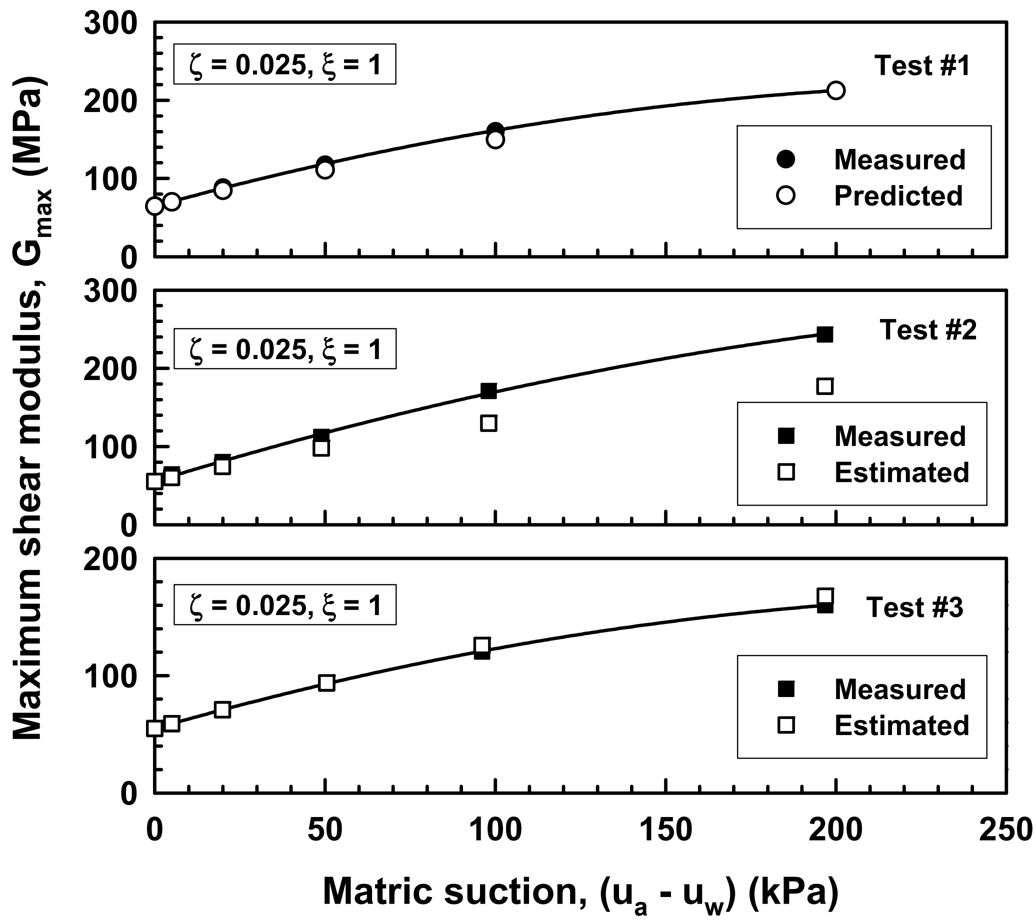

Figure 6.8 Comparison between the measured and the estimated G_{max} values for the data by Kim et al. (2003).

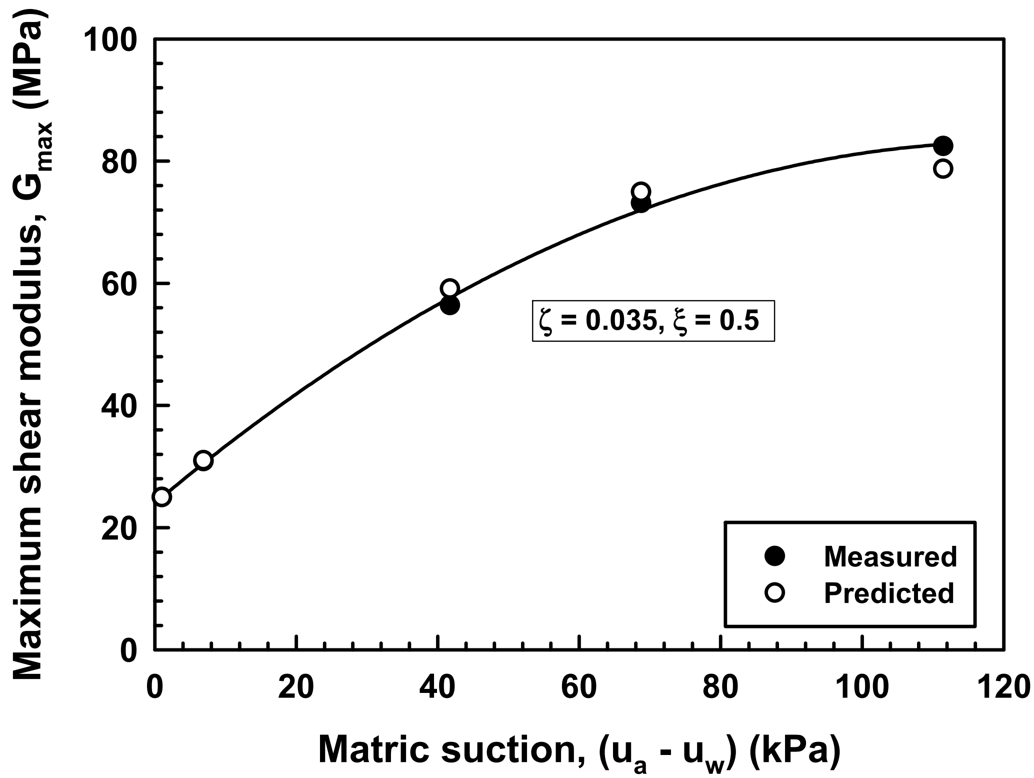

Figure 6.9 Comparison between the measured and the estimated G_{max} values for the data by Takkabutr (2006).

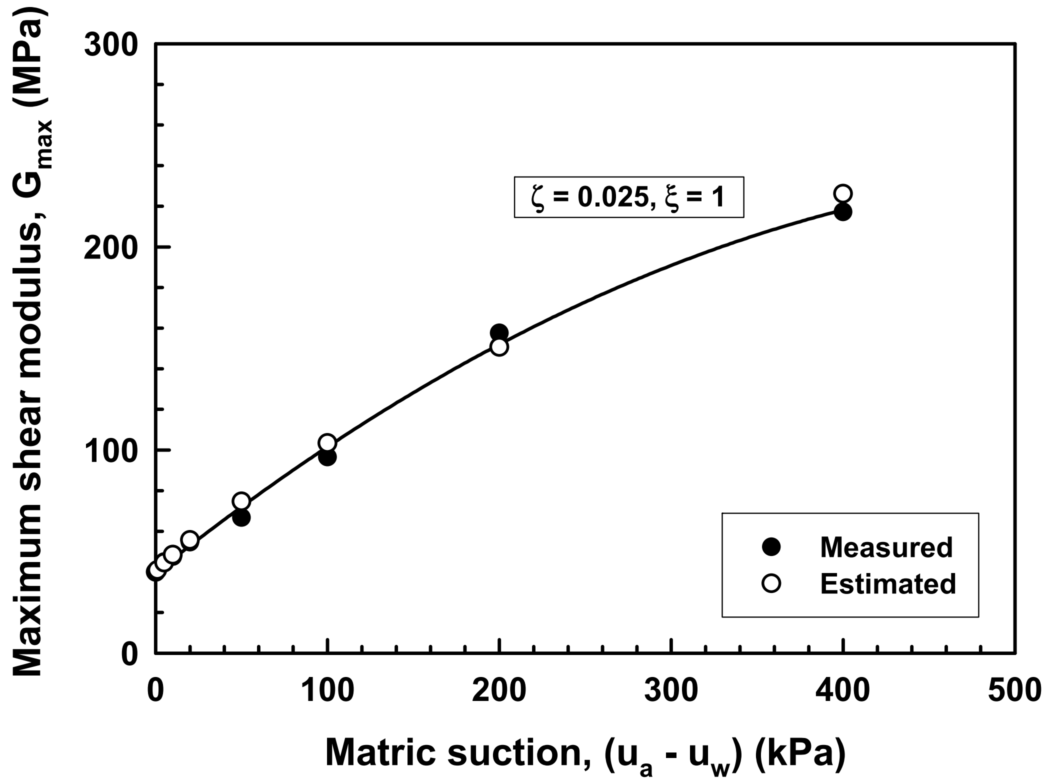

Figure 6.10 Comparison between the measured and the estimated G_{max} values for the data by Lee et al. (2007).

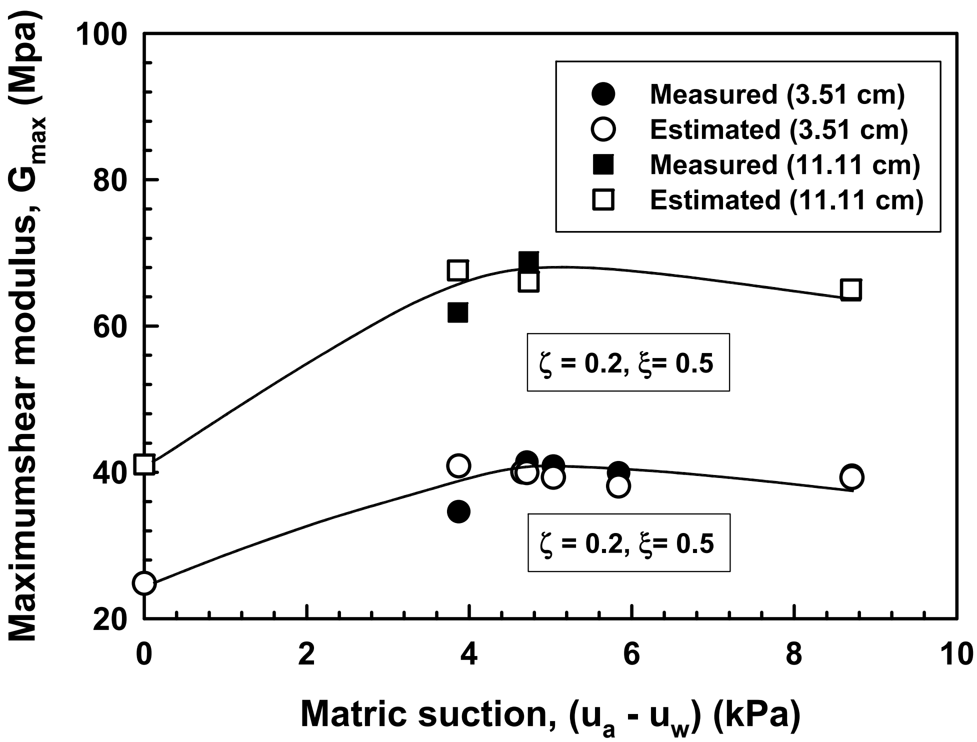

Figure 6.11 Comparison between the measured and the estimated G_{max} values for the data by Ghayoomi and McCartney (2011).

6.5.1 Fitting Parameter, ξ

The fitting parameter ξ for PN-, T-, and GM-sand are estimated to be 0.5 which is less compared to the fitting parameter value required for K- and L-sand (i.e. 1). According to the *USCS* (i.e. Unified Soil Classification System), PN-, T-, and GM-sand are classified as SP; on the other hand, K- and L-sand are classified as SW. This indicates that $\xi = 0.5$ and 1 are required for the soils classified as SP and SW, respectively. In case of the SP soils, the *SWCC* distributes in narrower range of matric suction value and G_{max} values change more drastically with respect to matric suction in comparison to SW soils. This characteristic behavior of the *SWCC* of the SP soils can be simulated by using lower values of parameter ξ.

6.5.2 Fitting Parameter, ζ

The fitting parameter ζ is estimated to be 0.35 for PN-sand, 0.2 for GM-sand, 0.035 for T-sand and 0.025 for K- and T-sand. The ζ value for PN-sand is 10 times greater than those for other sands. This can be attributed to the fact that in case of the PN-sand the range of the matric suction value corresponding to the transition zone (Figure 6.6) is the lowest compared to other sands. In other words, a higher value of fitting parameter ζ is required for the PN-sand to obtain most reasonable estimates.

Several studies showed that G_{max} of coarse-grained soils are closely related to gradation and particle shape of the soils (Hardin 1973, Chang and Ko 1986, Ishihara 1996, Menq 2003). According to Chang and Ko (1986), C_U is a key factor that influences on G_{max} of medium loose sand specimens; on the other hand, Menq (2003) concluded that D_{50} is a more important factor than C_U. In the present study, coefficient of uniformity C_U is adopted to correlate the fitting parameter, ζ with the gradation of the non-plastic sandy soils instead of D_{50} since no trends were found between ζ and D_{50}. The values for the fitting parameter, ζ are summarized in Table 4 along with the C_U values. In case of the PM-sand, the C_U value was calculated based on the assumed grain size distribution curve. The relationship between ζ and C_U is plotted in Figure 6.12. The ζ value rapidly decreases from 0.035 to 0.025 as the C_U value increases up to 2. The fitting parameter ζ

is relatively constant with a value of 0.025 for the C_U values greater than 6 (i.e. well-graded sandy soils). The ζ values for the C_U in the range of 2 to 6 cannot be confirmed due to the lack of date.

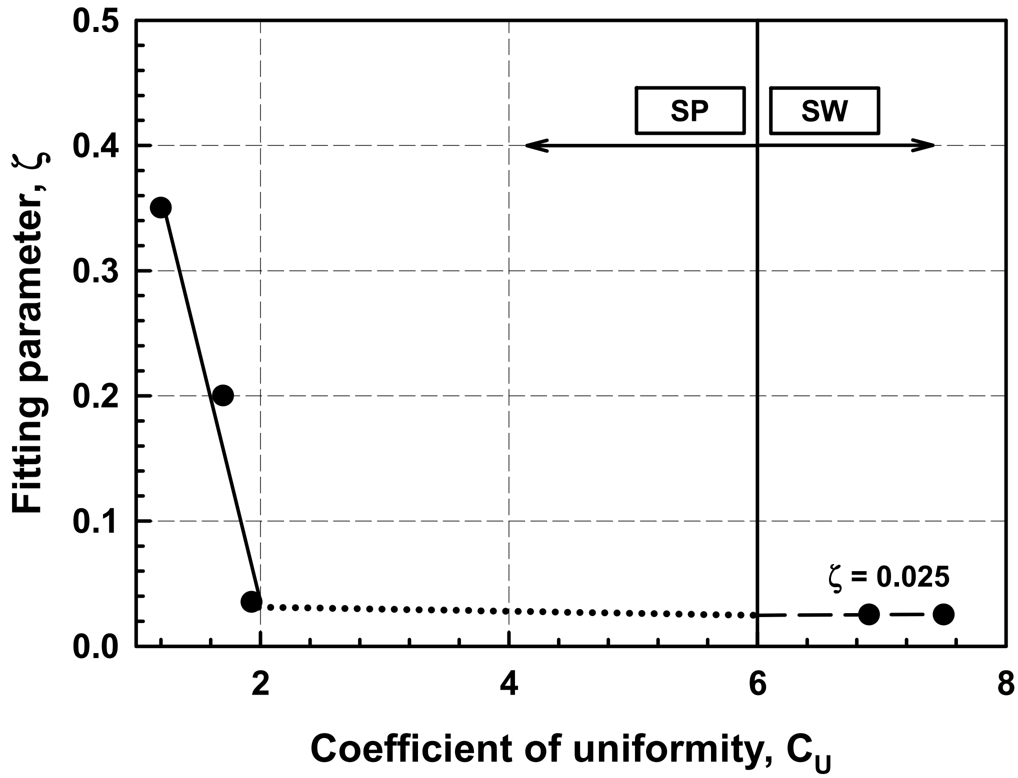

Figure 6.12 Variation of the fitting parameter, ζ with respect to coefficient of uniformity, C_U.

6.6 Limitations of the Proposed Semi-Empirical Model

(i) The semi-empirical shear modulus model proposed in this study is applicable for non-plastic sandy soils (i.e. I_p = 0 %) without taking account of the variation of void ratio (i.e. volume change) associated with water infiltration into the soils (i.e. change in matric suction).

(ii) The values for the fitting parameters, ξ and ζ suggested in this study are based on the non-plastic soils whose coefficient of uniformity and #200 passing % are in the range of 1.2 and 7.2 and less than 2.5%, respectively. The fitting parameters however can be reasonably well defined based on the soil classification (i.e. poorly or well-graded) and the coefficient of uniformity from the grain size distribution curve.

(iii) Kim et al. (2003) showed that there is good agreement between the shear moduli obtained in the laboratory (i.e. resonant column test) and in the field (cross-hole test) for unsaturated soils. On the contrary, the results from Lee et al. (2007) suggest that the maximum shear modulus from laboratory tests (i.e. bender element test) can be different from field test results (i.e. spectral analysis of surface wave and cross-hole test) due to differences in testing procedures, confining pressures and the compaction methods. However, their experiment results also showed that G_{max} versus gravimetric water content relationship from the laboratory tests is approximately parallel to the field studies results. These results are encouraging for implementing a correction factor into the proposed model to estimate G_{max} of unsaturated non-plastic sandy soils for field conditions. Larsson and Mulabdic (1991) also stated that G_{max} values from the laboratory tests are typically less than those from in-situ tests, which is mainly attributed to the sample disturbance. They suggested that this discrepancy can be overcome by using a strain-based correction factor.

6.7 Summary and Conclusions

A semi-empirical model is proposed to estimate the variation of maximum shear modulus, G_{max} of non-plastic sandy soils with respect to matric suction. The proposed model requires G_{max} under saturated condition and the *SWCC* along with two fitting parameters ξ and ζ. The two fitting parameters were determined by analyzing G_{max} values measured using bender element and resonant column tests. The analysis results showed that the fitting parameters can be well defined based on the soil classification and the coefficient of uniformity from the grain size distribution curve. The conclusions obtained from this study can be summarized as follow:

(i) The fitting parameter, $\xi = 0.5$ or 1 is required for poorly-graded and well-graded non-plastic sandy soils, respectively.

(ii) The fitting parameter, ζ is a function of the coefficient of uniformity, C_U. A value of $\zeta = 0.025$ can provide reasonable and yet conservative estimates for non-plastic sandy soils whose C_U values are greater than 2.

(iii) The proposed model can be used to estimate the variation of shear modulus in all the zones (i.e. boundary effect zone, transition zone and the residual zone) of the *SWCC*.

REFERENCES

Asslan, M. and Wuttke, F. 2012. Wave velocity change and small-strain stiffness in unsaturated soils: experimental investigation. *In* Proceedings of the 2nd European Conference on Unsaturated Soils (E-UNSAT 2012), Napoli, 355-362.

Airey, D.W. and Wood, D.M. 1987. An evaluation of direct simple shear tests on clay. *Géotechnique*, 37(1): 25-35.

Chang, N-Y. and Ko, H-Y. 1982 Effect of grain size distribution on dynamic properties and liquefaction potential of granular soils. Research Report R82-103, University of Colorado at Denver.

Cho, G. C. and Santamarina, J.C. 2001 Unsaturated particulate materials – particle-level studies. *Journal of Geotechnical and Geoenvironmental Engineering*, 127(1): 84-96.

Edil, T.B. and Sawangsuriya, A. 2005. Earthwork quality control using soil stiffness. *In* Proceedings of the 16th International Conference on Soil Mechanics and Geotechnical Engineering, Osaka, 1689-1692.

Ferreira, C., da Fonseca, A.V. and Santos, J. A. 2006. Comparison of simultaneous bender elements and resonant column tests on Porto residual soil. Soil Stress-Strain Behaviour: Measurement, Modeling and Analysis, 523-535.

Fredlund, D. G. and Rahardjo, H. 1993. *Soil mechanics for unsaturated soils*. John Wiley & Sons, New York.

Fredlund, D. G., Xing, A., Fredlund, M. D. and Barbour, S. L. 1996. Relationship of the unsaturated soil shear strength to the soil-water characteristic curve. *Canadian Geotechnical Journal*, 33(3): 440-448.

Ghayoomi, M. and McCartney, J. S. 2011. Measurement of small-strain shear moduli of partially saturated sand during infiltration in geotechnical centrifuge. *Geotechnical Testing Journal*, 34(5).

Hardin, B. O. 1978. The nature of stress-strain behaviors of soils. *In* Proceedings of the Geotechnical Engineering Division Specialty Conference on Earthquake Engineering and Soil Dynamics, ASCE, Pasadena, 1, 1 - 90.

Hardin, B. O. 1973. Shear modulus of gravel. Report TR74-73-CE19, Civil Engineering Department, University of Kentucky.

Hardin, B. O. and Drnevich, V. O. 1972. Shear modulus and damping in soils: measurements and parameter effect. *Journal of Geotechnical Engineering*, 98(6): 603-624.

Hardin, B. O. and Kalinski, M. E. 2005. Estimating the shear modulus of gravelly soils. *Journal of Geotechnical and Geoenvironmental Engineering*, 131(7): 867-875.

Hardin, B. O. and Richart, F. E. 1963. Elastic wave velocities in granular soils. *Journal of Soil Mechanics and Foundations Division*, ASCE, 89(1): 33-65.

Hoyos, L. R., Suescun, E. A. and Puppala, A. J. 2011. Small-strain stiffness of unsaturated soils using a suction-controlled resonant column device with bender elements. *In* Proceeding of Geo-Frontiers 2011 Conference, Dallas, 4313-4322.

Ishihara, K. 1996. *Soil behavior in earthquake geotechnics*. Oxford Science Publications, New York.

Kim, D. S., Seo, W. S. and Kim, M. J. 2003. Deformation characteristic of soils with variations of capillary pressure and water content. *Soils and Foundation*, 43(4): 71-79.

Kokusho, T. 1980. Cyclic triaxial test of dynamic soil properties for wide strain range. *Soils and Foundations*, 20(2): 45-60.

Kurtulus, A. Stokoe, K. H. 2008. In situ measurement of nonlinear shear modulus of silty soil. *Journal of Geotechnical and Geoenvironmental Engineering*, 134(10): 1531-1540.

Ladd, R. J. and Dutko, P. 1985. Small-strain measurements for stability of soft clays. In V. Koshla (ed.), Advances in the Art of Testing Soils Under Cyclic Conditions, 148-166,

Larsson, R. and Mulabdic, M. 1991. Shear moduli in Scandinavian clays; measurement of initial shear modulus with seismic cones. Report No. 40, Swedish Geotechnical Institute, Linkoping: 127.

Lee, S. H., Seo, W. S. and Kim, D. S. 2007. Evaluation of modulus of unsaturated compacted soils in various matric suctions using modified volumetric pressure plate extractor. *In* Proceedings of the 60th Canadian Geotechnical Conference, Ottawa, 1037-1044.

Mancuso, C., Vassallo, R. and d'Onofrio, A. 2002. Small strain behavior of a silty sand in controlled-suction resonant column - torsional shear tests. *Canadian Geotechnical Journal*, 39(1): 22-31.

Mendoza, C. E., Colmenares, J. E. and Merchán, V. E. 2005. Stiffness of an unsaturated compacted clayey soil at very small strains. *In* Proceedings of International Symposium on Advanced Experimental Unsaturated Soil Mechanics, Trento, 199-204.

Menq, F-Y. 2003. Dynamic properties of sandy and gravelly soils. PhD thesis, University of Texas at Austin

Nazarian, S. and Stokoe, K. H. 1983. Use of spectral analysis of surface waves for determination of moduli and thickness of pavement systems. Transportation Research Record 954, Transportation Research Board, Washington, D.C.

Ng, C. W. W. and Menzies, B. 2007. *Advanced unsaturated soil mechanics and engineering*, Taylor & Francis, New York and London.

Oh, W. T., Vanapalli, S. K. and Puppala, A. J. 2009. A semi-empirical model for the prediction of modulus of elastic for unsaturated soils. *Canadian Geotechnical Journal*, 46(8): 903-914.

Oh, W. T. and Vanapalli, S. K. 2011. Modelling the applied vertical stress and settlement relationship of shallow foundations in saturated and unsaturated sands. *Canadian Geotechnical Journal*, 48(3): 425-438.

Picornell, M. and Nazarian, S. 1998. Effect of soil suction on the low-strain shear modulus of soils. *In* Proceeding of the 2nd International Conference on Unsaturated Soil, Beijing, 102-107.

Qian, X., Gray, D. H. and Woods, R. D. 1993. Void and granulometry: effects and shear modulus of unsaturated soils. *Journal of Geotechnical Engineering*, 119(2): 295-314.

Richart, J. E., Hall, J. R. and Woods, R. O. 1970. *Vibrations of soils and foundations*. Prentice-Hall Inc, New Jersey.

Rinaldi, V. A., Santamarina, J. C. and Redolfi, E. R. 1998. Characterization of collapsible soils with combined geophysical and penetration testing. *In* Proceedings of the 1st International Conference on Site Characterization, ISC'98, Atlanta, 581-588.

Roesler, S. K. 1977. Correlation methods in soil dynamics. *In* Proceeding of DMSR77, Karlsruhe, 1, 309-334.

Sawangsuriya, A. 2006. Stiffness-suction-moisture relationship for compacted soils. PhD thesis, University of Wisconsin.

Sawangsuriya, A., Edil, T. B. and Bosscher, P. J. 2008. Modulus-suction-moisture relationship for compacted soils. *Canadian Geotechnical Journal*, 45(7): 973-983.

Seed, H. B. and Idriss, I. M. 1970. Soil moduli and damping factors for dynamic response analyses. Report EERC 70-10, Earthquake Engineering Research Center, University of California, Berkeley.

Shirley, D. J. and Anderson, A. L. 1975. Acoustic and engineering properties of sediments, Report ARL-TR-75-78, Applied Research Laboratory, University of Texas, Austin.

Takkabutr, P. 2006. Experimental investigations on small-strain stiffness properties of partially saturated soils via resonant column and bender element testing. PhD thesis, University of Texas, Arlington.

Vanapalli, S. K., Fredlund, D. G., Pufahl, D. E. and Clifton, A. W. 1996. Model for the prediction of shear strength with respect to soil suction. *Canadian Geotechnical Journal*, 33(3): 379-392.

Vanapalli, S. K. and Mohamed, F. M. O. 2007. Bearing capacity of model footings in unsaturated soils. *In* Proceedings of the 2nd International Conference on Unsaturated Soils, Weimar, 483-493.

Wu, S., Gray, D. H. and Richart, F. E. Jr. 1984. Capillary effect on dynamic modulus of sands and silts. *Journal of Geotechnical Engineering Division*, ASCE, 110(9): 1188-1203.

CHAPTER 7

SUMMARY AND CONCLUSIONS

7.1 General Introduction

In spite of several advancements over the past 50 years, implementation of the mechanics of unsaturated soils into conventional geotechnical engineering practice has been rather limited. This is mainly attributed to the lack of simple and reliable techniques or methodologies (or approaches) for (i) measuring soil suction values in field quickly and reliably and (ii) interpreting mechanical behavior of unsaturated soils. The main objective of this thesis research is to develop simple and reliable techniques, models or methodologies that can be reliably used in geotechnical engineering practice to estimate the mechanical properties extending mechanics of unsaturated soils.

The summary and conclusions from the studies undertaken in this thesis are summarized in the following sections.

7.2 Simple Techniques for Estimating Soil Suction of Unsaturated Soils

Two simple techniques are proposed to estimate suction values of as-compacted glacial till specimen (i.e. Indian Head till) in the range of 0 to 60,000 kPa. The first technique uses a conventional pocket penetrometer in the estimation of matric suction values lower than 300 kPa. The second technique uses conventional tensiometer to estimate relatively high suction values in the range of 1,200 to 60,000 kPa. The equilibrium suction values of the compacted glacial till specimens are respectively measured using axis-translation technique and a psychrometer for low and high suction values. There is a reasonably good comparison between the measured and the estimated suction values both in the low and high suction range.

7.3 Bearing Capacity of Unsaturated Soils

An approach is proposed to estimate the bearing capacity of unsaturated fine-grained soils (i.e. modified total stress approach) extending Skempton (1948)'s total stress approach based on the model footing tests results on statically compacted fine-grained soil samples (i.e. Indian Head till). The compacted soil samples are saturated and then subjected to varying degrees of natural air-drying to achieve different matric suction distribution profiles with depth below the model footing prior to loading them to failure conditions at constant rate (i.e. 1.14 mm/min). The results of the study suggest that the bearing capacity of unsaturated fine-grained soils can be estimated from conventional unconfined compression tests results without matric suction measurements. The proposed approach also provide good comparison between the measured and the estimated bearing capacity values for in-situ plate load test results in unsaturated fine-grained soils obtained with relatively large plates.

A semi-empirical model is proposed to estimate the variation of shear strength of unsaturated fine-grained soils from unconfined compression test results using the Soil-Water Characteristic Curve (*SWCC*) and unconfined compression test results under saturated condition along using two fitting parameters. Good agreement is observed between the measured shear strength and those estimated using the proposed model. This model can be effectively used to estimate the variation of bearing capacity of unsaturated fine-grained soils with respect to suction when the bearing capacity is interpreted using the modified total stress approach.

Finally, the model footing test results on a low plastic unsaturated fine-grained soil (i.e. I_p = 6%) were analyzed using both the *MESA* and the *MTSA*. The analyses results showed that the fitting parameter $\psi = 1$ (instead of 3) is required to estimate the bearing capacity of low plastic unsaturated fine-grained soils using the *MESA* assuming the local shear failure mode. The bearing capacity of low plastic unsaturated fine-grained soils can also be estimated more reliably using the *MTSA* with the fitting parameters $\upsilon = 1$ or 2 and μ values less than 10. In other words, the bearing capacity of low plastic unsaturated fine-grained soils can be interpreted using both the *MESA* and the *MTSA*.

7.4 Elastic Modulus of Unsaturated Soils

A semi-empirical model is proposed to estimate the variation of initial tangent elastic modulus, E_i of unsaturated coarse-grained soils with respect to matric suction using the *SWCC* and the initial tangent elastic modulus under saturated condition, $E_{i(sat)}$ along with two fitting parameters. This model is also extended to in-situ plate load and laboratory model footing tests results conducted in unsaturated fine-grained soils. The fitting parameter, $\beta = 1$ and 2 are recommended for coarse- and fine-grained soils, respectively. The fitting parameter, α is a function of plasticity index, I_p and the inverse of α (i.e. $1/\alpha$) non-linearly increases with increasing I_p. A better estimation of initial tangent elastic modulus of unsaturated soils can be achieved using upper and low boundary of the $1/\alpha$ versus I_p relationships depending of the rages of matric suction values.

7.5 Modelling the Stress versus Settlement Behavior of Shallow Foundations in Unsaturated Coarse-grained Soils

Two methodologies are proposed to simulate the applied vertical stress versus settlement behavior of model footing tests in both saturated and unsaturated sands based on the assumption that its behavior is elastic-perfectly plastic. In *Method I*, the stress versus settlement behavior is established as segments of two straight lines which represent linear elastic and perfect plastic behavior, respectively. In *Method II*, finite element analysis (i.e. *FEA*) is carried out using also the elastic-perfectly plastic model.

The results show that both the bearing capacity and the settlement of model footings in sands can be reasonably estimated using *Method I* for both saturated and unsaturated sandy soils. In case of the *Method II*, good agreement was observed between the measured and the estimated bearing capacity values, while the settlements were underestimated. The validity of the *Method II* was also checked using the footing ($B \times L$ = 1 m × 1 m) load test results in unsaturated sand.

The scale effect of plate size is an important parameter for reliable interpretation of model footing or in-situ plate load test results. Unlike saturated soils, the scale effect in unsaturated soils is function of not only the size of plate (or footing) but also of the representative matric suction value. In other words, if plate load tests are performed with two different sizes of plates on the soil whose suction distribution profile is non-uniform each stress versus settlement behavior corresponds to different representative suction value. Due to this reason, in the appendix, details of Large Tempe Cell that can be used to achieve the uniform suction distribution profile with depth are presented.

7.6 Shear Modulus of Unsaturated Soils

A semi-empirical model is proposed to estimate the variation of maximum shear modulus (G_{max}) of unsaturated non-plastic (i.e. I_p = 0%) sandy soils with respect to matric suction using the *SWCC* and G_{max} under saturated condition along with fitting parameters. To determine the proper fitting parameters, the shear modulus values measured using bender element and resonant column tests for five different unsaturated non-plastic sandy soils are analyzed. The results show that the fitting parameters can be defined based on the soil classification and the coefficient of uniformity from the grain size distribution curve. There is a good comparison between the measured G_{max} values of non-plastic sandy soils and those estimated using the proposed model.

7.7 Recommendations and Suggestions for Future Research Studies

The techniques (or methodologies) and models proposed in this thesis research are developed based on the experiment results for limited numbers of soils and analyzing few studies. More research studies are necessary in order to propose techniques and models that may be used for different types of soils considering different practical scenarios. For instance, suction measurement techniques proposed in Chapter 2 can be further improved by conducting more tests for the soils of various plasticity index values. In-situ plate load tests can be carried out in unsaturated fine-grained soils to improve the reliability of the modified total stress approach proposed in Chapter 3 for the estimation of bearing capacity of unsaturated fine-grained soils. These plate load tests results can also be used to check the validity of the elastic modulus model proposed in Chapter 4. The methodologies proposed in Chapter 5 to estimate the stress versus settlement behavior of model footing or in-situ plate load tests can be improved such that they can be extended to not only coarse-grained soils but also for fine-grained soils. The shear modulus model proposed in Chapter 6 can be strengthened by performing bender element or resonant column tests for the non-plastic sandy soils that have different coefficient of uniformity values.

APPENDIX

DESIGN OF LARGE TEMPE CELL TO ACHIEVE UNIFORM MATRIC SUCTION PROFILE

Figure App-1 shows the components of the Large Tempe Cell which were specially designed and constructed at the University of Ottawa. It consists of cylinder (300 mm in diameter × 300 mm in height), top plate, and bottom plate. Upper surface of the bottom plate is grooved in a spiral shape to facilitate easier movement of water (to flush air bubbles below the ceramic disk) in the system. The ceramic disk is glued to the bottom plate by filling the gap between the ceramic disk (air-entry value = 500 kPa) and the bottom plate using epoxy following the procedures provided by Power and Vanapalli (2010). The epoxy was build up in three layers by allowing each layer to be cured before the next layer was placed (Figure App-2).

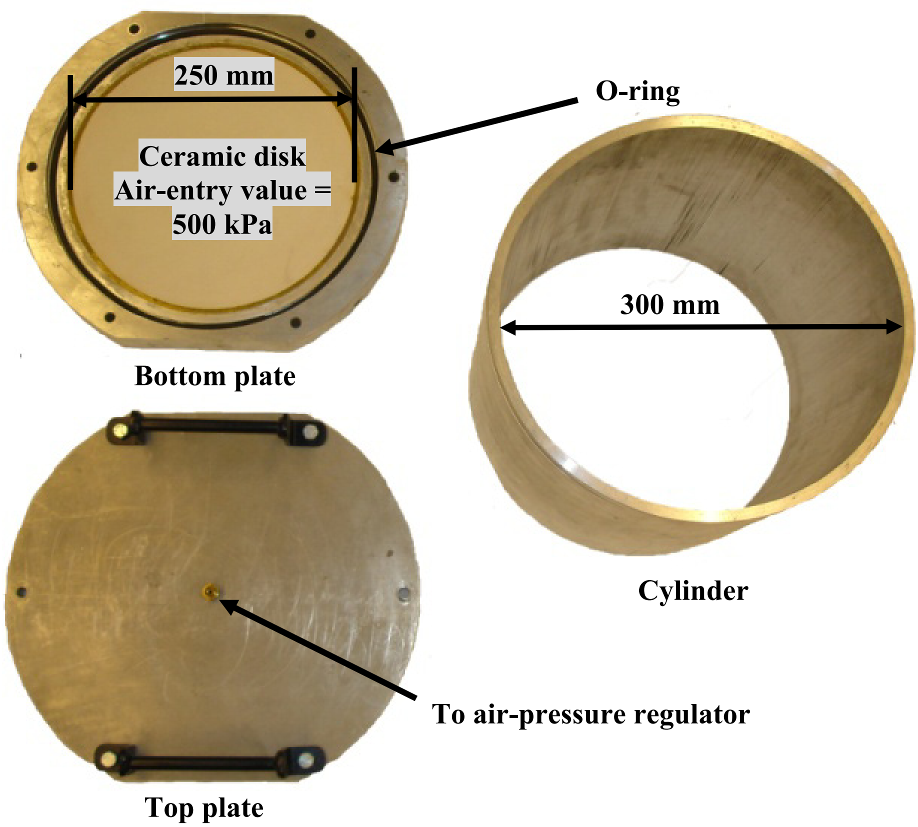

Figure App-1 Components of the Large Tempe Cell using axis-translation technique for conducting model footing test with constant matric suction distribution.

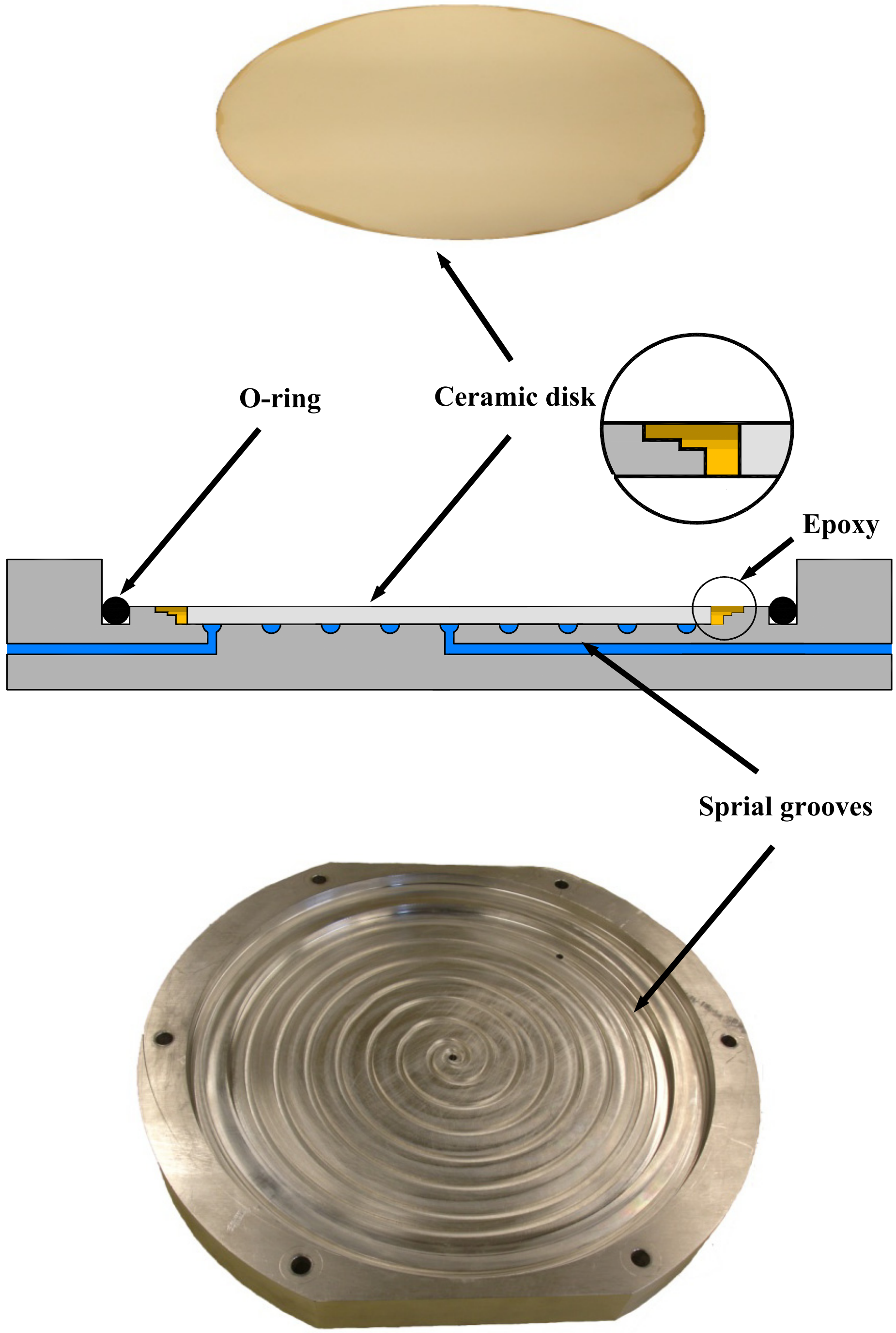

Figure App-2 Components of the bottom plate of the Large Tempe Cell.

The problems with Large Tempe Cell are associated with the leakage of both air and water in or out of the system. In the case of the equipment presented in this study, the most leakage susceptible area is the gap between the ceramic disk and bottom plate that was filled with epoxy. If any leakage in the system occurs during testing, the targeted matric suction value will not be reliable. Hence, it is necessary to monitor the amount of water coming out of the test system set up using an electronic scale (Figure App-3). Figure App-4 shows the amount of water collected over a period of time under the applied air-pressure of 6 kPa. As it can be seen, water comes out of the system at a constant rate until the suction value in the soil reaches equilibrium condition, which indicates that the matric suction value in the soil (i.e. 6 kPa) is reliable.

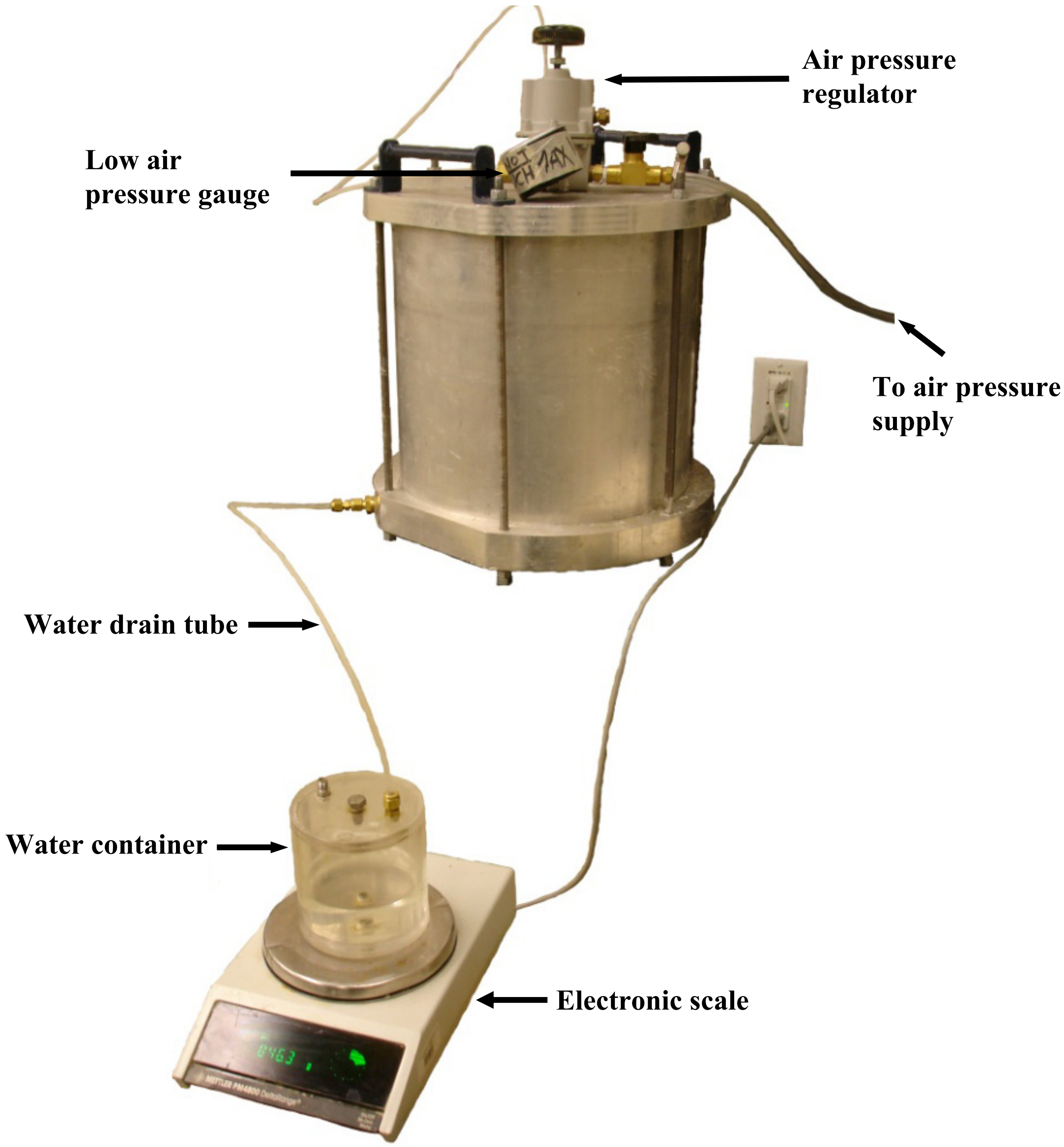

Figure App-3 Monitoring the drainage of water from the system setup under constant matric suction.

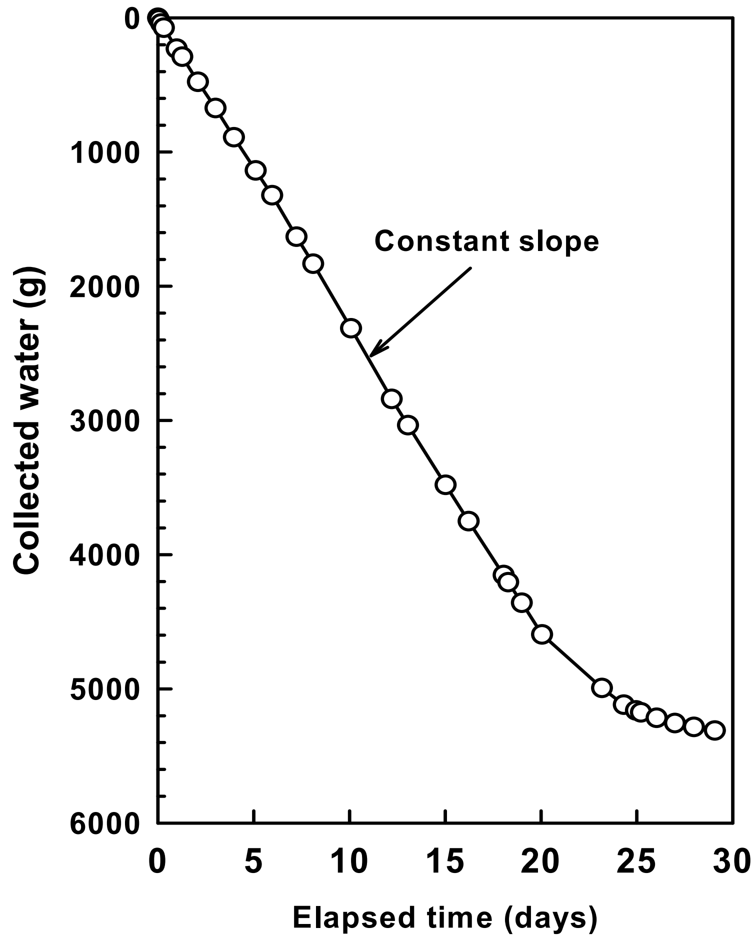

Figure App-4 Monitoring the amount of water from the test system with time.

REFERENCE

Power, K.C. and Vanapalli, S.K. 2010. Modified null pressure plate apparatus for measurement of matric suction. *Geotechnical Testing Journal*, 33(4).